University of Alberta

Gravity and Cyclonic Separation of Bidispersed Suspensions

by

Kelly Brian Roberge 

A thesis submitted to the Faculty of Graduate Studies and Research in partial fulfillment of the requirements for the degree of Master of Science.

in

Chemical Engineering

Department of Chemical and Materials Engineering

Edmonton, Alberta

Fall, 2005

Your file Votre référence
ISBN: 0-494-09272-6
Our file Notre référence
ISBN: 0-494-09272-6

For my wife, Susanna, and my parents, Ernie and Marie.

ABSTRACT:

The performance of a traditional gravity separation vessel with uniform feed injection was compared to tangentially-fed separation vessels with various output stream designs. Bidispersed suspensions were examined, consisting of various combinations of polymer beads and ceramic microspheres in salt water and fresh water solutions. Separation performance was measured for each system.

It was found that substantially improved separation performance over a simple gravity settler could be achieved by utilizing cyclonic separation via tangential feed injection. Cyclonic separation improved both product purity and recovery over a wide range of conditions. Notably, a simple cyclonic design featuring a tangential inlet achieved good light product recovery and heavy product quality, particularly at higher feed rates.

For the case of the gravity settler vessel, a theoretical model, based on mass balance and slip velocity, was used to model solids separation. The model predictions agreed well with the experimental measurements.

ACKNOWLEDGEMENTS

I would like to thank my advisor, Dr. Jacob Masliyah, for his guidance, support, and patience.

Thanks also to Syncrude Canada Ltd. and Barry Bara in particular for providing laboratory space and input through the initial part of my research.

I would like to acknowledge the Natural Sciences and Engineering Research Council through the NSERC Oil Sands Research Chair in Oil Sands Engineering for providing funding which made this thesis possible.

TABLE OF CONTENTS:

LIST OF TABLES:

LIST OF FIGURES:

NOMENCLATURE:

A	cross-sectional area of gravity settler, m^2
C	constant
C_D	coefficient of drag on a particle
D	diameter of a bounded container, m
d_p	particle diameter, m
F_D	fluid drag force, N
F_G	gravitational force, N
$F(\alpha_f, \Re_p)$	hindered settling function
g	gravitational acceleration, m/s^2
n	hindered settling exponent
N	number of particle species
Q	volumetric flow rate, m^3/s
R	drag force per unit surface area, N/m^2
$\Re_p$	particle Reynolds number
r	radial distance, m
u	velocity (of a fluid), m/s
v	velocity (of a solid), m/s

SYMBOLS:

α	volumetric fraction
ρ	density, kg/m^3
μ	viscosity, Pa·s
Ω	angular velocity, s^{-1}

SUBSCRIPTS:

batch	in a batch settler
F	in the feed stream
f	fluid
H	heavy particle species
i	particle species 'i'
j	index variable
L	light particle species
mono	monodispersed
M	in the mixed central zone
O	in the overflow
p	particle
rel	relative
Stokes	under Stokes flow
susp	suspension
U	in the underflow
∞	terminal velocity

1 - INTRODUCTION:

The majority of Canada's heavy hydrocarbons are found in Alberta's Athabasca oil sands. The oil sands are mixture of sand, bitumen, mineral rich clays, and water. The Athabasca oil sands deposit is, by itself, the largest petroleum resource in the world. According to the Alberta Energy and Utilities Board, the total remaining in-situ and mineable bitumen reserves are 174 billion barrels (AEUB 2004). To date, only 2 percent of the initial established crude bitumen reserve has been produced.

The Alberta oil sands are currently being developed by a method which combines aspects of mining, mineral processing, and hydrocarbon refining. The extraction of bitumen from oil sands is a process unique to the industry. The predominant extraction method is known as the Clark hot water process (1930).

The steps in the Clark hot water process are: (1) Oil sands are mined using surface mining techniques. Bitumen is a thick, sticky form of crude oil. At room temperature bitumen is extremely viscous and must be diluted with a solvent or heated before it can be liberated from the sand. (2) Hot water, chemical aids, and a significant amount of mechanical energy are required to detach bitumen from the sand grains. This process occurs in a tumbler or slurry pipeline, which also promotes aeration of the liberated bitumen droplets. (3) Subsequent separation of the bitumen dispersion and the solids occurs in a vertical gravity separation vessel. This is where the valuable bitumen is recovered from the unwanted solid material.

The bitumen froth from extraction is then mixed with a diluent (hydrocarbon solvent) and treated to reduce the amount of water and solids present in the bitumen froth. This treated diluted bitumen is suitable feedstock for the upgrading refinery. During the upgrading process, the diluent is separated and the bitumen is converted to synthetic crude oil.

Although bitumen extraction from oil sands is specific to Alberta, density-based separation is a classic industrial classification method with many applications. Differences in specific gravity are used to concentrate a desired product from the unwanted components. Vessels relying on gravity separation are in common use in the oil sands industry. Cyclones, which rely on centrifugal forces, are uncommon in oil sands extraction, but have potential for improved performance over gravity settlers.

1.1 - GRAVITY SEPARATION:

Gravity concentration methods separate species of different size and density by their relative movement in response to gravity and the resistance to motion offered by a viscous fluid. In a simple gravity separator, a feed stream - consisting of particles of a light phase and particles of a heavy phase, suspended in a fluid of intermediate density - is fed into a gravity settler and separated into underflow and overflow streams. The light particles tend to rise to the top, hence the overflow stream is rich in light particles. The heavy particles tend to settle to the bottom, and the underflow stream is rich in heavy particles.

Many factors influence the performance of a gravity separation vessel. Of the various mechanisms that play a role, *hydrodynamics* and *surface chemistry* are perhaps the two most important (Nasr-El-Din et al., 1988, 1990). Surface chemistry is important for systems relying on attachment between particles, drops, or bubbles as an intermediate stage before separation; as well as in systems where the particles are sufficiently small that their movement is dominated by colloidal forces. However, the actual separation of the differing phases is dominated by hydrodynamic forces. Gravity is the driving force for separation, and extremely large vessels are often required to provide sufficient surface area to achieve acceptable recovery.

Gravity separation vessels are the main equipment used for bitumen recovery in the oil sands industry. The primary separation stage at all existing commercial plants consists of

gravity settlers. Gravity separators can also be used for secondary recovery for tailings streams, or for froth cleaning of product streams. Primary extraction is the predominant role of gravity settlers in the oil sands industry, and this application deserves a more detailed description.

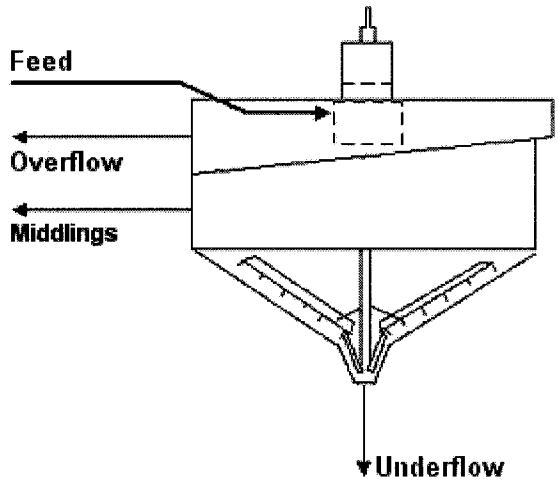

Figure 1-1. Typical Gravity Settler Design

Feed is introduced to the separation vessel via a centrally-located feed well and allowed to separate into a bitumen-rich upper layer and a sand-rich lower layer. Aerated bitumen, having a lower density than the surrounding fluid, rises to the top. Sand grains, being denser than the continuous fluid, sink to the bottom. The suspending fluid is a mixture of water, unaerated bitumen, and fine solids.

The aerated bitumen froth is recovered by continuously overflowing into launders, while an underflow tailings stream is withdrawn from the cone-shaped bottom. Most industrial vessels also withdraw a middlings stream of intermediate density and some designs incorporate a "froth underwash" stream of fresh water (not depicted).

The gravity separators used for secondary recovery are comparable to the primary separation vessels. Similar designs have also been used for froth cleaning, and the basic concept of density-based separation under gravity is also applied in froth treatment in the form of inclined plate settlers or stationary froth treatment.

1.2 - CYCLONIC SEPARATION:

The word 'cyclone' is used here as a general term for all tangentially-fed centrifugal separation devices. In a cyclone, centrifugal separation is achieved by tangential injection of feed, which induces centrifugal forces that act to separate the particles radially. Heavy particles are drawn to the outer zone of the cyclonic vessel and segregate along the edge. Light particles are drawn to the center of the vessel and tend to segregate in the central core. Thus, centrifugal forces act to separate particles across the cross-section of a cyclone, just as gravity acts to separate solids vertically in a gravity settler.

Various cyclone designs are used in industry. The most common type, the hydrocyclone (Figure 1-2), is one of the most important devices in mineral processing. Hydrocyclones are typically used for separation based on particle size, or for gas/liquid separation. As with gravity separators, cyclone performance is governed by hydrodynamics and surface chemistry. In most cyclones, hydronamic forces dominate since large centrifugal forces are induced.

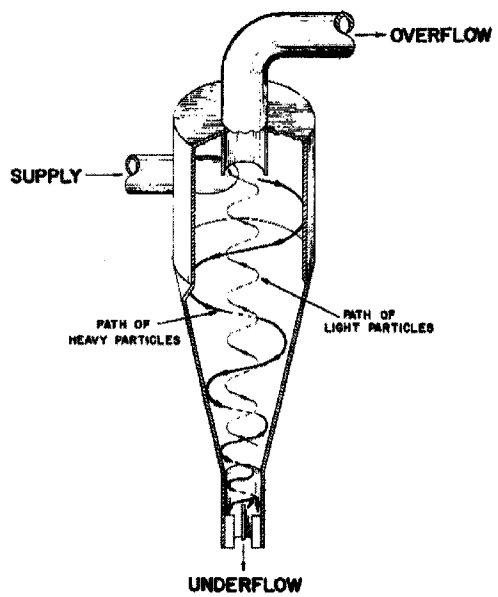

Figure 1-2. Typical Hydrocyclone Design

In fact, depending on the size of the vessel and the feed rate, centrifugal forces can be several orders of magnitude greater than gravity. Thus there is a strong driving force for particle separation and potential for improved separation compared to gravity separators.

Although hydroyclones are used for several applications in the oil sands industry, such as in the consolidated tailings process, these devices have yet to be in common use for bitumen production.

Cyclonic separation could be used at several stages in oil sand slurrying and bitumen extraction. For example, cyclones could be used in the mine to reject pebbles and coarse sand before hydrotransport. Potentially, at-face coarse solids removal could allow small, fully mobile slurry preparation units, instead of the current large fixed installations. Once proven in service, small cylones could potentially augment or replace the large gravity settlers used in primary extraction. Cyclonic separation vessels can also improve bitumen recovery in existing plants by reprocessing middlings or tailings streams. This is the application that has received the most attention to date.

In early 2002, cyclonic separation vessels (dubbed "cycloseparators") designed for tailings oil recovery were commissioned at Syncrude Canada Ltd.'s Mildred Lake Extraction Plant. These proprietary vessels depart significantly from the configurations of traditional cyclones.

1.3 - RESEARCH OBJECTIVE:

Traditionally, the design of gravity separation vessels is based on creating a uniform suspension throughout the entire feed zone and to have simple inlet and output streams from the vessel. Here, both approaches are challenged.

The performance of a traditional gravity separation vessel with uniform feed injection was compared to tangentially-fed separation vessels with various output stream designs. Although much research has been performed both on traditional gravity settlers and on hydrocyclones for mineral processing classification, there are few studies in the open literature for tangentially-fed separators of a more general design or purpose. Given the interest in non-conventional cyclones for oil sands extraction, there is a need for further theoretical and experimental investigation of particle separation in cyclonic vessels.

2 - THEORETICAL BACKGROUND:

Understanding the fundamentals of fluid-particle dynamics is essential for the analysis and design of gravity settlers and cyclones.

In Section 2.1, hydrodynamic drag on a single particle is considered. At low Reynolds number flow, the Navier-Stokes equation can be solved analytically. At higher Reynolds numbers, empirical relationships must be used. Both regimes are evaluated. Next, equations are given for the terminal velocity of a single particle at infinite dilution.

Section 2.2 discusses hindered settling of spherical particles in a suspension that is not infinitely dilute. First, the literature on monodispersed batch sedimentation is considered, and functions accounting for hindered settling effects are presented. Next, the settling velocity equations for batch sedimentation are generalized to particle slip velocities for continuous separation. Slip velocities are given for the continuous separation of monodispersed and polydispersed systems.

Next, Section 2.3 presents a model for the continuous separation of a bidispersed mixture of particles. Governing equations are first developed, followed by derived values of interest.

Finally, Section 2.4 considers the effects of swirling flow in cyclonic separators. While there is not yet a general model for cyclones of the design studied here, the physical laws which govern all swirling flows are examined.

2.1 - FLUID-PARTICLE DYNAMICS:

2.1.1 - LOW REYNOLDS NUMBER FLOW ($\Re_p < 0.1$):

The resistance to motion of a solid sphere in a fluid has been extensively studied for well over a century. The hydrodynamic drag force experienced by a single particle moving through a fluid at infinite dilution can be expressed as a relationship between the drag coefficient C_D and the particle Reynolds number $\Re_p$.

Derived from the Navier-Stokes equation, Stokes' Law gives the drag force, F_D, on a sphere under the condition of low Reynolds number flow known as 'creeping flow' (Stokes, 1891):

$$F_D = 3\,\pi\,\mu_f v_p\, d_p \qquad (2\text{-}1)$$

A sphere moving through a fluid projects an area equal to $\pi d_p^2/4$ in a plane perpendicular to the direction of motion. Therefore, R, the drag force per unit projected area of a particle in creeping flow is:

$$R = 4\frac{F_D}{\pi\, d_p^{\,2}} = 12\frac{\mu_f v_p}{d_p} \qquad (2\text{-}2)$$

Dividing by $\frac{1}{2}\rho_f v_p^2$ gives this expression in terms of dimensionless groups:

$$\frac{R}{\frac{1}{2}\rho_f v_p^{\,2}} = 24\frac{\mu_f}{\rho_f d_p v_p} \qquad (2\text{-}3)$$

In most literature, the drag coefficient C_D and particle Reynolds number $\Re_p$ are defined as:

$$C_D = \frac{R}{\frac{1}{2}\rho_f d_p^{\,2}} = 24\frac{\mu_f}{\rho_f d_p v_p} \qquad (2\text{-}4)$$

$$\Re_p = \frac{\rho_f d_p v_p}{\mu_f} \qquad (2\text{-}5)$$

This leads to a C_D-$\Re_p$ relationship of the following form:

$$C_D = 24\frac{1}{\Re_p} \qquad (2\text{-}6)$$

As noted above, this equation holds true only for low Reynolds number flows ($\Re_p < 0.1$).

2.1.2 - HIGH REYNOLDS NUMBER FLOW ($\Re_p > 0.1$):

At higher Reynolds numbers, analytical solutions are not possible and experimental correlations are used. Various relations have been proposed; some of the more common are listed in Table 2-1:

Table 2-1. Typical Equations for the Drag Coefficient of a Spherical Particle

Reference	$(C_D \Re_p)/24 =$	Region of Validity
Stokes (1891)	1	$\Re_p < 0.1$
Schiller & Naumann (1935)	$1 + 0.15\ \Re_p^{0.687}$	$\Re_p < 1000$
Dallaville (1948)	$(1 + 0.135\sqrt{\Re_p})^2$	$\Re_p < 3.5\times10^5$
Brauer & Stucker (1976)	$1 + 0.155\sqrt{\Re_p} + 0.0204\ \Re_p - \frac{2.01\times10^{-4}\ \Re_p^{(3/2)}}{1 + 3\times10^{-6}\ \Re_p^{(3/2)}}$	$\Re_p \le 3.5\times10^5$
Turton & Levenspiel (1986)	$1 + 0.173\ \Re_p^{0.657} + \frac{0.0172\ \Re_p}{1 + \frac{16300}{\Re_p^{1.09}}}$	$\Re_p \le 3.5\times10^5$
Khan & Richardson (1987)	$\frac{1}{24}\Re_p\left(2.25\frac{1}{\Re_p^{0.31}} + 0.36\ \Re_p^{0.06}\right)^{3.45}$	$\Re_p \subset (0.1, 3.5\times10^5)$

Particle Reynolds numbers ranged between 0.25 and 2.7 for the systems studied in this work; thus the Schiller and Naumann correlation was used. A more general C_D-$\Re_p$ relation than Eq. 2-6 valid for non-Stokes flow is therefore:

$$C_D = 24\frac{1 + 0.15\ \Re_p^{0.687}}{\Re_p} \qquad (2\text{-}7)$$

2.1.3 - PARTICLE SETTLING VELOCITY:

For a particle settling in a fluid, the gravitational force exerted on it is counteracted by viscous drag. The gravitational (or buoyant) force on a spherical particle is given by:

$$F_G = \frac{1}{6}\pi d_p^{\,3}(\rho_p - \rho_f) g \qquad (2\text{-}8)$$

Viscous forces at low Reynolds numbers (Stokes flow) were given by Eq. 2-1 as $3\pi\mu_f v_p d_p$. At terminal velocity, gravitational forces are balanced with viscous forces ($F_G = F_D$), leading to:

$$\frac{1}{6}\pi d_p^{\,3}(\rho_p - \rho_f) g = 3\pi\mu_f v_p d_p \qquad (2\text{-}9)$$

The terminal particle velocity under the conditions of Stokes flow, $v_{\infty,\,Stokes}$, is then given by:

$$v_{\infty,\,Stokes} = \frac{1}{18}\frac{g d_p^{\,2}(\rho_p - \rho_f)}{\mu_f} \qquad (2\text{-}10)$$

The more general equation for non-Stokes flow, again using Schiller and Naumann's relationship for C_D and $\Re_p$, is given by:

$$v_\infty = \frac{1}{18}\frac{g d_p^{\,2}(\rho_p - \rho_f)}{\mu_f(1 + 0.15\,\Re_p^{\,0.687})} \qquad (2\text{-}11)$$

This general equation was used for the systems studied in this work. $\Re_p$ here is calculated at the terminal velocity, v_∞.

2.2 - HINDERED SETTLING:

2.2.1 - BATCH SETTLING (MONODISPERSED SYSTEMS):

The settling of suspensions of monodispersed suspensions has been studied extensively, and the results have been summarized by Barnea and Mizrahi (1973), Garside and Al-Dibouni (1977), and Davis and Acrivos (1985). The settling velocity of a monodispersed suspension in a batch settler can be described by the expression:

$$v_{batch,\,mono} = v_{\infty}\, F(\alpha_f, \Re_p) \qquad (2\text{-}12)$$

$v_{batch,mono}$ is the hindered settling velocity of a monodispersed system in a closed system, v_{∞} is the terminal settling velocity of a single particle (from Section 2.1.3), and $F(\alpha_f, \Re_p)$ is a function of the volumetric fraction of fluid in a suspension and the particle Reynolds number.

Theoretical models have been constructed for extremely dilute systems, most notably by Batchelor (1982). For more concentrated systems, recent kinematic models in the form of central difference solutions of conservation equations have been developed by Bürger, Karlsen, Tory, and Wendland (2001) and Berres and Bürger (2003), but these must be solved numerically and empirical forms of $F(\alpha_f, \Re_p)$ are more often used in practice.

Several functions have been suggested by Richardson and Zaki (1954), Barnea and Mizrahi (1973), and Garside and Al-Dibouni (1977), as shown in Table 2-2. Other models include those of Steinour (1944), Brunkman (1947), Lewis et al. (1949), Hawksley (1951), and others.

Table 2-2. Some Functional Forms of $F(\alpha_f, \Re_p)$

Reference	$F(\alpha_f, \Re_p)$ =	Region of Validity
Richardson and Zaki (1954)	α_f^n	
where n =	$4.65 + 19.5\ d_p/D$	$\Re_p < 0.2$
	$(4.35 + 17.5\ d_p/D)\ \Re_p^{-0.03}$	$0.2 < \Re_p < 1$
	$(4.45 + 18.0\ d_p/D)\ \Re_p^{-0.1}$	$\Re_p \leq 3.5\times10^5$
	$4.45\ \Re_p^{-0.1}$	$1 < \Re_p < 200$
	2.39	$\Re_p > 500$
Barnea and Mizrahi (1973)	$\left(1 + (1-\alpha_f)^{(1/3)}\ \mathbf{e}^{\left(5/3\ \frac{1-\alpha_f}{\alpha_f}\right)}\right)^{-1}$	$10^{-3} < \Re_p < 3\times10^4$
Garside and Al-Dibouni (1977)	α_f^n	
where n =	$\frac{5.1-n}{n-2.7} = 0.1\ \Re_p^{0.9}$	$10^{-3} < \Re_p < 3\times10^4$
Rowe (1987)	α_f^n	
where n =	$\frac{4.7-n}{n-2.35} = 0.175\ \Re_p^{0.75}$	$10^{-3} < \Re_p < 3\times10^4$

The most widely used empirical form of $F(\alpha_f, \Re_p)$ is the Richardson and Zaki equation, where $F(\alpha_f, \Re_p) = \alpha_f^n$ and n is a function of the Reynolds number $\Re_p$, particle size d_p, and possibly vessel diameter D (in cases where wall effects are important). For the systems of interest in this study, n ranged from 4.12 to 4.62.

The Richardson-Zaki form of $F(\alpha_f, \Re_p)$ was found to be satisfactory for modelling experimental results. For discussion of other hindered settling equations, see Appendix 3.

The full expression for hindered particle velocity in a monodispersed batch settler, using the Richardson and Zaki form of $F(\alpha_f, \Re_p)$, is thus:

$$v_{batch,\ mono} = \frac{1}{18} \frac{g\, d_p^{\,2} (\rho_p - \rho_f)\, \alpha_f^{\,n}}{(1 + 0.15\ \Re_p^{\,0.687})\ \mu_f} \qquad (2\text{-}13)$$

Note that for suspensions of particles, the Reynolds number is also a function of α_f, the volume fraction of fluid. And when the particles are moving relative to a carrier fluid (as with continuous separation, covered next), the appropriate velocity term is $v_p - v_f$, the particle-fluid slip velocity, instead of v_p. The following general form of $\Re_p$, as given by Masliyah (1979), applies:

$$\Re_p = \frac{\rho_f d_p |v_p - v_f| \alpha_f}{\mu_f} \qquad (2\text{-}14)$$

Note that this simplifies to Eq. 2-5 in the case of $v_f = 0$ and $\alpha_f = 1$.

2.2.2 - CONTINUOUS SEPARATION (MONODISPERSED SYSTEMS):

The continuous gravity settling of a monodispersed suspension in a vertical column has received much research since the initial studies by Coe and Clevenver (1916), Kynch (1952), and Talmadge and Fitch (1955).

For continuous separators, the batch sedimentation velocity, $v_{batch,mono}$, shown in Eq. 2-13 must be reformulated in terms of the particle-fluid slip velocity, $v_p - v_f$. The general equation for a system of N particle species, as given by Smith (1966), is:

$$v_{batch,\,i} = v_{p,\,i} - v_f - \left(\sum_{j=1}^{N} (v_{p,j} - v_f)\, \alpha_j \right) \qquad (2\text{-}15)$$

For a monodispersed system, $N = 1$, and:

$$v_{batch} = v_p - v_f - (v_p - v_f)\,\alpha_p \tag{2-16a}$$

$$v_p - v_f - (v_p - v_f)\,\alpha_p = (v_p - v_f)\,(1 - \alpha_p) \tag{2-16b}$$

$$(v_p - v_f)\,(1 - \alpha_p) = (v_p - v_f)\,\alpha_f \tag{2-16c}$$

Therefore, converting from $v_{batch,mono}$ in Eq. 2-13, the particle slip velocity for the continuous separation of a monodispersed suspension is:

$$v_p - v_f = \frac{1}{18}\frac{g\,d_p^{\,2}\,(\rho_p - \rho_f)\,\alpha_f^{\,(n-1)}}{(1 + 0.15\,\Re_p^{\,0.687})\,\mu_f} \tag{2-17}$$

Note that the hindered settling exponent appropriate for such a system is related to the Richardson and Zaki exponent for batch settling by $n-1$.

2.2.3 - CONTINUOUS SEPARATION (POLYDISPERSED SYSTEMS):

In order to account for hydrodynamic interactions between different particle species, the drag force acting on a monodispersed particle species is assumed to apply for a polydispersed suspension. However, for a system of more than one particle species, there has been disagreement about the correct formulation for buoyant forces.

One choice is to assume that buoyant forces on a particle species depend on $\rho_p - \rho_{susp}$, where ρ_{susp} is defined for a system of N particle species as:

$$\rho_{susp} = \rho_f \alpha_f + \left(\sum_{j=1}^{N} \rho_{p,j}\,\alpha_{p,j} \right) \tag{2-18}$$

Using this approach, the generalization from v_{batch} to the slip velocity $v_{p,i}-v_f$ in a polydispersed system was given by Masliyah (1979) and Lockett and Bassoon (1979) and is known as the MLB Model:

$$v_{p,i}-v_f=\frac{1}{18}\frac{g\,d_{p,i}^{\,2}(\rho_{p,i}-\rho_{susp})\,\alpha_f^{(n-2)}}{(1+0.15\,\Re_{p,i}^{\,0.687})\,\mu_f} \qquad (2\text{-}19)$$

In this case, the appropriate hindered settling exponent is related to the Richardson and Zaki exponent for batch settling by $n-2$. Also note, for the case of a single particle settling at a low Reynolds number, $\alpha_f \rightarrow 1$ and $\Re_p \rightarrow 0$. Eq. 2-19 simplifies to the form for Stokes flow as given in Eq. 2-10.

As an aside, one can also derive the monodispersed relationship (shown Eq. 2-17) from the polydispersed equation by noting the following:

$$\rho_p-\rho_{susp}=\rho_p-\alpha_p\rho_p-\alpha_f\rho_f \qquad (2\text{-}20a)$$

$$\rho_p-\alpha_p\rho_p-\alpha_f\rho_f=\rho_p(1-\alpha_p)-\alpha_f\rho_f \qquad (2\text{-}20b)$$

$$\rho_p(1-\alpha_p)-\alpha_f\rho_f=\alpha_f\rho_p-\alpha_f\rho_f \qquad (2\text{-}20c)$$

$$\alpha_f\rho_p-\alpha_f\rho_f=\alpha_f(\rho_p-\rho_f) \qquad (2\text{-}20d)$$

2.3 - MATHEMATICAL MODEL:

The fluid-particle slip velocities developed in the previous sections can be used to help model and understand the behavior of industrial separation vessels. A number of approaches have been used to model the behaviour of continuous gravity settlers. Of these, the Masliyah Model (Masliyah et al., 1981) is among the clearest and most easily implemented. It is inspired by the standard one-dimensional wave model for sedimentation (Kynch, 1952). The simplest form of the model, for bidispersed systems, is considered here.

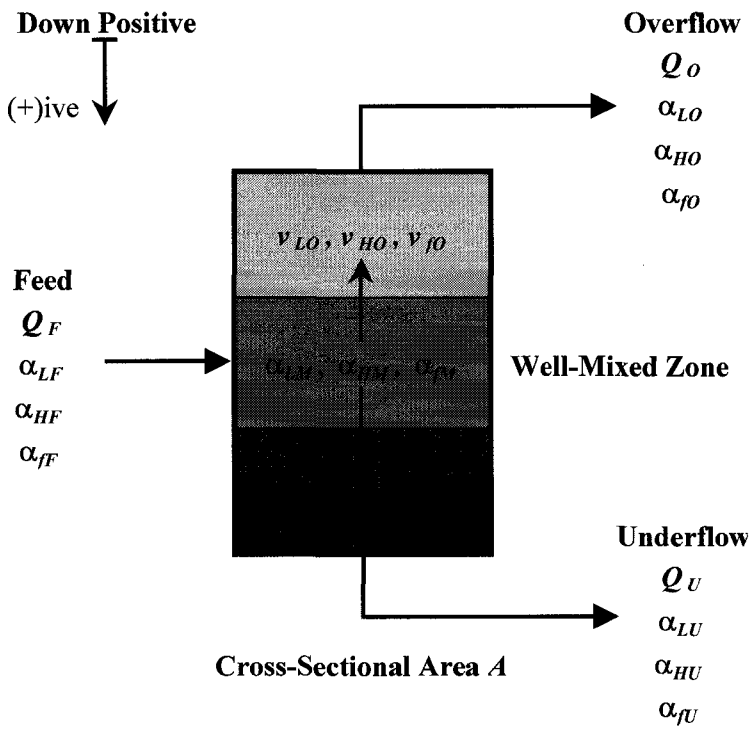

Figure 2-1. Schematic of a Continuous Gravity Settler for the Mathematical Model

2.3.1 - GOVERNING EQUATIONS:

Consider the case as shown in Figure 2.1. Feed enters a continuous gravity settler into a well-mixed zone that is assumed to be of uniform concentration. The composition of this zone is not necessarily that of the feed stream. This mixed zone supplies the suspension to the underflow and overflow streams. If the downward fluid velocity is larger than the rise velocity of the light particles it can carry the light particles across the lower boundary of the mixed zone to report to the underflow stream. Otherwise the light particles can only cross the upper boundary of the mixed zone to report to the overflow stream. Similar constraints apply to the heavy particle species at the upper boundary of the mixed zone.

Referring to Figure 2-1, volumetric balances over the well-mixed source zone are given by:

Light particle species:

$$\alpha_{LM} v_{LU} A - \alpha_{LM} v_{LO} A = Q_F \alpha_{LF} \qquad (2\text{-}21)$$

Heavy particle species:

$$\alpha_{HM} v_{HU} A - \alpha_{HM} v_{HO} A = Q_F \alpha_{HF} \qquad (2\text{-}22)$$

Fluid phase:

$$\alpha_{fM} v_{fU} A - \alpha_{fM} v_{fO} A = Q_F \alpha_{fF} \qquad (2\text{-}23)$$

Q_F is the volumetric flow rate of a feed having light and heavy particle volume fractions of α_{LF} and α_{HF}, respectively, and a fluid fraction of α_{fF}. The volume fractions of light particles, heavy particles, and fluid in the well-mixed zone are α_{LM}, α_{HM}, and α_{fM}, respectively. v_{LU} and v_{LO} are the velocities of the light particles at the underflow and overflow boundaries, while the velocities of the heavy particles and fluid are v_{HU}, v_{HO}, v_{fU} and v_{fO}. A is the vessel cross-sectional area. The downward direction is taken as positive.

The vertical velocity of the light particles at the overflow boundary is given by:

$$v_{LO} - v_{fO} = v_{L,\infty} \mathrm{F}(\alpha_f, \Re_p) \qquad (2\text{-}24)$$

Similarly, the vertical velocity of the light particles at the underflow boundary is:

$$v_{LU} - v_{fU} = v_{L,\infty} \mathrm{F}(\alpha_f, \Re_p) \qquad (2\text{-}25)$$

And the velocities of heavy particles at the overflow and underflow boundaries are:

$$v_{HO} - v_{fO} = v_{H,\infty} \mathrm{F}(\alpha_f, \Re_p) \qquad (2\text{-}26)$$

$$v_{HU} - v_{fU} = v_{H,\infty} \mathrm{F}(\alpha_f, \Re_p) \qquad (2\text{-}27)$$

Thus, the slip velocity equations (Eq. 2-24 to 2-27) take the form as shown in Eq. 2-19, assuming the Richardson-Zaki relation for $F(\alpha_f, \Re_p)$.

There is an additional physical constraint that must be considered here. Light particles can enter the underflow only when the downward fluid velocity is larger than the rise velocity of the particles themselves, but they cannot enter the mixed zone from the lower boundary. Likewise, heavy particles cannot enter the mixed zone from the upper overflow boundary. Thus, $v_{LU} \geq 0$ and $v_{HO} \leq 0$, respectively.

In addition to the volumetric balances and velocity equations, the withdrawl rate of either the underflow or overflow stream must be specified. The underflow stream flow rate is given by:

$$\alpha_{LM} v_{LU} A + \alpha_{HM} v_{HU} A + \alpha_{fM} v_{fU} A = Q_U \qquad (2\text{-}28)$$

A final equation can be constructed by observing that the sum of volume fractions in the well-mixed zone must equal 1:

$$\alpha_{LM} + \alpha_{HM} + \alpha_{fM} = 1 \qquad (2\text{-}29)$$

Thus, the model consists of a total of nine equations - three volumetric balances, four slip velocity equations at the upper and lower boundaries, an equation for withdrawl rate of either the underflow or overflow, and a constraint on source zone volume fractions.

The nine unknowns to be solved for are the volumetric concentrations in the well-mixed zone (α_{LM}, α_{HM}, and α_{fM}) and the velocities of each species at the underflow and overflow boundaries (v_{LU}, v_{HU}, and v_{fU}; v_{LO}, v_{HO}, and v_{fO}).

In summary, equations 2-21 to 2-29 provide a simple model for the continuous separation

of a bidispersed suspension in a gravity separation vessel in the absence of any lateral concentration gradients.

2.3.2 - DERIVED QUANTITIES:

Once the composition in the well-mixed zones and the interface velocities are calculated, the volume fractions of each species in the overflow and underflow streams can be determined:

$$\alpha_{LO} = \frac{A|v_{LO}|\alpha_{LM}}{Q_F - Q_U} \qquad (2\text{-}30)$$

$$\alpha_{HO} = \frac{A|v_{HO}|\alpha_{HM}}{Q_F - Q_U} \qquad (2\text{-}31)$$

$$\alpha_{LU} = \frac{A|v_{LU}|\alpha_{LM}}{Q_U} \qquad (2\text{-}32)$$

$$\alpha_{HU} = \frac{A|v_{HU}|\alpha_{HM}}{Q_U} \qquad (2\text{-}33)$$

Finally, the particle recovery, defined as the fraction that particle species collected in the stream compared to the total amount in the feed, for each product stream can be calculated:

$$R_{LO} = \frac{A|v_{LO}|\alpha_{LM}}{Q_F \alpha_{LF}} \qquad (2\text{-}34)$$

$$R_{HO} = \frac{A|v_{HO}|\alpha_{HM}}{Q_F \alpha_{HF}} \qquad (2\text{-}35)$$

$$R_{LU} = \frac{A|v_{LU}|\alpha_{LM}}{Q_F \alpha_{LF}} \qquad (2\text{-}36)$$

$$R_{HU} = \frac{A|v_{HU}|\alpha_{HM}}{Q_F \alpha_{HF}} \qquad (2\text{-}37)$$

Appendix 3 gives sample calculations for the model predictions of a given system. A Gauss-Siedel iterative method was used, with a relaxation factor of 0.8. Within 20 iterations, solutions converged with a tolerance of 10^{-6}. All gravity separation figures shown in Chapter 4 and Appendix 5 include predictions made using this model.

2.4- SWIRLING FLOW

Thus far in this chapter, only gravity separation has been discussed. For cyclones and other equipment which utilize swirling flow, separation is driven by centrifugal acceleration instead of gravity. For such systems, a cylindrical coordinate system (r-θ-z) is more appropriate.

2.4.1 - FLUID ELEMENT IN SWIRLING FLOW:

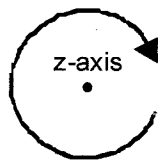

Figure 2-2. Swirling Flow

Take an arbitrary *fluid* element (as opposed to a solid particle) rotating in an orbit with radius r around some center point which lies upon the z-axis (extending vertically out of the page). This fluid will accelerate towards the center - if it did not accelerate, it would continue in a straight path tangent to its orbit about the center point. This inward acceleration is termed 'centripetal acceleration'. Centripetal acceleration leads to an apparent force away from the z-axis, termed 'centrifugal force', equal to the mass of the element times the centripetal acceleration.

For a fluid element, the centrifugal force is balanced by a radial force arising from the pressure gradient. For this case, the momentum equation balance in the radial direction, expressed on a per unit volume basis, from Bird, Stewart, and Lightfoot (BSL) (1960), is:

$$-\frac{\rho_f u_\theta^{\,2}}{r} = \frac{dP}{dr} \qquad (2\text{-}38)$$

Thus, the pressure in a swirling flow increases with r, and this static pressure gradient creates a force which acts towards the z-axis - thus keeping the element in its path around the center.

If we assume that the centerline coincides with the direction of gravity, then the momentum balance along the z-axis, as given by BSL (1960), is:

$$0 = \frac{dP}{dz} + \rho_f g \qquad (2\text{-}39)$$

This leaves just the momentum balance in the θ direction. Equations can be derived for two types of ideal swirling flows:

- Forced vortex flow, which is swirling flow with the same tangential velocity distribution as in *solid body rotation*; and
- *Free vortex flow*, which is the way an ideal, frictionless fluid would swirl.

In solid body rotation no shear occurs between fluid layers in the r-direction. All fluid elements have the same angular velocity, Ω (rad/s), and the tangential velocity u_θ (m/s) is given by:

$$u_\theta = \Omega\, r \qquad (2\text{-}40)$$

At the other extreme, in free vortex flow the swirling fluid has no viscosity. In such a fluid, an element rotating at a smaller radius from center has a higher tangential velocity from conservation of momentum and $u_\theta \cdot r$ equals a constant, C, so that:

$$u_\theta = \frac{C}{r} \qquad (2\text{-}41)$$

For real swirling flows, the tangential velocity distribution is intermediate between these two extremes. Typically, solid body rotation dominates near the center, and free vortex flow dominates at larger r.

2.4.2 - PARTICLE MOTION IN SWIRLING FLOW:

Next, consider a *particle* moving in a swirling flow. The momentum balance in the r-direction differs from that of an equivalent fluid element. The forces from the pressure gradient will not keep a particle on a circular path around the center point unless the particle's density exactly matches that of the fluid.

Assuming the particle moves with the same tangential velocity as the fluid, the centrifugal force acts in the same way as the gravitational force in a non-cyclonic system. The equations of particle motion from previous sections still apply, but instead of g, the acceleration term becomes v_θ^2/r. The centrifugal force is then equal to the mass of the particle times this centrifugal acceleration. Under Stokes' flow conditions, a particle will move with a terminal radial velocity of:

$$v_{r,\,Stokes} = \frac{1}{18}\frac{v_\theta^{\,2}\, d_p^{\,2}\,(\rho_p - \rho_f)}{r\,\mu_f} \qquad (2\text{-}42)$$

Or, for the more general case of higher Reynolds number flow:

$$v_r = \frac{1}{18}\frac{v_\theta^{\,2}\, d_p^{\,2}\,(\rho_p - \rho_f)}{r\,\mu_f\,(1 + 0.15\,\Re_p^{\,0.687})} \qquad (2\text{-}43)$$

Heavy particles entering a cyclone thus experience an inward-directed drag and an

outward-directed centrifugal force, and they move towards the outer edge of the cyclone. For particles lighter than the carrier fluid, the situation is reversed, and they move towards the center. Thus, particles of differing density are separated radially by centrifugal forces. Unlike gravity, which is (in practice) constant, the centrifugal force is a function of tangential velocity and vessel size. Therefore, much higher accelerational forces are possible in a centrifugal vessel than in a gravity separator.

Unfortunately, for the type of cyclonic separators investigated here, no general model exists to predict the performance of such vessels. Further empirical work is required in this field.

3 - EXPERIMENTAL SET-UP AND PROCEDURE:

The capabilities of three different designs of gravity and cyclonic separation vessels were evaluated. Experiments were conducted with two different fluid-particle systems. Bidispersed particle suspensions, made up of monosized polymer beads and/or hollow ceramic microspheres of different density were used to model industrial systems of interest. The carrier fluids were salt water or tap water with densities between those of the particles. For each vessel design and fluid-particle system, tests were performed at several different feed rates, and at each feed rate, the split ratio (defined as the volume fraction of the feed stream that reports to a given product stream) was varied. From each run, the flow rates and compositions for the feed, overflow, and underflow streams were measured to derive overall separation performance.

A basic schematic of the experimental set-up is shown below:

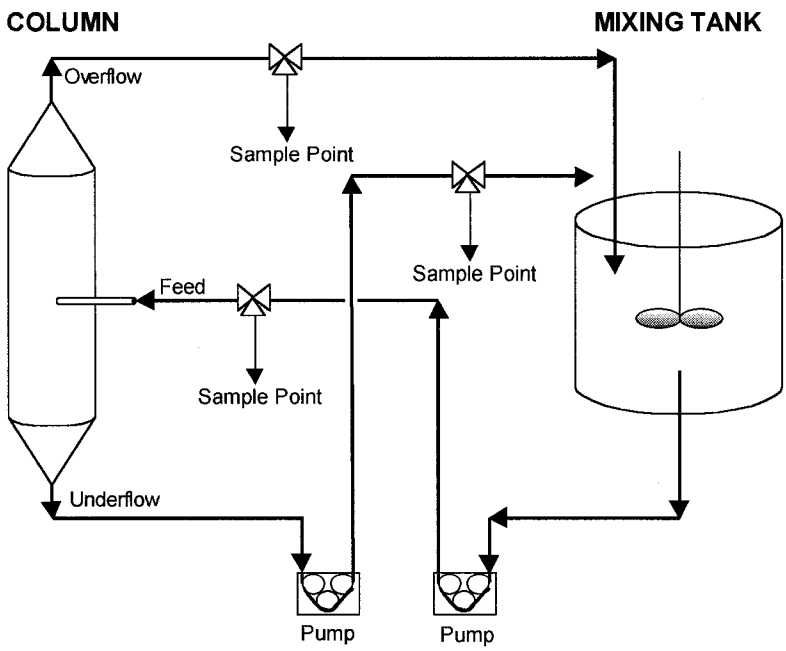

Figure 3-1. Experimental Set-Up Schematic

3.1 - COLUMN DESIGN:

Three column designs were investigated, designated Column A (Figure 3-2), Column B (Figure 3-3), and Column C (Figure 3-4).

The basic dimensions of each column were identical; all three had a cylindrical section 8 cm in diameter and 24 cm high. For Columns A and B, top and bottom conical sections each added another 8 cm to the height, while the ends of Column C were flat. The conical ends of Columns A and B were intended to eliminate any dead zones where the particles might accumulate, while the flat ends of Column C were intended to facilitate its tangential outlet stream. Each column had one or more inlet streams, an overflow outlet, and an underflow outlet. All inlets and outlets had an inner diameter of 0.95 cm. All three columns were made of clear glass to allow for flow visualization.

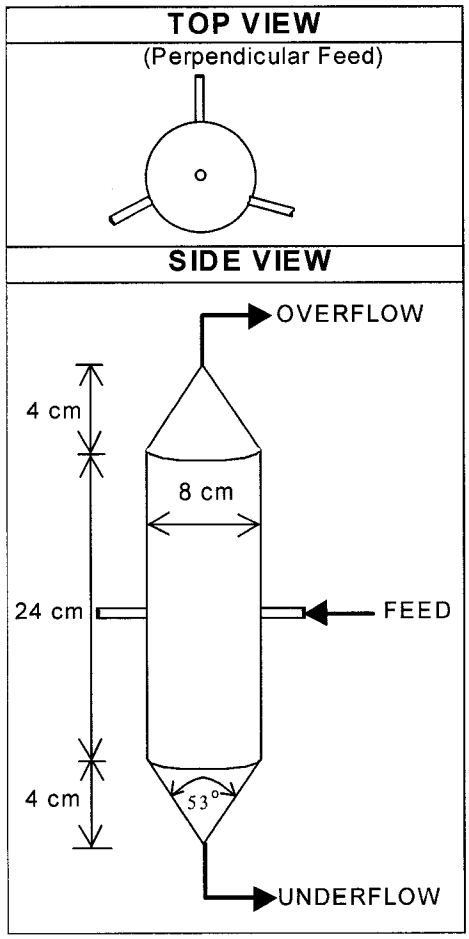

Figure 3-2. Detail View of Column A

In Column A, the feed was split into three equal substreams which were radially injected by inlet pipes spaced equally around the perimeter of the column (Figure 3-2). These inlet pipes were midway up the column. This feed introduction method creates a well-mixed central zone in the separation column with no vortex or swirl. Above and below this central zone, the column tapered to a cone where the overflow and underflow streams were withdrawn. Since there were no centrifugal effects, only the force of gravity acts to induce separation, and Column A simulates a traditional gravitational settling vessel. Unlike previous investigations of bidispersed particle separation by Nasr-El-Din et al. (1988, 1990), this separation column had a relatively large cross-sectional area compared to its height.

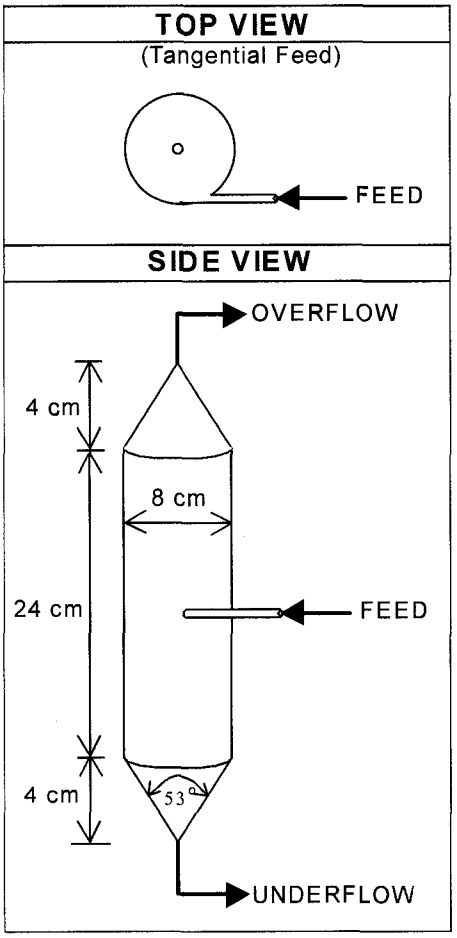

Figure 3-3. Detail View of Column B

Column B was of similar dimensions to Column A, but fed tangentially (Figure 3-3). A single feed stream was introduced by a tangential inlet midway up the column, imparting a swirling motion to the slurry. This generates a vortex in the column and induces centrifugal forces on the particles in the vessel. Particles in this column experience both gravitational and centripetal acceleration. Depending on the injection velocity, either gravity or centrifugal forces can dominate. The conical ends were identical to Column A. Column B is similar to hydrocyclones used in mineral processing, but not identical (it does not have a vortex finder, for example). The different design provides flow patterns within the vessel are not the same as in a standard hydrocyclone.

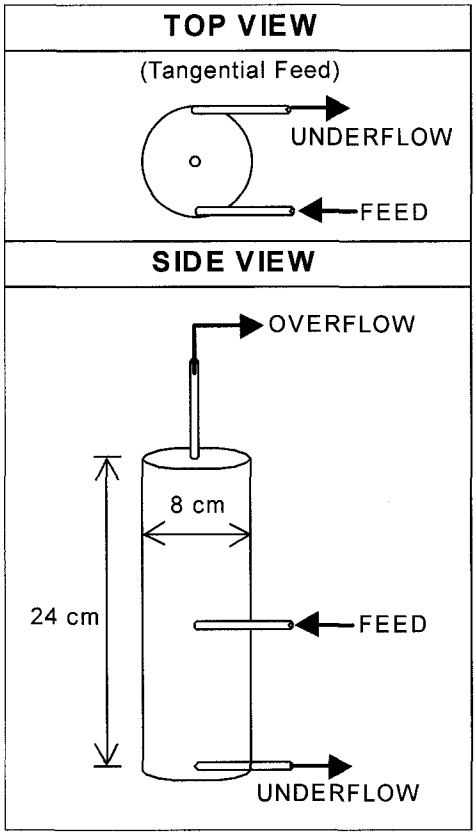

Figure 3-4. Detail View of Column C

Column C had a different configuration from the other two columns. It had the same feed injection system as Column B - a single tangential feed at the midway point, however the overflow and underflow were withdrawn in a different manner (Figure 3-4). Both the top and bottom of the vessel were flat, and while the overflow was withdrawn from the center point, the underflow was withdrawn tangentially. The intention of the tangential underflow was to improve the withdrawal of heavy particles from near the vessel wall at the bottom.

3.2 - SYSTEM PREPARATION:

The separation of two different fluid-particle systems were tested. Light and heavy particle fractions of known size and composition were used to simulate industrial systems of interest. Several distinct particle types were tested; polystyrene beads (two size

fractions), polymethyl methacrylate beads, and z-light ceramic microspheres. Near-monosized particles were used in all experiments.

System I consisted of light polystyrene beads (d_p=386 μm, ρ_p=1052 kg/m^3) and heavy polymethyl methacrylate beads (d_p=194 μm, ρ_p=1184 kg/m^3) in a salt water solution (ρ_f=1067 kg/m^3, μ_f=1.41 mPa·s). Volumetric concentrations in System I were α_{LF}=0.058, α_{HF}=0.122, and α_{fF}=0.820.

System II consisted of light z-light ceramic microspheres (d_p=137 μm, ρ_p=749 kg/m^3) and heavy polystyrene beads (d_p=459 μm, ρ_p=1052 kg/m^3) in tap water (ρ_f=997 kg/m^3, μ_f=0.931 mPa·s). Volumetric concentrations in System II were α_{LF}=0.134, α_{HF}=0.163, and α_{fF}=0.703.

The following tables summarize the particle properties of both systems:

Table 3-1. System I Particle Summary (α_{LF} = 0.058, α_{HF} = 0.122, α_{fF} = 0.820)

Particle Type	Sieve Passing Size (μm)	Mean Particle Diameter (μm)	Particle Density (kg/m^3)
Polystyrene (Light Particles)	355-417	386	1052
Polymethyl Methacrylate (Heavy Particles)	177-210	194	1184

Table 3-2. System II Particle Summary (α_{LF} = 0.134, α_{HF} = 0.163, α_{fF} = 0.703)

Particle Type	Sieve Passing Size (μm)	Mean Particle Diameter (μm)	Particle Density (kg/m^3)
Z-Light Microspheres (Light Particles)	125-149	137	749
Polystyrene (Heavy Particles)	417-500	459	1052

Obtaining monosized fractions of any given particle species is not a trivial task. For these experiments, tight particle size fractions were achieved by laborious sorting from bulk

particle mixtures. A process of dry sieving followed by wet sieving was used. Static charge on the particles was a major concern during this preparation, particularly for the polymer beads.

All particles were first dry sieved in Ro-Tap sieve shakers. The Ro-Tap testing sieve shaker is the standard machine for automatically carrying out sieve-test procedures. Small strips of "Bounce" fabric softener sheets (used in clothes laundering) were included in each sieve. This ensured that static repulsion did not inhibit the free passage of the polymer beads from one sieve to another (this problem was not experienced with the ceramic microspheres). Two iterations of dry sieving were performed on all particles used in tests to ensure that truly monosized particles were obtained.

After dry-sieving, the particles were placed in water and allowed to sit for an extended period of time (at least three days). Then, they were wet-sieved to check whether immersion in the fluid had induced swelling or shrinkage. A drop of Triton-X surfactant was added to the particles in top sieve and mixed in to reduce static effects. Wet sieving indicated that there had been no measurable size change, though some flocculation did occur once the surfactant had been completely washed away. This step also washed away any contaminating dust (which was a challenge with the ceramic microspheres).

The wet-sieved particles were then stored in their carrier fluid in plastic sampling containers until needed. The representative particle size for each fraction was assumed to be the average value of the screen passing sizes (above and below).

After using the same particles in tests over an extended period of time, the particles were again wet sieved to check whether swelling or erosion had occurred. For the polymer beads, there was no holdup on the larger sieves and only trace particles reported to smaller size fractions. Thus it was deduced that no alteration in particle size had occurred during testing. When the ceramic microspheres were wet-sieved, some of the particles were smaller; it appeared that some had broken into smaller fragments. This amount

represented less than 2% of the total (2.4 grams out of the 123 grams tested), and thus was considered negligible.

Two different carrier fluids were used: salt water for System I and tap water for System II, both at room temperature (22±3 °C). The following table summarizes the properties of each carrier fluid :

Table 3-3. Carrier Fluid Summary

Carrier Fluid	Fluid Density (kg/m^3)	Fluid Viscosity (mPa·s)
System I (Salt Water Solution)	1067	1.41
System II (Tap Water)	997	0.931

Commercial table salt was added to tap water to obtain a salt water solution (System I). A hygrometer was used to measure the density of the salt water solution and a value of 1067 kg/m^3 was selected for testing. It was found that mineral impurities in the salt created cloudy conditions. Before being used in experiments, the top 80% or so was decanted off into a separate container. The original mixing tank was rinsed out, washing away the sedimented minerals, then the decanted salt water was added back into the mixing tank. The resulting salt water was transparent.

No special preparations were required for the tap water (System II).

The total height of the mixture was marked in the tank, and daily density measurements were performed to ensure that the salt concentration remained constant. On occasion, fresh water would be added to the mixture to balance evaporation.

Into both the systems, a drop of surfactant (Triton-X) was stirred in before adding particles. This ensured that no particle flocculation occurred. On the one occasion when *several* drops of surfactant were mistakenly added to the system, enormous quantities of

bubbles resulted. The tank, column, and tubing had to be cleaned and the particles washed before testing could resume.

Periodically, the system required cleaning to remove products of corrosion and other contaminants. In each case, the particles were washed in tap water then added back into the system in the manner described above. Repeat tests were performed to ensure the results were the same as before cleaning.

3.3 - EXPERIMENTAL SET-UP:

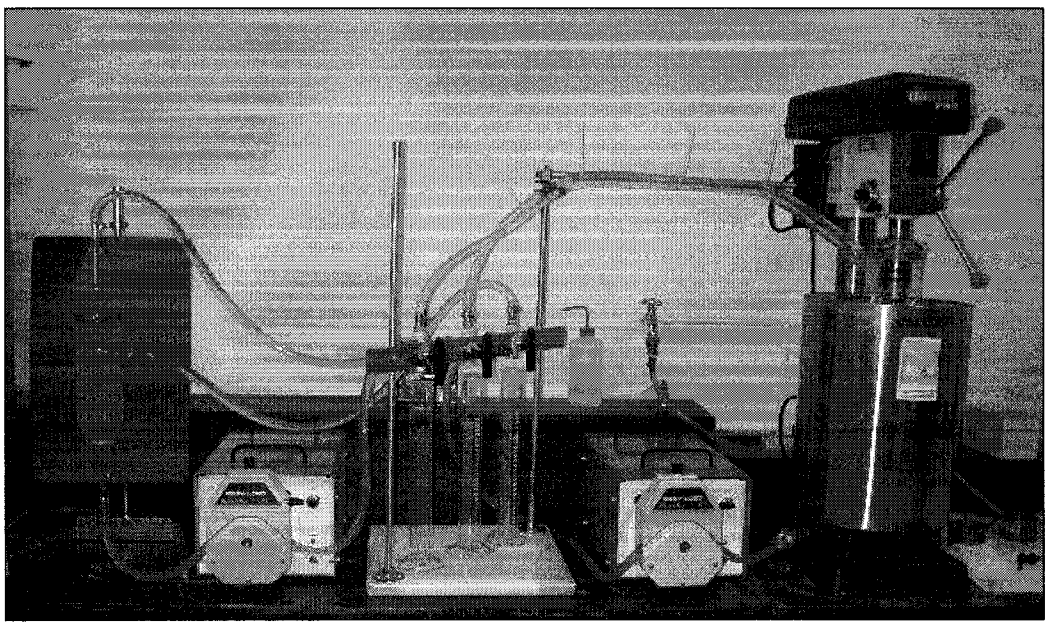

Figure 3-5. Experimental Set-Up Photograph

An experimental set-up similar to that of Nasr-El-Din et al. (1988, 1990) was used for the investigations detailed here. As shown in Figure 3-5, the equipment consisted of a separation column, a mixing tank equipped with a stirrer, two peristaltic pumps, three sampling ports, and connecting hoses. Each separation column was mounted on a steel stand in a vertical position. The mixing tank, stirred with a modified drill press, contained the particle/fluid mixture. One peristaltic pump introduced feed into the middle of the separation column (feed configuration varied with column design). The

second pump was used to control the underflow withdrawal rate, and thus, the overall vessel split ratio. The overflow and underflow streams were both continuously returned to the mixing tank, except during sampling. The loop had three sampling ports; one each on the feed, overflow, and underflow; to measure the composition of the streams.

3.4 - EXPERIMENTAL PROCEDURE:

A different procedure for measuring fractions of particles in the samples was employed from that previously outlined in the literature by Law et al. (1986) and Nasr-El-Din et al. (1988, 1990). A simple and rapid volumetric technique was used.

For each column design and particle-fluid system over a wide range of feed rates, the following measurements were made:

- Flow rates of feed, overflow, and underflow (as well as the split ratio of overflow and underflow to feed).
- Bulk particle concentrations in each stream were measured and converted to true volumetric concentrations.
- From these values, the recovery of light and heavy particle species in the overflow and underflow were calculated.

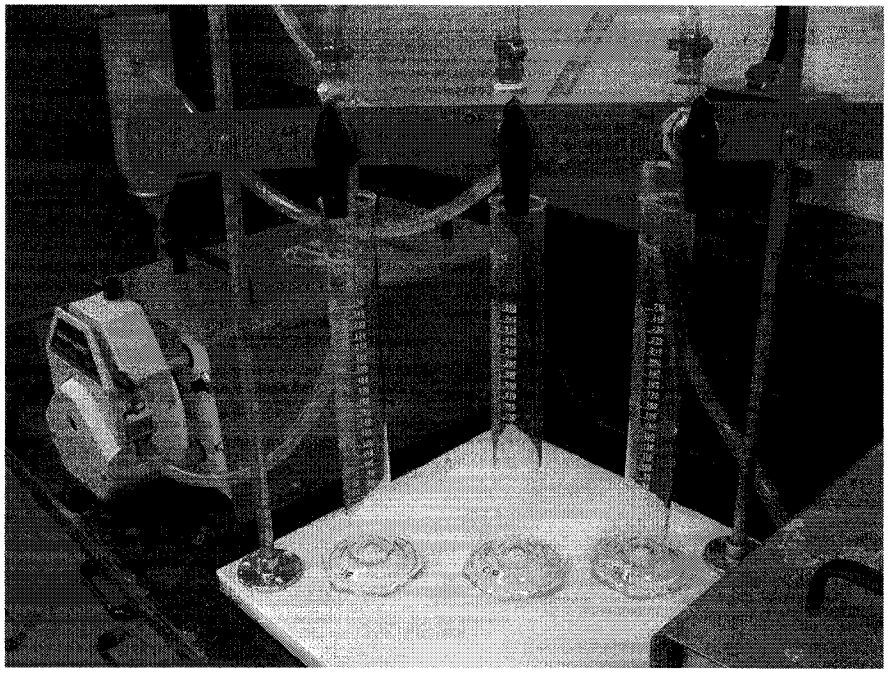

Figure 3-6. Photograph of UF, OF, and Feed Cylinders

Each experiment was operated at a constant feed composition, feed flow rate, and underflow split ratio. After circulating the slurry until steady state conditions were reached, samples were taken and measured in the following manner:

- Three samples were collected; one each for the underflow, overflow, and feed streams (in that order). See Figure 3-6.
- The total weight of the sample was first measured.

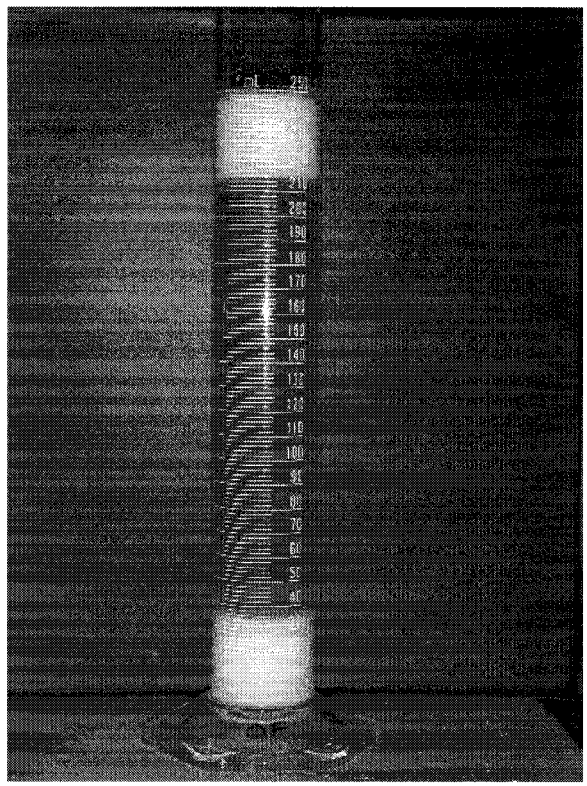

Figure 3-7. Measuring Volumes of Light and Heavy Particles

- Sufficient time was given for the light and heavy particles to completely separate and settle in the cylinder (typically 1-5 minutes). (See Figure 3-7.) The cylinder was swirled slightly during settling to ensure complete particle segregation.
- Total sample volume, the volume occupied by heavy particles, and the volume occupied by light particles were measured. These particle volumes were the bulk (random) packed volume of the solids.

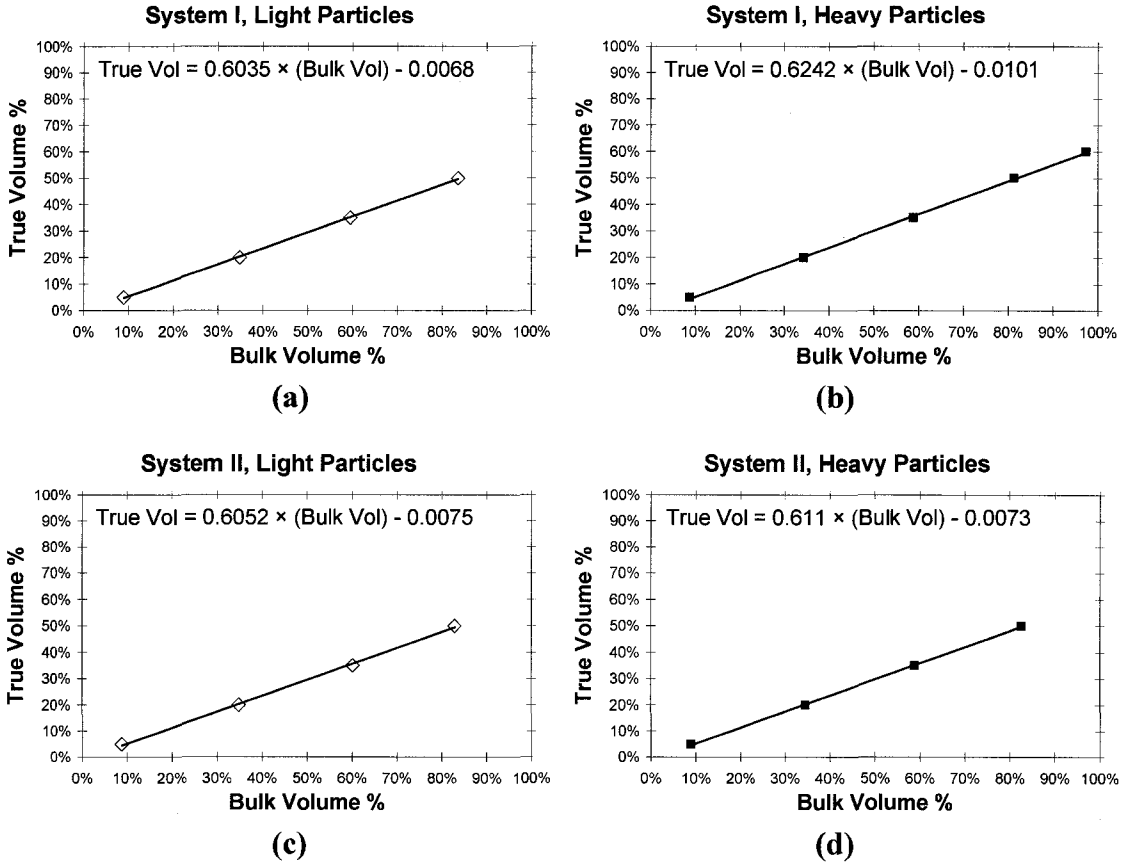

Figures 3-8a, b, c, d. Volumetric Calibration Curves

- The concentration of light and heavy particles was calculated by comparing these bulk volumes to calibration curves (see Figures 3-8a through 3-8d).
- Finally, the contents of each cylinder were returned to the mixing tank to restore and maintain a constant feed concentration.

After several measurements were made at a given feed rate, the underflow split ratio was adjusted, the system was allowed to reach steady state conditions again, and more samples were obtained.

After a range of split ratios were tested, the feed rate was changed and the process repeated. Likewise, the same procedure was followed for each column design and slurry system.

3.4.1 - NOTES ON THE EXPERIMENTAL PROCEDURE:

Appendix 1 gives a more detailed experimental procedure.

The mixing tank volume was 20 litres; separation columns had a volume of 1.5 litres; sample size was approximately 250 ml. Depending on the feed rate, residence times for the system ranged from 2.9 minutes to 8.2 minutes. Column residence times ranged from 13 seconds to 37 seconds. At the start of a series of tests, the system was allowed to run for at least 5 system residence times to reach steady state conditions. Likewise, between sample runs, the system was allowed to run for at least 5 column residence times.

Experiments were conducted at room temperature ($22 \pm 3\,^{\circ}C$).

Samples of the overflow, underflow, and feed streams were taken by diverting the whole of each stream into graduated cylinders. Sample volumes of 200-250 ml were small enough not to disrupt the system, but large enough to avoid sampling errors.

Because of varying column design and slurry properties, identical pump settings did not yield the same flow rates between experiments. The following rates were tested:

Table 3-4. Experimental Feed Rates

	Feed Rate (ml/s)
Feed Rate 1	38.9 to 43.8
Feed Rate 2	55.8 to 59.5
Feed Rate 3	74.2 to 84.0
Feed Rate 4	102 to 118

For each feed rate, the underflow withdrawal rate as a fraction of the feed flow rate (referred to as the underflow split ratio) was varied from 0.1 to 0.9. Solids concentration in the feed remained constant as the feed rate was changed. As the split ratio approached 0 or 1, it was very difficult to operate the system as the solids concentration would reach the maximum packing concentration resulting in plugging of the lines.

The flow rates of each stream were measured separately at each pump setting to determine exact flow rates. Following the procedure, mass balance checks have shown good agreement between input and output streams to within ±5%. Measurements were repeated three or more times at each test point to reduce experimental error.

Bulk volume measurements from the experiments were converted to true volumetric concentrations. For each particle-fluid system, calibration curves were developed. Known amounts of particle species were mixed with carrier fluid and poured into the measurement cylinders and allowed to settle. Sample calculations are included in Appendix 2.

4 - RESULTS AND DISCUSSION:

In this chapter, gravity separation results from Column A are discussed, followed by the cyclonic separation results from Columns B and C. Throughout the discussion, the following terms are often used:

Normalized Particle Concentration: All particle concentrations have been normalized against the overall concentration of each species in the feed. For example, the normalized concentration of light particles in the overflow is α_{LO}/α_{LF}. Normalization allows comparison between different particle-slurry systems in a more consistent manner.

Split Ratio: The split ratio is the volume fraction of the feed stream that reports to a given product stream. Both the overflow (OF) and underflow (UF) split ratios can be defined as Q_O/Q_F and Q_U/Q_F, respectively. For ease of reference, both the UF and OF split ratios are given on all applicable graphs. The UF split ratio is shown on the x-axis because it was the control variable. Unless otherwise noted, the phrase "split ratio" is used in the text to refer to the UF split ratio.

Recovery: The recovery of a given species in a product stream is defined as the fraction of that particle species collected in the stream compared to the total amount in the feed, expressed as a percentage. (Volumetric and mass recoveries are identical since each species has uniform density.) For example, recovery of light particles in the overflow stream is given by:

$$R_{LO} = \frac{\alpha_{LO} Q_O}{\alpha_{LF} Q_F} \qquad (4\text{-}1)$$

Thus, at a high overflow split ratio (i.e., most of the feed reports to the OF), the recovery of light particles in that stream would approach 100%.

Particle and Slurry Velocities: Shown in Table 4-1 for each particle species are the Reynolds numbers and terminal velocities at infinite dilution, as calculated using Eq. 2-5 and 2-11 respectively. Peak bulk vertical slurry velocities are given in Table 4-2. By comparing the magnitudes of these values, one can get a feel for the behavior of the particles in a gravity settler. For example, note how small the rise velocity is of the light particles in System I. At high flow rates, the bulk slurry velocity can approach 30× the value of the particle rise velocity. Under such conditions, one would expect that the light particles would simply travel with the bulk slurry flow, and that particle recovery would simply be proportional to the split ratio (as discussed in Section 4.2).

Table 4-1. Particle Reynolds Numbers and Terminal Velocities

Fluid-Particle System	$\Re_p$	v_∞ (mm/s)
System I, Light Particles	0.239	-0.82
System I, Heavy Particles	0.237	1.61
System II, Light Particles	0.372	-2.58
System II, Heavy Particles	2.588	5.27

Table 4-2. Bulk Vertical Slurry Velocities

Feed Rate (ml/s)	Maximum Value (mm/s)
Feed Rate 1	±8.7
Feed Rate 2	±12.0
Feed Rate 3	±17.0
Feed Rate 4	±24.0

Comparing particle v_∞ values against the bulk slurry velocity is not useful in predicting the behavior of cyclonic separators, however. (See Sections 4.3 and 4.4)

4.1 - SUMMARY OF RESULTS:

Tables 4-3 to 4-8, below, give a *very basic* comparative summary of results from each column. Product quality and recovery are compared for light and heavy particles at low and high feed rates. The comparison is intended to provide an at-a-glance synopsis of the overall experimental results. *Please refer to the specific results for each individual test system for full analysis.* In the tables, a check mark (✓) denotes generally "good" performance, while a cross (×) denotes generally "poor" performance, compared to the other vessels tested.

Table 4-3a. Light Particle Quality and Recovery for Column A at Low Feed Rates

	Low Q_U/Q_F				High Q_U/Q_F			
Overflow	Light Particle Quality	×	Light Particle Recovery	×	Light Particle Quality	✓	Light Particle Recovery	✓
Underflow	Light Particle Quality	×	Light Particle Recovery	×	Light Particle Quality	×	Light Particle Recovery	×

Table 4-3b. Heavy Particle Quality and Recovery for Column A at Low Feed Rates

	Low Q_U/Q_F				High Q_U/Q_F			
Overflow	Heavy Particle Quality	×	Heavy Particle Recovery	×	Heavy Particle Quality	×	Heavy Particle Recovery	×
Underflow	Heavy Particle Quality	✓	Heavy Particle Recovery	✓	Heavy Particle Quality	×	Heavy Particle Recovery	×

Table 4-4a. Light Particle Quality and Recovery for Column A at High Feed Rates

	Low Q_U/Q_F				High Q_U/Q_F			
Overflow	Light Particle Quality	×	Light Particle Recovery	×	Light Particle Quality	×	Light Particle Recovery	×
Underflow	Light Particle Quality	×	Light Particle Recovery	×	Light Particle Quality	×	Light Particle Recovery	×

Table 4-4b. Heavy Particle Quality and Recovery for Column A at High Feed Rates

	Low Q_U/Q_F				High Q_U/Q_F			
Overflow	Heavy Particle Quality	×	Heavy Particle Recovery	×	Heavy Particle Quality	×	Heavy Particle Recovery	×
Underflow	Heavy Particle Quality	×	Heavy Particle Recovery	×	Heavy Particle Quality	×	Heavy Particle Recovery	×

Table 4-5a. Light Particle Quality and Recovery for Column B at Low Feed Rates

	Low Q_U/Q_F				High Q_U/Q_F			
Overflow	Light Particle Quality	×	Light Particle Recovery	✓	Light Particle Quality	×	Light Particle Recovery	×
Underflow	Light Particle Quality	×	Light Particle Recovery	×	Light Particle Quality	×	Light Particle Recovery	✓

Table 4-5b. Heavy Particle Quality and Recovery for Column B at Low Feed Rates

	Low Q_U/Q_F				High Q_U/Q_F			
Overflow	Heavy Particle Quality	×	Heavy Particle Recovery	×	Heavy Particle Quality	×	Heavy Particle Recovery	✓
Underflow	Heavy Particle Quality	✓	Heavy Particle Recovery	×	Heavy Particle Quality	×	Heavy Particle Recovery	×

Table 4-6a. Light Particle Quality and Recovery for Column B at High Feed Rates

	Low Q_U/Q_F				High Q_U/Q_F			
Overflow	Light Particle Quality	×	Light Particle Recovery	✓	Light Particle Quality	×	Light Particle Recovery	×
Underflow	Light Particle Quality	×	Light Particle Recovery	×	Light Particle Quality	×	Light Particle Recovery	✓

Table 4-6b. Heavy Particle Quality and Recovery for Column B at High Feed Rates

	Low Q_U/Q_F				High Q_U/Q_F			
Overflow	Heavy Particle Quality	×	Heavy Particle Recovery	×	Heavy Particle Quality	✓	Heavy Particle Recovery	×
Underflow	Heavy Particle Quality	✓	Heavy Particle Recovery	×	Heavy Particle Quality	×	Heavy Particle Recovery	×

Table 4-7a. Light Particle Quality and Recovery for Column C at Low Feed Rates

	Low Q_U/Q_F				High Q_U/Q_F			
Overflow	Light Particle Quality	×	Light Particle Recovery	✓	Light Particle Quality	×	Light Particle Recovery	×
Underflow	Light Particle Quality	×	Light Particle Recovery	×	Light Particle Quality	×	Light Particle Recovery	✓

Table 4-7b. Heavy Particle Quality and Recovery for Column C at Low Feed Rates

	Low Q_U/Q_F				High Q_U/Q_F			
Overflow	Heavy Particle Quality	×	Heavy Particle Recovery	×	Heavy Particle Quality	×	Heavy Particle Recovery	×
Underflow	Heavy Particle Quality	✓	Heavy Particle Recovery	×	Heavy Particle Quality	×	Heavy Particle Recovery	✓

Table 4-8a. Light Particle Quality and Recovery for Column C at High Feed Rates

	Low Q_U/Q_F				High Q_U/Q_F			
Overflow	Light Particle Quality	×	Light Particle Recovery	✓	Light Particle Quality	✓	Light Particle Recovery	×
Underflow	Light Particle Quality	×	Light Particle Recovery	×	Light Particle Quality	×	Light Particle Recovery	×

Table 4-8b. Heavy Particle Quality and Recovery for Column C at High Feed Rates

	Low Q_U/Q_F				High Q_U/Q_F			
Overflow	Heavy Particle Quality	×	Heavy Particle Recovery	×	Heavy Particle Quality	×	Heavy Particle Recovery	×
Underflow	Heavy Particle Quality	✓	Heavy Particle Recovery	×	Heavy Particle Quality	×	Heavy Particle Recovery	✓

4.2 - COLUMN A - EFFECT OF SPLIT RATIO:

4.2.1 - SYSTEM I:

Figure 4-1 shows the normalized concentrations of light particles in the overflow and underflow streams as a function of split ratio for Column A, System I (5.8 vol % polystyrene and 12.2 vol % polymethyl methacrylate), at a feed rate of 40.6 ml/s. The solid lines represent the model predictions, which agree reasonably well with the experimental results. Error bars (shown on this graph only) denote confidence intervals in the measured values. The normalized feed concentration is indicated by a horizontal dashed line.

Even at this low feed rate, the particle concentrations in the product streams do not deviate much from the feed concentration. Only at the lowest and highest split ratios tested (0.32 and 0.69) did the light particles noticeably concentrate in either of the product streams.

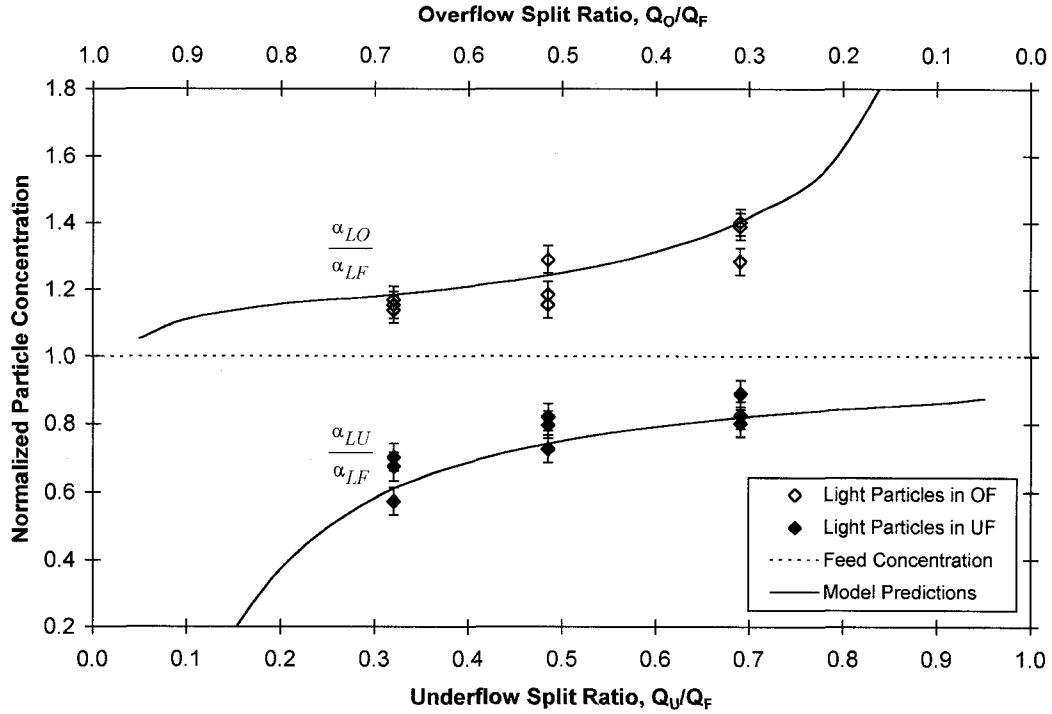

Figure 4-1. Concentrations of Light Particles in Overflow and Underflow for Column A, System I (α_{LF} = 0.058, α_{HF} = 0.122), Feed Rate 40.6 ml/s

Figure 4-2 shows the product stream concentrations of heavy particles for Column A, System I, at a feed rate of 40.6 ml/s. Again, good agreement with model predictions was achieved. At high UF split ratios (about 0.69), the upward fluid velocity is sufficiently low that fewer heavy particles report to the overflow. At UF split ratios lower than about 0.32, the concentration of heavy particles in the underflow is high. Like in Figure 4-1, the settling velocity at infinite dilution of the heavy particles is not large in magnitude compared to the fluid velocity, and Figure 4-2 is nearly a reverse image of the graph for light particles.

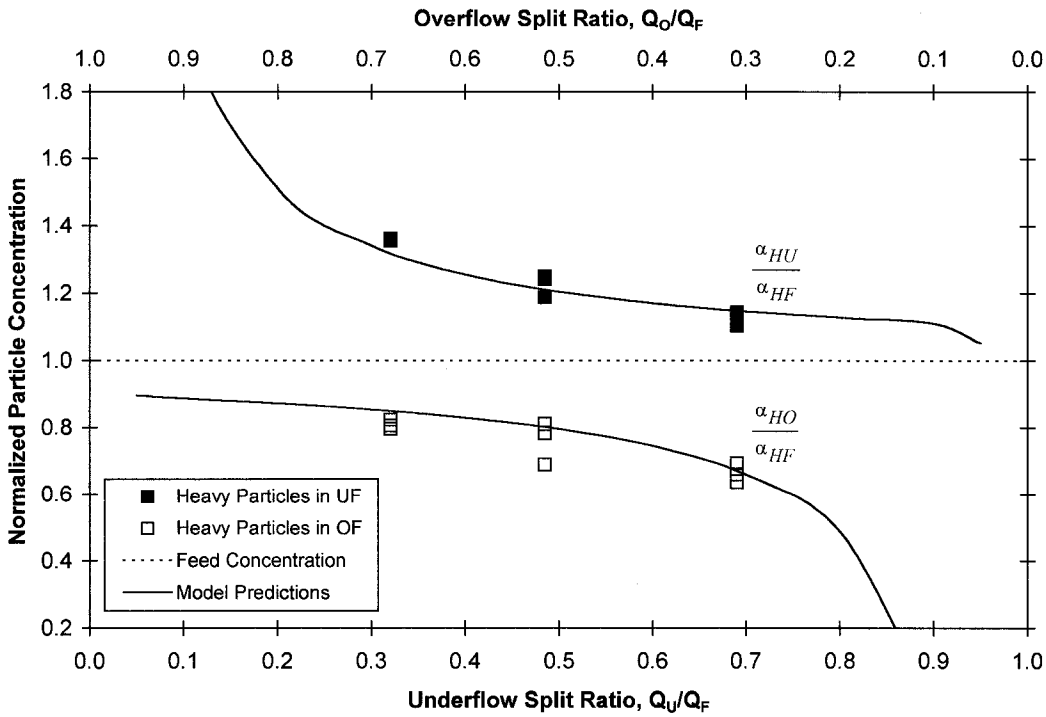

Figure 4-2. Concentrations of Heavy Particles in Overflow and Underflow for Column A, System I (α_{LF} = 0.058, α_{HF} = 0.122), Feed Rate 40.6 ml/s

While product stream concentrations are a useful measure of efficiency for designs based on purity specifications, overall recovery is another important test of separator performance. Figure 4-3 shows the recoveries of light particles in the overflow and underflow streams as a function of the split ratio for Column A, System I, at a feed rate of 40.6 ml/s. Figure 4-4 shows the same for heavy particles. Good agreement with model predictions was achieved. Because of the low v_∞ values of the particles in System I, 100% recovery was not achieved with any of the tests performed. For System II, however, this was not the case.

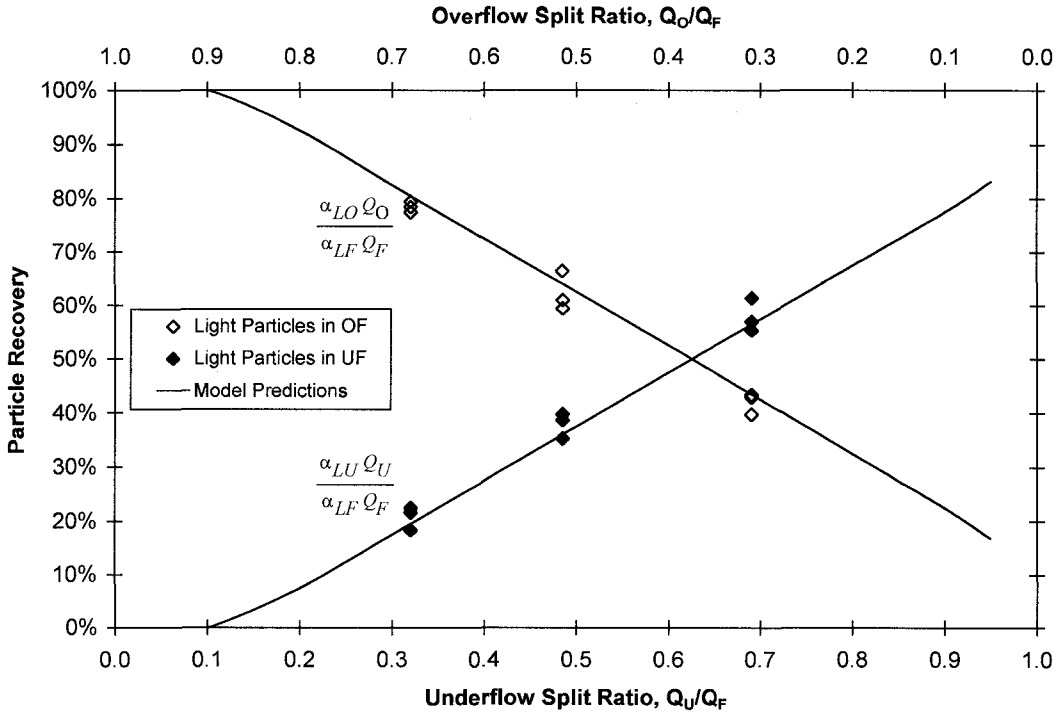

Figure 4-3. Recoveries of Light Particles in Overflow and Underflow for Column A, System I (α_{LF} = 0.058, α_{HF} = 0.122), Feed Rate 40.6 ml/s

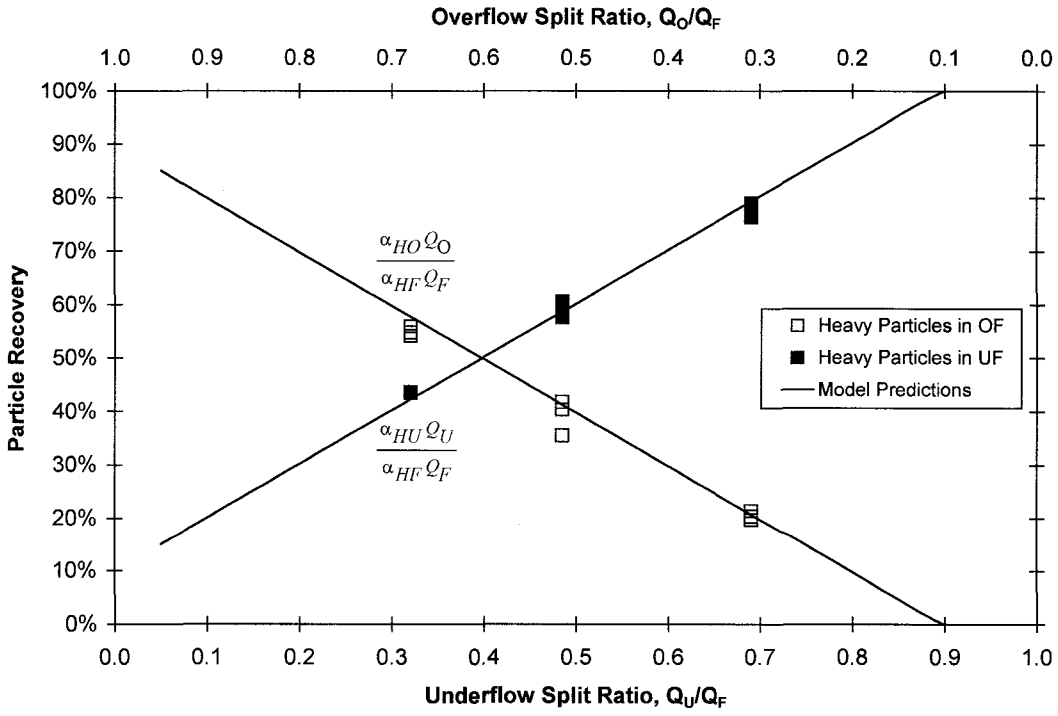

Figure 4-4. Recoveries of Heavy Particles in Overflow and Underflow for Column A, System I (α_{LF} = 0.058, α_{HF} = 0.122), Feed Rate 40.6 ml/s

4.2.2 - SYSTEM II:

Figure 4-5 shows the normalized concentrations of light particles in the overflow and underflow streams as a function of the split ratio for Column A, System II (13.4 vol % z-light microspheres and 16.3 vol % polystyrene), at a feed rate of 38.9 ml/s. Experimental results agree closely with model predictions, which is somewhat surprising for such a concentrated system. Here, v_∞ of the light particles is higher than for System I, hence concentrations in the product streams diverge greatly from that of the feed. At UF split ratios of less than about 0.2, nearly all the light particles in the feed are recovered in the overflow stream. The concentration of light particles in the underflow is nearly zero. Note the abrupt change in slope of the model prediction curve for light particles in overflow at this split ratio. According to the model, this comes about because of the switch in case from having only one particle species in the overflow to two particle species.

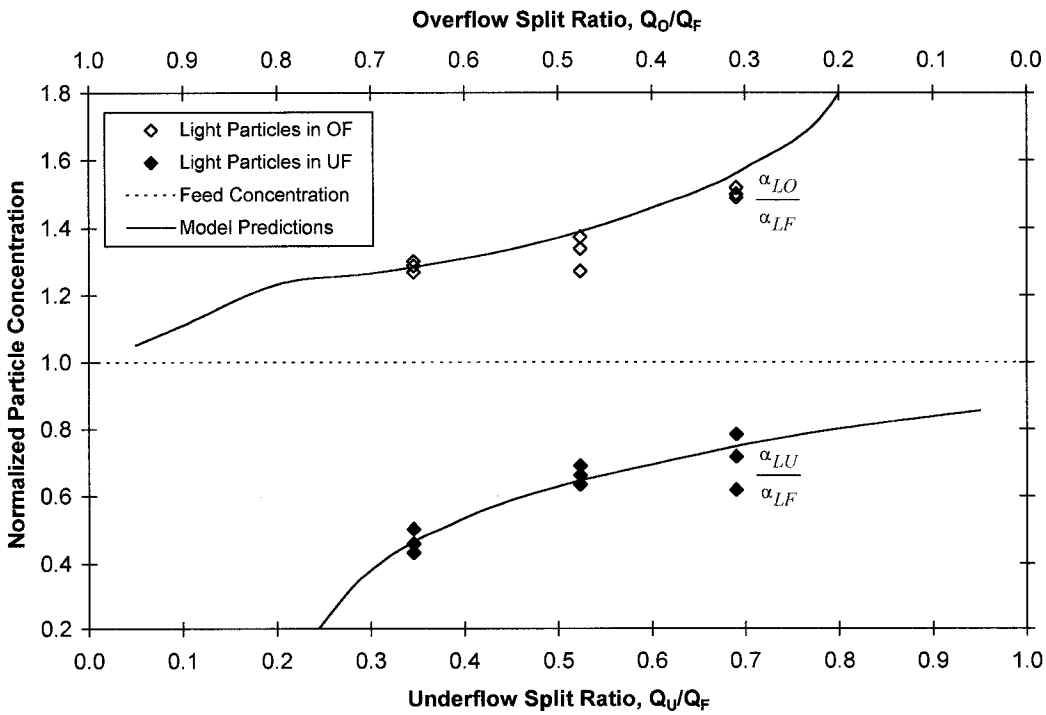

Figure 4-5. Concentrations of Light Particles in Overflow and Underflow for Column A, System II ($\alpha_{LF} = 0.134$, $\alpha_{HF} = 0.163$), Feed Rate 38.9 ml/s

Figure 4-6 shows the product stream concentrations of heavy particles for Column A, System II, at a feed rate of 38.9 ml/s. There is some difference between experimental results and model predictions, likely due to additional particle-particle interactions due to higher solids concentrations in this system. In contrast to System I, the magnitudes of v_∞ for the light and heavy particles in System II are much larger. The appearance is very different from Figure 4-2. In particular, at UF split ratios higher than about 0.6, the model predicts that virtually no heavy particles are present in the overflow. Here, the low upward fluid velocity is not sufficient to carry any heavy particles to the overflow stream. Note the abrupt change in slope of the model prediction at that point. At UF split ratios lower than about 0.35, the concentration of heavy particles in the underflow increases dramatically.

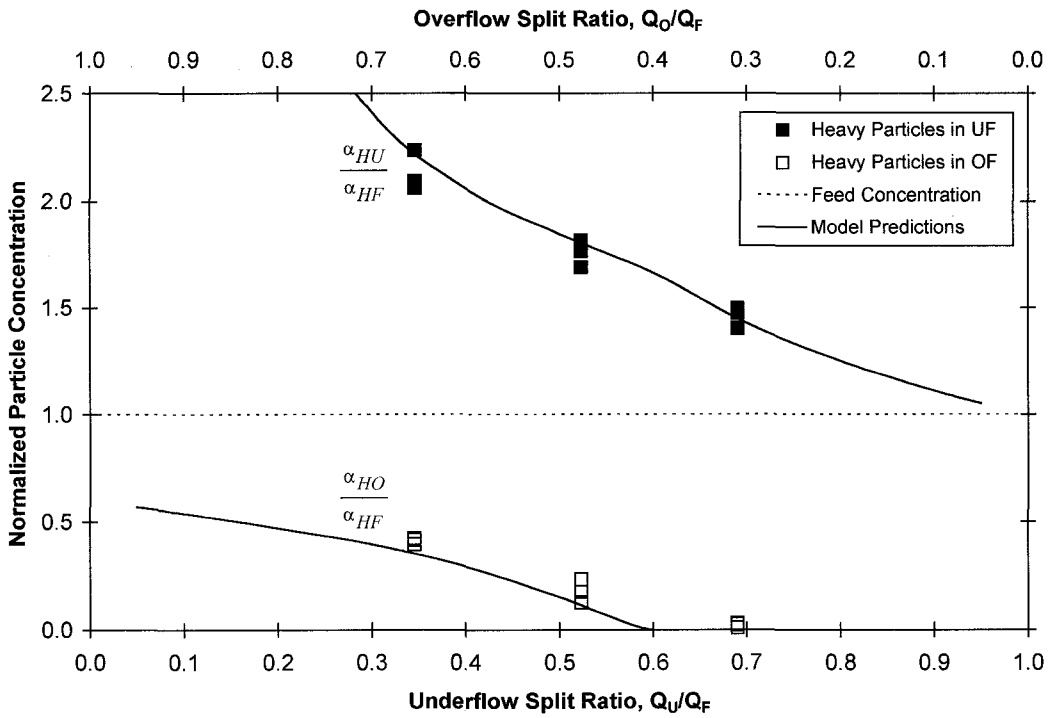

Figure 4-6. Concentrations of Heavy Particles in Overflow and Underflow for Column A, System II (α_{LF} = 0.134, α_{HF} = 0.163), Feed Rate 38.9 ml/s

Figure 4-7 shows the recoveries of light particles in the overflow and underflow streams as a function of the split ratio for Column A, System II, at a feed rate of 38.9 ml/s. Figure 4-8 shows the same for heavy particles. Predictions of light particle recovery were good;

however the recovery of heavy particles in the UF is over-predicted, and conversely, recovery of in the OF under-predicted. Nasr-El-Din et al.(1990), noted more extreme deviations from theory at high concentrations due to particle segregation, and a similar effect is likely occurring here. The different behaviour of this slurry system due to higher particle terminal velocities is readily apparent from these graphs. According to the model, 100% recovery of light particles in the overflow occurs at split ratios below about 0.2 (Figure 4-7). For heavy particles, near 100% recovery was experimentally measured at split ratios above 0.6 (Figure 4-8), in agreement with model predictions.

As noted by Nasr-El-Din et al. (1988), 100% recovery of heavy particles in the underflow only implies that all the heavy particles in the feed have reported to the underflow. In particular, it does not exclude the presence of any light particles in the underflow stream, as was shown in Figure 4-5.

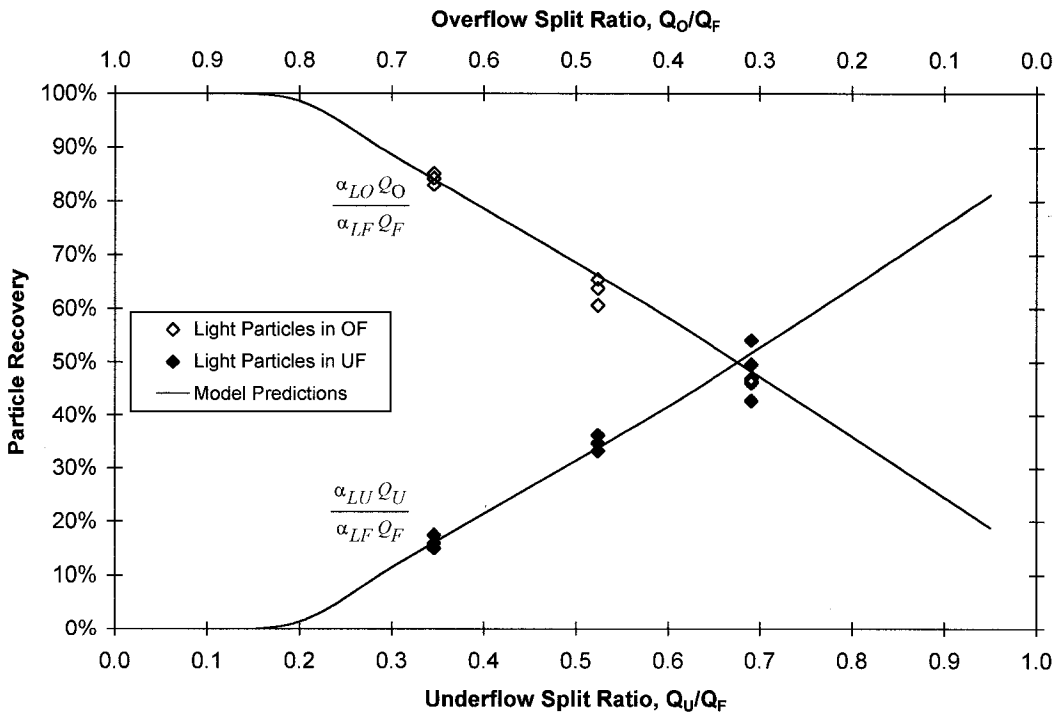

Figure 4-7. Recoveries of Light Particles in Overflow and Underflow for Column A, System II (α_{LF} = 0.134, α_{HF} = 0.163), Feed Rate 38.9 ml/s

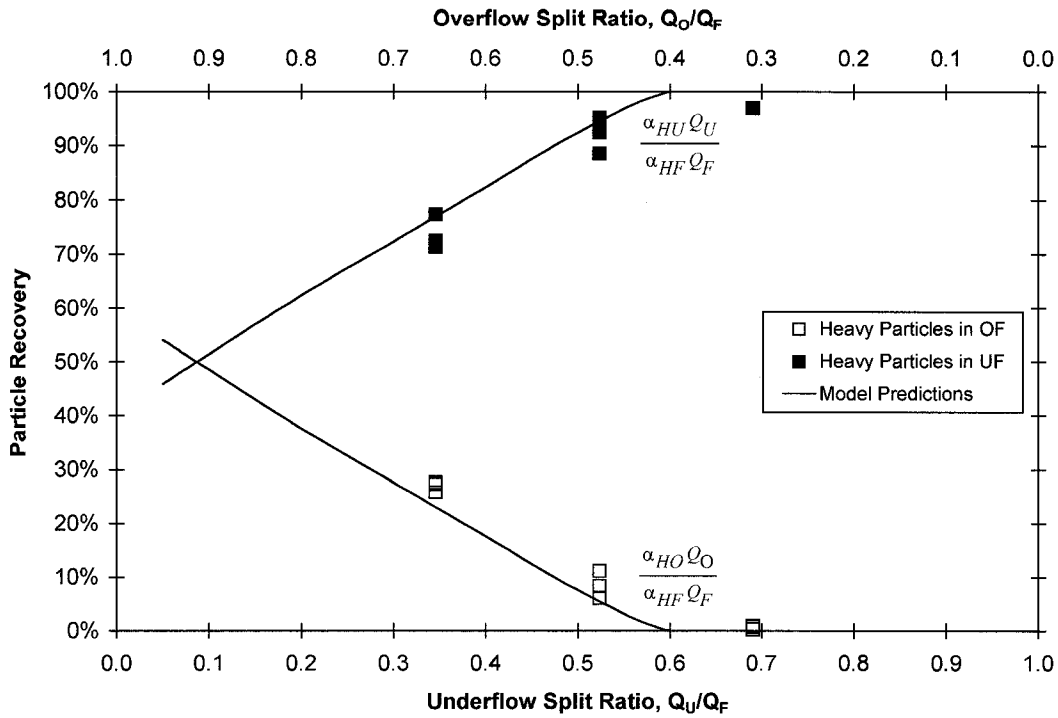

Figure 4-8. Recoveries of Heavy Particles in Overflow and Underflow for Column A, System II (α_{LF} = 0.134, α_{HF} = 0.163), Feed Rate 38.9 ml/s

As shown in Figures 4-1 to 4-8, particle concentrations and recoveries in the product stream vary with split ratio depending on the terminal velocity of the particle species. Agreement with model predictions in all cases was good or excellent, except for heavy particle results for System II.

Split ratio effects are most obvious at low feed flow rates, where the effects of hindered settling on movement are relatively large compared to the bulk fluid flow. In the extreme case of zero feed flow - *i.e.*, a batch settler - particle concentration is limited only by packing factors and recovery is always 0% or 100% in a given product 'stream'. Industrial processes, however, must operate at high throughputs to be profitable, so experiments at high feed flow rates are important.

4.3 - COLUMN A - EFFECT OF FEED RATE:

4.3.1 - SYSTEM I:

Figures 4-9, 4-10, and 4-11 show the product stream concentrations of light particles for System I (the same as in Figure 4-1) but at higher feed flow rates of 59.4 ml/s, 81.5 ml/s, and 117 ml/s. At these rates, more tests were possible, as were experiments at extreme split ratios. It can be seen that model predictions still agree reasonably well with most experimental results. In Figure 4-10, however, very high concentrations were measured in the overflow stream in some tests. As the overall feed rate increases, the upward and downward fluid velocities increase as well. As can be seen, more of the light particles are carried with the fluid to the underflow and overflow, and product stream concentrations are closer to that of the feed. Split ratio has little effect on product concentration, except at very high and very low values. The limit of no separation (*i.e.*, no differential settling) can nearly be achieved for light particles at high feed flow rates (Figure 4-11). This is due to the very low terminal velocity of the particles relative to the fluid flow.

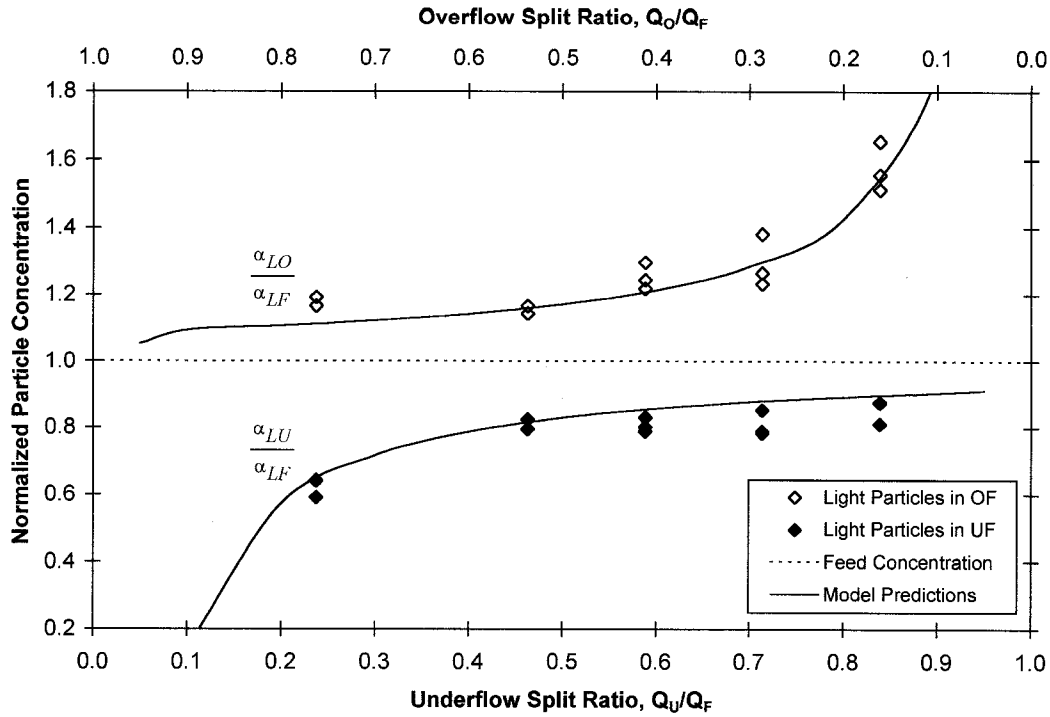

Figure 4-9. Concentrations of Light Particles in Overflow and Underflow for Column A, System I (α_{LF} = 0.058, α_{HF} = 0.122), Feed Rate 59.4 ml/s

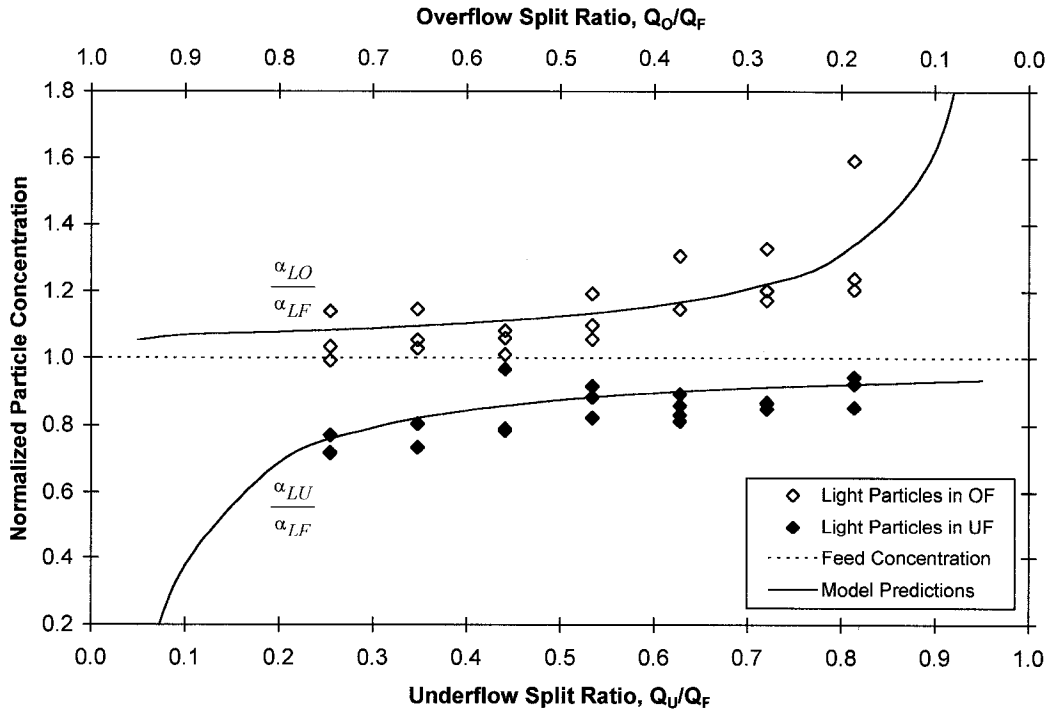

Figure 4-10. Concentrations of Light Particles in Overflow and Underflow for Column A, System I (α_{LF} = 0.058, α_{HF} = 0.122), Feed Rate 81.5 ml/s

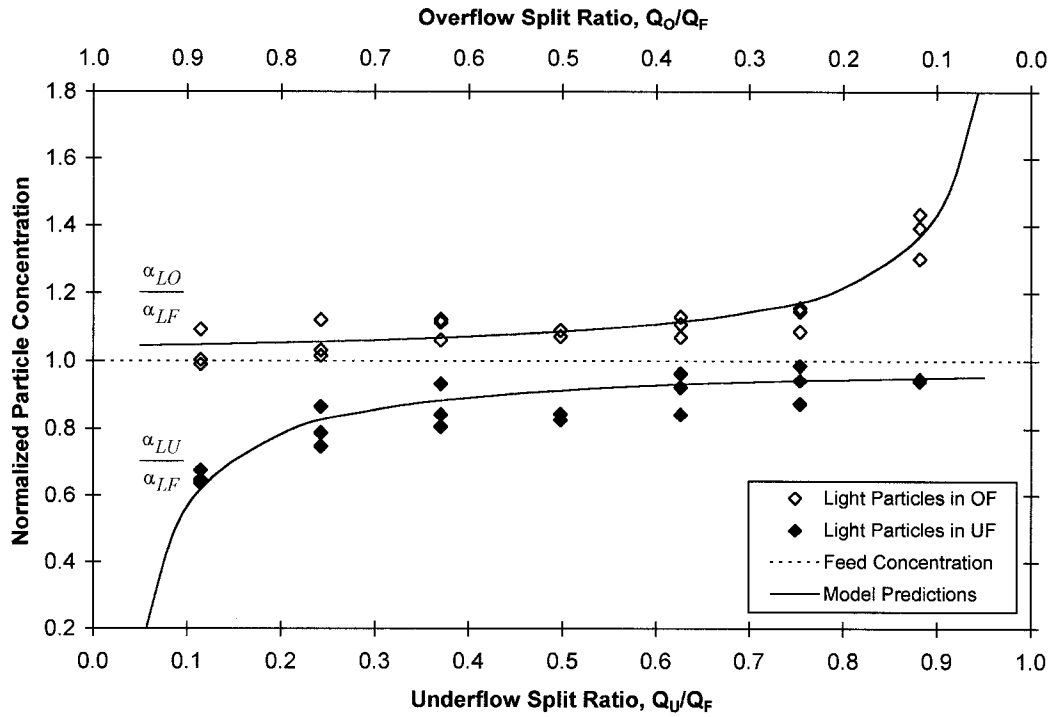

Figure 4-11. Concentrations of Light Particles in Overflow and Underflow for Column A, System I (α_{LF} = 0.058, α_{HF} = 0.122), Feed Rate 117 ml/s

Figures 4-12a through 4-12d show the recoveries of light particles in overflow streams as a function of the split ratio for Column A, System I, at all feed rates. Graphs of recoveries at individual feed rates can be found in Appendix 5. As can be seen, there is very little variation of recovery with feed rate. In fact, it is very difficult to make out the differences between recoveries at the different feed rates at all. At high flow rates, the performance is very close to the limit of no separation (i.e., it approaches the behaviour of a simple flow splitter, where particle recovery in a stream equals the split ratio).

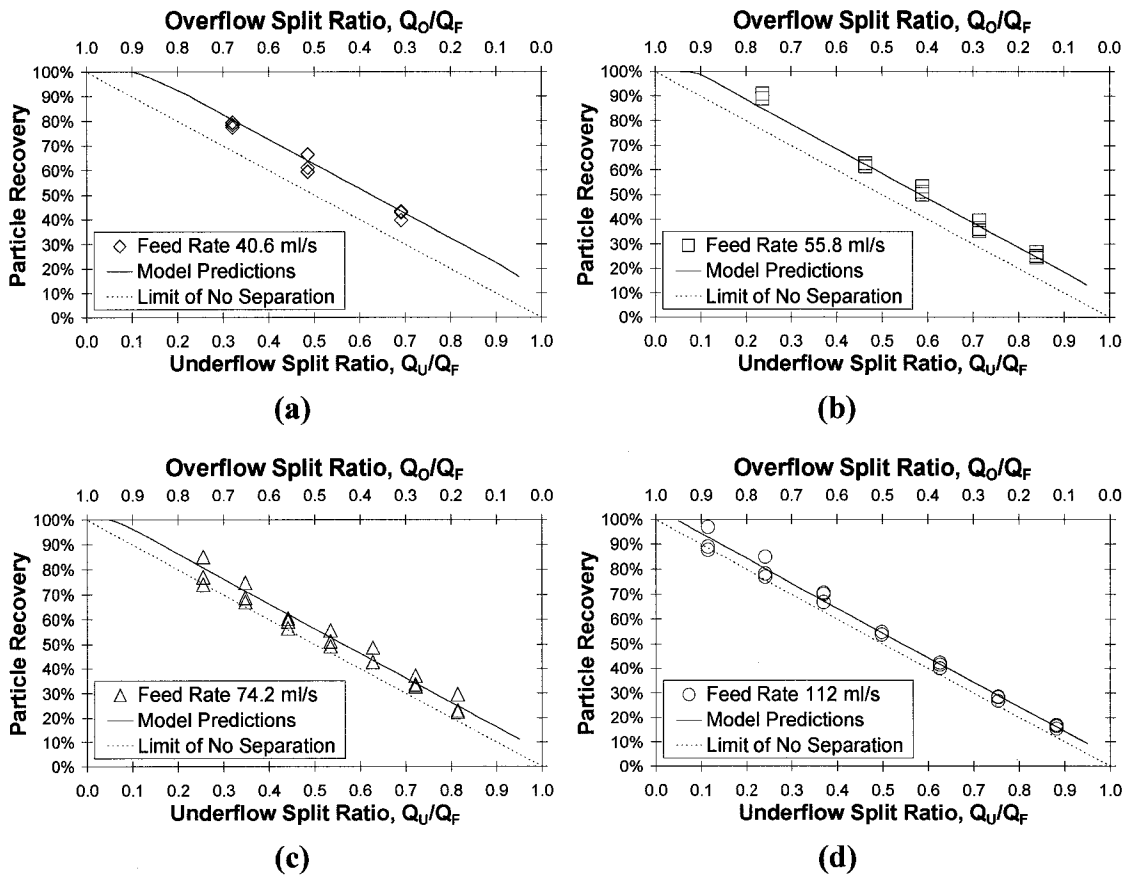

Figures 4-12a, b, c, d. Recoveries of Light Particles in Overflow of Column A, System I ($\alpha_{LF} = 0.058$, $\alpha_{HF} = 0.122$), all Feed Rates

Consistent results for concentration and recovery were measured for heavy particles. In System I, the behaviour of light particles in the overflow mirrors that of heavy particles in the underflow, therefore heavy particle concentrations and recoveries are not discussed in depth. Refer to the additional figures in Appendix 5 for details.

4.3.2 - SYSTEM II:

Figures 4-13, 4-14, and 4-15 show the product stream concentrations of heavy particles for Column A, System II at feed rates of 55.8 ml/s, 74.2 ml/s, and 102 ml/s (compare with Figure 4-6 for 36.9 ml/s). Agreement with model predictions is very good. The only exception is the results in Figure 4-13 at a split ratio of 0.6, which is possibly due to experimenter error. Compared to System I, particle concentrations in the product streams

show a stronger dependence on feed rate. As the flow increases, the degree of differential separation decreases, and the product stream concentrations approach that of the feed. These results reinforce the conclusions of Nasr-El-Din et al. (1988). The critical split ratio, where the overflow stream goes from having only light particles to both light and heavy, increases as the feed rate increases (*i.e.*, the separator has to be run under more extreme conditions to achieve a high-purity product).

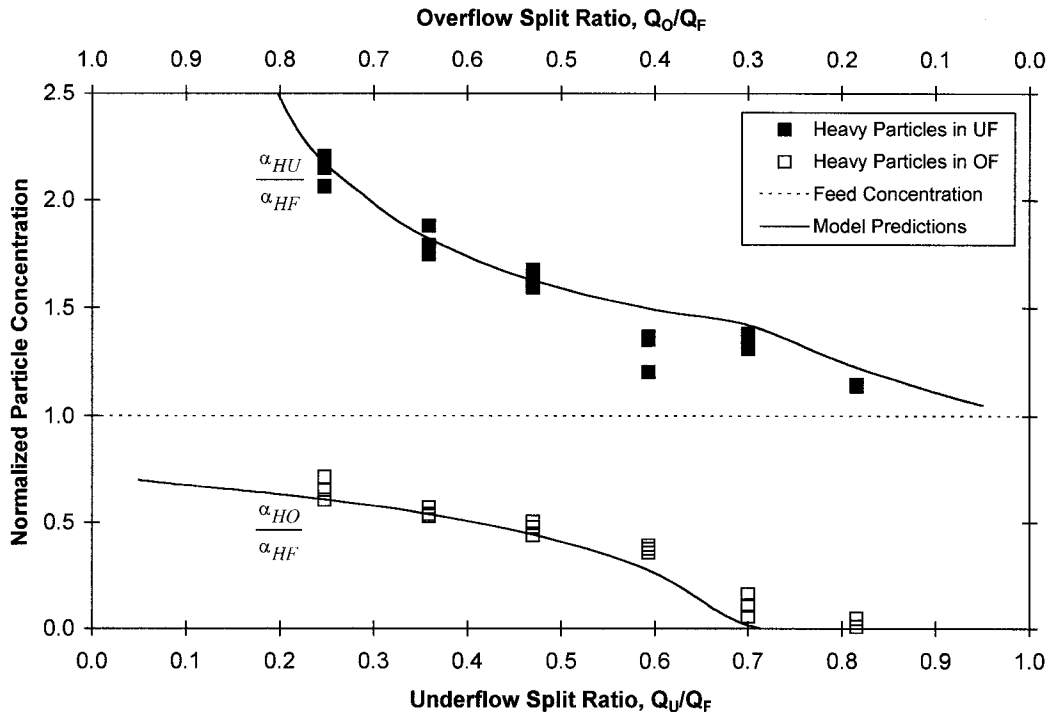

Figure 4-13. Concentrations of Heavy Particles in Overflow and Underflow for Column A, System II (α_{LF} = 0.134, α_{HF} = 0.163), Feed Rate 55.8 ml/s

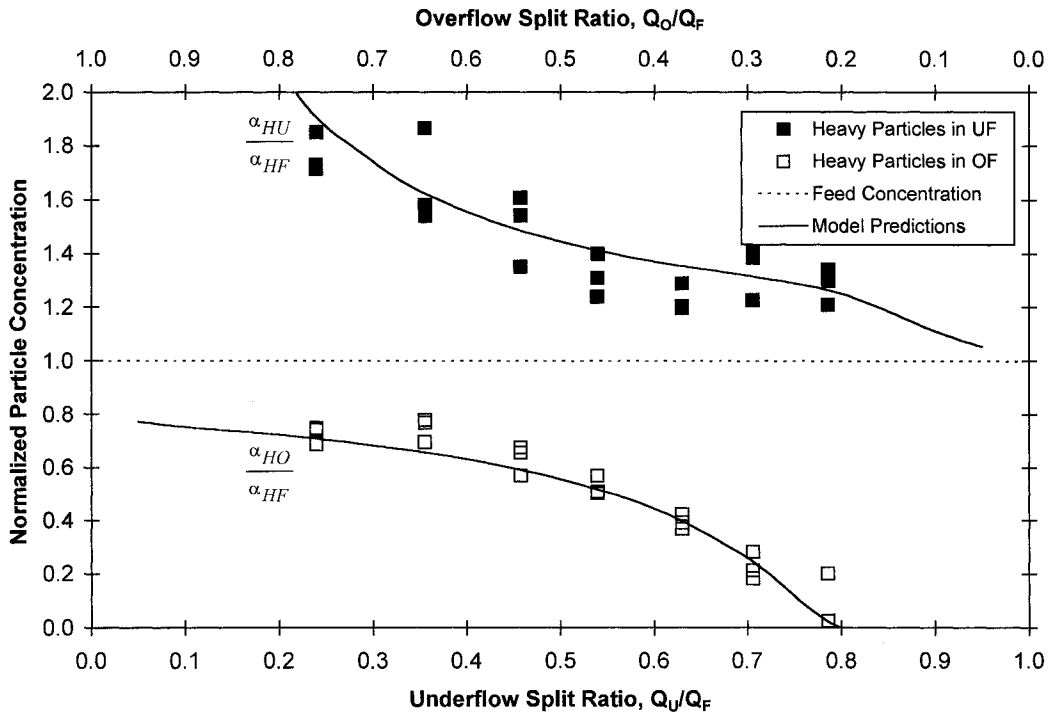

Figure 4-14. Concentrations of Heavy Particles in Overflow and Underflow for Column A, System II (α_{LF} = 0.134, α_{HF} = 0.163), Feed Rate 74.2 ml/s

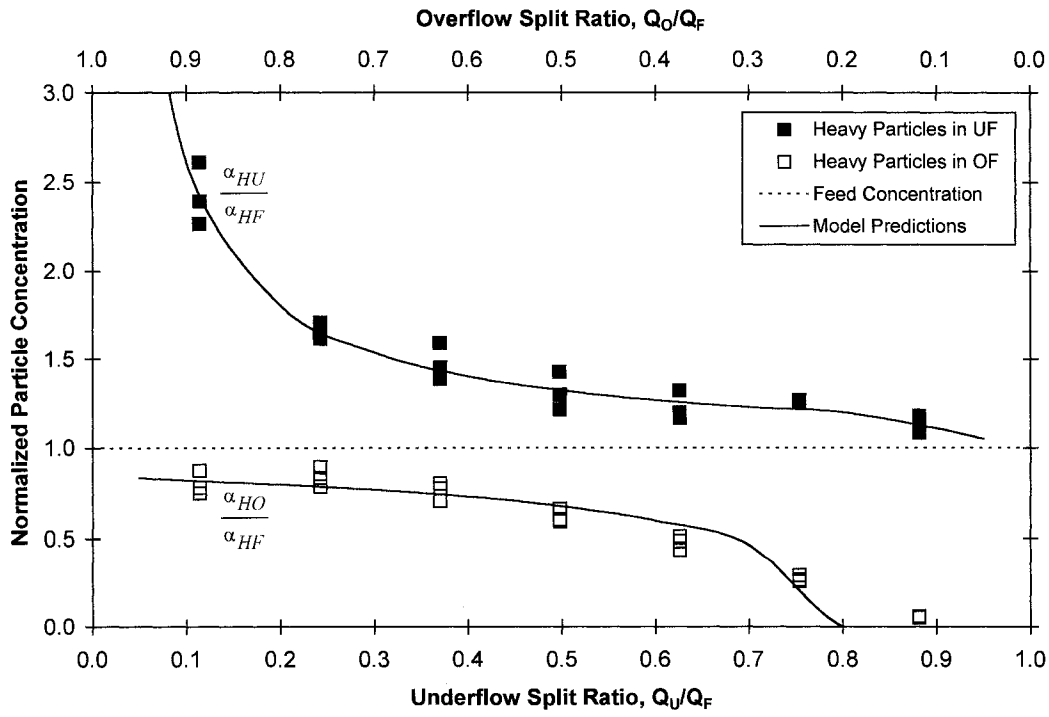

Figure 4-15. Concentrations of Heavy Particles in Overflow and Underflow for Column A, System II (α_{LF} = 0.134, α_{HF} = 0.163), Feed Rate 102 ml/s

Figures 4-16a through 4-16d show the recoveries of heavy particles in underflow streams as a function of the split ratio for Column A, System II, at all feed rates. As expected, there is more variation of recovery with feed rate for this slurry system. Although experimental results match reasonably well with model predictions, it is still difficult to distinguish between different flow rates at some split ratios. And even though the terminal velocity of heavy particles is higher than in System I, performance still approaches the limit of no separation at high feed rates.

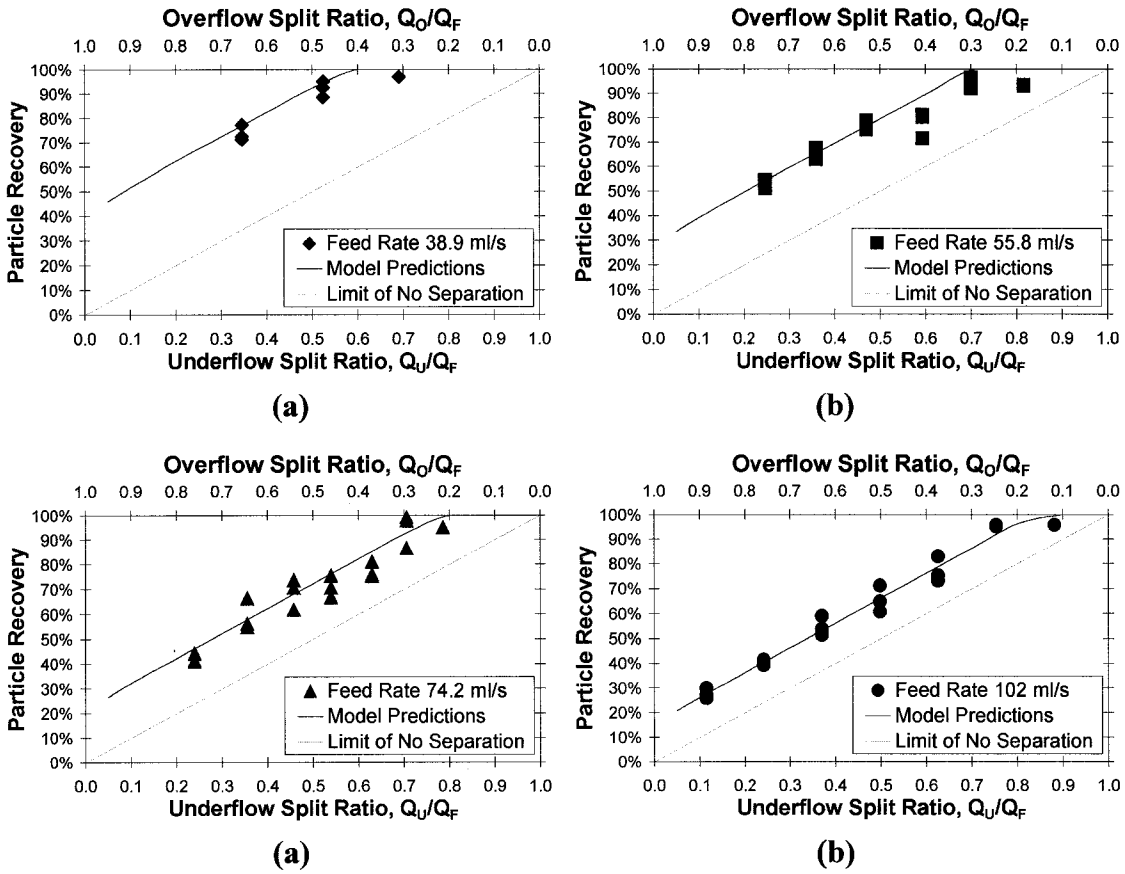

Figure 4-16a, b, c, d. Recoveries of Heavy Particles in Underflows of Column A, System II (α_{LF} = 0.134, α_{HF} = 0.163), all Feed Rates

Since concentrations and recoveries for Column A match closely with expected performance and with model predictions, these results are used as the baseline for comparing other designs.

As with System I, additional graphs are available in Appendix 5.

4.4 - COLUMN B - EFFECT OF CYCLONIC FLOW:

Figure 4-17 shows the normalized concentrations of light particles in the overflow and underflow streams as a function of the split ratio for Column B, System I, at a feed rate of 41.3 ml/s. The set-up is virtually identical to Column A, except that feed is introduced to the vessel tangentially instead of perpendicular to the vessel (as shown in Figure 3-3). At a glance, it is clear that the separation behaviour of this vessel is significantly different than Column A. In general, product concentrations are closer to that of the feed over the range of split ratios tested - the vessel does not concentrate light particles to the same extent as a simple gravity settler. Above an UF split ratio of about 0.76, the expected particle concentrations actually reverse - the concentration of light particles in the underflow is higher than that in the overflow. Visual observations (see Section 4.5) suggest that the light particles concentrate in a narrow stream at the center of the vessel. When the net downward velocity is sufficiently high, the entire stream is drawn to the underflow product, with relatively fewer particles reporting to the overflow.

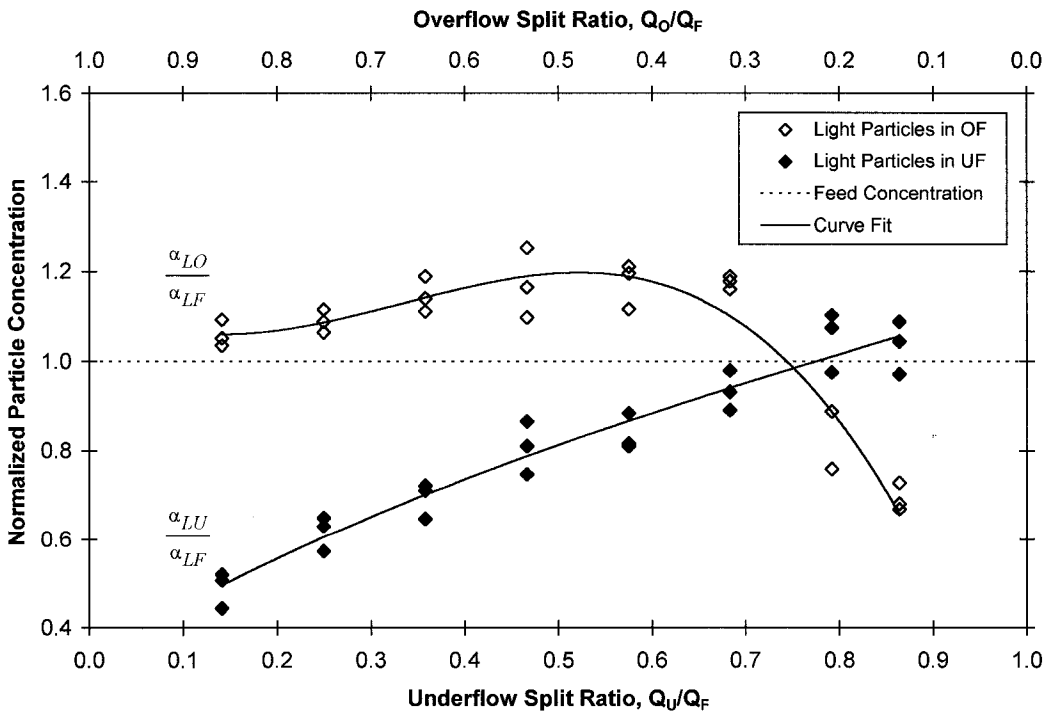

Figure 4-17. Concentrations of Light Particles in Overflow and Underflow for Column B, System I (α_{LF} = 0.058, α_{HF} = 0.122), Feed Rate 41.3 ml/s

Figure 4-18 shows the normalized concentrations of heavy particles in the overflow and underflow streams as a function of the split ratio for Column B, System I, at a feed rate of 41.3 ml/s. This is analogous to the gravity separation case in Figure 4-2. Heavy particle concentration performance is much better than for light particles. At UF split ratios below about 0.6, the tangentially-fed vessel also performs better than an equivalent vessel with normal feed injection, likely due to the centrifugal forces causing particle segregation across the vessel. If product purity is a motivating factor in process design, this cyclonic vessel would work better than a gravity settler for concentrating heavy particles. As was shown in Figure 4-17, contamination with light particles is also relatively low at these split ratios.

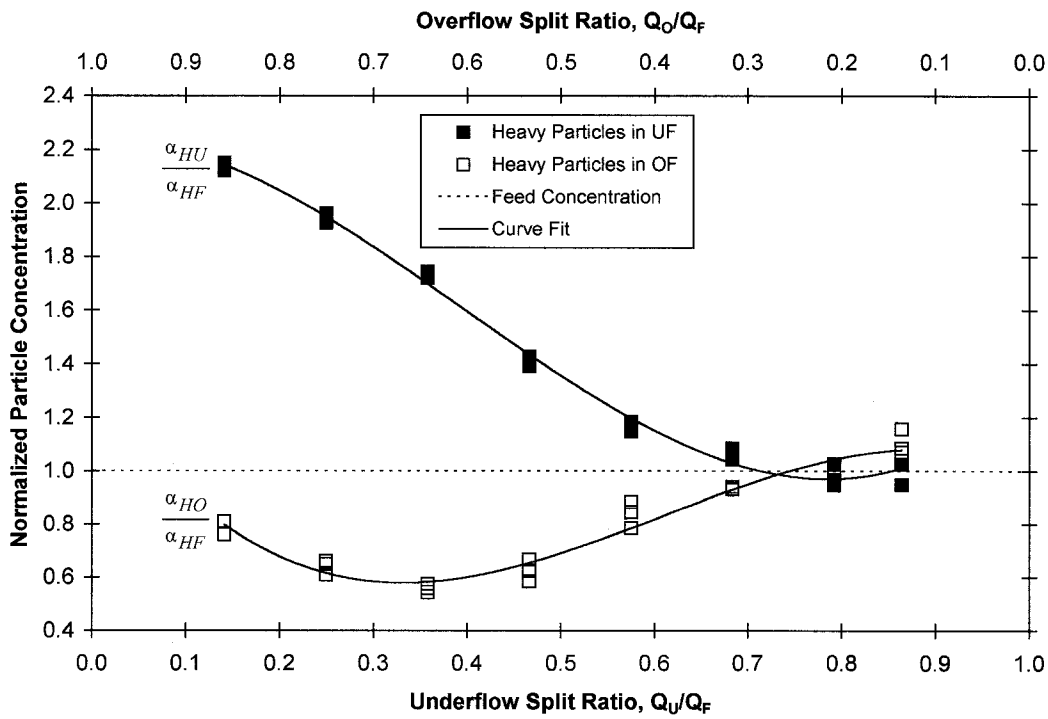

Figure 4-18. Concentrations of Heavy Particles in Overflow and Underflow for Column B, System I (α_{LF} = 0.058, α_{HF} = 0.122), Feed Rate 41.3 ml/s

Since centrifugal force is proportional to v_θ^2, one would expect the performance of a cyclonic vessel to increasingly deviate from that of a gravity settler with increasing feed rate. Figures 4-19, 4-20, and 4-21 show the product stream concentrations of light

particles for the same system as Figure 4-17 but at higher feed rates of 59.5 ml/s, 83.5 ml/s, and 118 ml/s. As the flow rate to the vessel increases, concentrations diverge further than comparable results shown in Figures 4-9, 4-10, and 4-11. Overall system behaviour becomes very symmetric with split ratio, and from visual observations seems entirely dependent on fluid flow in the vessel. At high feed flow rates, and hence high rotational speed, a central core consisting of highly concentrated light particles forms, and depending on the split ratio, can report almost solely to overflow or solely to the underflow. As shown, the concentration of light particles in the underflow approaches zero as split ratios approach zero, and concentration of light particles in the overflow approaches zero as split ratios approach unity. This is far more effective performance than compared to the separation shown in Figure 4-11.

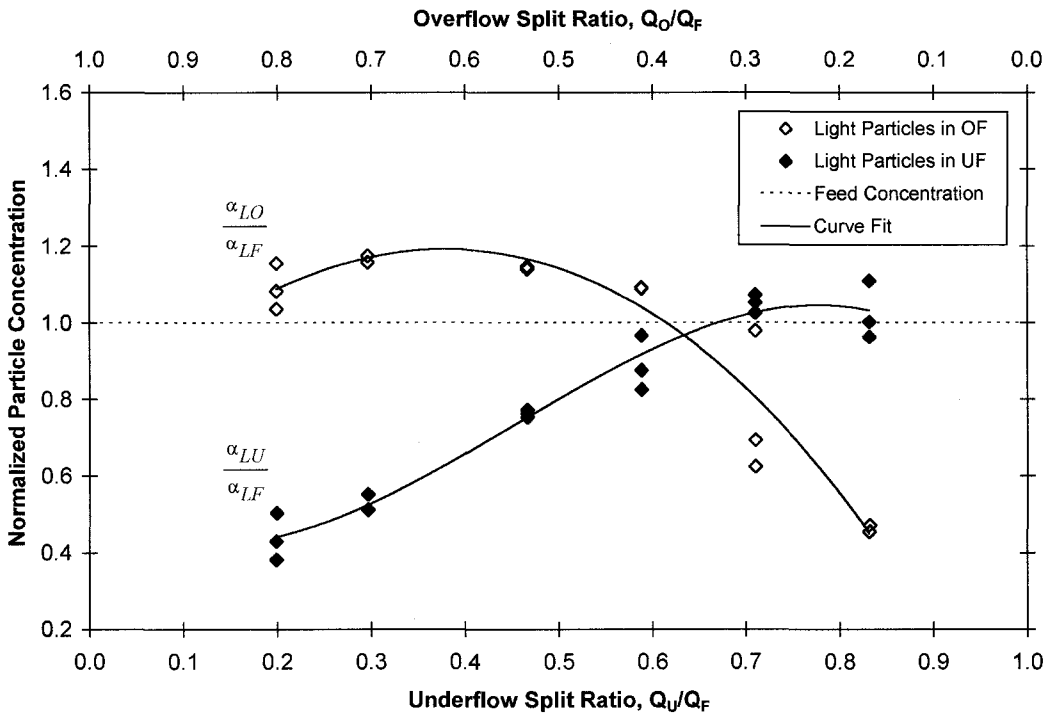

Figure 4-19. Concentrations of Light Particles in Overflow and Underflow for Column B, System I (α_{LF} = 0.058, α_{HF} = 0.122), Feed Rate 59.5 ml/s

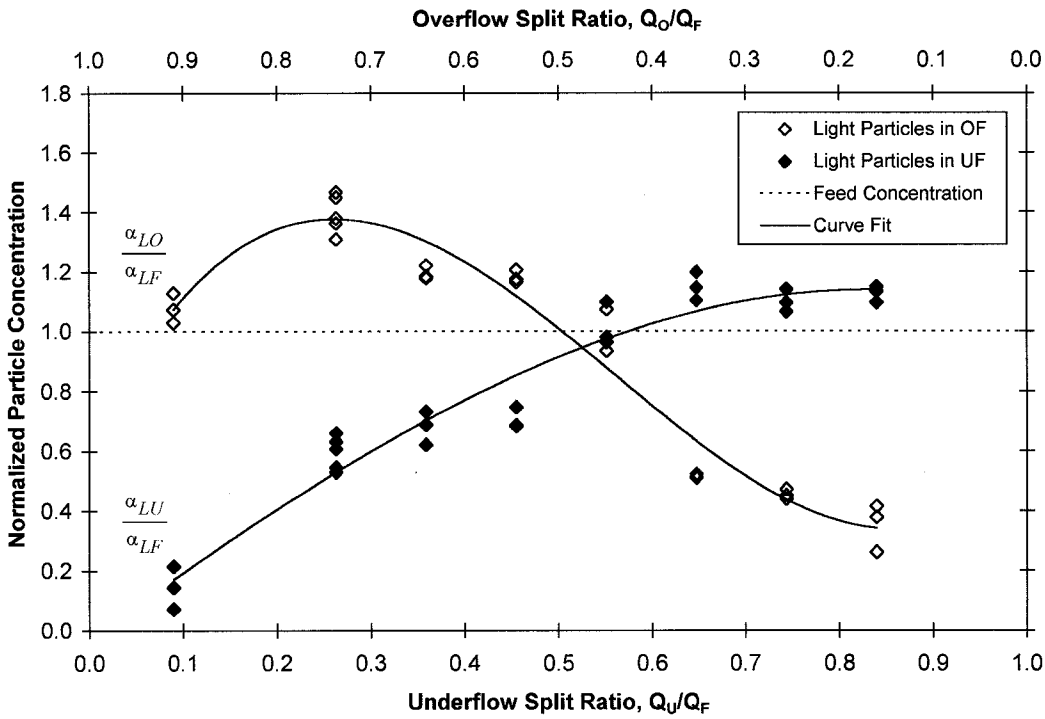

Figure 4-20. Concentrations of Light Particles in Overflow and Underflow for Column B, System I (α_{LF} = 0.058, α_{HF} = 0.122), Feed Rate 83.5 ml/s

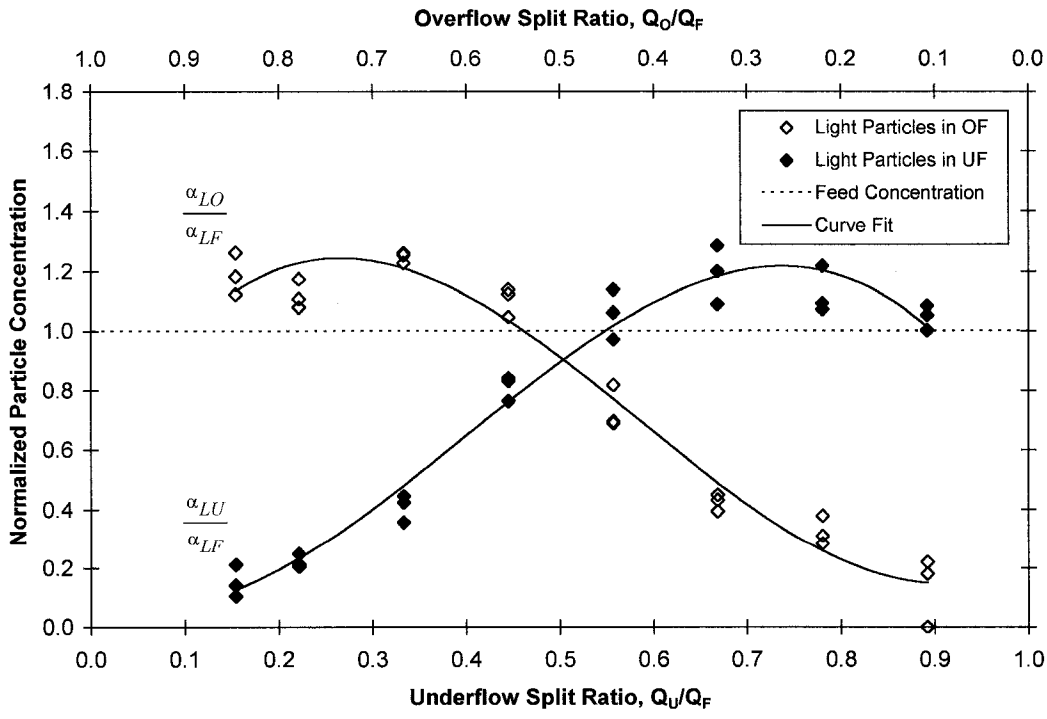

Figure 4-21. Concentrations of Light Particles in Overflow and Underflow for Column B, System I (α_{LF} = 0.058, α_{HF} = 0.122), Feed Rate 118 ml/s

Performance with heavy particles is also interesting. Figures 4-22, 4-23, and 4-24 show the product stream concentrations of heavy particles at higher flow rates. Again, the graphs become highly symmetric with split ratio as feed rates increase and high concentrations are reached at extreme split ratios. Underflow samples at low split ratios were highly concentrated, with high volume fractions of heavy particles. Unlike the light particles, heavy particles did not visibly concentrate in a given zone within the vessel. Instead, they appeared to be evenly distributed except at the outlets. At very low split ratios, the central core of light particles appeared to be "sucked" into the overflow, and the flow of these particles looked to be "crowding out" the heavy particles at that outlet. The reverse was true at high split ratios. Performance appeared to be highly dominated by flow patterns within the vessel instead of differential or hindered settling. Once again, this is in sharp contrast to the results using Column A.

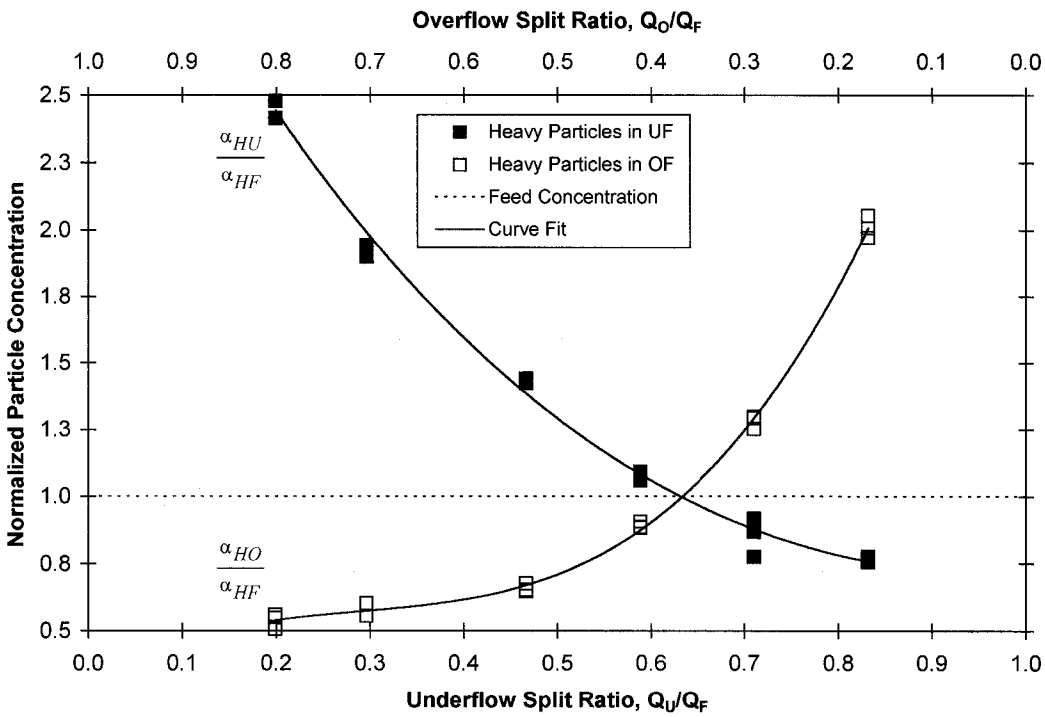

Figure 4-22. Concentrations of Heavy Particles in Overflow and Underflow for Column B, System I (α_{LF} = 0.058, α_{HF} = 0.122), Feed Rate 59.5 ml/s

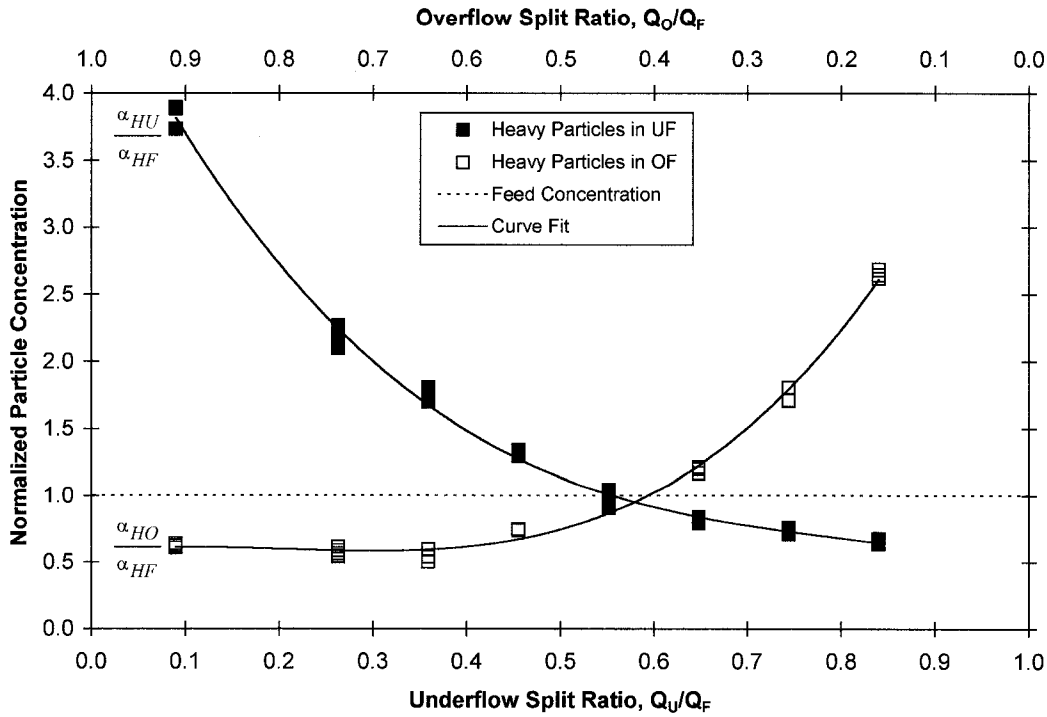

Figure 4-23. Concentrations of Heavy Particles in Overflow and Underflow for Column B, System I (α_{LF} = 0.058, α_{HF} = 0.122), Feed Rate 83.5 ml/s

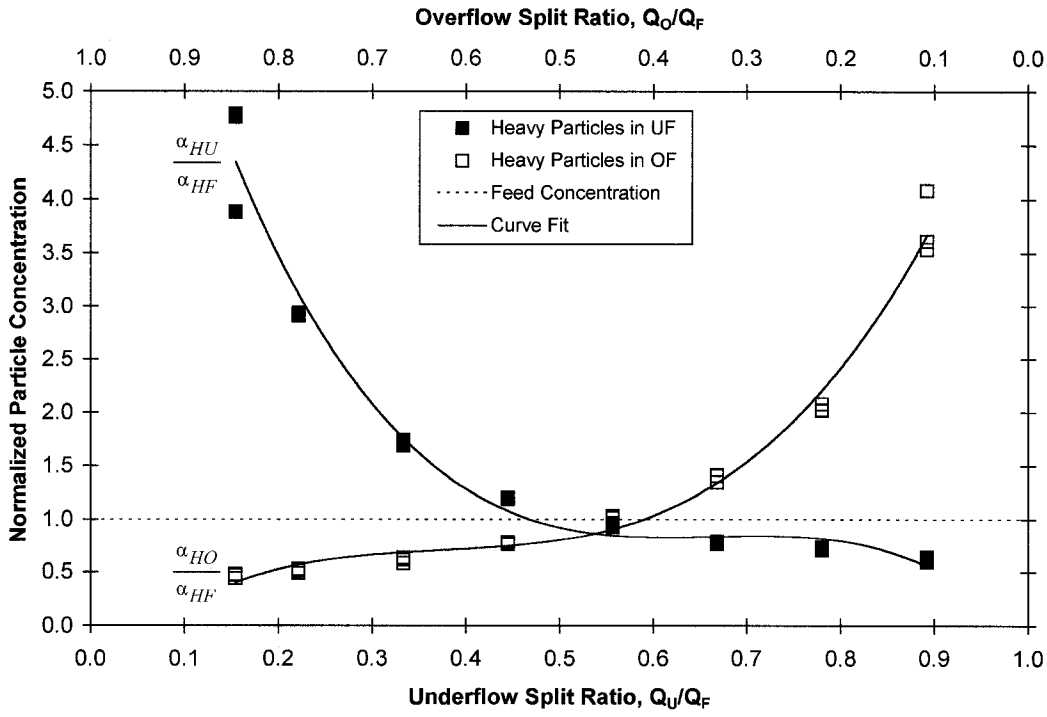

Figure 4-24. Concentrations of Heavy Particles in Overflow and Underflow for Column B, System I (α_{LF} = 0.058, α_{HF} = 0.122), Feed Rate 118 ml/s

Figures 4-25 and 4-26 show the recoveries of light particles in the overflow and underflow streams as a function of the split ratio for Column B, System I, at feed rates of 41.3 ml/s and 118 ml/s, respectively. At low flow rates, the recovery of light particles is comparable to that of Column A (Figure 4-5). At high flow rates and split ratios, recovery of particles tend towards 0% or 100% (i.e., perfect separation occurs). At an UF split ratio of about 0.15, recovery of light particles in the overflow exceeds 95%. Thus, at high throughputs, Column B yields superior recovery of light particles than was recorded in any of the tests with Column A.

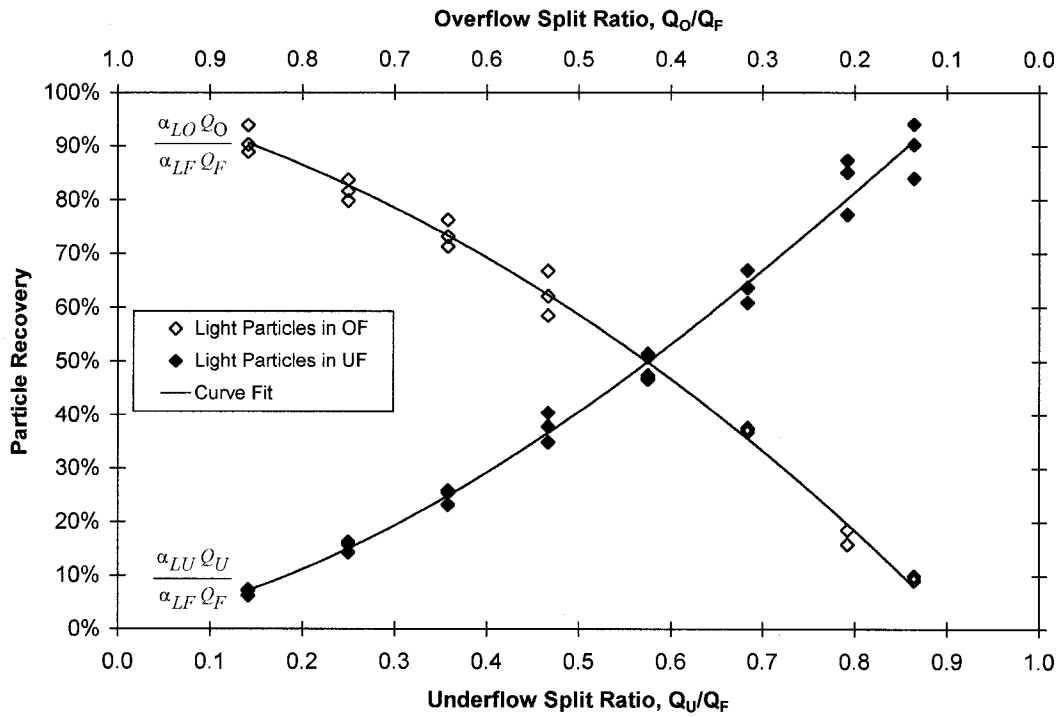

Figure 4-25. Recoveries of Light Particles in Overflow and Underflow for Column B, System I (α_{LF} = 0.058, α_{HF} = 0.122), Feed Rate 41.3 ml/s

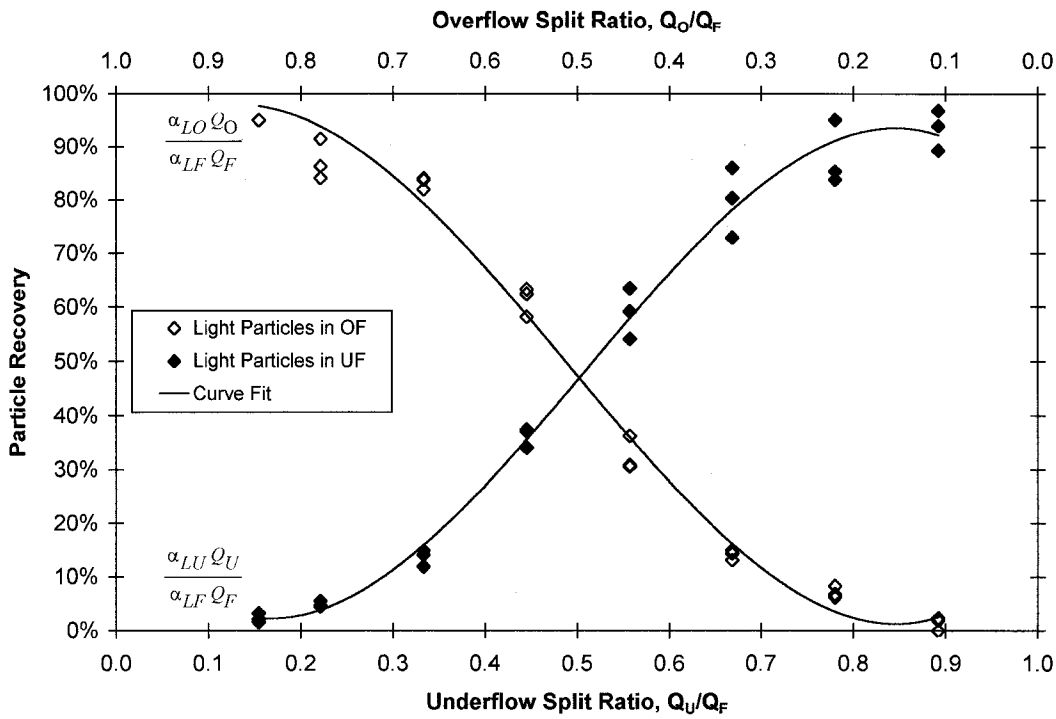

Figure 4-26. Recoveries of Light Particles in Overflow and Underflow for Column B, System I (α_{LF} = 0.058, α_{HF} = 0.122), Feed Rate 118 ml/s

Figure 4-27 shows heavy particle recovery at a low flow rate (41.3 ml/s), while Figure 4-28 shows the same at a high flow rate (118 ml/s). As can be seen, heavy particle recovery in Column B was reasonable at low flow rates, but did not improve with increased flow as was observed with light particle recovery.

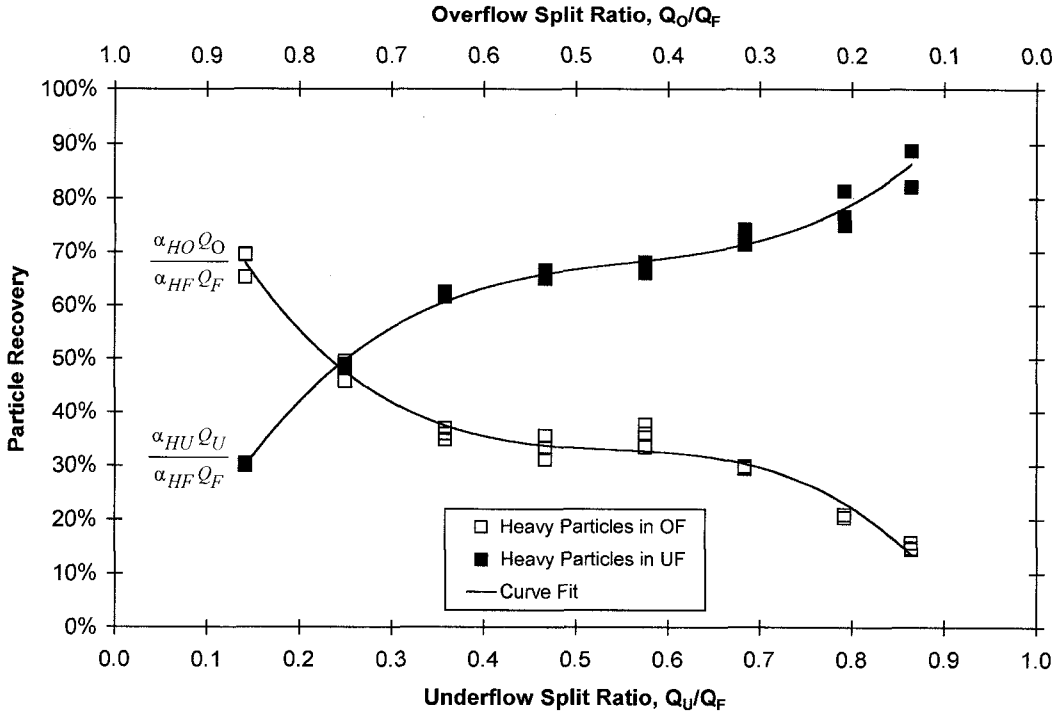

Figure 4-27. Recoveries of Heavy Particles in Overflow and Underflow for Column B, System I (α_{LF} = 0.058, α_{HF} = 0.122), Feed Rate 41.3 ml/s

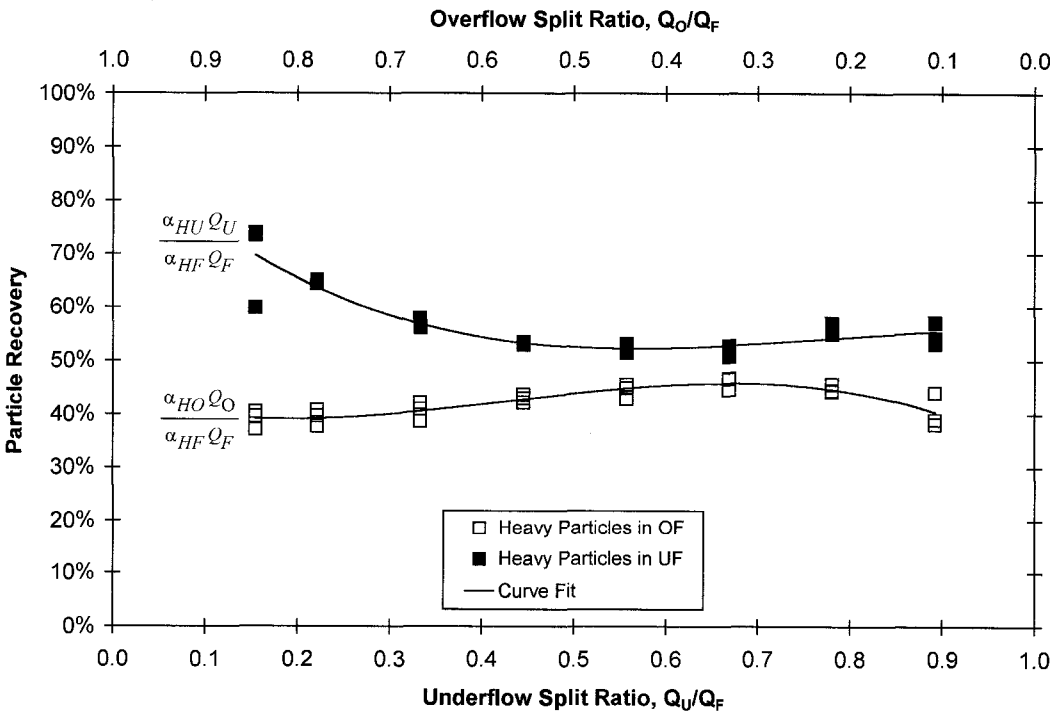

Figure 4-28. Recoveries of Heavy Particles in Overflow and Underflow for Column B, System I (α_{LF} = 0.058, α_{HF} = 0.122), Feed Rate 118 ml/s

Combining the information on particle concentration with the recovery results, one could envision a tangentially-fed vessel with a similar design to Column B delivering high recovery of a light product while simultaneously yielding a high-density heavy stream for a difficult-to-separate slurry like System I. At low UF split ratios, for example, near 100% recovery of light particles could be achieved in the overflow with a concentration of heavy particles in the underflow 5× of that of the feed. For such applications, a design based on Column B would actually operate better at higher throughputs, a useful trait for an industrial process.

4.5 - COLUMN C - EFFECT OF TANGENTIAL OUTLET:

Figures 4-29 to 4-38 depict the concentration and recovery results for Column C. Column C is similar to Column B except that the underflow is withdrawn tangentially and the ends of the vessel are flat, instead of conical. It was thought that a tangential underflow outlet would enhance recovery of heavy particles in that stream, since the heavy species would migrate preferentially to the outer edge of the vessel. Unfortunately, that was not what was found.

Figures 4-29, 4-30, and 4-31 show the normalized concentrations of light particles in the overflow and underflow streams as a function of the split ratio for Column C, System I, at feed rates of 43.8 ml/s, 58.7 ml/s, and 84.0 ml/s. At low feed rates, Column C does a poorer job of concentrating light particles than either Column A or Column B. Indeed, Column C appears to act more like a *mixer* than a *separation vessel*. With increasing feed rate, however, Column C produces an overflow stream with a higher concentration of light particles than either Columns A or B (though with very low light particle recovery - see Figure 4-36).

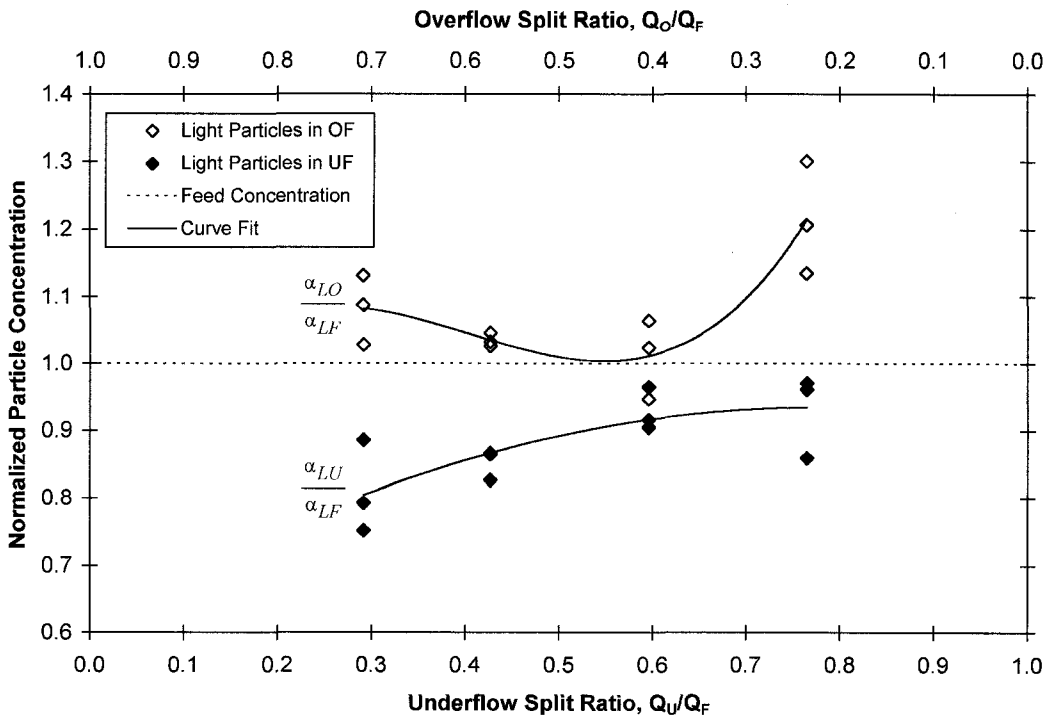

Figure 4-29. Concentrations of Light Particles in Overflow and Underflow for Column C, System I (α_{LF} = 0.058, α_{HF} = 0.122), Feed Rate 43.8 ml/s

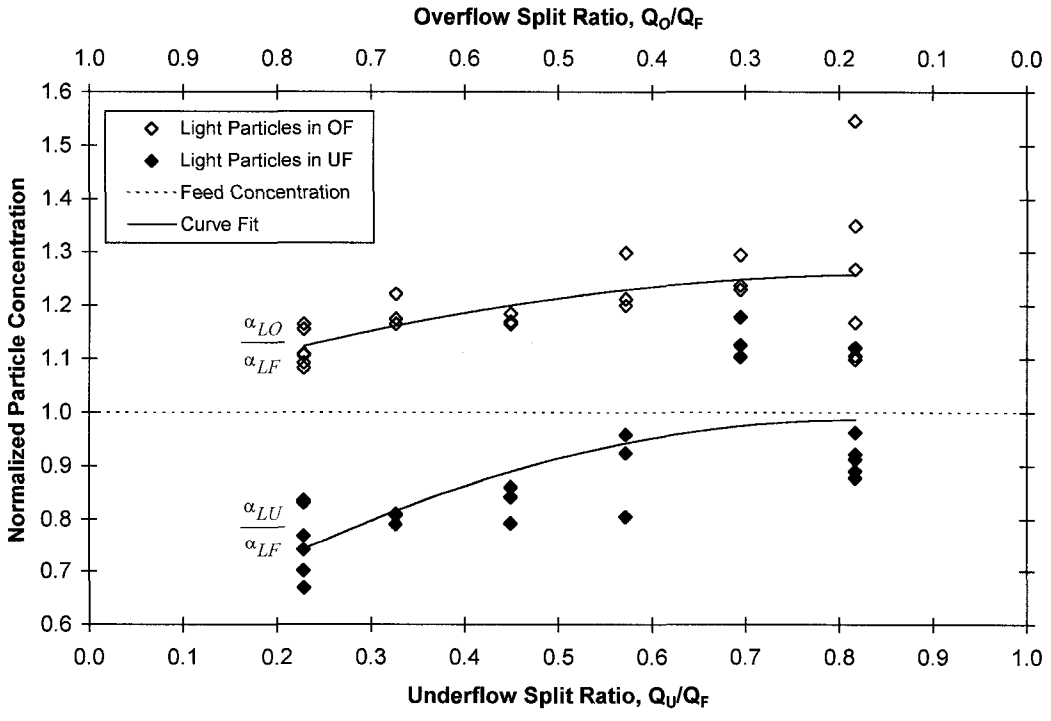

Figure 4-30. Concentrations of Light Particles in Overflow and Underflow for Column C, System I (α_{LF} = 0.058, α_{HF} = 0.122), Feed Rate 58.7 ml/s

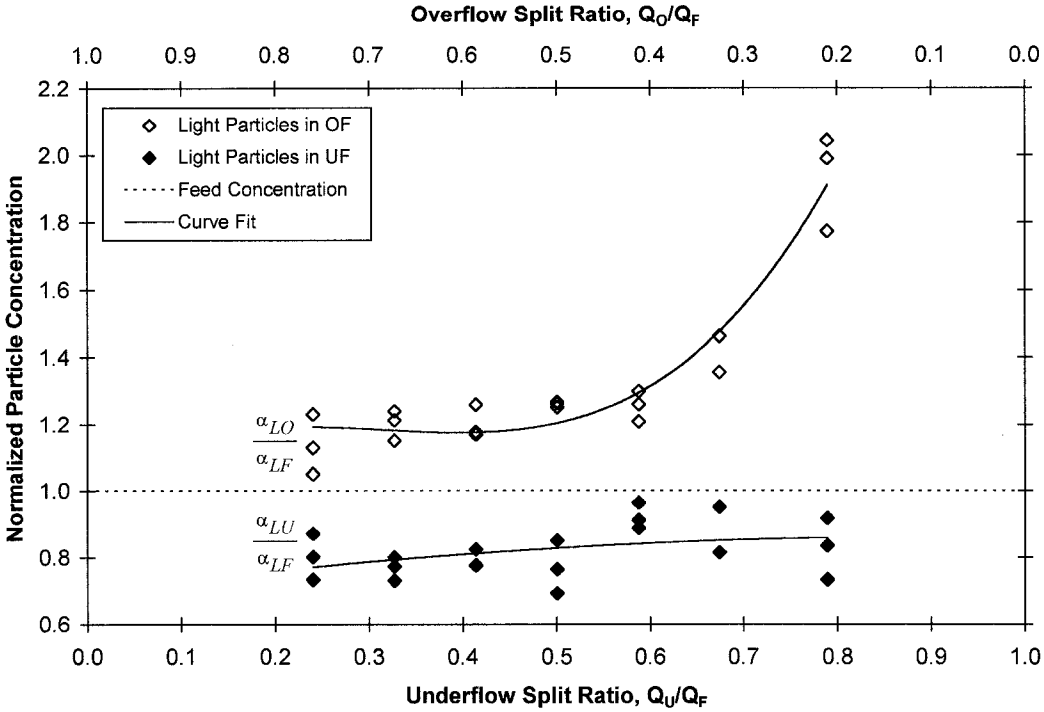

Figure 4-31. Concentrations of Light Particles in Overflow and Underflow for Column C, System I (α_{LF} = 0.058, α_{HF} = 0.122), Feed Rate 84.0 ml/s

Figures 4-32, 4-33, and 4-34 show the product stream concentrations of heavy particles. As stated earlier, it was hoped that the tangential underflow outlet configuration would enhance vessel performance. It was found that although heavy phase concentration was slightly higher than in Column A, performance was much poorer than Column B for all feed rates. A tangential outlet, therefore, does not improve the *quality* of the underflow product.

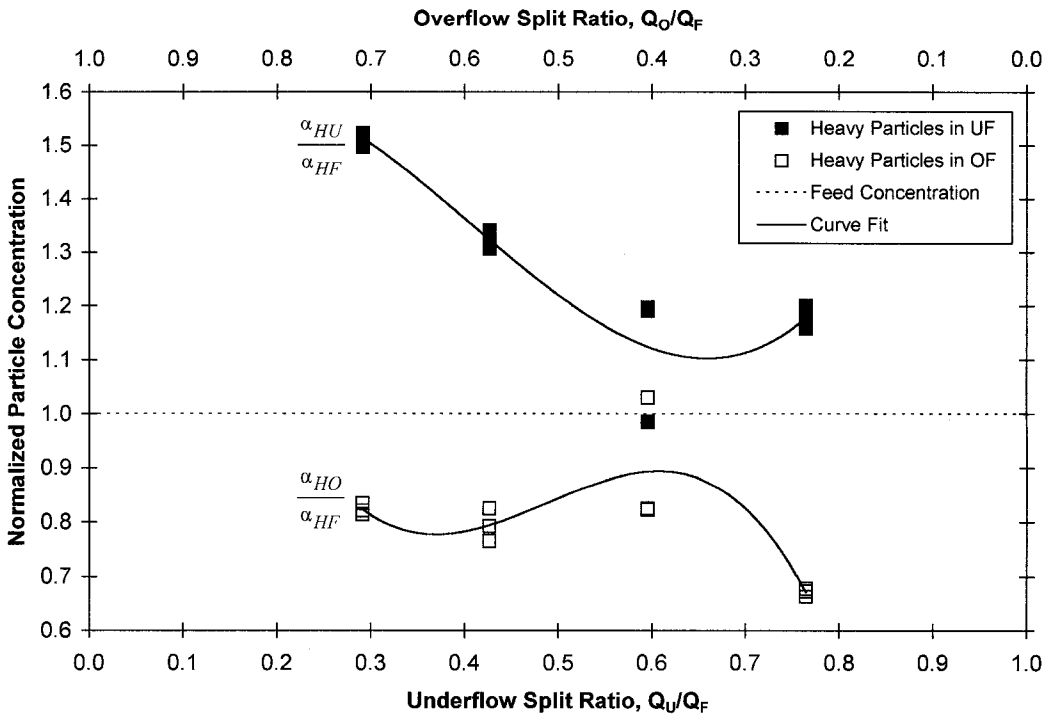

Figure 4-32. Concentrations of Heavy Particles in Overflow and Underflow for Column C, System I (α_{LF} = 0.058, α_{HF} = 0.122), Feed Rate 43.8 ml/s

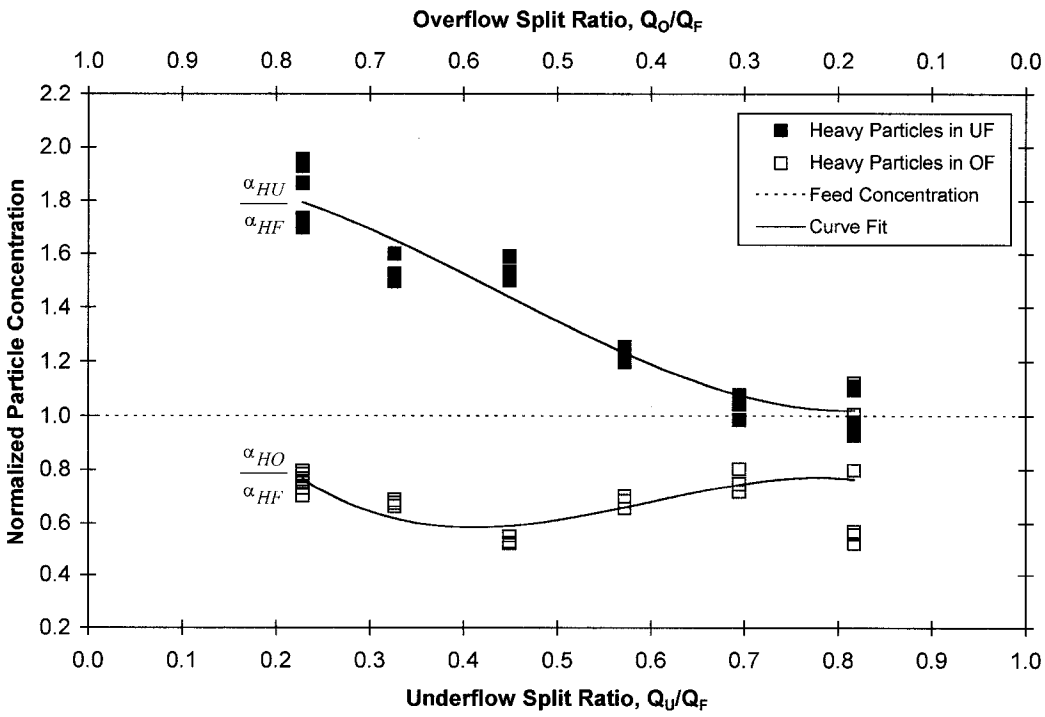

Figure 4-33. Concentrations of Heavy Particles in Overflow and Underflow for Column C, System I (α_{LF} = 0.058, α_{HF} = 0.122), Feed Rate 58.7 ml/s

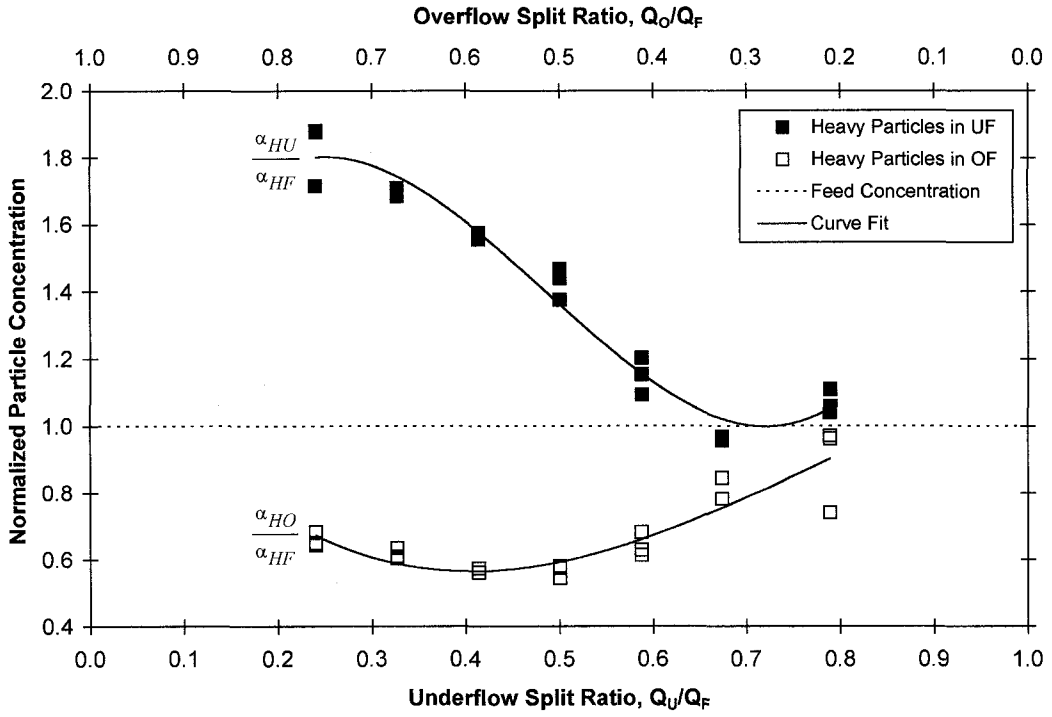

Figure 4-34. Concentrations of Heavy Particles in Overflow and Underflow for Column C, System I (α_{LF} = 0.058, α_{HF} = 0.122), Feed Rate 84.0 ml/s

Figures 4-35 and 4-36 show the recoveries of light particle species at low and high feed rates. As can be seen, recovery of light particles to the overflow was generally inferior compared to both Column A and Column B. Column C does yield higher light particle recoveries at low underflow split ratios, but only in a narrow operating range. A vessel built in the manner of Column C would be a poor design for recovery of a light phase product (such as aerated bitumen) under most operating regimes of interest.

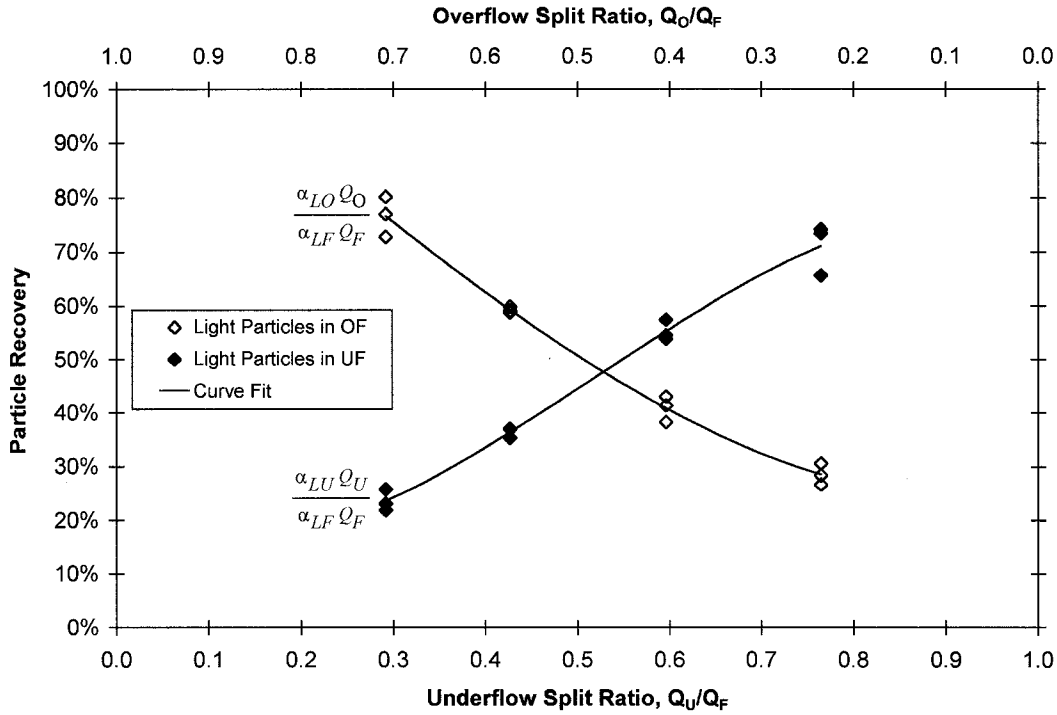

Figure 4-35. Recoveries of Light Particles in Overflow and Underflow for Column C, System I (α_{LF} = 0.058, α_{HF} = 0.122), Feed Rate 43.8 ml/s

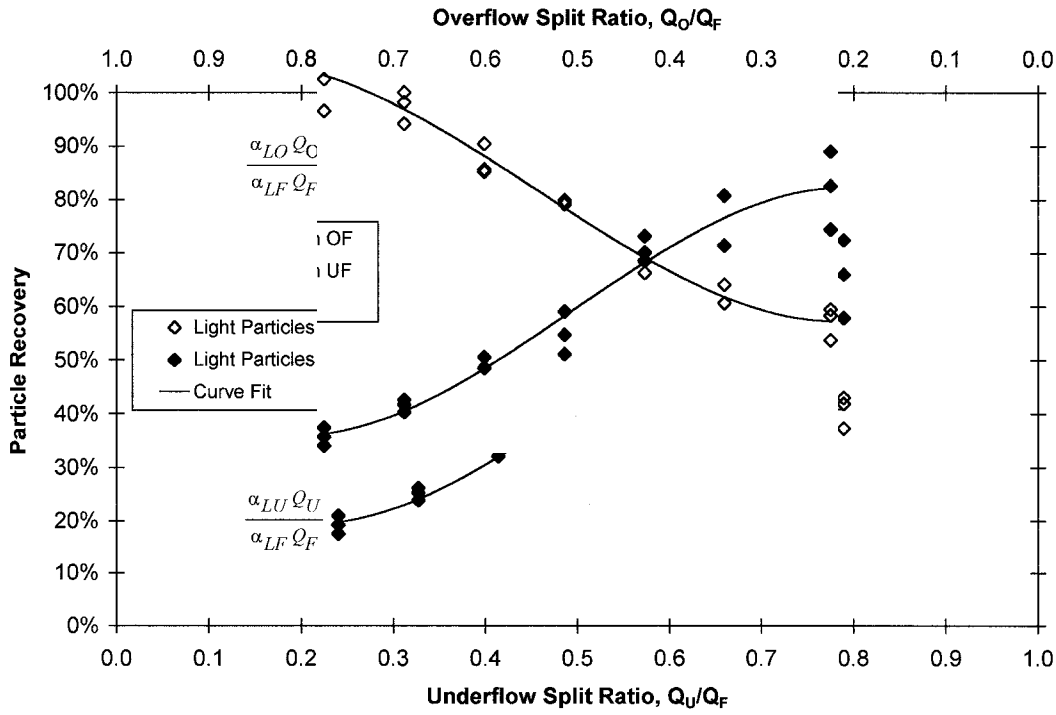

Figure 4-36. Recoveries of Light Particles in Overflow and Underflow for Column C, System I (α_{LF} = 0.058, α_{HF} = 0.122), Feed Rate 84.0 ml/s

Figures 4-37 and 4-38 show the recoveries of heavy particle species at low and high feed rates. At all split ratios, heavy particle recovery in the underflow for Column C was superior compared to Column A and Column B. Unlike the other tangentially-fed vessel, performance did not dramatically improve at higher feed rates.

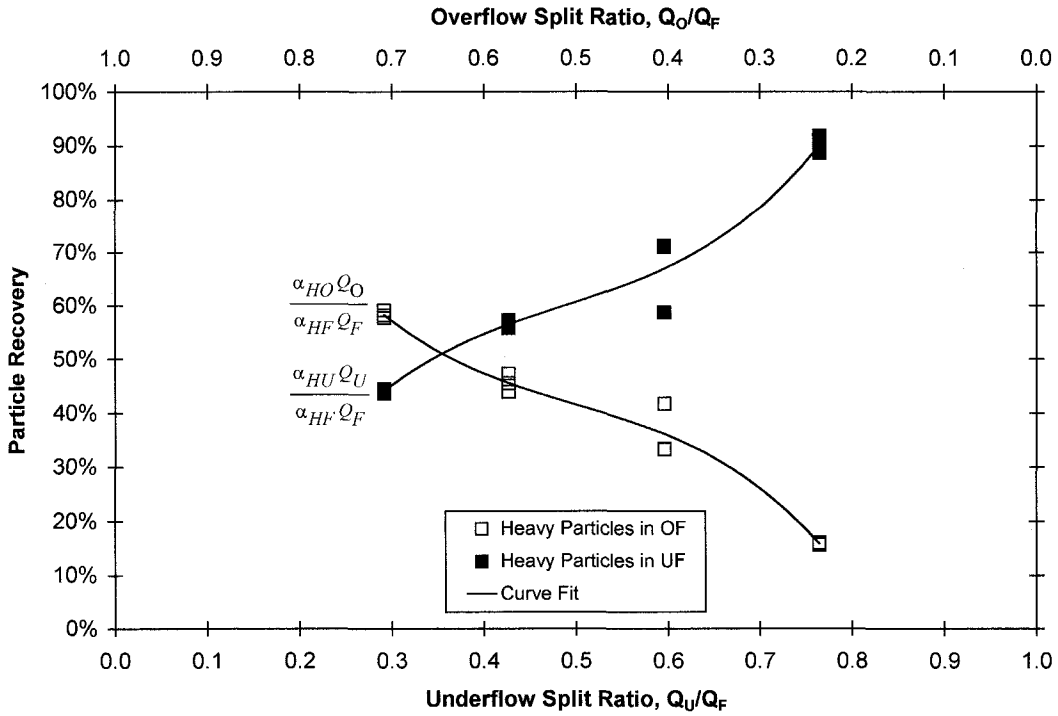

Figure 4-37. Recoveries of Heavy Particles in Overflow and Underflow for Column C, System I (α_{LF} = 0.058, α_{HF} = 0.122), Feed Rate 43.8 ml/s

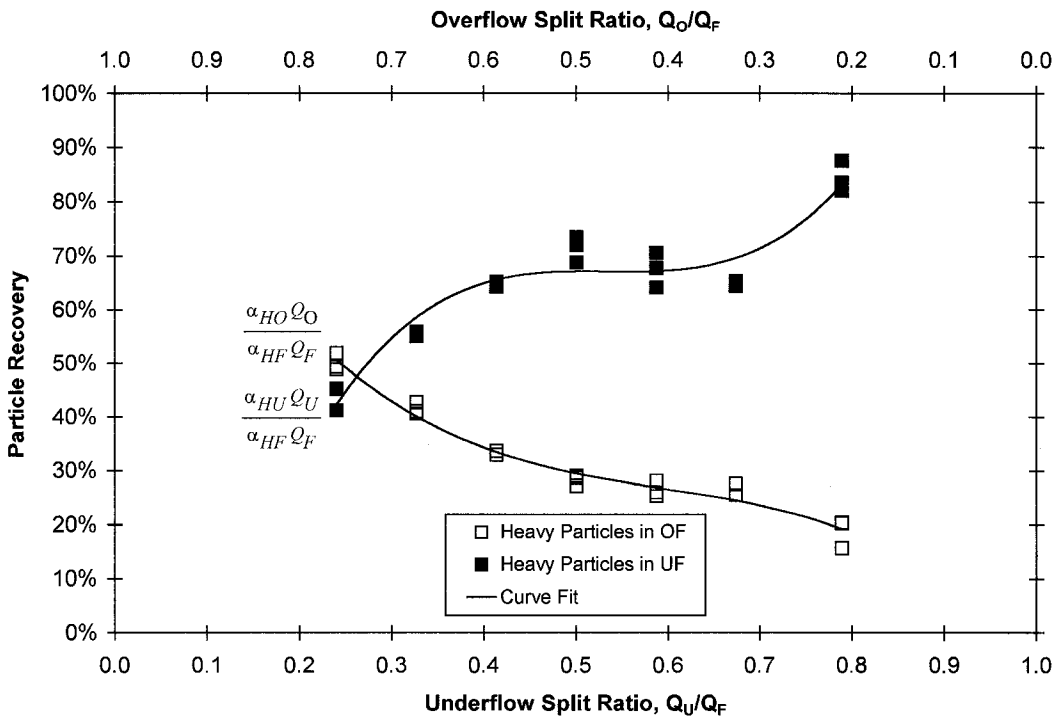

Figure 4-38. Recoveries of Heavy Particles in Overflow and Underflow for Column C, System I (α_{LF} = 0.058, α_{HF} = 0.122), Feed Rate 84.0 ml/s

The tangential underflow in Column C had the expected effect of increasing the heavy phase recovery, even at low feed rates. However, in most other respects this column design performed poorly compared to the others tested. A vessel of this design could see use recovering heavy phase particles where purity is not a concern.

4.6 - VISUAL OBSERVATIONS:

During the experimental phase, attempts were made to dye several of the particle species - most notably using rhodamine B dye using an acetone technique described by Fessas (1983). Unfortunately, no suitable procedure could be found that did not significantly degrade the polymer beads. In the end, undyed particles were used, making it more difficult to visually distinguish between species, but interesting observations could still be made.

In the case of the simple gravity separation experiments (Column A), particles appeared

to be evenly distributed throughout the column. For both Systems I and II, no internal structure could be discerned. Even though System II had a high solids concentration, no fingering or other lateral instabilities were noted. No major interesting visual phenomenon were noted, with the exception that at extreme split ratios, the product outlet was nearly plugged with particles.

In several previous studies of simple gravity separators, Nasr-El-Din et al. (1989, 1990), definite zones of particle segregation were seen. This was very apparent when lateral segregation was a factor, particularly in Nasr-El-Din (1990). In this study, however, with the thickness of the column and high particle density, no segregation in Column A was noted.

For the tangentially-fed experiments with Column B, much more interesting phenomena were seen. At even relatively low feed rates, the light particles segregated to the middle of the column under centrifugal force. This was visible as a thin, well-defined "vortex" along the very center of the vessel. As the split ratio varied, the majority of the light particles in the center followed the bulk particle flow.

Photographs of this phenomenon are much easier to discern with colours inverted so the images are presented in negative. The central core of light particles appears as a distinct black line in the photographs below (Figures 4-39 and 4-40) of Column B, System I, at a Feed rate of 118 ml/s. The behaviour of the light particles changes with increasing UF split ratios (from left to right) from reporting mainly to the overflow to the product reporting mainly to the underflow. This observed particle segregation is supported by the recovery results, as shown in Figure 4-21. At lower feed rates, this visual effect was less noticeable, and the recovery measurements less spectacular.

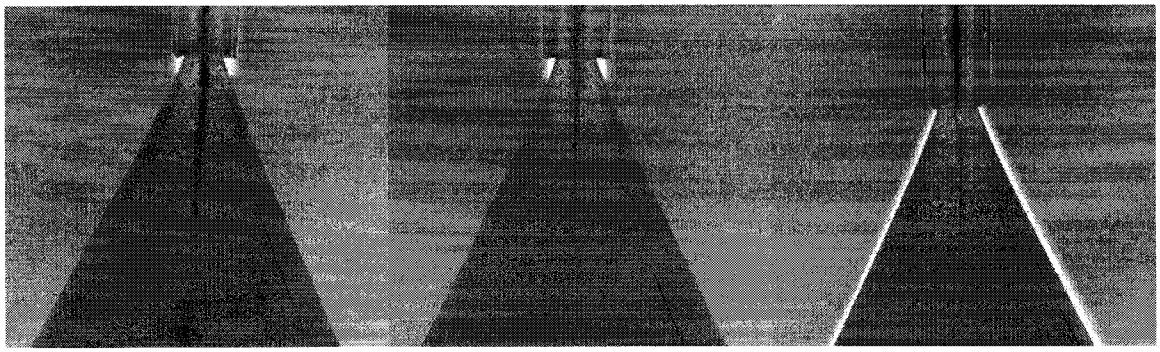

Figure 4-39. Overflow Photographs at UF Split Ratios of 0.15, 0.45, and 0.78 of Column B, System I (α_{LF} = 0.058, α_{HF} = 0.122), Feed Rate 118 ml/s

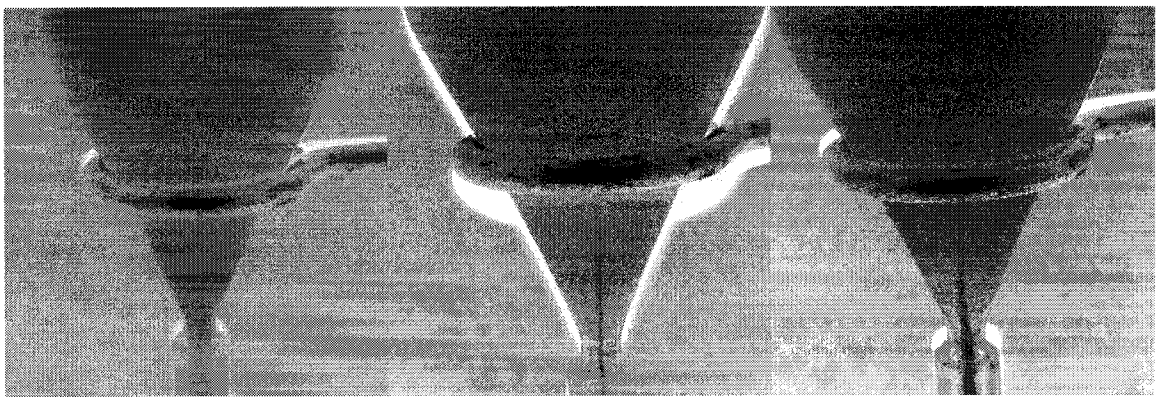

Figure 4-40. Underflow Photographs at UF Split Ratios of 0.15, 0.45, and 0.78 of Column B, System I (α_{LF} = 0.058, α_{HF} = 0.122), Feed Rate 118 ml/s

Note from the photographs that the centerline is thicker when reporting to the overflow than when it reports to the underflow, even for near-symmetric splits. There appeared to be less "plugging" around the outlets than with Column A, although from the photographs it can be seen that the central core still occupies almost the outlet at extreme split ratios.

The sole observation of note during experiments with Column C was that the tangential outlet appeared less "overloaded" at extremely high split ratios than the conical design of Columns A or B. This may explain, in part, the higher recovery values for heavy particles of this vessel.

5 - CONCLUSIONS:

It was found that the method of slurry feed injection to a separation vessel has a large impact on its performance, as does the overall vessel geometry.

Experimental results with the traditional gravity separator (Column A) were consistent with predictions made with the Masliyah model. Schiller and Naumann's C_D-$\Re_p$ relationship and the Richardson-Zaki form of $F(\alpha_f, \Re_p)$ were found to be satisfactory.

Substantially improved product quality and recovery compared to a simple gravity settler was achieved by utilizing cyclonic separation via tangential feed injection (Column B). Cyclonic separation improved both product quality and recovery over a wide range of conditions, even for difficult-to-separate mixtures (e.g., System I).

Experiments with a cyclonic design featuring tangential outlet (Column C) achieved good recovery of heavy particles under some conditions, namely at higher split ratios, though product quality was not enhanced. In general, Column C did not perform well compared to other designs.

5.1 - RECOMMENDATIONS:

One can envision a tangentially-fed vessel with a similar design to Column B delivering high recovery of a light product while simultaneously yielding a high-density heavy stream for a difficult-to-separate slurry. At low underflow split ratios, for example, near 100% recovery of light particles can be achieved in the overflow with a concentration of heavy particles in the underflow five times of that of the feed. At high feed rates, centrifugal forces dominate over gravitational forces, so the vessel can be operated in any orientation with system performance governed by split ratio. Such a vessel actually operates better at higher throughputs, a useful trait for an industrial process.

Vessels based around the design of Column C could also find use, though in a narrower range of applications. In situations where heavy particle recovery is the key parameter, such a separator is superior to either Column A or B.

Tangentially fed-vessels of a design similar to Columns B and C have in fact been used industrially alongside gravity separation vessels to recover residual bitumen from fine solids in a light hydrocarbon tailings stream. These vessels were commissioned at Syncrude Canada Ltd.'s Mildred Lake Extraction Plant by the author in early 2002, though the specific equipment design and results are proprietary. It is recommended that further research and development into cyclonic separation vessels be performed and their use in the hydrocarbon industry be expanded.

REFERENCES:

Alberta Energy and Utilities Board (AEUB). "Statistical Series (ST) 2004-98: Alberta's Reserves 2003 and Supply/Demand Outlook 2004-2013 May 2004." Revised June 2004 ISSN 1499-1179.

Al-Naafa, M., and S. Selim. "Sedimentation of Monodisperse and Bidisperse Hard-Sphere Colloidal Suspensions". *AIChE Journal*, **38**, 10, 1618-1630. (1992).

Barnea, E., and J. Mizrahi. "A Generalized Approach to the Fluid Dynamics of Particulate Systems: Part 1. General Correlation for Fluidization and Sedimentation in Solid Multiparticle Systems". *Chemical Engineering Journal*, **5**, 171-189. (1973).

Batchelor, G. "Sedimentation in a Dilute Polydisperse System of Interacting Spheres: Part 1. General Theory". *J. Fluid Mech.*, **119**, 379-408. (1982).

Batchelor, G., and C. Wen. "Sedimentation in a Dilute Polydisperse System of Interactive Spheres: Part 2. Numerical Results". *J. Fluid Mech.*, **124**, 495-528. (1982).

Berres, S., and R. Bürger. "On Gravity and Centrifugal Settling of Polydisperse Suspensions Forming Compressible Sediments". *International Journal of Solids and Structures*, **40**, 4965-4987. (2003).

Bürger, R., K. H. Karlsen, E. M. Tory, and W. L. Wendland. "Model Equations and Instability Regions for the Sedimentation of Polydisperse Suspensions of Spheres". *UCLA Computational and Applied Mathematics Report*, Los Angeles. (2001).

Bird , R. B., W. E. Stewart, and E. N. Lightfoot (BSL). *Transport Phenomena*, John Wiley & Sons, 1960.

Bisschops, M., K. Lubyen, and L. van der Wielen. "Hydrodynamics of Countercurrent Two-Phase Flow in a Centrifugal Field". *AIChE Journal*, **47**, 6, 1263-1276. (2001).

Brauer, H. and D. Sucker. "Umströmung von Platten, Zylindern und Kugeln". *Chem. Ing. Tech.*, **48**, 665-671. (1976).

Bürger, R., and W. Wendland. "Sedimentation and Suspension Flows: Historical Perspective and Some Recent Developments". *Journal of Engineering Mathematics*, **41**, 101-116. (2001).

Cheung, M., R. Powell, and M. McCarthy. "Sedimentation of Noncolloidal Bidisperse Suspensions". *AIChE Journal*, **42**, 1, 271-276. (1996).

Clark, K. A. *Can. Min. Met. Bull.*, **212**, 1385-1395. (1930).

Concha, F., and R. Bürger. "A Century of Research in Sedimentation and Thickening". *KONA*, **20**, 38-70. (2003).

Coe, H. S. and G. H Clevenger. "Methods for Determining the Capabilities of Slime-Settling Tanks". *Trans. AIME*, **55**, 356-385. (1916).

Dallavalle, J. M. *Micromeritics: The Technology of Fine Particles*, 2nd ed. Pitman: New York, 1948.

Davis, R., and A. Acrivos. "Sedimentation of Noncolloidal Particles at Low Reynolds Numbers". *Ann. Rev. Fluid Mech.*, **17**, 91-118. (1985).

Davis, R., and H. Gecol. "Hindered Settling Function with No Empirical Parameters for Polydisperse Suspensions". *AIChE Journal*, **40**, 3, 570-575. (1994).

Di Felice, R. "The Sedimentation Velocity of Dilute Suspensions of Nearly Monosized Spheres". *International Journal of Multiphase Flow*, **25**, 559-574. (1999).

Fessas, Y. *On the Settling of Model Suspensions Promoted by Rigid Buoyant Particles.* Ph.D. Thesis. (1983).

Garside, J. and M. Al-Dibouni. "Velocity-Voidage Relationships for Fluidization and Sedimentation in Solid-Liquid Systems". *Ind. Eng. Chem., Process Des. Dev.*, **16**, 2, 206-214. (1977).

Khan, A., and J. Richardson. "The Resistance to Motion of a Solid Sphere in a Fluid". *Chem. Eng. Comm.*, **62**, 135-150. (1987).

Kynch, G. J. "A Theory of Sedimentation". *Trans. Faraday Soc.*, **48**, 166-176. (1952).

Law, H., J. Masliyah, R. MacTaggart, and K. Nandakumar. "Gravity Separation of Bidisperse Suspensions of Light and Heavy Particle Species". *Chemical Engineering Science*, **42**, 7, 1527-1538. (1987).

Lockett, M. J. and K. S. Bassoon. "Sedimentation of Binary Particle Mixtures". *Powder Technology*, **24**, 1-7. (1979)

Maarten, B., H. Verweij, and V. Breedveld. "Evaluation of Instability Criterion for Bidisperse Sedimentation". *Particle Technology and Fluidization*, **47**, 1, 45-52. (2001).

Masliyah, J. "Hindered Settling in a Multi-Species Particle System". *Chemical Engineering Science*, **34**, 1166-1168. (1979).

Masliyah, J., T. Kwong, and F. Seyer. "Theoretical and Experimental Studies of a Gravity Separation Vessel". *I&EC Process Design & Development*, **20**, 154-160. (1981).

Mirza, S., and J. Richardson. "Sedimentation of Particles of Two or More Sizes". *Chemical Engineering Science*, **34**, 447-454. (1979).

Nasr-El-Din, H., J. Masliyah, K. Nandakumar, and H. Law. "Continuous Gravity Separation of a Bidisperse Suspension in a Vertical Column". *Chemical Engineering Science*, **43**, 12, 3225-3234. (1988).

Nasr-El-Din, H., J. Masliyah, and K. Nandakumar. "Continuous Gravity Separation of Concentrated Bidisperse Suspensions in a Vertical Column". *Chemical Engineering Science*, **45**, 4, 849-857. (1990).

Patwardhan, V., and C. Tien. "Sedimentation and Liquid Fluidization of Solid Particles of Different Sizes and Densities". *Chemical Engineering Science*, **40**, 7, 1051-1060. (1985).

Richardson, J., and W. Zaki. "Sedimentation and Fluidisation: Part 1". *Trans. Instn Chem. Engrs*, **32**, 35-53. (1954).

Rowe, P. N., "A Convenient Empirical Equation for Estimation of the Richardson-Zaki Exponent". *Chemical Engineering Science*, **43**, 2795-2796. (1987).

Schiller L. and A. Naumann. *Z. Ver. Deut. Ing.*, **77**, 318. (1935)

Smith, T. N. "The Sedimentation of Particles Having a Dispersion of Sizes". *Trans. Instn. Chem. Engrs.*, **43**, 69-73. (1966)

Stokes, G. G. *Mathematical and Physical Paper III*, Cambridge University Press. (1891)

Talmadge, W. P. and E. Fitch. "Determining Thickener Unit Areas". *Ind. Engng. Chem*, **47**, 38-41. (1955)

Turton, R. and O. Levenspiel. "A Short Note on the Drag Correlation for Spheres". *Powder Technology*, **47**, 83-86. (1986)

Weiland, R., Y. Fessas, and B. Ramarao. "On Instabilities Arising During Sedimentation of Two-Component Mixtures of Solids". *J. Fluid. Mech.*, **142**, 383-389. (1984).

Wills, B. A. *Mineral Processing Technology*, 6th ed. Butterworth Heinemann, 1997.

Xue, B., and Y. Sun. Modeling of Sedimentation of Polydisperse Spherical Beads with a Broad Size Distribution. *Chemical Engineering Science*, **58**, 1531-1543. (2003).

APPENDIX 1 - DETAILED EXPERIMENTAL PROCEDURE:

- Select setting for Feed and UF and turn on paristaltic pumps.
- Turn on stirrer for mixing tank.
    - Note that mixing tank volume is ~20 litres; wait at least 5 system residence times before taking first sample at a given Feed and UF rate.
        - If feed = 40.6 ml/s = 2.4 l/min = 8.2 minute residence time.
        - If feed = 59.4 ml/s = 3.6 l/min = 5.6 minute residence time.
        - If feed = 81.3 ml/s = 4.9 l/min = 4.1 minute residence time.
        - If feed = 117 ml/s = 7.0 l/min = 2.9 minute residence time.
- Divert entire UF stream to 250 ml cylinder, then resume normal flow.
- Divert entire OF stream to 250 ml cylinder, then resume normal flow.
- Divert entire Feed stream to 250 ml cylinder, then resume normal flow.
- Weigh each cylinder (to obtain ρ_{slurry}).
- Wait for layers to settle, tapping & stirring slightly to ensure complete segregation.
    - Level of heavy particle interface.
    - Level of light particle interface.
    - Upper level of light particles.
- Compare settled volumes of heavy and light particles to calibration curve to obtain true values for UF, OF, and Feed compositions.
- Return samples back to mix tank. (Combined samples are ~600 ml which is ~3% of total system volume.) If necessary, wash particles which remain in cylinders onto a separate sieve to return to system at a later time.

- Repeat sampling procedure three times to obtain representative samples.
    - Note that separation columns are ~1.5 litres in volume (Column C is ~1.2 litres); wait at least 5 column residence times between sample runs.
        - If feed = 40.6 ml/s = 2.4 l/min = ~37 second residence time.
        - If feed = 59.4 ml/s = 3.6 l/min = ~ 25 second residence time.
        - If feed = 81.3 ml/s = 4.9 l/min = ~ 18 second residence time.
        - If feed = 117 ml/s = 7.0 l/min = ~ 13 second residence time.

- Change UF pump rate to test new split ratio, and repeat entire procedure. Measure at as many split ratios as feasible (actual number will depend on Feed flow rate).

- Change Feed pump rate to new setting and repeat entire procedure (varying UF) to test different split ratios. Measure at as many feed flow rates as feasible.

- Change column and repeat entire procedure (varying UF and Feed) to perform vessel comparisons. Test all three columns.

- Change tank composition and repeat entire procedure (varying UF, Feed, and column) to test dependence on system properties. Test both system compositions in this manner.

APPENDIX 2 - SAMPLE CALCULATIONS:

As mentioned in Chapter 3, bulk volume measurements from experiments were converted to true volumetric concentrations using the calibration curves depicted in Figures 3-8a through 3-8d.

The equations used to calculate true volume from bulk volume for light and heavy particicles of System II are repeated here:

System II, Light particle species:

$$\text{True Volume} = 0.6052 \times (\text{Bulk Volume}) - 0.0068 \qquad \text{(A2-1)}$$

System II, Heavy particle species:

$$\text{True Volume} = 0.6110 \times (\text{Bulk Volume}) - 0.0073 \qquad \text{(A2-2)}$$

For this example, consider the case of Column A, System II, at a feed rate of 55.8 ml/s. The following measurements were taken at an UF split ratio of 0.346:

Table A2-1. Sample Volume Calculations

				Bulk Volume %		True Volume %	
UF Readings				$\alpha_{LU, Bulk}$	$\alpha_{HU, Bulk}$	$\alpha_{LU, True}$	$\alpha_{HU, True}$
0.0	29.5	102.0	236.0	12.5%	56.8%	6.8%	34.0%
OF Readings				$\alpha_{LO, Bulk}$	$\alpha_{HO, Bulk}$	$\alpha_{LO, True}$	$\alpha_{HO, True}$
0.0	67.5	198.5	227.0	29.8%	12.6%	17.3%	6.9%
UF Readings				$\alpha_{LU, Bulk}$	$\alpha_{HU, Bulk}$	$\alpha_{LU, True}$	$\alpha_{HU, True}$
0.0	25.0	91.0	230.5	10.8%	60.5%	5.8%	36.3%
OF Readings				$\alpha_{LO, Bulk}$	$\alpha_{HO, Bulk}$	$\alpha_{LO, True}$	$\alpha_{HO, True}$
0.0	67.8	202.6	231.0	29.3%	12.3%	17.0%	6.8%
UF Readings				$\alpha_{LU, Bulk}$	$\alpha_{HU, Bulk}$	$\alpha_{LU, True}$	$\alpha_{HU, True}$
0.0	26.0	100.0	227.5	11.4%	56.0%	6.2%	33.5%
OF Readings				$\alpha_{LO, Bulk}$	$\alpha_{HO, Bulk}$	$\alpha_{LO, True}$	$\alpha_{HO, True}$
0.0	69.0	202.5	229.5	30.1%	11.7%	17.4%	6.4%

APPENDIX 3 - MODEL COMPARISONS:

The mathematical model introduced in Chapter 2 (see Section 2.3) was used to predict the performance of Column A for various figures in Chapter 4 and Appendix 5. However, different forms of $F(\alpha_f, \Re_p)$ in Eq. 2-25 to 2-28 lead to different predictions (see Section 2.2) when using this model.

Figures A3-1 through A3-4 show experimental results as well as model predictions for Column A, System II, at a feed rate of 55.8 ml/s (chosen as an example). The forms of $F(\alpha_f, \Re_p)$ referred to are given in Table 2-2. It was found that the widely utilized relationship suggested by Richardson and Zaki generally yielded the closest match to the experimental results. Thus, this form of $F(\alpha_f, \Re_p)$ was depicted on the graphs in Chapter 4 and Appendix 5.

Also included are samples of the model calculation worksheets that were used (Tables A3-1 and A3-2). In all cases, a Gauss-Siedel iterative method was used, with a relaxation factor of 0.8. Within 20 iterations, solutions converged with a tolerance of 10^{-6}.

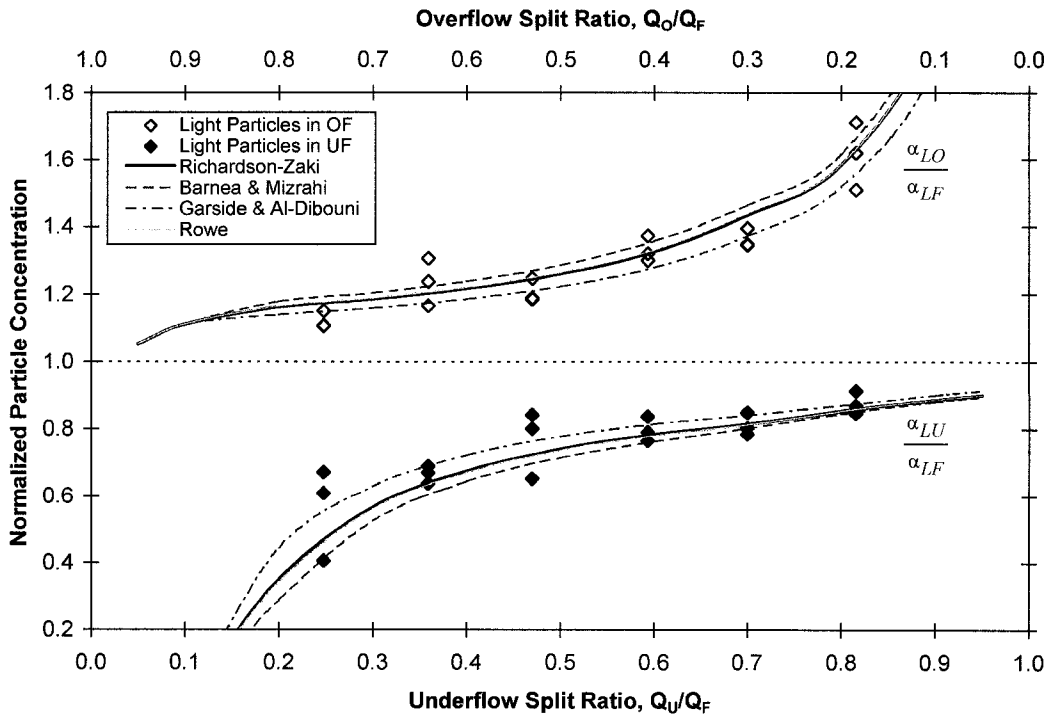

Figure A3-1. Measured and Predicted Light Particle Concentrations for Column A, System II (α_{LF} = 0.134, α_{HF} = 0.163), Feed Rate 55.8 ml/s

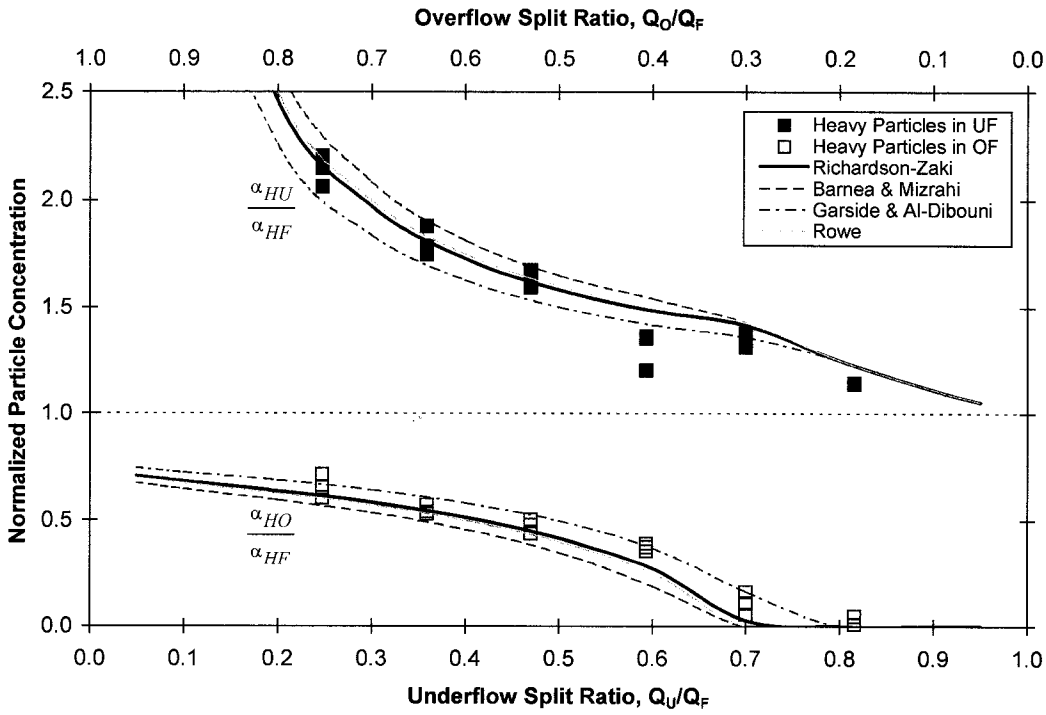

Figure A3-2. Measured and Predicted Heavy Particle Concentrations for for Column A, System II (α_{LF} = 0.134, α_{HF} = 0.163), Feed Rate 55.8 ml/s

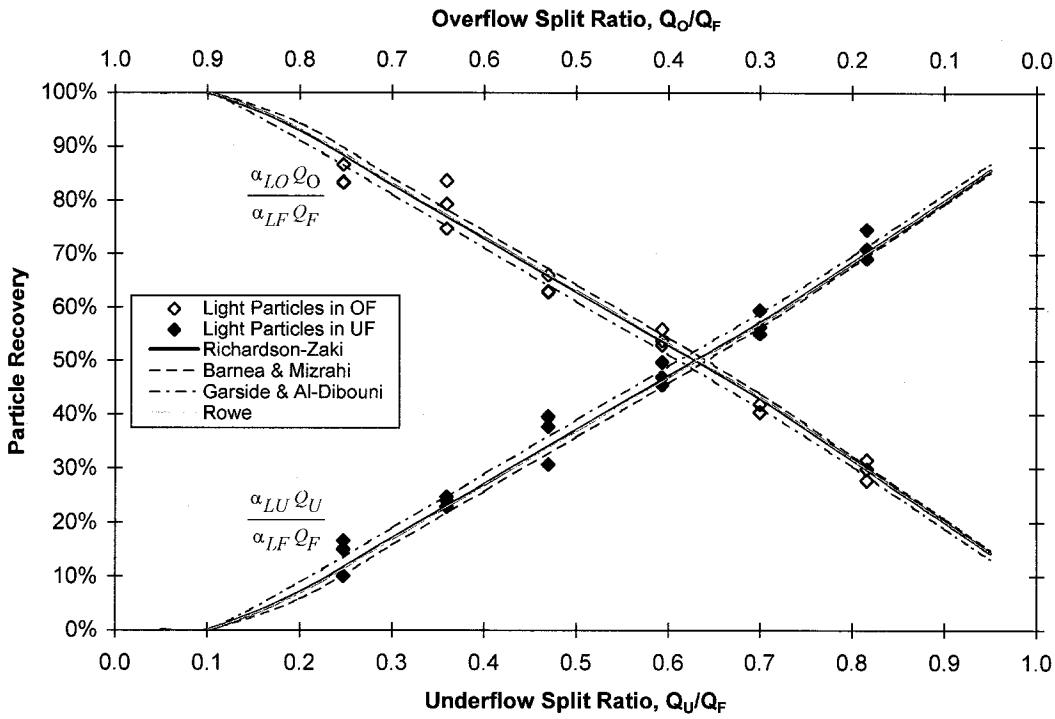

Figure A3-3. Measured and Predicted Light Particle Recoveries for Column A, System II (α_{LF} = 0.134, α_{HF} = 0.163), Feed Rate 55.8 ml/s

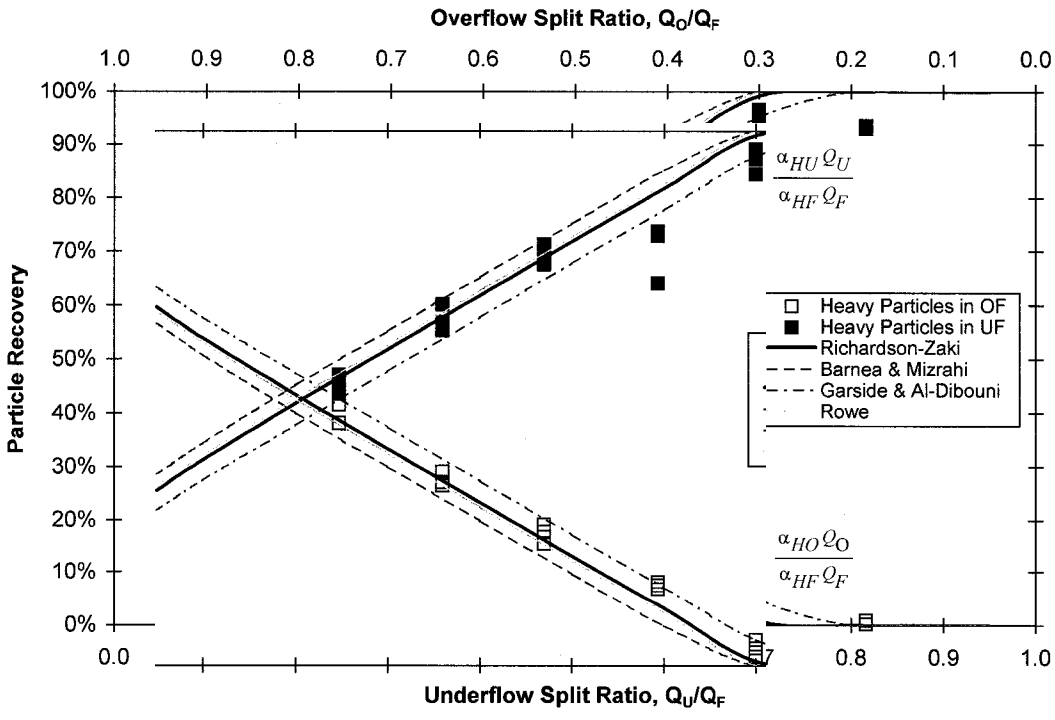

Figure A3-4. Measured and Predicted Heavy Particle Recoveries for Column A, System II (α_{LF} = 0.134, α_{HF} = 0.163), Feed Rate 55.8 ml/s

Table A3-1. Sample Model Calculation Worksheets for Column A, System II (α_{LF} = 0.134, α_{HF} = 0.163), Feed Rate 55.8 ml/s

System Parameters			mks Units
Q_F	55.8 mL/s	=	5.58E-05 m^3/s
D	80 mm	=	8.00E-02 m
A	5027 mm^2	=	5.03E-03 m^2
g	9.81 m/s^2	=	9.81E+00 m/s^2

Component Properties			mks Units
α_{LF}	13.4 vol %	=	0.134 vol frac
α_{HF}	16.3 vol %	=	0.163 vol frac
α_{fF}	70.3 vol %	=	0.703 vol frac
d_L	137 μm	=	1.37E-04 m
ρ_L	749 kg/m^3	=	7.49E+02 kg/m^3
d_H	459 μm	=	4.59E-04 m
ρ_H	1052 kg/m^3	=	1.05E+03 kg/m^3
ρ_f	997 kg/m^3	=	9.97E+02 kg/m^3
μ_f	0.931 mPa*s	=	9.31E-04 Pa*s

v_{Stokes} & Re_{Stokes}			mks Units	% Error
$v_{L,Stokes}$	-2.731 mm/s	=	-2.73E-03 m/s	+6.04%
$v_{H,Stokes}$	6.712 mm/s	=	6.71E-03 m/s	+23.17%
$Re_{L,Stokes}$	0.401	=	4.01E-01	+50.73%
$Re_{H,Stokes}$	3.298	=	3.30E+00	+75.09%

v_{inf} & Re_{inf}			mks Units	v_{Dummy}
$v_{L,inf}$	-2.575 mm/s	=	-2.58E-03 m/s	-2.575
$v_{H,inf}$	5.450 mm/s	=	5.45E-03 m/s	5.450
$Re_{L,inf}$	0.266	=	2.66E-01	
$Re_{H,inf}$	1.884	=	1.88E+00	

Richardson-Zaki	
n_L	4.56
n_H	4.27

Barnea & Mizrahi	
$F(\alpha_F)$	0.426

Garside & Al-Dibouni	
n_L	5.03
n_H	4.74

Rowe	
n_L	4.56
n_H	4.18

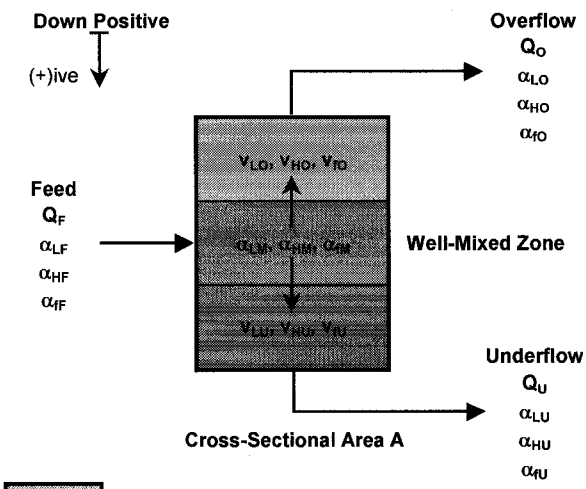

Table A3-2. Sample Numerical Analysis for Various Forms of $F(\alpha_f, \Re_p)$

Richardson-Zaki Hindered Settling Numerics

Iteration Parameters	
Q_U/Q_F	0.050
Q_O	5.30E-05 m^3/s
Q_U	2.79E-06 m^3/s
W	0.8

Max. Error:	0.000024%

Variables	Guess	1	2		19	20	Final	% Error
α_{LM}	**0.1177**	0.1531	0.1108		0.1236	0.1236	**0.1236**	0.000000%
α_{HM}	**0.1656**	0.2153	0.1419		0.1645	0.1645	**0.1645**	0.000001%
α_{fM}	**0.7167**	0.6316	0.7472		0.7120	0.7120	**0.7120**	0.000000%
ρ_{susp}	**977.2**	971.2	977.7		975.7	975.7	**975.7**	0.000000%
Re_{LO}	**0.10903**	0.10903	0.01542		0.10584	0.10584	**0.10584**	0.000000%
v_{LO}	**-0.00919**	-0.01277	-0.01190		-0.01204	-0.01204	**-0.01204**	0.000000%
Re_{LU}	**0.02416**	0.02416	0.11693		0.00598	0.00598	**0.00598**	0.000023%
v_{LU}	**0.00000**	0.00206	0.00000		0.00000	0.00000	**0.00000**	0.000000%
Re_{HO}	**1.28918**	1.28918	1.26167		1.28715	1.28715	**1.28715**	0.000002%
v_{HO}	**-0.00449**	-0.00887	-0.00700		-0.00735	-0.00735	**-0.00735**	0.000000%
Re_{HU}	**1.28918**	1.28918	0.74393		1.28715	1.28715	**1.28715**	0.000003%
v_{HU}	**0.00343**	0.00572	0.00329		0.00362	0.00362	**0.00362**	0.000001%
v_{fO}	**-0.00815**	-0.01294	-0.01053		-0.01103	-0.01103	**-0.01103**	0.000000%
v_{fU}	**-0.00023**	0.00332	-0.00133		-0.00006	-0.00006	**-0.00006**	0.000024%

Barnea & Mizrahi Hindered Settling Numerics

Iteration Parameters	
Q_U/Q_F	0.050
Q_O	5.30E-05 m^3/s
Q_U	2.79E-06 m^3/s
W	0.8

Max. Error:	0.000000%

Variables	Guess	1	2		19	20	Final	% Error
α_{LM}	**0.1160**	0.1509	0.1103		0.1222	0.1222	**0.1222**	0.000000%
α_{HM}	**0.1659**	0.2157	0.1421		0.1647	0.1647	**0.1647**	0.000000%
α_{fM}	**0.7181**	0.6334	0.7476		0.7131	0.7131	**0.7131**	0.000000%
ρ_{susp}	**977.7**	971.7	977.8		976.1	976.1	**976.1**	0.000000%
v_{LO}	**-0.00932**	-0.01295	-0.01201		-0.01217	-0.01217	**-0.01217**	0.000000%
v_{LU}	**0.00000**	0.00191	0.00000		0.00000	0.00000	**0.00000**	0.000000%
v_{HO}	**-0.00416**	-0.00849	-0.00670		-0.00700	-0.00700	**-0.00700**	0.000000%
v_{HU}	**0.00374**	0.00608	0.00356		0.00395	0.00395	**0.00395**	0.000000%
v_{fO}	**-0.00821**	-0.01301	-0.01058		-0.01108	-0.01108	**-0.01108**	0.000000%
v_{fU}	**-0.00030**	0.00324	-0.00141		-0.00013	-0.00013	**-0.00013**	0.000000%

Garside & Al-Dibouni Hindered Settling Numerics

Iteration Parameters	
Q_U/Q_F	0.050
Q_O	5.30E-05 m^3/s
Q_U	2.79E-06 m^3/s
W	0.8

Max. Error:	0.000088%

Variables	Guess	1	2		19	20	Final	% Error
α_{LM}	**0.1207**	0.1569	0.1116		0.1259	0.1259	**0.1259**	0.000000%
α_{HM}	**0.1650**	0.2146	0.1415		0.1640	0.1640	**0.1640**	0.000001%
α_{fM}	**0.7143**	0.6285	0.7469		0.7101	0.7101	**0.7101**	0.000000%
ρ_{susp}	**976.5**	970.2	977.4		975.1	975.1	**975.1**	0.000000%
Re_{LO}	**0.09196**	0.09196	0.02933		0.08930	0.08930	**0.08930**	0.000001%
v_{LO}	**-0.00896**	-0.01255	-0.01170		-0.01182	-0.01182	**-0.01182**	0.000000%
Re_{LU}	**0.01459**	0.01459	0.10712		0.00374	0.00374	**0.00374**	0.000088%
v_{LU}	**0.00000**	0.00228	0.00000		0.00000	0.00000	**0.00000**	0.000000%
Re_{HO}	**1.11848**	1.11848	1.09313		1.11387	1.11387	**1.11387**	0.000002%
v_{HO}	**-0.00490**	-0.00933	-0.00740		-0.00777	-0.00777	**-0.00777**	0.000000%
Re_{HU}	**1.11848**	1.11848	0.57666		1.11387	1.11387	**1.11387**	0.000003%
v_{HU}	**0.00305**	0.00531	0.00291		0.00323	0.00323	**0.00323**	0.000001%
v_{fO}	**-0.00809**	-0.01287	-0.01048		-0.01096	-0.01096	**-0.01096**	0.000000%
v_{fU}	**-0.00014**	0.00344	-0.00124		0.00004	0.00004	**0.00004**	0.000017%

Rowe Hindered Settling Numerics

Iteration Parameters	
Q_U/Q_F	0.050
Q_O	5.30E-05 m^3/s
Q_U	2.79E-06 m^3/s
W	0.8

Max. Error:	0.000020%

Variables	Guess	1	2		19	20	Final	% Error
α_{LM}	**0.1175**	0.1528	0.1107		0.1234	0.1234	**0.1234**	0.000000%
α_{HM}	**0.1656**	0.2153	0.1419		0.1645	0.1645	**0.1645**	0.000001%
α_{fM}	**0.7169**	0.6319	0.7473		0.7121	0.7121	**0.7121**	0.000000%
ρ_{susp}	**977.3**	971.2	977.7		975.8	975.8	**975.8**	0.000000%
Re_{LO}	**0.10915**	0.10915	0.01547		0.10593	0.10593	**0.10593**	0.000000%
v_{LO}	**-0.00921**	-0.01280	-0.01192		-0.01206	-0.01206	**-0.01206**	0.000000%
Re_{LU}	**0.02621**	0.02621	0.11661		0.00807	0.00807	**0.00807**	0.000010%
v_{LU}	**0.00000**	0.00205	0.00000		0.00000	0.00000	**0.00000**	0.000000%
Re_{HO}	**1.32574**	1.32574	1.29868		1.32441	1.32441	**1.32441**	0.000002%
v_{HO}	**-0.00440**	-0.00878	-0.00691		-0.00726	-0.00726	**-0.00726**	0.000000%
Re_{HU}	**1.32574**	1.32574	0.78048		1.32441	1.32441	**1.32441**	0.000003%
v_{HU}	**0.00351**	0.00582	0.00336		0.00371	0.00371	**0.00371**	0.000000%
v_{fO}	**-0.00817**	-0.01296	-0.01055		-0.01104	-0.01104	**-0.01104**	0.000000%
v_{fU}	**-0.00025**	0.00330	-0.00135		-0.00008	-0.00008	**-0.00008**	0.000020%

APPENDIX 4 - TABLES OF RESULTS:

Table A4-1. System Summary Chart

Column A, System I, All Feed Rates

Component Densities		Other Properties	
ρ_L (kg/m^3)	1052	d_L (μm)	386
ρ_H (kg/m^3)	1184	d_H (μm)	194
ρ_f (kg/m^3)	1067	μ_f (mPa*s)	1.41

System Compostion	
α_{LF}	0.0577
α_{HF}	0.1223
α_{fF}	0.8200

Overall Density	
ρ_{avg} (kg/m^3)	1080.4

System Flow Rates			
	M_F (g/s)	Q_F (m^3/s)	Q_F (ml/s)
Rate 1	43.83	4.06E-05	40.6
Rate 2	64.17	5.94E-05	59.4
Rate 3	88.01	8.15E-05	81.5
Rate 4	126.90	1.17E-04	117

Column A, System II, All Feed Rates

Component Densities		Other Properties	
ρ_L (kg/m^3)	749	d_L (μm)	137
ρ_H (kg/m^3)	1052	d_H (μm)	459
ρ_f (kg/m^3)	997	μ_f (mPa*s)	0.931

System Compostion	
α_{LF}	0.1340
α_{HF}	0.1625
α_{fF}	0.7035

Overall Density	
ρ_{avg} (kg/m^3)	973.0

System Flow Rates			
	M_F (g/s)	Q_F (m^3/s)	Q_F (ml/s)
Rate 1	37.82	3.89E-05	38.9
Rate 2	54.29	5.58E-05	55.8
Rate 3	72.18	7.42E-05	74.2
Rate 4	99.28	1.02E-04	102

Column B, System I, All Feed Rates

Component Densities		Other Properties	
ρ_L (kg/m^3)	1052	d_L (μm)	386
ρ_H (kg/m^3)	1184	d_H (μm)	194
ρ_f (kg/m^3)	1067	μ_f (mPa*s)	1.41

System Compostion	
α_{LF}	0.0577
α_{HF}	0.1223
α_{fF}	0.8200

Overall Density	
ρ_{avg} (kg/m^3)	1080.4

System Flow Rates			
	M_F (g/s)	Q_F (m^3/s)	Q_F (ml/s)
Rate 1	44.57	4.13E-05	41.3
Rate 2	64.25	5.95E-05	59.5
Rate 3	90.26	8.35E-05	83.5
Rate 4	127.90	1.18E-04	118

Column C, System I, All Feed Rates

Component Densities		Other Properties	
ρ_L (kg/m^3)	1052	d_L (μm)	386
ρ_H (kg/m^3)	1184	d_H (μm)	194
ρ_f (kg/m^3)	1067	μ_f (mPa*s)	1.41

System Compostion	
α_{LF}	0.0577
α_{HF}	0.1223
α_{fF}	0.8200

Overall Density	
ρ_{avg} (kg/m^3)	1080.4

System Flow Rates			
	M_F (g/s)	Q_F (m^3/s)	Q_F (ml/s)
Rate 1	47.33	4.38E-05	43.8
Rate 2	63.38	5.87E-05	58.7
Rate 3	90.75	8.40E-05	84.0

Table A4-2. Experimental Results for Column A, System I, All Flow Rates

Feed Composition	
α_{LF}	0.058
α_{HF}	0.122
α_{RF}	0.820

Column A - Flow Rate 1 - Concentration

UF SR	OF SR	α_{LU}	α_{HU}	α_{LO}	α_{HO}
0.320	0.680	0.040	0.166	0.067	0.101
0.320	0.680	0.033	0.166	0.066	0.099
0.320	0.680	0.039	0.166	0.067	0.097
0.485	0.515	0.047	0.145	0.068	0.096
0.485	0.515	0.046	0.152	0.067	0.099
0.485	0.515	0.042	0.153	0.074	0.084
0.691	0.309	0.051	0.135	0.074	0.078
0.691	0.309	0.046	0.140	0.081	0.085
0.691	0.309	0.048	0.139	0.080	0.081

Column A - Flow Rate 1 - Normalized Concentration

UF SR	OF SR	α_{LU}	α_{HU}	α_{LO}	α_{HO}
0.320	0.680	0.702	1.360	1.169	0.823
0.320	0.680	0.573	1.366	1.139	0.806
0.320	0.680	0.675	1.361	1.154	0.796
0.485	0.515	0.820	1.188	1.184	0.783
0.485	0.515	0.797	1.243	1.154	0.810
0.485	0.515	0.726	1.249	1.290	0.689
0.691	0.309	0.869	1.105	1.284	0.638
0.691	0.309	0.802	1.143	1.401	0.693
0.691	0.309	0.825	1.139	1.388	0.659

Column A - Flow Rate 1 - Recovery

UF SR	OF SR	R_{LU}	R_{HU}	R_{LO}	R_{HO}
0.320	0.680	22.5%	43.6%	79.4%	55.9%
0.320	0.680	18.4%	43.4%	77.4%	54.8%
0.320	0.680	21.6%	43.6%	78.4%	54.1%
0.485	0.515	39.8%	57.6%	61.0%	40.3%
0.485	0.515	38.7%	60.3%	59.4%	41.7%
0.485	0.515	35.2%	60.6%	66.4%	35.5%
0.691	0.309	61.4%	76.3%	39.7%	19.7%
0.691	0.309	56.4%	78.9%	43.3%	21.4%
0.691	0.309	57.0%	78.7%	42.9%	20.4%

Column A - Flow Rate 2 - Concentration

UF SR	OF SR	α_{LU}	α_{HU}	α_{LO}	α_{HO}
0.238	0.762	0.037	0.181	0.067	0.116
0.238	0.762	0.034	0.171	0.069	0.123
0.463	0.537	0.046	0.146	0.066	0.107
0.463	0.537	0.048	0.147	0.067	0.104
0.588	0.412	0.046	0.150	0.070	0.111
0.588	0.412	0.048	0.143	0.072	0.101
0.588	0.412	0.045	0.145	0.075	0.098
0.714	0.286	0.045	0.136	0.073	0.091
0.714	0.286	0.045	0.135	0.080	0.085
0.714	0.286	0.049	0.142	0.071	0.093
0.839	0.161	0.051	0.141	0.095	0.089
0.839	0.161	0.047	0.134	0.087	0.082
0.839	0.161	0.051	0.143	0.090	0.074

Column A - Flow Rate 2 - Normalized Concentration

UF SR	OF SR	α_{LU}	α_{HU}	α_{LO}	α_{HO}
0.238	0.762	0.641	1.477	1.166	0.946
0.238	0.762	0.591	1.396	1.192	1.003
0.463	0.537	0.795	1.197	1.144	0.872
0.463	0.537	0.824	1.201	1.166	0.847
0.588	0.412	0.802	1.228	1.218	0.911
0.588	0.412	0.830	1.170	1.244	0.823
0.588	0.412	0.788	1.186	1.297	0.801
0.714	0.286	0.768	1.116	1.265	0.748
0.714	0.286	0.763	1.105	1.361	0.698
0.714	0.286	0.852	1.162	1.233	0.764
0.839	0.161	0.875	1.154	1.654	0.730
0.839	0.161	0.811	1.097	1.513	0.672
0.839	0.161	0.877	1.166	1.566	0.604

Column A - Flow Rate 2 - Recovery

UF SR	OF SR	R_{LU}	R_{HU}	R_{LO}	R_{HO}
0.238	0.762	15.2%	35.1%	88.9%	72.1%
0.238	0.762	14.0%	33.2%	90.9%	76.5%
0.463	0.537	36.5%	55.4%	61.4%	46.8%
0.463	0.537	38.1%	55.6%	62.6%	45.5%
0.588	0.412	47.2%	72.3%	50.1%	37.5%
0.588	0.412	48.8%	68.8%	51.2%	33.9%
0.588	0.412	46.4%	69.8%	53.4%	33.0%
0.714	0.286	56.2%	79.6%	36.2%	21.4%
0.714	0.286	55.9%	78.9%	39.5%	20.0%
0.714	0.286	60.8%	82.9%	35.3%	21.9%
0.839	0.161	73.5%	96.8%	26.6%	11.8%
0.839	0.161	68.0%	92.0%	24.4%	10.8%
0.839	0.161	73.6%	97.9%	25.0%	9.7%

Column A - Flow Rate 3 - Concentration

UF SR	OF SR	α_{LU}	α_{HU}	α_{LO}	α_{HO}
0.255	0.745	0.044	0.176	0.057	0.124
0.255	0.745	0.041	0.156	0.060	0.121
0.255	0.745	0.041	0.159	0.066	0.111
0.348	0.652	0.046	0.145	0.061	0.105
0.348	0.652	0.046	0.139	0.066	0.109
0.348	0.652	0.042	0.160	0.059	0.118
0.441	0.559	0.056	0.134	0.058	0.105
0.441	0.559	0.046	0.132	0.061	0.099
0.441	0.559	0.045	0.140	0.062	0.098
0.534	0.466	0.051	0.138	0.061	0.098
0.534	0.466	0.047	0.136	0.063	0.100
0.534	0.466	0.053	0.128	0.069	0.096
0.628	0.372	0.050	0.132	0.066	0.096
0.628	0.372	0.052	0.129	0.066	0.092
0.628	0.372	0.048	0.136	0.075	0.096
0.628	0.372	0.047	0.130	0.066	0.099
0.721	0.279	0.049	0.127	0.069	0.086
0.721	0.279	0.050	0.127	0.068	0.096
0.721	0.279	0.050	0.141	0.077	0.095
0.814	0.186	0.053	0.125	0.070	0.082
0.814	0.186	0.054	0.127	0.092	0.080
0.814	0.186	0.049	0.133	0.071	0.081

Column A - Flow Rate 3 - Normalized Concentration

UF SR	OF SR	α_{LU}	α_{HU}	α_{LO}	α_{HO}
0.255	0.745	0.771	1.439	0.993	1.011
0.255	0.745	0.717	1.279	1.034	0.993
0.255	0.745	0.719	1.302	1.140	0.910
0.348	0.652	0.804	1.184	1.054	0.856
0.348	0.652	0.805	1.140	1.146	0.894
0.348	0.652	0.734	1.231	1.029	0.964
0.441	0.559	0.967	1.092	1.011	0.880
0.441	0.559	0.790	1.079	1.060	0.812
0.441	0.559	0.785	1.141	1.081	0.802
0.534	0.466	0.884	1.125	1.056	0.802
0.534	0.466	0.823	1.110	1.098	0.814
0.534	0.466	0.917	1.051	1.193	0.788
0.628	0.372	0.859	1.062	1.146	0.787
0.628	0.372	0.892	1.053	1.146	0.754
0.628	0.372	0.831	1.110	1.306	0.788
0.628	0.372	0.813	1.065	1.146	0.809
0.721	0.279	0.860	1.038	1.203	0.705
0.721	0.279	0.868	1.042	1.173	0.786
0.721	0.279	0.866	1.149	1.328	0.778
0.814	0.186	0.923	1.025	1.206	0.672
0.814	0.186	0.944	1.041	1.593	0.658
0.814	0.186	0.854	1.087	1.239	0.662

Column A - Flow Rate 3 - Recovery

UF SR	OF SR	R_{LU}	R_{HU}	R_{LO}	R_{HO}
0.255	0.745	19.6%	36.6%	74.0%	75.3%
0.255	0.745	18.3%	32.6%	77.1%	74.0%
0.255	0.745	18.3%	33.2%	86.0%	67.8%
0.348	0.652	28.0%	41.2%	68.7%	55.8%
0.348	0.652	28.0%	39.7%	74.7%	58.3%
0.348	0.652	25.5%	42.8%	67.1%	62.9%
0.441	0.559	42.6%	48.2%	56.5%	48.0%
0.441	0.559	34.8%	47.6%	59.3%	45.4%
0.441	0.559	34.6%	50.3%	60.4%	44.8%
0.534	0.466	47.2%	60.1%	49.2%	37.4%
0.534	0.466	43.9%	59.3%	51.1%	37.9%
0.534	0.466	49.0%	56.1%	55.6%	36.7%
0.628	0.372	53.9%	67.9%	42.7%	29.3%
0.628	0.372	56.0%	66.1%	42.7%	28.1%
0.628	0.372	52.1%	69.7%	48.6%	29.3%
0.628	0.372	51.0%	66.8%	42.7%	30.1%
0.721	0.279	61.3%	74.8%	33.6%	19.7%
0.721	0.279	62.6%	75.1%	32.8%	21.9%
0.721	0.279	62.4%	82.8%	37.1%	21.7%
0.814	0.186	75.1%	83.4%	22.4%	12.5%
0.814	0.186	76.8%	84.7%	29.6%	12.2%
0.814	0.186	69.5%	88.4%	23.0%	12.3%

Column A - Flow Rate 4 - Concentration

UF SR	OF SR	α_{LU}	α_{HU}	α_{LO}	α_{HO}
0.114	0.886	0.037	0.165	0.057	0.117
0.114	0.886	0.039	0.157	0.058	0.112
0.114	0.886	0.037	0.150	0.063	0.122
0.242	0.758	0.050	0.143	0.060	0.105
0.242	0.758	0.043	0.133	0.059	0.113
0.242	0.758	0.045	0.136	0.066	0.131
0.370	0.630	0.054	0.132	0.064	0.107
0.370	0.630	0.049	0.132	0.061	0.112
0.370	0.630	0.047	0.134	0.065	0.104
0.498	0.502	0.048	0.129	0.063	0.105
0.498	0.502	0.049	0.127	0.062	0.110
0.626	0.374	0.056	0.127	0.062	0.102
0.626	0.374	0.049	0.124	0.065	0.103
0.626	0.374	0.053	0.126	0.064	0.113
0.754	0.246	0.057	0.130	0.066	0.092
0.754	0.246	0.050	0.130	0.063	0.098
0.754	0.246	0.054	0.129	0.067	0.073
0.882	0.118	0.054	0.126	0.083	0.050
0.882	0.118	0.054	0.127	0.080	0.052
0.882	0.118	0.055	0.130	0.076	0.062

Column A - Flow Rate 4 - Normalized Concentration

UF SR	OF SR	α_{LU}	α_{HU}	α_{LO}	α_{HO}
0.114	0.886	0.639	1.350	0.990	0.953
0.114	0.886	0.676	1.281	1.004	0.918
0.114	0.886	0.647	1.223	1.094	0.998
0.242	0.758	0.866	1.166	1.032	0.860
0.242	0.758	0.747	1.084	1.016	0.926
0.242	0.758	0.788	1.110	1.121	1.072
0.370	0.630	0.933	1.077	1.113	0.876
0.370	0.630	0.842	1.079	1.062	0.916
0.370	0.630	0.806	1.100	1.122	0.847
0.498	0.502	0.826	1.051	1.091	0.858
0.498	0.502	0.844	1.036	1.072	0.897
0.626	0.374	0.963	1.037	1.070	0.832
0.626	0.374	0.842	1.017	1.130	0.842
0.626	0.374	0.922	1.027	1.108	0.926
0.754	0.246	0.986	1.065	1.146	0.755
0.754	0.246	0.875	1.065	1.087	0.801
0.754	0.246	0.942	1.056	1.156	0.600
0.882	0.118	0.941	1.022	1.433	0.411
0.882	0.118	0.942	1.040	1.393	0.421
0.882	0.118	0.948	1.065	1.301	0.506

Column A - Flow Rate 4 - Recovery

UF SR	OF SR	R_{LU}	R_{HU}	R_{LO}	R_{HO}
0.114	0.886	7.3%	15.4%	87.7%	84.4%
0.114	0.886	7.7%	14.7%	88.9%	81.3%
0.114	0.886	7.4%	14.0%	96.8%	88.4%
0.242	0.758	21.0%	28.3%	78.2%	66.2%
0.242	0.758	18.1%	26.3%	77.0%	70.2%
0.242	0.758	19.1%	26.9%	84.9%	81.2%
0.370	0.630	34.5%	39.9%	70.1%	56.2%
0.370	0.630	31.2%	39.9%	66.9%	57.7%
0.370	0.630	29.9%	40.7%	70.7%	53.3%
0.498	0.502	41.1%	52.3%	54.8%	43.1%
0.498	0.502	42.0%	51.6%	53.8%	45.0%
0.626	0.374	60.3%	64.9%	40.0%	31.1%
0.626	0.374	52.7%	63.7%	42.3%	31.5%
0.626	0.374	57.7%	64.3%	41.4%	34.6%
0.754	0.246	74.3%	80.2%	28.2%	18.6%
0.754	0.246	66.9%	80.3%	26.7%	19.7%
0.754	0.246	71.0%	79.6%	26.5%	14.8%
0.882	0.118	83.0%	90.1%	16.9%	4.9%
0.882	0.118	83.1%	91.7%	16.5%	5.0%
0.882	0.118	83.4%	93.9%	15.4%	6.0%

Table A4-3. Experimental Results for Column A, System II, All Flow Rates

Feed Composition	
α_{LF}	0.134
α_{HF}	0.163
α_{IF}	0.703

Column A - Flow Rate 1 - Concentration

UF SR	OF SR	α_{LU}	α_{HU}	α_{LO}	α_{HO}
0.346	0.654	0.068	0.340	0.173	0.069
0.346	0.654	0.058	0.363	0.170	0.068
0.346	0.654	0.062	0.335	0.174	0.064
0.524	0.476	0.085	0.295	0.184	0.029
0.524	0.476	0.089	0.275	0.171	0.021
0.524	0.476	0.093	0.267	0.179	0.038
0.691	0.309	0.105	0.239	0.203	0.005
0.691	0.309	0.096	0.244	0.200	0.004
0.691	0.309	0.083	0.228	0.201	0.001

Column A - Flow Rate 1 - Normalized Concentration

UF SR	OF SR	α_{LU}	α_{HU}	α_{LO}	α_{HO}
0.346	0.654	0.504	2.093	1.268	0.422
0.346	0.654	0.433	2.236	1.269	0.417
0.346	0.654	0.459	2.062	1.301	0.394
0.524	0.476	0.634	1.816	1.374	0.176
0.524	0.476	0.662	1.690	1.272	0.128
0.524	0.476	0.691	1.766	1.339	0.234
0.691	0.309	0.784	1.473	1.518	0.031
0.691	0.309	0.718	1.498	1.490	0.025
0.691	0.309	0.619	1.404	1.500	0.009

Column A - Flow Rate 1 - Recovery

UF SR	OF SR	R_{LU}	R_{HU}	R_{LO}	R_{HO}
0.346	0.654	17.4%	72.4%	84.2%	27.6%
0.346	0.654	15.0%	77.3%	83.0%	27.2%
0.346	0.654	15.9%	71.3%	85.1%	25.8%
0.524	0.476	33.2%	95.1%	65.5%	8.4%
0.524	0.476	34.7%	88.5%	60.6%	6.1%
0.524	0.476	36.2%	92.5%	63.8%	11.2%
0.691	0.309	54.1%	101.7%	47.0%	0.9%
0.691	0.309	49.6%	103.5%	46.1%	0.8%
0.691	0.309	42.7%	96.9%	46.4%	0.3%

Column A - Flow Rate 2 - Concentration

UF SR	OF SR	α_{LU}	α_{HU}	α_{LO}	α_{HO}
0.247	0.753	0.090	0.368	0.148	0.116
0.247	0.753	0.054	0.335	0.149	0.106
0.247	0.753	0.082	0.349	0.154	0.088
0.359	0.641	0.086	0.284	0.175	0.086
0.359	0.641	0.093	0.305	0.156	0.088
0.359	0.641	0.090	0.291	0.166	0.093
0.470	0.530	0.107	0.272	0.167	0.082
0.470	0.530	0.088	0.259	0.159	0.078
0.470	0.530	0.113	0.264	0.159	0.071
0.593	0.407	0.106	0.222	0.184	0.061
0.593	0.407	0.112	0.220	0.174	0.064
0.593	0.407	0.103	0.196	0.177	0.059
0.700	0.300	0.108	0.220	0.180	0.018
0.700	0.300	0.105	0.213	0.181	0.009
0.700	0.300	0.114	0.224	0.187	0.026
0.816	0.184	0.116	0.186	0.217	0.002
0.816	0.184	0.114	0.186	0.229	0.008
0.816	0.184	0.122	0.185	0.202	0.001

Column A - Flow Rate 2 - Normalized Concentration

UF SR	OF SR	α_{LU}	α_{HU}	α_{LO}	α_{HO}
0.247	0.753	0.672	2.203	1.106	0.713
0.247	0.753	0.406	2.062	1.108	0.651
0.247	0.753	0.609	2.147	1.151	0.605
0.359	0.641	0.639	1.747	1.306	0.530
0.359	0.641	0.690	1.880	1.166	0.540
0.359	0.641	0.671	1.790	1.237	0.571
0.470	0.530	0.802	1.676	1.247	0.504
0.470	0.530	0.654	1.594	1.189	0.478
0.470	0.530	0.842	1.628	1.186	0.438
0.593	0.407	0.791	1.367	1.373	0.376
0.593	0.407	0.837	1.353	1.300	0.393
0.593	0.407	0.766	1.204	1.319	0.357
0.700	0.300	0.803	1.352	1.345	0.109
0.700	0.300	0.786	1.312	1.347	0.056
0.700	0.300	0.849	1.380	1.395	0.162
0.816	0.184	0.869	1.146	1.620	0.010
0.816	0.184	0.848	1.144	1.712	0.047
0.816	0.184	0.914	1.139	1.510	0.009

Column A - Flow Rate 2 - Recovery

UF SR	OF SR	R_{LU}	R_{HU}	R_{LO}	R_{HO}
0.247	0.753	16.6%	54.5%	83.2%	53.7%
0.247	0.753	10.0%	51.0%	83.4%	49.0%
0.247	0.753	15.1%	53.1%	86.6%	45.5%
0.359	0.641	23.0%	62.8%	83.7%	34.0%
0.359	0.641	24.8%	67.5%	74.7%	34.6%
0.359	0.641	24.1%	64.3%	79.3%	36.6%
0.470	0.530	37.7%	78.7%	66.1%	26.7%
0.470	0.530	30.7%	74.9%	63.0%	25.3%
0.470	0.530	39.6%	76.5%	62.9%	23.2%
0.593	0.407	46.9%	81.1%	55.8%	15.3%
0.593	0.407	49.7%	80.2%	52.9%	16.0%
0.593	0.407	45.4%	71.4%	53.7%	14.5%
0.700	0.300	56.2%	94.6%	40.3%	3.3%
0.700	0.300	55.0%	91.9%	40.4%	1.7%
0.700	0.300	59.5%	96.6%	41.8%	4.9%
0.816	0.184	70.9%	93.5%	29.8%	0.2%
0.816	0.184	69.2%	93.3%	31.5%	0.9%
0.816	0.184	74.5%	92.9%	27.8%	0.2%

Column A - Flow Rate 3 - Concentration

UF SR	OF SR	α_{LU}	α_{HU}	α_{LO}	α_{HO}
0.240	0.760	0.091	0.281	0.152	0.112
0.240	0.760	0.061	0.301	0.157	0.120
0.240	0.760	0.078	0.279	0.160	0.121
0.356	0.644	0.093	0.303	0.149	0.113
0.356	0.644	0.092	0.260	0.159	0.126
0.356	0.644	0.101	0.257	0.154	0.125
0.458	0.542	0.110	0.260	0.156	0.107
0.458	0.542	0.105	0.261	0.159	0.110
0.458	0.542	0.080	0.219	0.163	0.093
0.540	0.460	0.132	0.227	0.162	0.082
0.540	0.460	0.115	0.201	0.152	0.083
0.540	0.460	0.095	0.213	0.154	0.092
0.629	0.371	0.100	0.195	0.176	0.060
0.629	0.371	0.118	0.196	0.165	0.069
0.629	0.371	0.105	0.209	0.174	0.064
0.706	0.294	0.122	0.199	0.161	0.035
0.706	0.294	0.120	0.225	0.169	0.046
0.706	0.294	0.115	0.226	0.195	0.030
0.786	0.214	0.119	0.211	0.184	0.004
0.786	0.214	0.123	0.218	0.223	0.033
0.786	0.214	0.121	0.197	0.206	0.004

Column A - Flow Rate 3 - Normalized Concentration

UF SR	OF SR	α_{LU}	α_{HU}	α_{LO}	α_{HO}
0.240	0.760	0.682	1.729	1.133	0.687
0.240	0.760	0.606	1.850	1.171	0.741
0.240	0.760	0.584	1.715	1.196	0.747
0.356	0.644	0.693	1.867	1.113	0.695
0.356	0.644	0.686	1.539	1.182	0.778
0.356	0.644	0.755	1.579	1.146	0.768
0.458	0.542	0.824	1.541	1.161	0.656
0.458	0.542	0.785	1.608	1.183	0.675
0.458	0.542	0.597	1.350	1.215	0.570
0.540	0.460	0.988	1.399	1.205	0.504
0.540	0.460	0.862	1.239	1.136	0.509
0.540	0.460	0.709	1.309	1.160	0.568
0.629	0.371	0.750	1.197	1.315	0.368
0.629	0.371	0.879	1.205	1.230	0.423
0.629	0.371	0.781	1.289	1.295	0.392
0.706	0.294	0.910	1.226	1.205	0.213
0.706	0.294	0.898	1.384	1.262	0.283
0.706	0.294	0.861	1.406	1.451	0.183
0.786	0.214	0.889	1.298	1.370	0.024
0.786	0.214	0.918	1.342	1.663	0.202
0.786	0.214	0.903	1.209	1.539	0.025

Column A - Flow Rate 3 - Recovery

UF SR	OF SR	R_{LU}	R_{HU}	R_{LO}	R_{HO}
0.240	0.760	16.4%	41.4%	86.1%	52.3%
0.240	0.760	14.5%	44.3%	89.0%	56.4%
0.240	0.760	14.0%	41.1%	91.0%	56.8%
0.356	0.644	24.6%	66.4%	71.7%	44.8%
0.356	0.644	24.4%	54.8%	76.2%	50.1%
0.356	0.644	26.9%	56.2%	73.9%	49.5%
0.458	0.542	37.7%	70.6%	63.0%	35.6%
0.458	0.542	35.9%	73.6%	64.2%	36.6%
0.458	0.542	27.3%	61.8%	65.9%	30.9%
0.540	0.460	53.3%	75.5%	55.5%	23.2%
0.540	0.460	46.5%	66.8%	52.3%	23.4%
0.540	0.460	38.2%	70.6%	53.0%	26.2%
0.629	0.371	47.2%	75.4%	46.7%	13.6%
0.629	0.371	55.4%	75.8%	45.6%	15.7%
0.629	0.371	49.2%	81.1%	48.0%	14.5%
0.706	0.294	64.2%	86.5%	35.5%	6.3%
0.706	0.294	63.3%	97.7%	37.1%	8.3%
0.706	0.294	60.8%	99.2%	42.7%	5.4%
0.786	0.214	69.9%	102.0%	29.3%	0.5%
0.786	0.214	72.1%	105.4%	35.6%	4.3%
0.786	0.214	70.9%	95.0%	33.0%	0.5%

Column A - Flow Rate 4 - Concentration

UF SR	OF SR	α_{LU}	α_{HU}	α_{LO}	α_{HO}
0.114	0.886	0.050	0.368	0.156	0.122
0.114	0.886	0.050	0.389	0.136	0.142
0.114	0.886	0.073	0.424	0.137	0.127
0.242	0.758	0.091	0.262	0.136	0.145
0.242	0.758	0.097	0.275	0.149	0.128
0.242	0.758	0.087	0.277	0.143	0.136
0.370	0.630	0.103	0.236	0.136	0.126
0.370	0.630	0.101	0.225	0.144	0.115
0.370	0.630	0.103	0.269	0.154	0.130
0.498	0.502	0.111	0.196	0.138	0.097
0.498	0.502	0.111	0.211	0.162	0.108
0.498	0.502	0.115	0.232	0.163	0.098
0.626	0.374	0.119	0.215	0.170	0.083
0.626	0.374	0.119	0.190	0.152	0.079
0.626	0.374	0.107	0.195	0.177	0.071
0.754	0.246	0.134	0.205	0.162	0.041
0.754	0.246	0.124	0.205	0.159	0.047
0.754	0.246	0.125	0.206	0.191	0.043
0.882	0.118	0.126	0.192	0.218	0.009
0.882	0.118	0.136	0.186	0.215	0.008
0.882	0.118	0.116	0.177	0.197	0.009

Column A - Flow Rate 4 - Normalized Concentration

UF SR	OF SR	α_{LU}	α_{HU}	α_{LO}	α_{HO}
0.114	0.886	0.371	2.266	1.166	0.750
0.114	0.886	0.375	2.394	1.012	0.873
0.114	0.886	0.548	2.612	1.019	0.780
0.242	0.758	0.680	1.615	1.012	0.894
0.242	0.758	0.723	1.692	1.114	0.786
0.242	0.758	0.647	1.707	1.064	0.834
0.370	0.630	0.767	1.452	1.012	0.774
0.370	0.630	0.755	1.387	1.072	0.707
0.370	0.630	0.768	1.694	1.160	0.802
0.498	0.502	0.827	1.218	1.026	0.595
0.498	0.502	0.826	1.300	1.134	0.662
0.498	0.502	0.860	1.428	1.214	0.606
0.626	0.374	0.887	1.325	1.272	0.512
0.626	0.374	0.885	1.170	1.136	0.486
0.626	0.374	0.800	1.201	1.323	0.436
0.754	0.246	0.996	1.261	1.209	0.255
0.754	0.246	0.929	1.261	1.187	0.267
0.754	0.246	0.936	1.270	1.427	0.263
0.882	0.118	0.929	1.181	1.629	0.057
0.882	0.118	1.008	1.148	1.601	0.051
0.882	0.118	0.864	1.086	1.468	0.058

Column A - Flow Rate 4 - Recovery

UF SR	OF SR	R_{LU}	R_{HU}	R_{LO}	R_{HO}
0.114	0.886	4.2%	25.9%	103.2%	66.4%
0.114	0.886	4.3%	27.4%	89.6%	77.3%
0.114	0.886	6.3%	29.9%	90.3%	69.1%
0.242	0.758	16.5%	39.1%	76.7%	67.7%
0.242	0.758	17.5%	41.0%	84.4%	59.5%
0.242	0.758	15.7%	41.4%	80.6%	63.2%
0.370	0.630	28.4%	53.8%	63.7%	48.7%
0.370	0.630	27.9%	51.4%	67.5%	44.5%
0.370	0.630	28.4%	59.0%	72.4%	50.5%
0.498	0.502	41.2%	60.7%	51.5%	29.9%
0.498	0.502	41.1%	64.7%	56.9%	33.2%
0.498	0.502	42.8%	71.1%	61.0%	30.4%
0.626	0.374	55.5%	82.9%	47.6%	19.1%
0.626	0.374	55.4%	73.2%	42.5%	18.2%
0.626	0.374	50.1%	75.2%	49.5%	16.3%
0.754	0.246	75.1%	95.1%	29.8%	6.3%
0.754	0.246	70.0%	95.1%	29.2%	7.1%
0.754	0.246	70.6%	95.7%	35.1%	6.5%
0.882	0.118	81.9%	104.1%	19.3%	0.7%
0.882	0.118	88.9%	101.2%	18.9%	0.6%
0.882	0.118	76.1%	95.8%	17.4%	0.7%

Table A4-4. Experimental Results for Column B, System I, All Flow Rates

Feed Composition	
α_{LF}	0.058
α_{HF}	0.122
α_{rF}	0.820

Column B - Trial Runs - Concentration

UF SR	OF SR	α_{LU}	α_{HU}	α_{LO}	α_{HO}
0.322	0.678	0.034	0.218	0.071	0.070
0.322	0.678	0.037	0.222	0.065	0.069
0.322	0.678	0.035	0.221	0.068	0.070
0.467	0.533	0.044	0.168	0.068	0.075
0.467	0.533	0.044	0.167	0.067	0.072
0.467	0.533	0.043	0.164	0.067	0.076
0.828	0.172	0.058	0.126	0.060	0.099
0.828	0.172	0.056	0.126	0.059	0.108
0.828	0.172	0.056	0.127	0.062	0.106

Column B - Trial Runs - Normalized Concentration

UF SR	OF SR	α_{LU}	α_{HU}	α_{LO}	α_{HO}
0.322	0.678	0.587	1.785	1.236	0.576
0.322	0.678	0.640	1.813	1.133	0.566
0.322	0.678	0.608	1.811	1.172	0.571
0.467	0.533	0.766	1.377	1.186	0.614
0.467	0.533	0.760	1.363	1.168	0.587
0.467	0.533	0.747	1.339	1.168	0.625
0.828	0.172	1.010	1.027	1.046	0.811
0.828	0.172	0.976	1.031	1.015	0.884
0.828	0.172	0.967	1.035	1.073	0.868

Column B - Trial Runs - Recovery

UF SR	OF SR	R_{LU}	R_{HU}	R_{LO}	R_{HO}
0.322	0.678	18.9%	57.5%	83.6%	39.1%
0.322	0.678	20.6%	58.4%	76.8%	38.4%
0.322	0.678	19.6%	58.3%	79.4%	38.7%
0.467	0.533	35.7%	64.3%	63.3%	32.7%
0.467	0.533	35.5%	63.6%	62.3%	31.3%
0.467	0.533	34.9%	62.5%	62.3%	33.3%
0.828	0.172	83.7%	85.0%	18.0%	13.9%
0.828	0.172	80.8%	85.4%	17.4%	15.2%
0.828	0.172	80.1%	85.7%	18.5%	14.9%

Column B - Flow Rate 1 - Concentration

UF SR	OF SR	α_{LU}	α_{HU}	α_{LO}	α_{HO}
0.141	0.859	0.026	0.263	0.060	0.093
0.141	0.859	0.030	0.262	0.061	0.099
0.141	0.859	0.029	0.259	0.063	0.099
0.250	0.750	0.038	0.240	0.061	0.075
0.250	0.750	0.033	0.240	0.064	0.079
0.250	0.750	0.036	0.236	0.063	0.081
0.358	0.642	0.037	0.212	0.069	0.086
0.358	0.642	0.042	0.210	0.064	0.088
0.358	0.642	0.041	0.213	0.066	0.070
0.467	0.533	0.050	0.172	0.067	0.071
0.467	0.533	0.043	0.175	0.072	0.076
0.467	0.533	0.047	0.170	0.063	0.081
0.575	0.425	0.047	0.143	0.070	0.096
0.575	0.425	0.047	0.145	0.069	0.103
0.575	0.425	0.051	0.140	0.064	0.108
0.684	0.316	0.054	0.129	0.069	0.115
0.684	0.316	0.051	0.126	0.067	0.114
0.684	0.316	0.057	0.133	0.068	0.114
0.792	0.208	0.064	0.118	0.044	0.123
0.792	0.208	0.062	0.116	0.044	0.123
0.792	0.208	0.056	0.126	0.051	0.120
0.864	0.136	0.060	0.116	0.039	0.142
0.864	0.136	0.063	0.126	0.042	0.133
0.864	0.136	0.056	0.126	0.039	0.131

Column B - Flow Rate 1 - Normalized Concentration

UF SR	OF SR	α_{LU}	α_{HU}	α_{LO}	α_{HO}
0.141	0.859	0.444	2.149	1.035	0.760
0.141	0.859	0.521	2.141	1.051	0.809
0.141	0.859	0.508	2.121	1.093	0.810
0.250	0.750	0.650	1.959	1.064	0.610
0.250	0.750	0.573	1.960	1.116	0.649
0.250	0.750	0.631	1.926	1.088	0.680
0.358	0.642	0.647	1.731	1.188	0.543
0.358	0.642	0.722	1.721	1.111	0.559
0.358	0.642	0.710	1.743	1.140	0.574
0.467	0.533	0.866	1.404	1.165	0.584
0.467	0.533	0.748	1.427	1.252	0.624
0.467	0.533	0.811	1.392	1.098	0.666
0.575	0.425	0.817	1.173	1.211	0.786
0.575	0.425	0.811	1.183	1.195	0.846
0.575	0.425	0.885	1.148	1.116	0.883
0.684	0.316	0.932	1.055	1.188	0.941
0.684	0.316	0.891	1.043	1.160	0.931
0.684	0.316	0.979	1.084	1.178	0.933
0.792	0.208	1.103	0.966	0.760	1.004
0.792	0.208	1.074	0.946	0.760	1.004
0.792	0.208	0.975	1.027	0.889	0.979
0.864	0.136	1.044	0.949	0.669	1.158
0.864	0.136	1.068	1.027	0.728	1.086
0.864	0.136	0.971	1.027	0.681	1.071

Column B - Flow Rate 1 - Recovery

UF SR	OF SR	R_{LU}	R_{HU}	R_{LO}	R_{HO}
0.141	0.859	6.3%	30.4%	88.9%	65.3%
0.141	0.859	7.4%	30.2%	90.3%	69.4%
0.141	0.859	7.2%	30.0%	93.8%	69.6%
0.250	0.750	16.2%	48.9%	79.8%	45.7%
0.250	0.750	14.3%	48.9%	83.7%	48.7%
0.250	0.750	15.8%	48.1%	81.6%	49.5%
0.358	0.642	23.2%	62.0%	76.3%	34.8%
0.358	0.642	25.9%	61.6%	71.3%	35.9%
0.358	0.642	25.4%	62.4%	73.2%	36.8%
0.467	0.533	40.4%	65.5%	62.1%	31.2%
0.467	0.533	34.9%	66.6%	66.8%	33.3%
0.467	0.533	37.8%	64.9%	63.6%	35.5%
0.575	0.425	47.0%	67.5%	51.4%	33.4%
0.575	0.425	46.6%	68.0%	50.8%	35.9%
0.575	0.425	50.9%	66.0%	47.4%	37.5%
0.684	0.316	63.7%	72.1%	37.6%	29.8%
0.684	0.316	60.9%	71.3%	36.7%	29.5%
0.684	0.316	66.9%	74.1%	37.3%	29.5%
0.792	0.208	87.3%	76.5%	15.8%	20.9%
0.792	0.208	85.1%	74.9%	15.8%	20.9%
0.792	0.208	77.2%	81.3%	18.5%	20.4%
0.864	0.136	90.3%	82.0%	9.1%	15.7%
0.864	0.136	94.0%	88.7%	9.9%	14.7%
0.864	0.136	84.0%	88.7%	9.2%	14.5%

Column B - Flow Rate 2 - Concentration

UF SR	OF SR	α_{LU}	α_{HU}	α_{LO}	α_{HO}
0.199	0.801	0.022	0.295	0.067	0.062
0.199	0.801	0.025	0.306	0.063	0.067
0.199	0.801	0.029	0.303	0.060	0.068
0.296	0.704	0.032	0.238	0.067	0.074
0.296	0.704	0.030	0.232	0.068	0.068
0.467	0.533	0.043	0.174	0.066	0.083
0.467	0.533	0.044	0.176	0.066	0.080
0.467	0.533	0.045	0.174	0.066	0.079
0.588	0.412	0.056	0.129	0.063	0.108
0.588	0.412	0.048	0.134	0.063	0.108
0.588	0.412	0.051	0.133	0.063	0.111
0.710	0.290	0.062	0.106	0.057	0.159
0.710	0.290	0.059	0.095	0.036	0.153
0.710	0.290	0.061	0.112	0.040	0.158
0.832	0.168	0.058	0.095	0.027	0.241
0.832	0.168	0.056	0.093	0.026	0.251
0.832	0.168	0.064	0.096	0.026	0.246

Column B - Flow Rate 2 - Normalized Concentration

UF SR	OF SR	α_{LU}	α_{HU}	α_{LO}	α_{HO}
0.199	0.801	0.382	2.414	1.155	0.506
0.199	0.801	0.430	2.501	1.083	0.549
0.199	0.801	0.503	2.477	1.037	0.559
0.296	0.704	0.552	1.945	1.158	0.602
0.296	0.704	0.512	1.898	1.175	0.554
0.467	0.533	0.753	1.422	1.141	0.677
0.467	0.533	0.763	1.441	1.147	0.653
0.467	0.533	0.773	1.424	1.145	0.648
0.588	0.412	0.967	1.059	1.090	0.887
0.588	0.412	0.825	1.094	1.093	0.884
0.588	0.412	0.876	1.087	1.092	0.907
0.710	0.290	1.073	0.868	0.979	1.298
0.710	0.290	1.027	0.775	0.624	1.252
0.710	0.290	1.053	0.917	0.693	1.291
0.832	0.168	1.003	0.776	0.472	1.972
0.832	0.168	0.963	0.757	0.454	2.053
0.832	0.168	1.110	0.777	0.456	2.009

Column B - Flow Rate 2 - Recovery

UF SR	OF SR	R_{LU}	R_{HU}	R_{LO}	R_{HO}
0.199	0.801	7.6%	48.0%	92.6%	40.6%
0.199	0.801	8.5%	49.7%	86.8%	44.0%
0.199	0.801	10.0%	49.3%	83.1%	44.8%
0.296	0.704	16.3%	57.6%	81.5%	42.4%
0.296	0.704	15.2%	56.2%	82.7%	39.0%
0.467	0.533	35.2%	66.4%	60.8%	36.1%
0.467	0.533	35.6%	67.2%	61.2%	34.9%
0.467	0.533	36.0%	66.4%	61.1%	34.6%
0.588	0.412	56.9%	62.3%	44.9%	36.5%
0.588	0.412	48.5%	64.4%	45.0%	36.4%
0.588	0.412	51.5%	64.0%	45.0%	37.3%
0.710	0.290	76.2%	61.7%	28.4%	37.6%
0.710	0.290	72.9%	55.0%	18.1%	36.3%
0.710	0.290	74.7%	65.1%	20.1%	37.4%
0.832	0.168	83.4%	64.6%	7.9%	33.2%
0.832	0.168	80.1%	63.0%	7.6%	34.6%
0.832	0.168	92.3%	64.6%	7.7%	33.8%

Column B - Flow Rate 3 - Concentration

UF SR	OF SR	α_{LU}	α_{HU}	α_{LO}	α_{HO}
0.090	0.910	0.012	0.456	0.062	0.076
0.090	0.910	0.008	0.475	0.065	0.078
0.090	0.910	0.004	0.476	0.059	0.074
0.359	0.641	0.036	0.215	0.070	0.066
0.359	0.641	0.042	0.208	0.068	0.061
0.359	0.641	0.040	0.221	0.068	0.073
0.263	0.737	0.038	0.272	0.079	0.072
0.263	0.737	0.035	0.257	0.080	0.075
0.263	0.737	0.037	0.262	0.085	0.069
0.263	0.737	0.032	0.267	0.076	0.067
0.263	0.737	0.031	0.277	0.084	0.066
0.455	0.545	0.040	0.168	0.067	0.090
0.455	0.545	0.039	0.162	0.068	0.091
0.455	0.545	0.043	0.164	0.070	0.091
0.551	0.449	0.057	0.113	0.062	0.111
0.551	0.449	0.056	0.116	0.054	0.112
0.551	0.449	0.063	0.128	0.054	0.112
0.648	0.352	0.066	0.101	0.030	0.148
0.648	0.352	0.064	0.102	0.030	0.147
0.648	0.352	0.089	0.097	0.029	0.143
0.744	0.256	0.063	0.093	0.027	0.209
0.744	0.256	0.062	0.087	0.025	0.220
0.744	0.256	0.068	0.088	0.026	0.209
0.840	0.160	0.065	0.078	0.024	0.320
0.840	0.160	0.068	0.080	0.015	0.328
0.840	0.160	0.063	0.083	0.022	0.323

Column B - Flow Rate 3 - Normalized Concentration

UF SR	OF SR	α_{LU}	α_{HU}	α_{LO}	α_{HO}
0.090	0.910	0.216	3.733	1.073	0.623
0.090	0.910	0.144	3.884	1.128	0.639
0.090	0.910	0.072	3.893	1.029	0.607
0.359	0.641	0.621	1.760	1.220	0.538
0.359	0.641	0.732	1.699	1.178	0.502
0.359	0.641	0.689	1.805	1.184	0.596
0.263	0.737	0.660	2.226	1.363	0.588
0.263	0.737	0.608	2.099	1.380	0.615
0.263	0.737	0.633	2.139	1.467	0.562
0.263	0.737	0.546	2.183	1.309	0.545
0.263	0.737	0.530	2.268	1.450	0.540
0.455	0.545	0.686	1.295	1.165	0.739
0.455	0.545	0.684	1.327	1.175	0.745
0.455	0.545	0.747	1.339	1.205	0.747
0.551	0.449	0.981	0.926	1.073	0.905
0.551	0.449	0.963	0.946	0.934	0.916
0.551	0.449	1.098	1.048	0.934	0.916
0.648	0.352	1.145	0.829	0.514	1.213
0.648	0.352	1.103	0.836	0.523	1.198
0.648	0.352	1.198	0.791	0.510	1.168
0.744	0.256	1.094	0.760	0.473	1.710
0.744	0.256	1.066	0.708	0.441	1.802
0.744	0.256	1.140	0.717	0.452	1.707
0.840	0.160	1.134	0.638	0.415	2.619
0.840	0.160	1.149	0.652	0.262	2.685
0.840	0.160	1.096	0.675	0.378	2.643

Column B - Flow Rate 3 - Recovery

UF SR	OF SR	R_{LU}	R_{HU}	R_{LO}	R_{HO}
0.090	0.910	1.9%	33.5%	97.6%	56.7%
0.090	0.910	1.3%	34.9%	102.7%	58.2%
0.090	0.910	0.6%	35.0%	93.7%	55.3%
0.359	0.641	22.3%	63.2%	78.2%	34.4%
0.359	0.641	26.3%	61.0%	75.5%	32.2%
0.359	0.641	24.7%	64.8%	75.9%	36.2%
0.263	0.737	17.4%	58.5%	100.5%	43.3%
0.263	0.737	16.0%	55.2%	101.7%	45.3%
0.263	0.737	16.6%	56.3%	108.1%	41.5%
0.263	0.737	14.4%	57.4%	96.5%	40.2%
0.263	0.737	13.9%	59.6%	106.9%	39.8%
0.455	0.545	31.2%	59.0%	63.5%	40.2%
0.455	0.545	31.1%	60.4%	64.0%	40.6%
0.455	0.545	34.0%	61.0%	65.7%	40.7%
0.551	0.449	54.1%	51.1%	48.1%	40.6%
0.551	0.449	53.1%	52.2%	41.9%	41.1%
0.551	0.449	60.6%	57.8%	41.9%	41.1%
0.648	0.352	74.2%	53.7%	18.1%	42.7%
0.648	0.352	71.4%	54.2%	18.4%	42.2%
0.648	0.352	77.6%	51.3%	16.0%	41.2%
0.744	0.256	81.4%	56.6%	12.1%	43.8%
0.744	0.256	79.3%	52.7%	11.3%	46.2%
0.744	0.256	84.8%	53.4%	11.6%	43.7%
0.840	0.160	95.2%	53.6%	6.6%	41.9%
0.840	0.160	96.5%	54.8%	4.2%	42.9%
0.840	0.160	92.1%	56.7%	6.1%	42.3%

Column B - Flow Rate 4 - Concentration

UF SR	OF SR	α_{LU}	α_{HU}	α_{LO}	α_{HO}
0.154	0.846	0.012	0.474	0.065	0.054
0.154	0.846	0.006	0.585	0.073	0.057
0.154	0.846	0.008	0.582	0.068	0.059
0.221	0.779	0.012	0.356	0.068	0.059
0.221	0.779	0.012	0.359	0.062	0.062
0.221	0.779	0.014	0.357	0.064	0.064
0.333	0.667	0.026	0.212	0.071	0.071
0.333	0.667	0.021	0.207	0.073	0.075
0.333	0.667	0.024	0.206	0.072	0.077
0.445	0.555	0.048	0.146	0.085	0.096
0.445	0.555	0.044	0.147	0.080	0.093
0.445	0.555	0.049	0.146	0.086	0.095
0.557	0.443	0.066	0.114	0.040	0.118
0.557	0.443	0.061	0.113	0.040	0.124
0.557	0.443	0.056	0.117	0.047	0.126
0.669	0.331	0.063	0.094	0.025	0.173
0.669	0.331	0.074	0.093	0.023	0.172
0.669	0.331	0.069	0.097	0.026	0.165
0.780	0.220	0.063	0.087	0.016	0.254
0.780	0.220	0.070	0.089	0.022	0.247
0.780	0.220	0.062	0.086	0.018	0.248
0.892	0.108	0.058	0.073	0.000	0.499
0.892	0.108	0.061	0.078	0.013	0.432
0.892	0.108	0.063	0.074	0.010	0.442

Column B - Flow Rate 4 - Normalized Concentration

UF SR	OF SR	α_{LU}	α_{HU}	α_{LO}	α_{HO}
0.154	0.846	0.212	3.880	1.124	0.439
0.154	0.846	0.106	4.787	1.264	0.469
0.154	0.846	0.142	4.759	1.183	0.479
0.221	0.779	0.205	2.909	1.175	0.485
0.221	0.779	0.212	2.937	1.080	0.510
0.221	0.779	0.249	2.922	1.109	0.523
0.333	0.667	0.446	1.737	1.229	0.580
0.333	0.667	0.358	1.690	1.261	0.614
0.333	0.667	0.424	1.686	1.256	0.632
0.445	0.555	0.832	1.195	1.125	0.786
0.445	0.555	0.765	1.203	1.048	0.761
0.445	0.555	0.841	1.191	1.140	0.775
0.557	0.443	1.140	0.933	0.696	0.967
0.557	0.443	1.063	0.926	0.690	1.013
0.557	0.443	0.972	0.955	0.818	1.029
0.669	0.331	1.090	0.772	0.432	1.411
0.669	0.331	1.267	0.759	0.395	1.405
0.669	0.331	1.201	0.789	0.450	1.345
0.780	0.220	1.094	0.714	0.284	2.078
0.780	0.220	1.219	0.731	0.379	2.016
0.780	0.220	1.073	0.706	0.311	2.024
0.892	0.108	1.001	0.596	0.000	4.080
0.892	0.108	1.053	0.640	0.220	3.534
0.892	0.108	1.065	0.607	0.181	3.612

Column B - Flow Rate 4 - Recovery

UF SR	OF SR	R_{LU}	R_{HU}	R_{LO}	R_{HO}
0.154	0.846	3.3%	59.9%	95.0%	37.2%
0.154	0.846	1.6%	73.9%	106.8%	39.6%
0.154	0.846	2.2%	73.5%	100.1%	40.5%
0.221	0.779	4.6%	64.4%	91.5%	37.8%
0.221	0.779	4.7%	65.0%	84.1%	39.7%
0.221	0.779	5.5%	64.7%	86.3%	40.7%
0.333	0.667	14.9%	57.9%	81.9%	38.7%
0.333	0.667	11.9%	56.3%	84.1%	41.0%
0.333	0.667	14.1%	56.2%	83.7%	42.1%
0.445	0.555	37.0%	53.2%	62.4%	43.6%
0.445	0.555	34.0%	53.5%	58.1%	42.2%
0.445	0.555	37.4%	53.0%	63.3%	43.0%
0.557	0.443	63.5%	51.9%	30.9%	42.8%
0.557	0.443	59.2%	51.5%	30.6%	44.9%
0.557	0.443	54.1%	53.2%	36.2%	45.6%
0.669	0.331	72.9%	51.6%	14.3%	46.8%
0.669	0.331	86.0%	50.7%	13.1%	46.6%
0.669	0.331	80.3%	52.8%	14.9%	44.6%
0.780	0.220	86.3%	55.7%	6.2%	45.6%
0.780	0.220	96.1%	57.0%	8.3%	44.3%
0.780	0.220	83.8%	55.1%	6.8%	44.4%
0.892	0.108	89.3%	53.2%	0.0%	44.0%
0.892	0.108	94.0%	57.1%	2.4%	38.1%
0.892	0.108	96.8%	54.2%	1.9%	38.9%

Table A4-5. Experimental Results for Column C, System I, All Flow Rates

Feed Composition	
α_{LF}	0.058
α_{HF}	0.122
α_{FF}	0.820

Column C - Flow Rate 1 - Concentration

UF SR	OF SR	α_{LU}	α_{HU}	α_{LO}	α_{HO}
0.292	0.708	0.051	0.186	0.065	0.102
0.292	0.708	0.046	0.183	0.063	0.100
0.292	0.708	0.043	0.186	0.059	0.100
0.427	0.573	0.048	0.160	0.060	0.097
0.427	0.573	0.050	0.164	0.059	0.101
0.427	0.573	0.050	0.162	0.060	0.094
0.596	0.404	0.053	0.146	0.055	0.126
0.596	0.404	0.052	0.120	0.059	0.101
0.596	0.404	0.056	0.146	0.061	0.101
0.765	0.235	0.050	0.147	0.066	0.083
0.765	0.235	0.056	0.144	0.070	0.082
0.765	0.235	0.055	0.142	0.075	0.081

Column C - Flow Rate 1 - Normalized Concentration

UF SR	OF SR	α_{LU}	α_{HU}	α_{LO}	α_{HO}
0.292	0.708	0.886	1.522	1.132	0.834
0.292	0.708	0.793	1.496	1.088	0.821
0.292	0.708	0.752	1.521	1.028	0.814
0.427	0.573	0.827	1.306	1.046	0.793
0.427	0.573	0.866	1.341	1.026	0.825
0.427	0.573	0.865	1.322	1.032	0.766
0.596	0.404	0.916	1.197	0.947	1.031
0.596	0.404	0.905	0.985	1.024	0.823
0.596	0.404	0.965	1.191	1.064	0.825
0.765	0.235	0.869	1.200	1.135	0.678
0.765	0.235	0.970	1.176	1.206	0.673
0.765	0.235	0.961	1.159	1.301	0.664

Column C - Flow Rate 1 - Recovery

UF SR	OF SR	R_{LU}	R_{HU}	R_{LO}	R_{HO}
0.292	0.708	25.8%	44.4%	80.2%	59.1%
0.292	0.708	23.1%	43.6%	77.0%	58.2%
0.292	0.708	21.9%	44.3%	72.8%	57.7%
0.427	0.573	36.3%	55.8%	59.9%	45.5%
0.427	0.573	37.0%	57.2%	58.8%	47.3%
0.427	0.573	36.9%	56.4%	59.2%	43.9%
0.596	0.404	54.6%	71.3%	38.3%	41.7%
0.596	0.404	53.9%	58.7%	41.4%	33.3%
0.596	0.404	57.5%	70.9%	43.0%	33.3%
0.765	0.235	65.7%	91.7%	26.7%	16.0%
0.765	0.235	74.2%	90.0%	28.4%	15.8%
0.765	0.235	73.5%	88.6%	30.6%	15.6%

Column C - Flow Rate 2 - Concentration

UF SR	OF SR	α_{LU}	α_{HU}	α_{LO}	α_{HO}
0.228	0.772	0.048	0.212	0.064	0.096
0.228	0.772	0.039	0.208	0.067	0.092
0.228	0.772	0.048	0.208	0.064	0.097
0.228	0.772	0.040	0.239	0.063	0.093
0.228	0.772	0.043	0.228	0.063	0.089
0.228	0.772	0.044	0.236	0.067	0.086
0.326	0.674	0.046	0.196	0.068	0.083
0.326	0.674	0.047	0.186	0.067	0.084
0.326	0.674	0.047	0.183	0.071	0.081
0.572	0.428	0.055	0.153	0.070	0.080
0.572	0.428	0.053	0.147	0.075	0.086
0.572	0.428	0.046	0.149	0.069	0.084
0.449	0.551	0.049	0.194	0.068	0.063
0.449	0.551	0.046	0.187	0.068	0.064
0.449	0.551	0.050	0.184	0.067	0.067
0.695	0.305	0.065	0.128	0.071	0.088
0.695	0.305	0.064	0.132	0.075	0.091
0.695	0.305	0.068	0.121	0.071	0.099
0.817	0.183	0.065	0.119	0.073	0.098
0.817	0.183	0.053	0.114	0.078	0.123
0.817	0.183	0.051	0.119	0.089	0.137
0.817	0.183	0.053	0.135	0.063	0.063
0.817	0.183	0.056	0.134	0.064	0.068
0.817	0.183	0.051	0.134	0.067	0.070

Column C - Flow Rate 2 - Normalized Concentration

UF SR	OF SR	α_{LU}	α_{HU}	α_{LO}	α_{HO}
0.228	0.772	0.832	1.734	1.107	0.783
0.228	0.772	0.669	1.702	1.165	0.766
0.228	0.772	0.836	1.697	1.109	0.794
0.228	0.772	0.702	1.953	1.092	0.764
0.228	0.772	0.741	1.865	1.083	0.730
0.228	0.772	0.769	1.929	1.165	0.703
0.326	0.674	0.791	1.600	1.175	0.676
0.326	0.674	0.808	1.525	1.165	0.687
0.326	0.674	0.811	1.496	1.222	0.664
0.572	0.428	0.959	1.253	1.212	0.656
0.572	0.428	0.924	1.199	1.299	0.700
0.572	0.428	0.805	1.223	1.200	0.683
0.449	0.551	0.842	1.589	1.170	0.518
0.449	0.551	0.793	1.532	1.185	0.524
0.449	0.551	0.861	1.501	1.165	0.550
0.695	0.305	1.125	1.044	1.230	0.719
0.695	0.305	1.104	1.076	1.294	0.747
0.695	0.305	1.178	0.966	1.238	0.801
0.817	0.183	1.121	0.976	1.268	0.798
0.817	0.183	0.922	0.929	1.349	1.005
0.817	0.183	0.878	0.973	1.546	1.120
0.817	0.183	0.912	1.106	1.099	0.519
0.817	0.183	0.963	1.099	1.106	0.557
0.817	0.183	0.890	1.096	1.168	0.569

Column C - Flow Rate 2 - Recovery

UF SR	OF SR	R_{LU}	R_{HU}	R_{LO}	R_{HO}
0.228	0.772	19.0%	39.6%	85.4%	60.4%
0.228	0.772	15.3%	38.9%	89.9%	58.3%
0.228	0.772	19.1%	38.7%	85.6%	61.3%
0.228	0.772	16.0%	44.6%	84.3%	59.0%
0.228	0.772	16.9%	42.6%	83.6%	56.3%
0.228	0.772	17.5%	44.0%	89.1%	54.3%
0.326	0.674	25.8%	52.2%	79.1%	45.5%
0.326	0.674	26.4%	49.8%	78.5%	46.3%
0.326	0.674	26.5%	48.8%	82.3%	44.7%
0.572	0.428	54.8%	71.6%	51.9%	28.1%
0.572	0.428	52.8%	68.6%	55.6%	30.0%
0.572	0.428	46.0%	69.9%	51.4%	29.2%
0.449	0.551	37.8%	71.4%	64.4%	28.5%
0.449	0.551	35.6%	68.8%	65.3%	28.9%
0.449	0.551	38.7%	67.4%	64.2%	30.3%
0.695	0.305	78.2%	72.5%	37.6%	22.0%
0.695	0.305	76.7%	74.8%	39.5%	22.8%
0.695	0.305	81.8%	68.5%	37.8%	24.5%
0.817	0.183	91.6%	79.8%	23.2%	14.6%
0.817	0.183	75.3%	75.9%	24.7%	18.4%
0.817	0.183	71.7%	79.5%	28.3%	20.5%
0.817	0.183	74.5%	90.5%	20.1%	9.5%
0.817	0.183	78.7%	89.8%	20.2%	10.2%
0.817	0.183	72.8%	89.6%	21.3%	10.4%

Column C - Flow Rate 3 - Concentration

UF SR	OF SR	α_{LU}	α_{HU}	α_{LO}	α_{HO}
0.240	0.760	0.050	0.210	0.071	0.079
0.240	0.760	0.046	0.229	0.065	0.084
0.240	0.760	0.042	0.230	0.061	0.079
0.327	0.673	0.045	0.208	0.070	0.074
0.327	0.673	0.046	0.206	0.072	0.074
0.327	0.673	0.042	0.209	0.067	0.078
0.414	0.586	0.048	0.193	0.068	0.070
0.414	0.586	0.045	0.190	0.068	0.070
0.414	0.586	0.045	0.192	0.073	0.069
0.501	0.499	0.049	0.179	0.073	0.067
0.501	0.499	0.040	0.176	0.073	0.071
0.501	0.499	0.044	0.168	0.072	0.070
0.588	0.412	0.053	0.147	0.075	0.075
0.588	0.412	0.056	0.134	0.073	0.077
0.588	0.412	0.051	0.141	0.070	0.083
0.674	0.326	0.047	0.118	0.084	0.103
0.674	0.326	0.055	0.117	0.078	0.096
0.789	0.211	0.042	0.136	0.118	0.091
0.789	0.211	0.063	0.127	0.102	0.119
0.789	0.211	0.048	0.129	0.115	0.118

Column C - Flow Rate 3 - Normalized Concentration

UF SR	OF SR	α_{LU}	α_{HU}	α_{LO}	α_{HO}
0.240	0.760	0.872	1.714	1.231	0.643
0.240	0.760	0.803	1.877	1.131	0.683
0.240	0.760	0.734	1.880	1.053	0.650
0.327	0.673	0.773	1.702	1.213	0.609
0.327	0.673	0.801	1.684	1.240	0.603
0.327	0.673	0.731	1.708	1.153	0.635
0.414	0.586	0.825	1.575	1.170	0.574
0.414	0.586	0.778	1.555	1.178	0.574
0.414	0.586	0.776	1.569	1.260	0.562
0.501	0.499	0.862	1.468	1.264	0.544
0.501	0.499	0.693	1.439	1.268	0.582
0.501	0.499	0.765	1.374	1.253	0.575
0.588	0.412	0.912	1.202	1.300	0.613
0.588	0.412	0.965	1.093	1.261	0.629
0.588	0.412	0.889	1.153	1.209	0.661
0.674	0.326	0.815	0.968	1.462	0.845
0.674	0.326	0.952	0.956	1.356	0.782
0.789	0.211	0.734	1.109	2.044	0.740
0.789	0.211	0.918	1.040	1.774	0.970
0.789	0.211	0.836	1.058	1.990	0.962

Column C - Flow Rate 3 - Recovery

UF SR	OF SR	R_{LU}	R_{HU}	R_{LO}	R_{HO}
0.240	0.760	21.0%	41.2%	93.5%	48.9%
0.240	0.760	19.3%	45.1%	85.9%	51.9%
0.240	0.760	17.6%	45.2%	80.0%	49.3%
0.327	0.673	25.3%	55.7%	81.6%	41.0%
0.327	0.673	26.2%	55.1%	83.5%	40.6%
0.327	0.673	23.9%	55.9%	77.6%	42.7%
0.414	0.586	34.2%	65.2%	68.6%	33.6%
0.414	0.586	32.2%	64.4%	69.0%	33.6%
0.414	0.586	32.1%	65.0%	73.9%	32.9%
0.501	0.499	42.6%	73.5%	63.1%	27.2%
0.501	0.499	34.7%	72.1%	63.3%	29.0%
0.501	0.499	38.3%	68.8%	62.5%	28.7%
0.588	0.412	53.6%	70.6%	53.6%	25.3%
0.588	0.412	56.7%	64.2%	52.0%	25.9%
0.588	0.412	52.2%	67.8%	49.9%	28.1%
0.674	0.326	54.9%	65.3%	47.6%	27.5%
0.674	0.326	64.2%	64.5%	44.2%	25.5%
0.789	0.211	58.0%	87.5%	43.0%	15.6%
0.789	0.211	72.5%	82.1%	37.4%	20.4%
0.789	0.211	66.0%	83.5%	41.9%	20.3%

APPENDIX 5 - COLLECTED GRAPHS:

FIGURES A5-1 to A5-17 - COLUMN A, SYSTEM I
FIGURES A5-18 to A5-34 - COLUMN A, SYSTEM II
FIGURES A5-35 to A5-50 - COLUMN B, SYSTEM I
FIGURES A5-51 to A5-62 - COLUMN C, SYSTEM I

Appendix 5 contains the results of some tests not depicted in Chapter 4. For ease of reference, all figures are repeated here and pairs of graphs from the same set of tests are shown on each page.

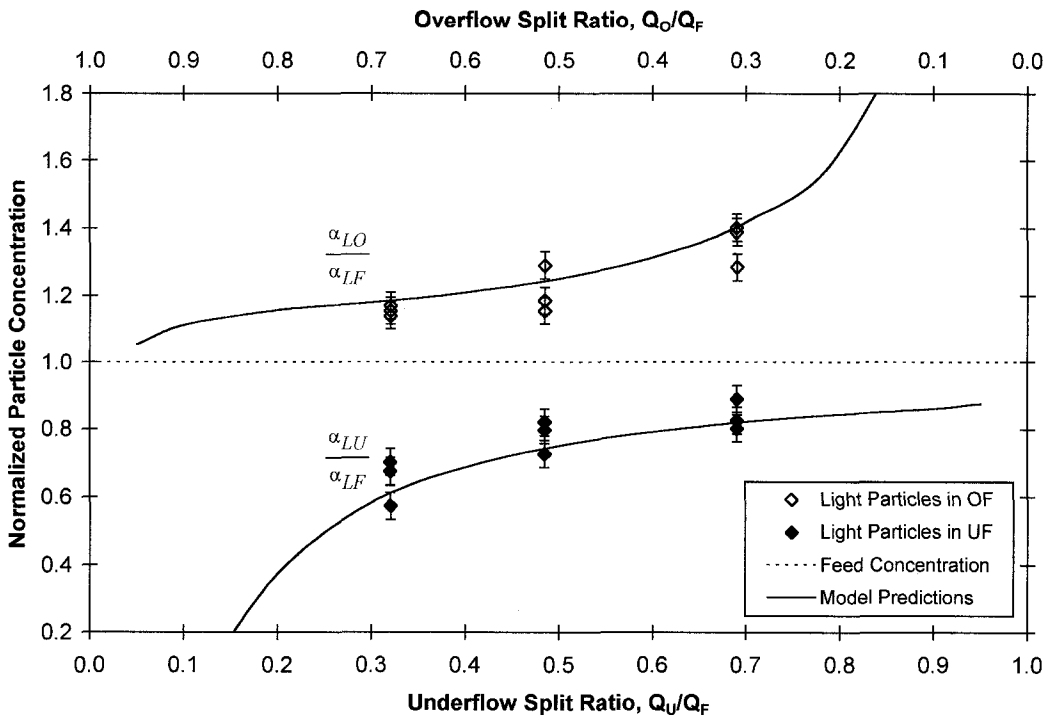

Figure A5-1. Concentrations of Light Particles in Overflow and Underflow for Column A, System I (α_{LF} = 0.058, α_{HF} = 0.122), Feed Rate 40.6 ml/s

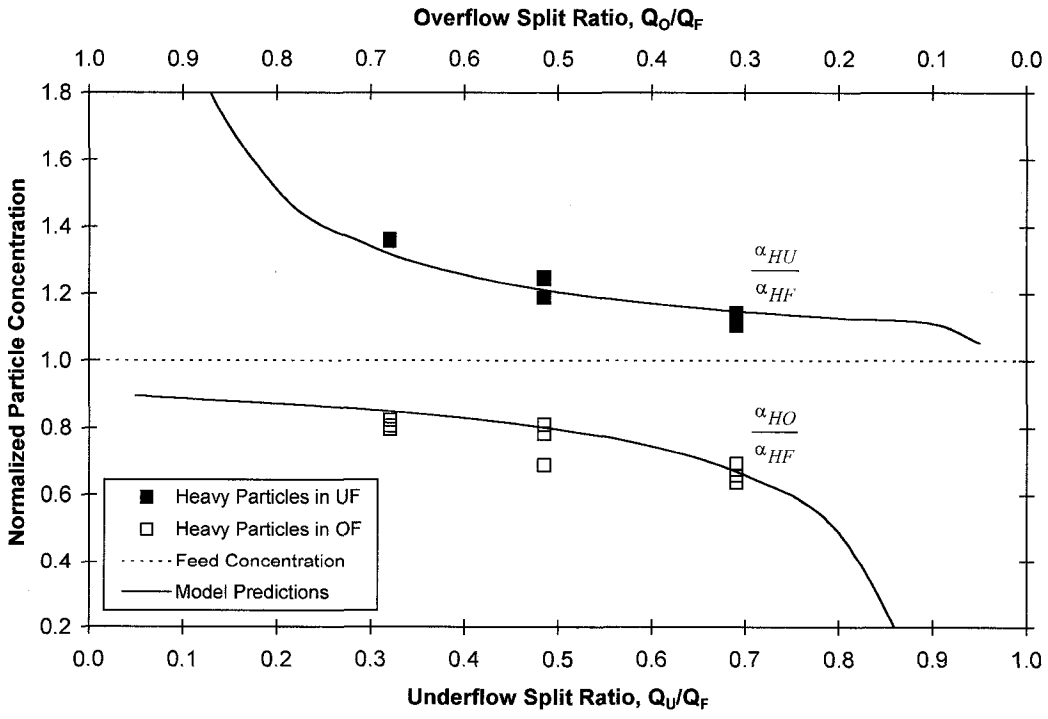

Figure A5-2. Concentrations of Heavy Particles in Overflow and Underflow for Column A, System I (α_{LF} = 0.058, α_{HF} = 0.122), Feed Rate 40.6 ml/s

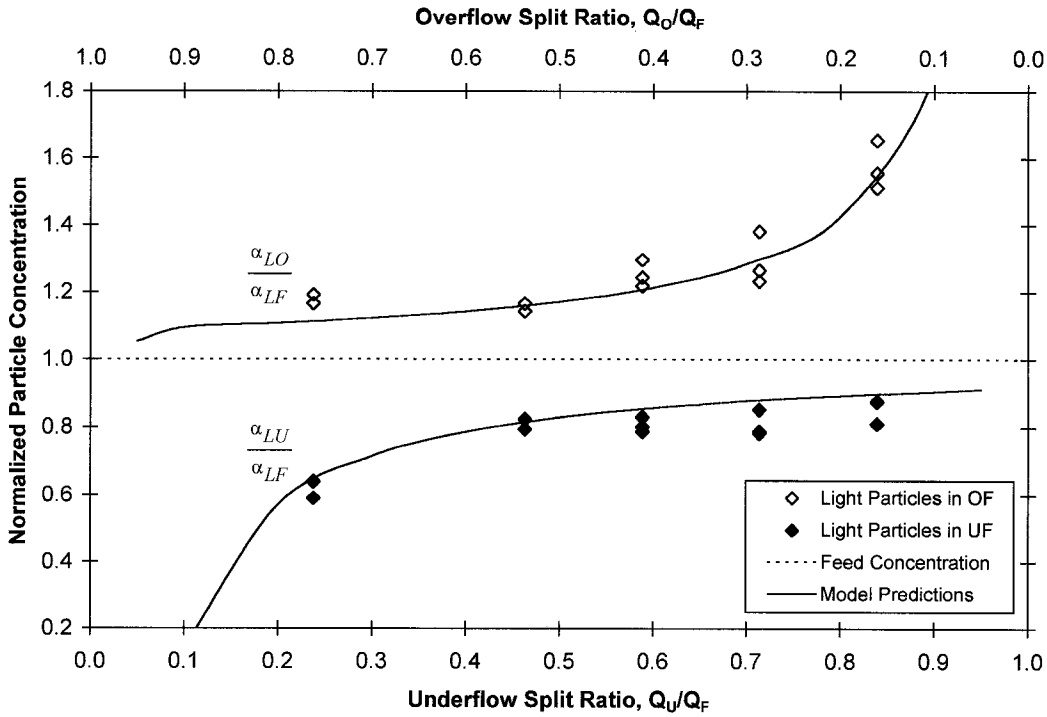

Figure A5-3. Concentrations of Light Particles in Overflow and Underflow for Column A, System I (α_{LF} = 0.058, α_{HF} = 0.122), Feed Rate 59.4 ml/s

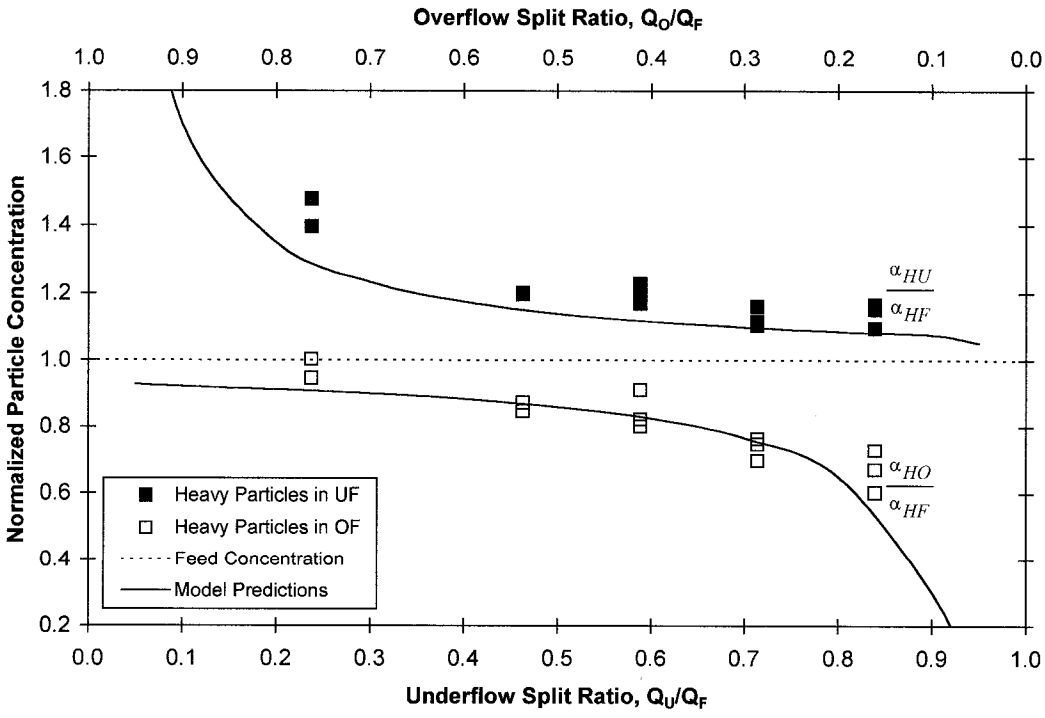

Figure A5-4. Concentrations of Heavy Particles in Overflow and Underflow for Column A, System I (α_{LF} = 0.058, α_{HF} = 0.122), Feed Rate 59.4 ml/s

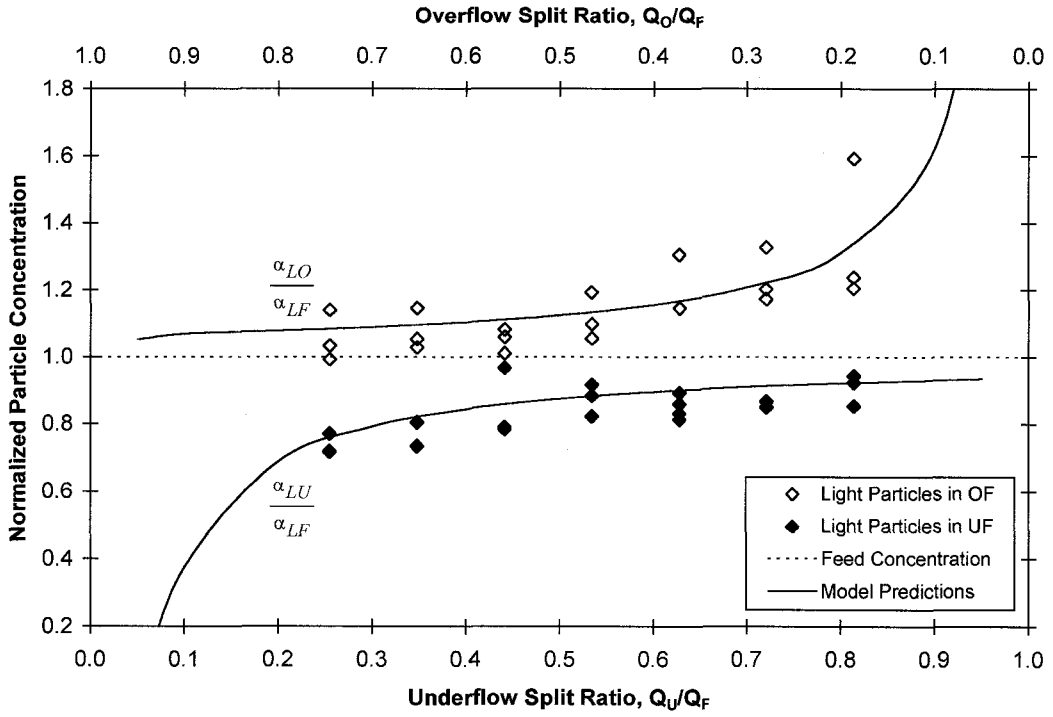

Figure A5-5. Concentrations of Light Particles in Overflow and Underflow for Column A, System I (α_{LF} = 0.058, α_{HF} = 0.122), Feed Rate 81.5 ml/s

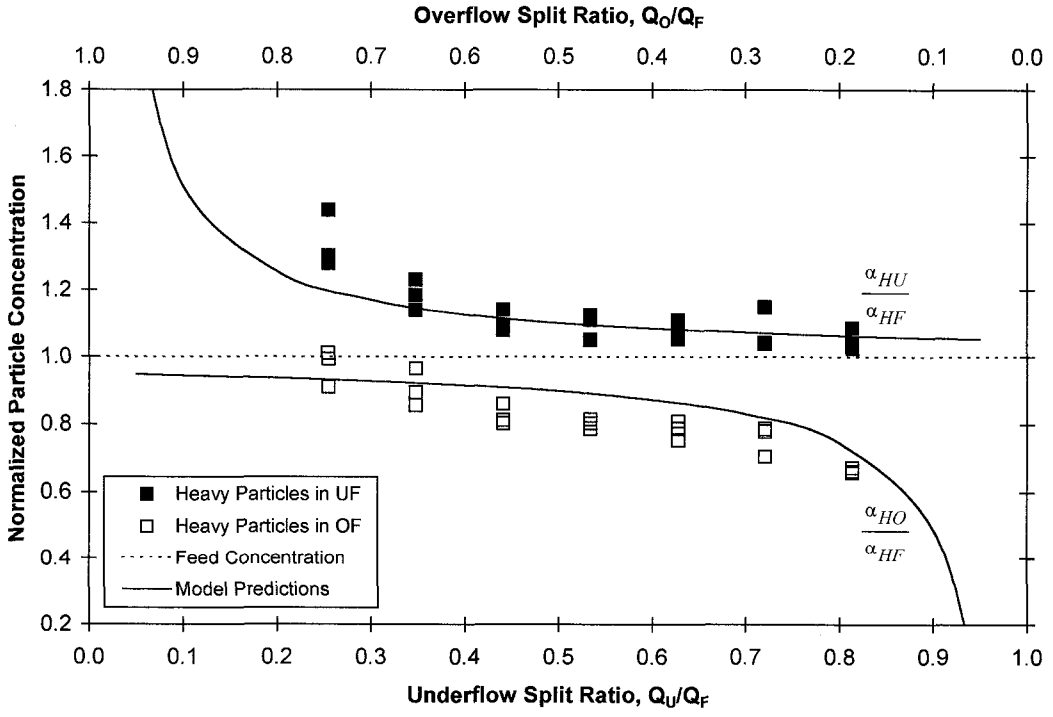

Figure A5-6. Concentrations of Heavy Particles in Overflow and Underflow for Column A, System I (α_{LF} = 0.058, α_{HF} = 0.122), Feed Rate 81.5 ml/s

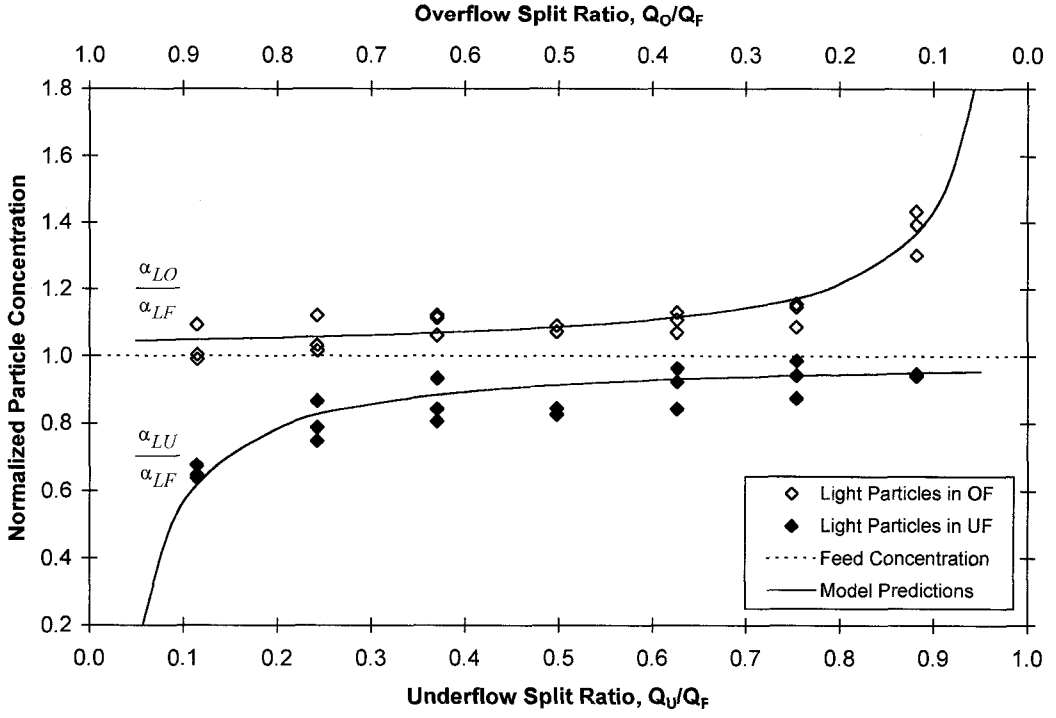

Figure A5-7. Concentrations of Light Particles in Overflow and Underflow for Column A, System I (α_{LF} = 0.058, α_{HF} = 0.122), Feed Rate 117 ml/s

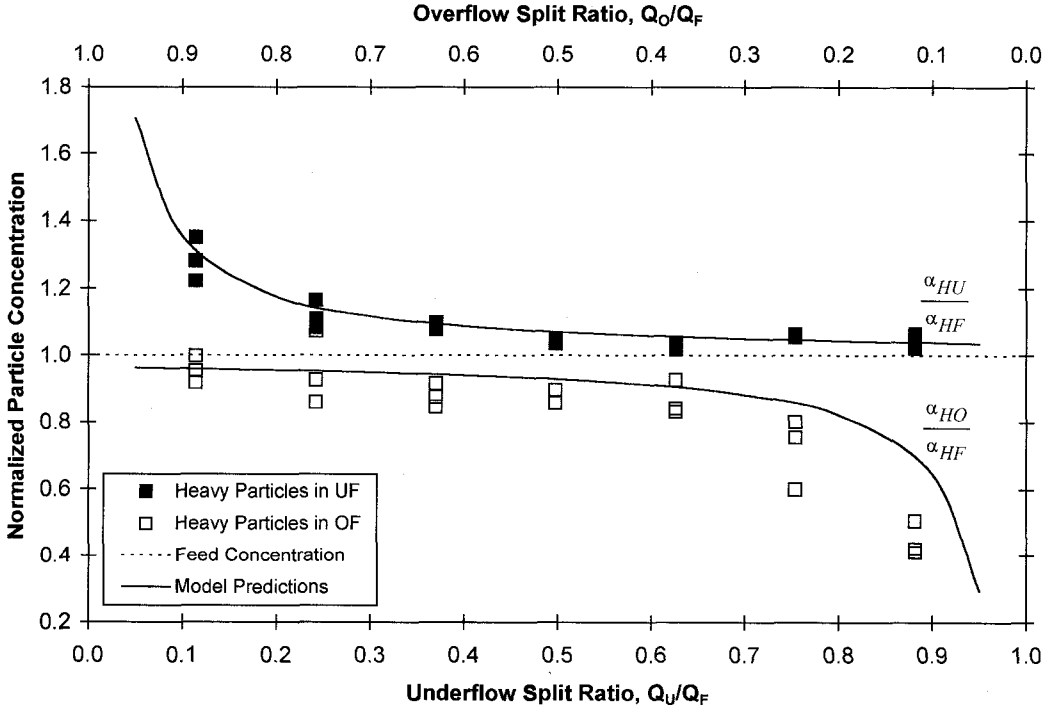

Figure A5-8. Concentrations of Heavy Particles in Overflow and Underflow for Column A, System I (α_{LF} = 0.058, α_{HF} = 0.122), Feed Rate 117 ml/s

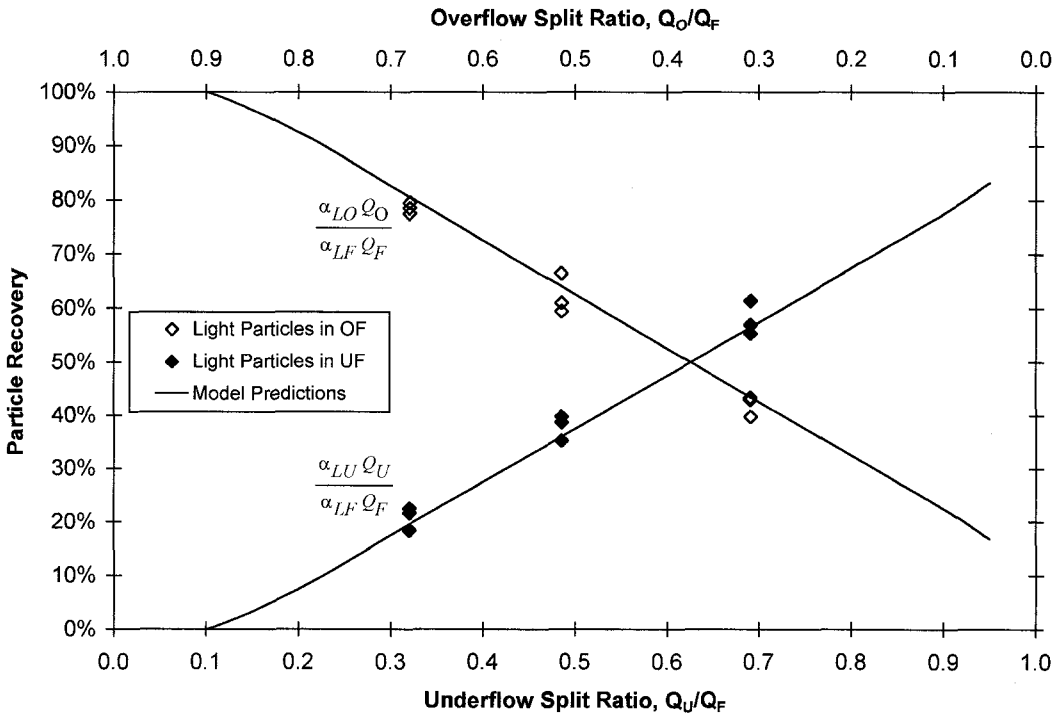

Figure A5-9. Recoveries of Light Particles in Overflow and Underflow for Column A, System I (α_{LF} = 0.058, α_{HF} = 0.122), Feed Rate 40.6 ml/s

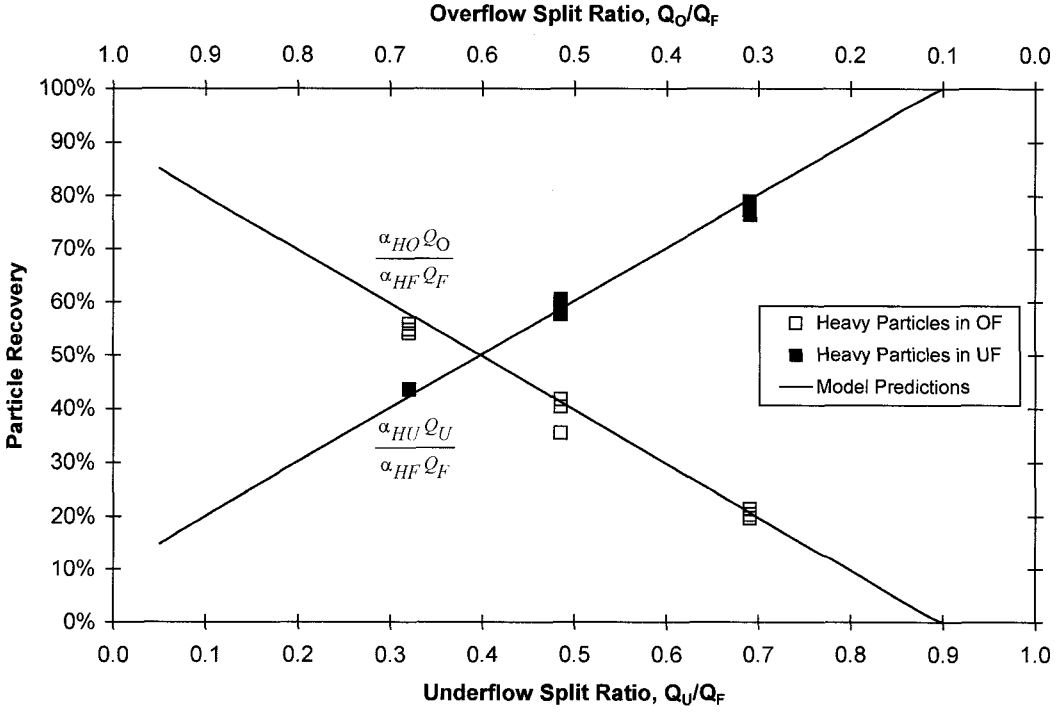

Figure A5-10. Recoveries of Heavy Particles in Overflow and Underflow for Column A, System I (α_{LF} = 0.058, α_{HF} = 0.122), Feed Rate 40.6 ml/s

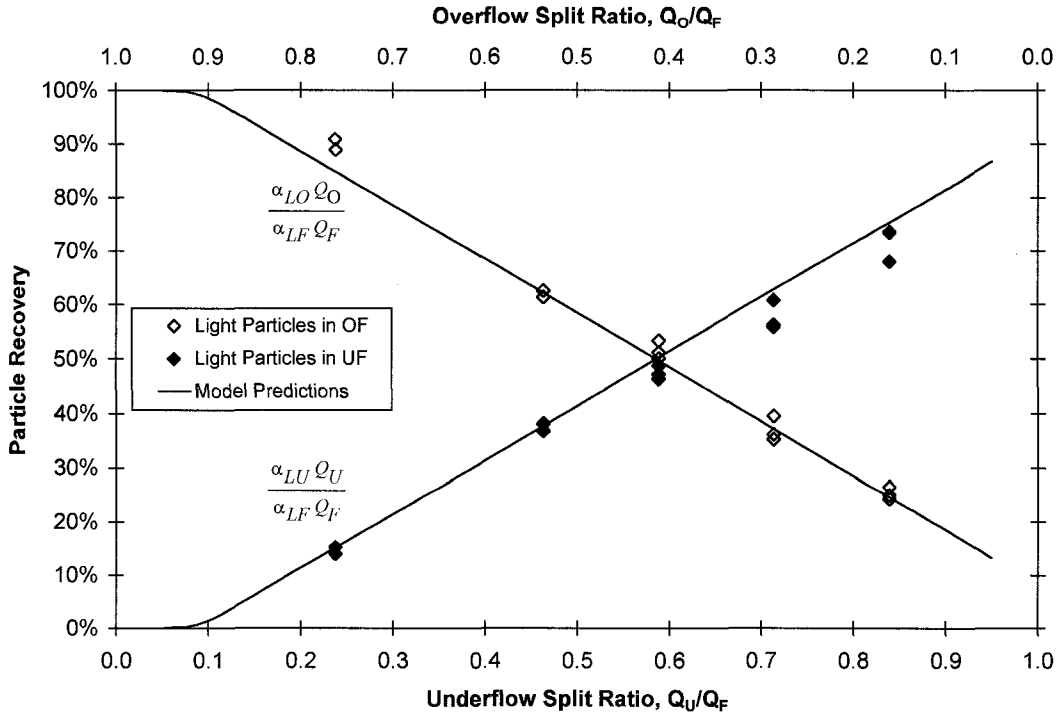

Figure A5-11. Recoveries of Light Particles in Overflow and Underflow for Column A, System I (α_{LF} = 0.058, α_{HF} = 0.122), Feed Rate 59.4 ml/s

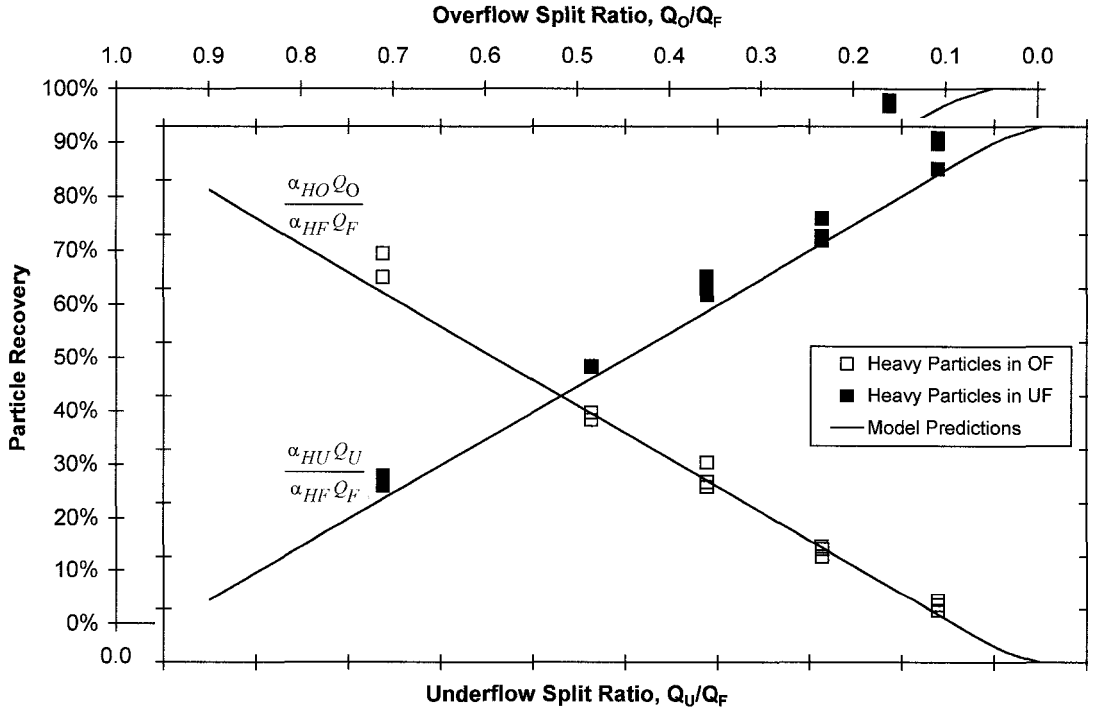

Figure A5-12. Recoveries of Heavy Particles in Overflow and Underflow for Column A, System I (α_{LF} = 0.058, α_{HF} = 0.122), Feed Rate 59.4 ml/s

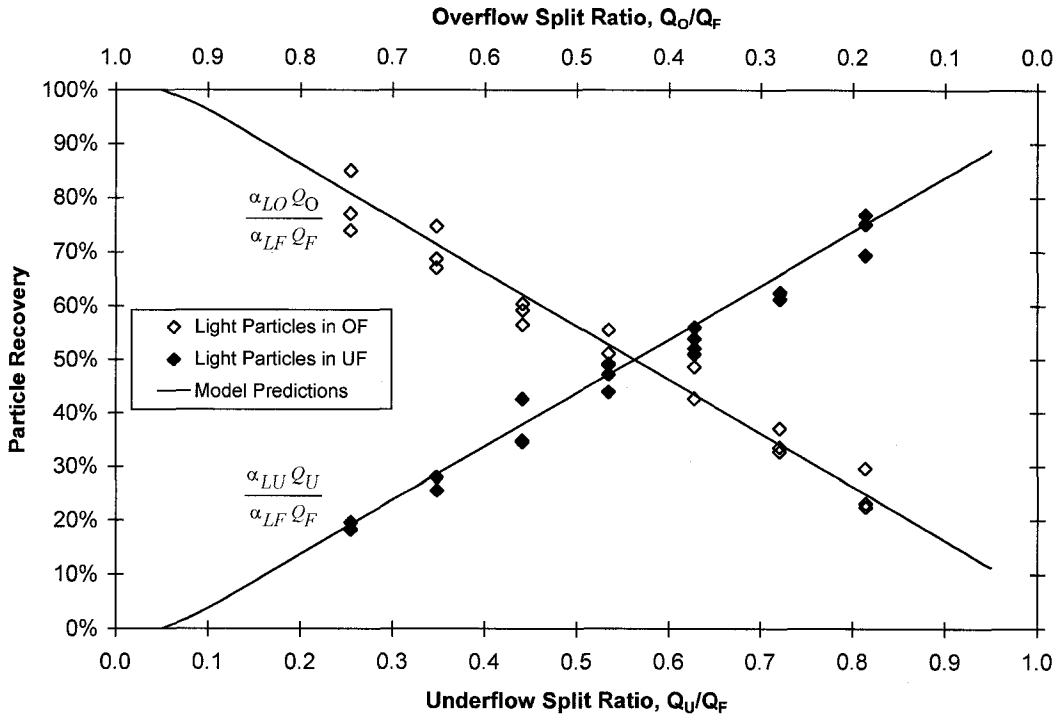

Figure A5-13. Recoveries of Light Particles in Overflow and Underflow for Column A, System I (α_{LF} = 0.058, α_{HF} = 0.122), Feed Rate 81.5 ml/s

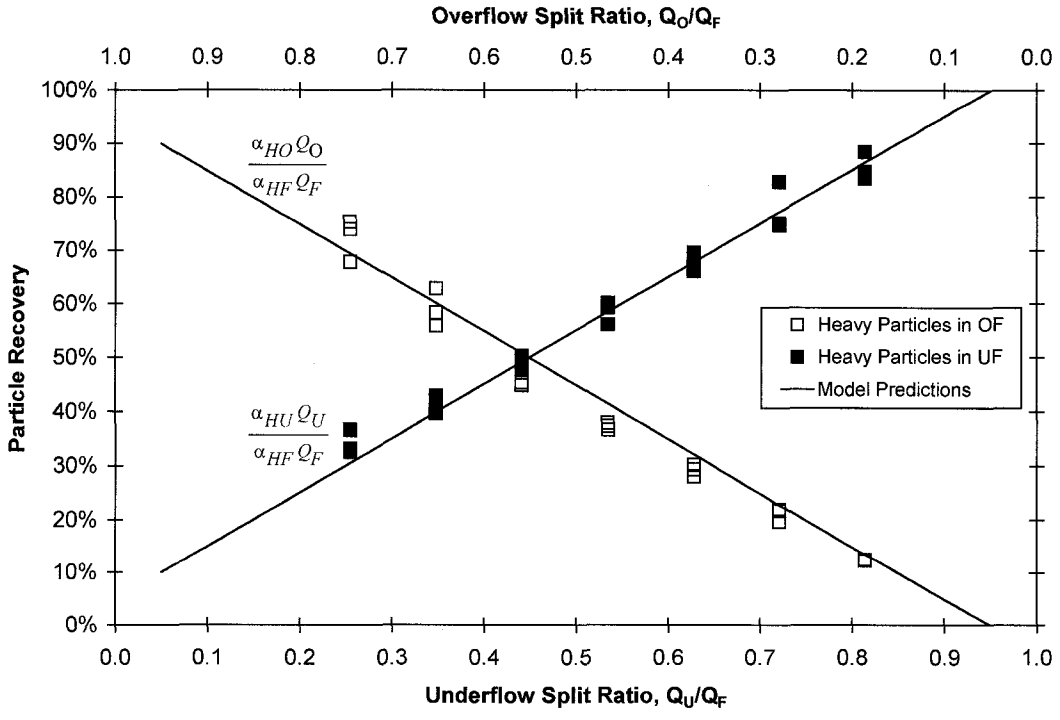

Figure A5-14. Recoveries of Heavy Particles in Overflow and Underflow for Column A, System I (α_{LF} = 0.058, α_{HF} = 0.122), Feed Rate 81.5 ml/s

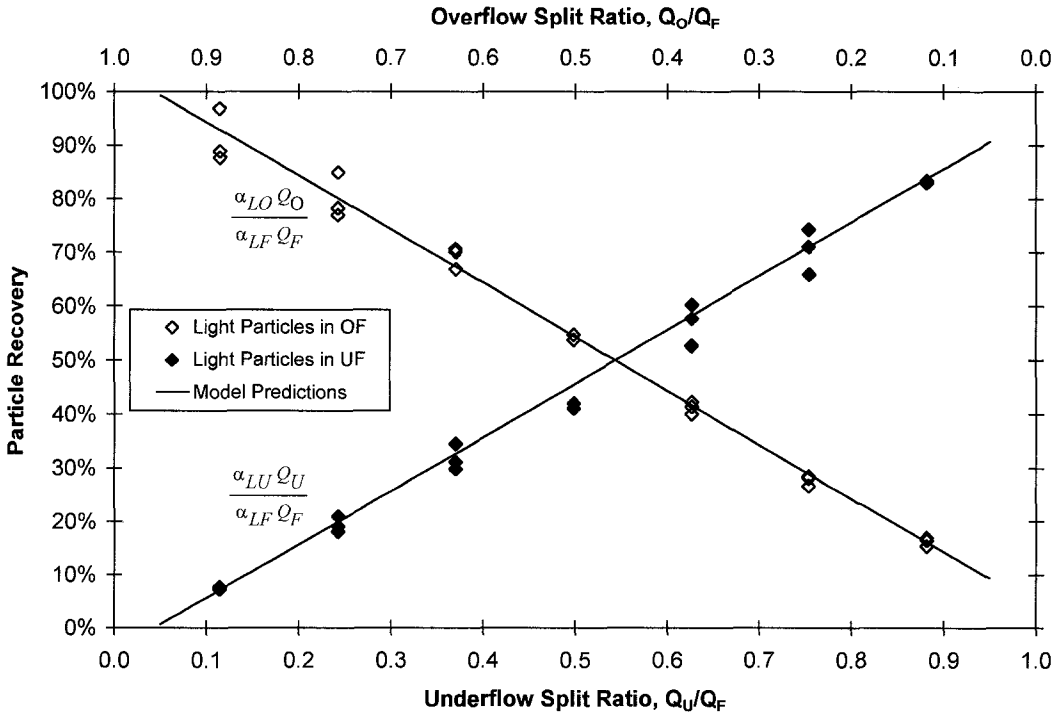

Figure A5-15. Recoveries of Light Particles in Overflow and Underflow for Column A, System I (α_{LF} = 0.058, α_{HF} = 0.122), Feed Rate 117 ml/s

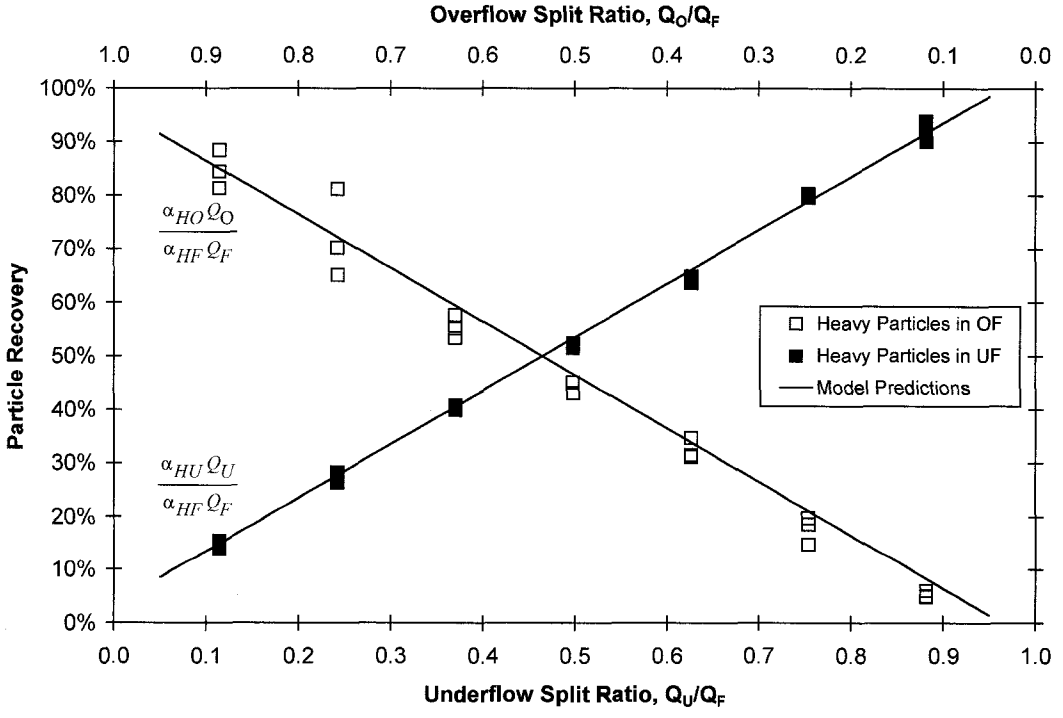

Figure A5-16. Recoveries of Heavy Particles in Overflow and Underflow for Column A, System I (α_{LF} = 0.058, α_{HF} = 0.122), Feed Rate 117 ml/s

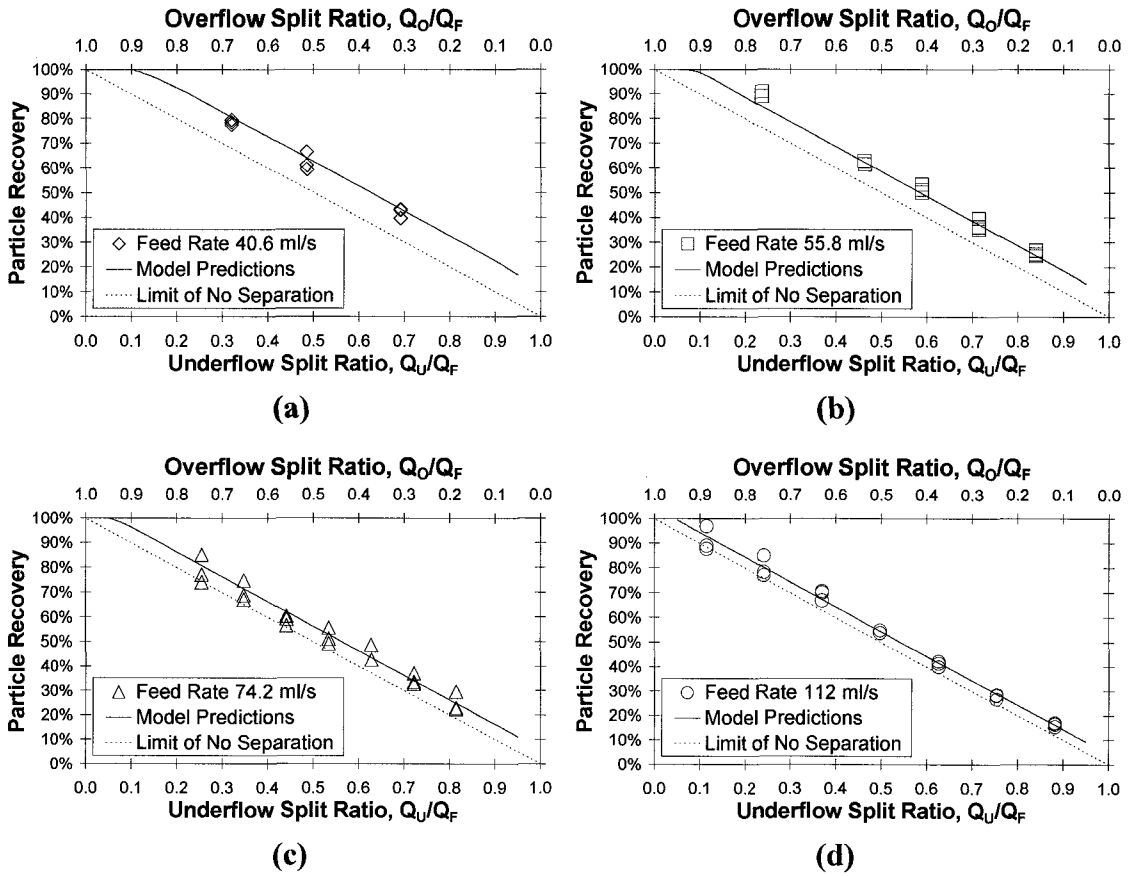

Figures A5-17a, b, c, d. Recoveries of Light Particles in Overflows of Column A, System I ($\alpha_{LF} = 0.058$, $\alpha_{HF} = 0.122$), all Feed Rates

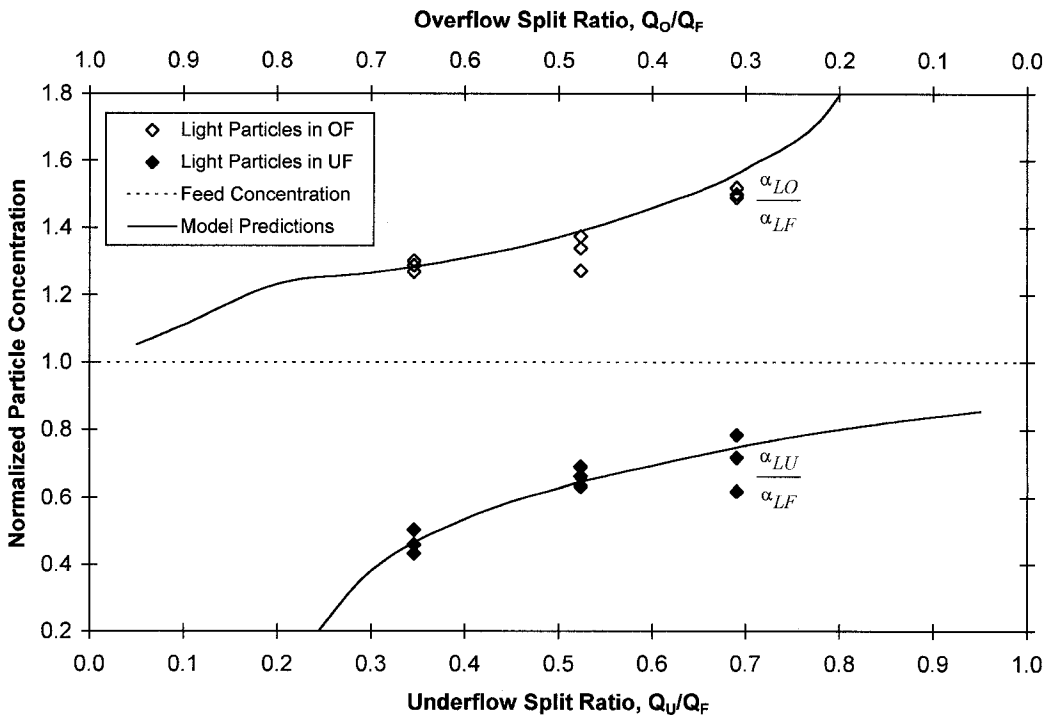

Figure A5-18. Concentrations of Light Particles in Overflow and Underflow for Column A, System II (α_{LF} = 0.134, α_{HF} = 0.163), Feed Rate 38.9 ml/s

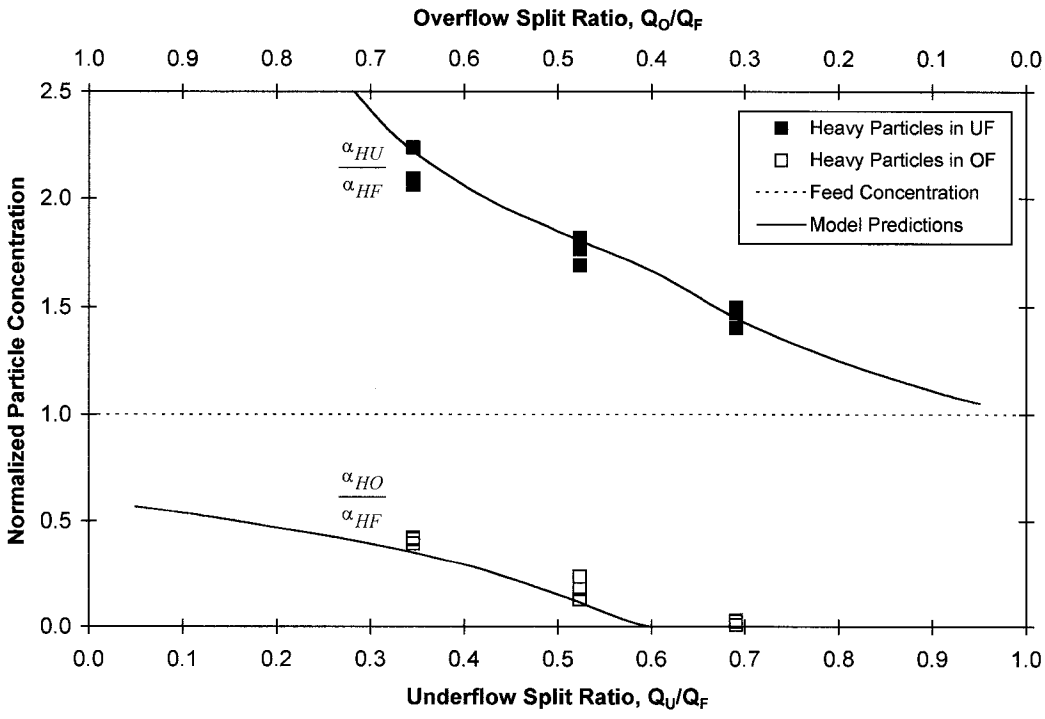

Figure A5-19. Concentrations of Heavy Particles in Overflow and Underflow for Column A, System II (α_{LF} = 0.134, α_{HF} = 0.163), Feed Rate 38.9 ml/s

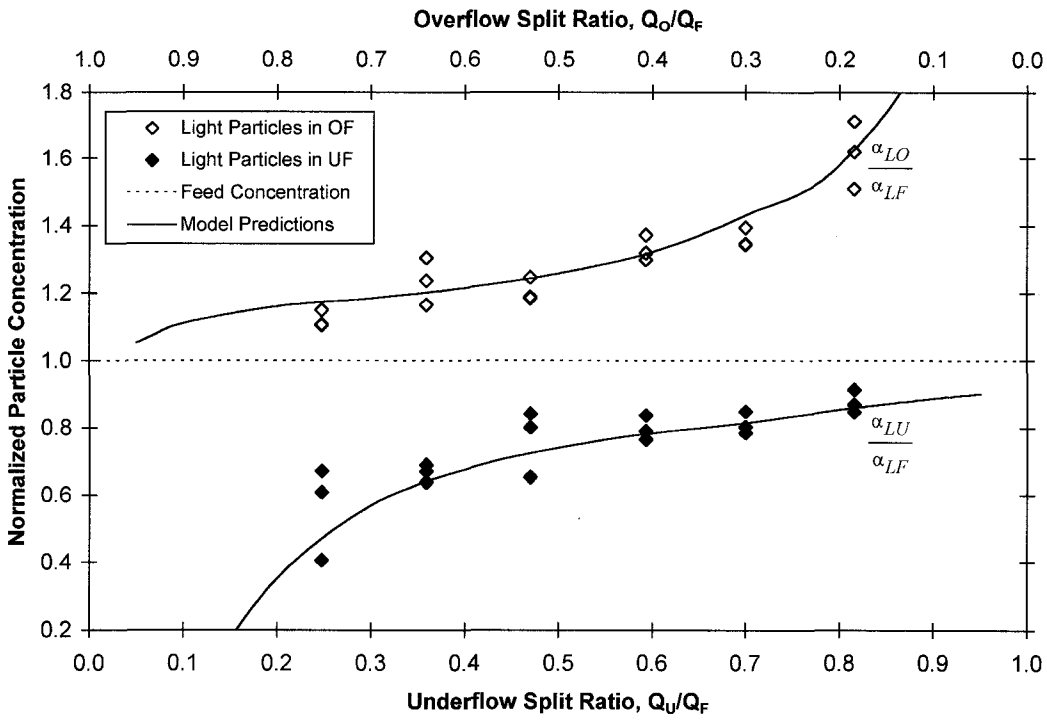

Figure A5-20. Concentrations of Light Particles in Overflow and Underflow for Column A, System II (α_{LF} = 0.134, α_{HF} = 0.163), Feed Rate 55.8 ml/s

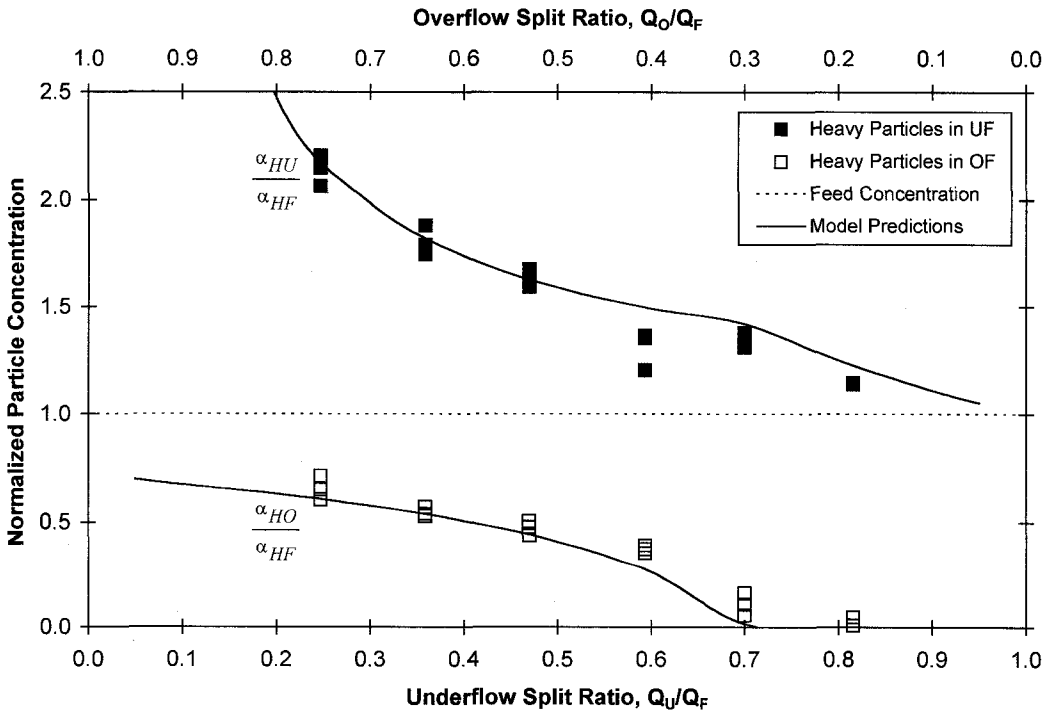

Figure A5-21. Concentrations of Heavy Particles in Overflow and Underflow for Column A, System II (α_{LF} = 0.134, α_{HF} = 0.163), Feed Rate 55.8 ml/s

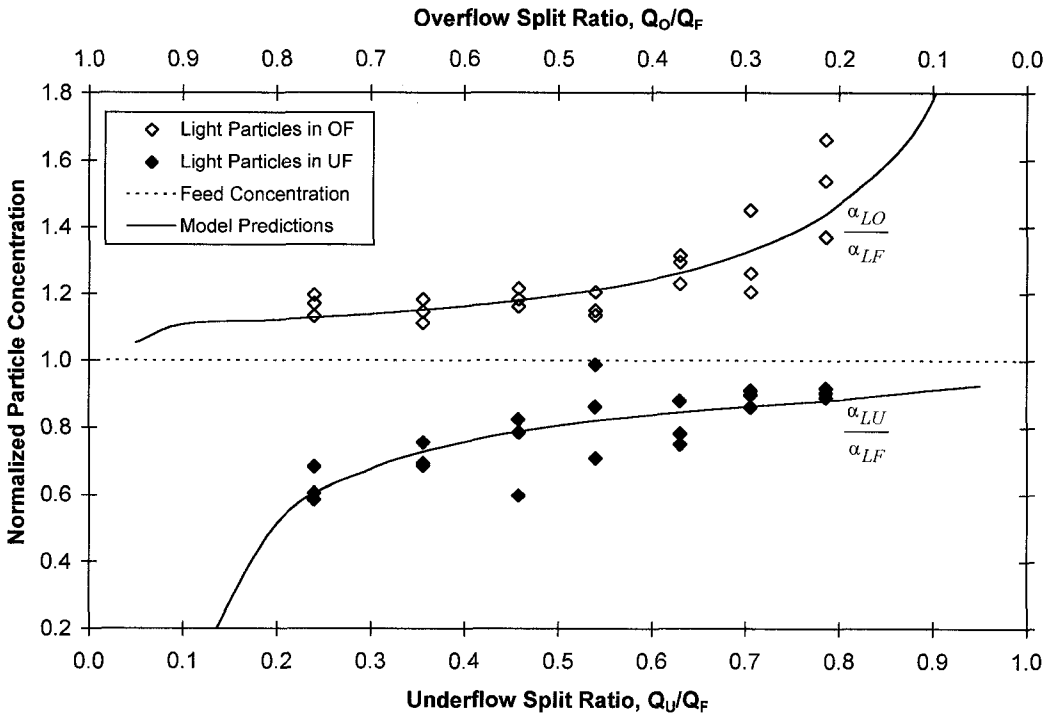

Figure A5-22. Concentrations of Light Particles in Overflow and Underflow for Column A, System II (α_{LF} = 0.134, α_{HF} = 0.163), Feed Rate 74.2 ml/s

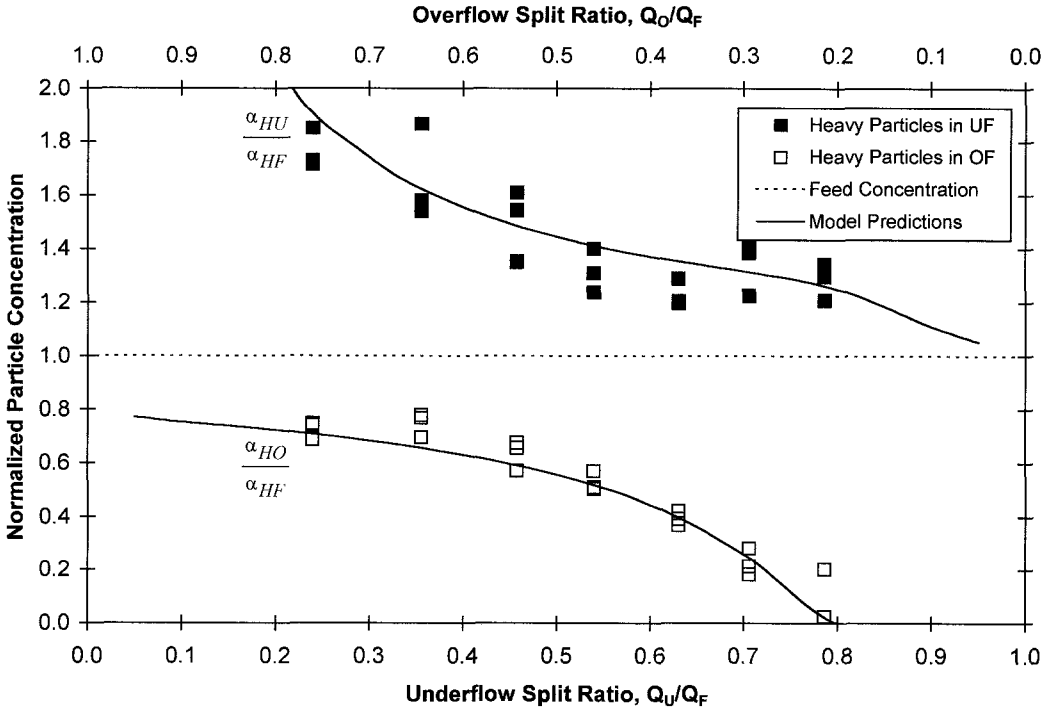

Figure A5-23. Concentrations of Heavy Particles in Overflow and Underflow for Column A, System II (α_{LF} = 0.134, α_{HF} = 0.163), Feed Rate 74.2 ml/s

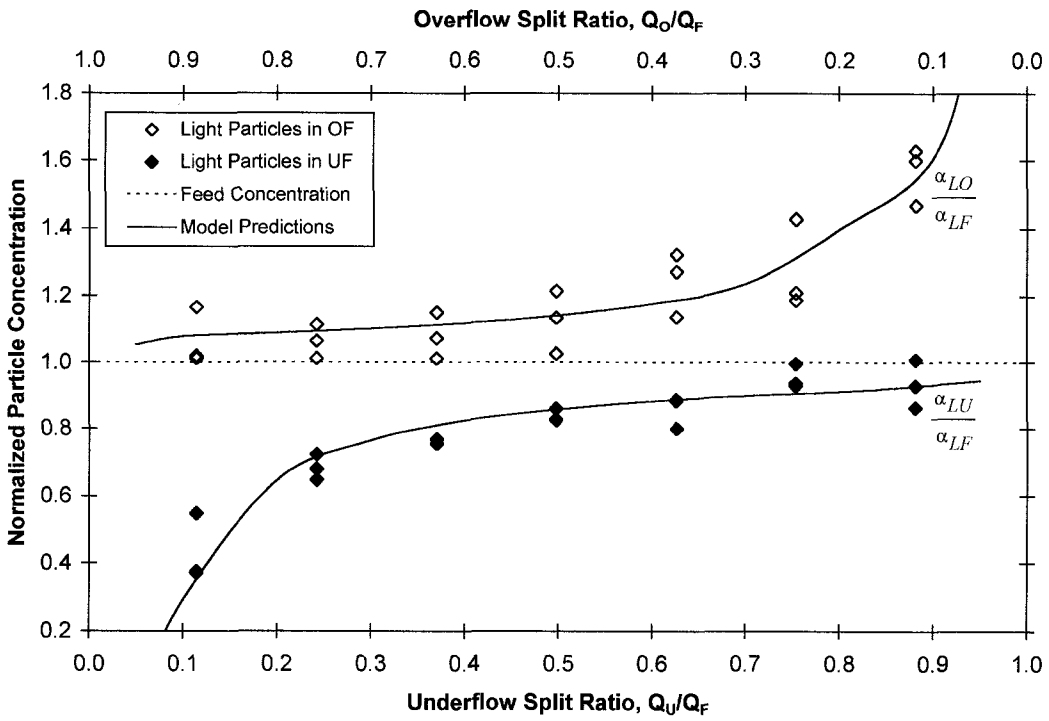

Figure A5-24. Concentrations of Light Particles in Overflow and Underflow for Column A, System II (α_{LF} = 0.134, α_{HF} = 0.163), Feed Rate 102 ml/s

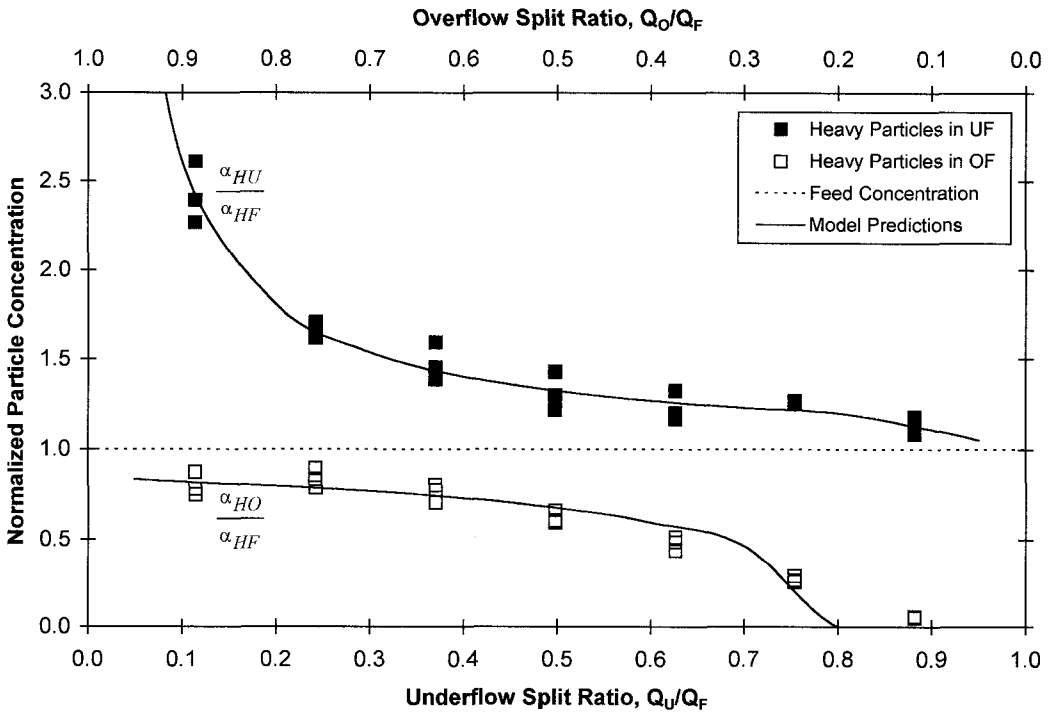

Figure A5-25. Concentrations of Heavy Particles in Overflow and Underflow for Column A, System II (α_{LF} = 0.134, α_{HF} = 0.163), Feed Rate 102 ml/s

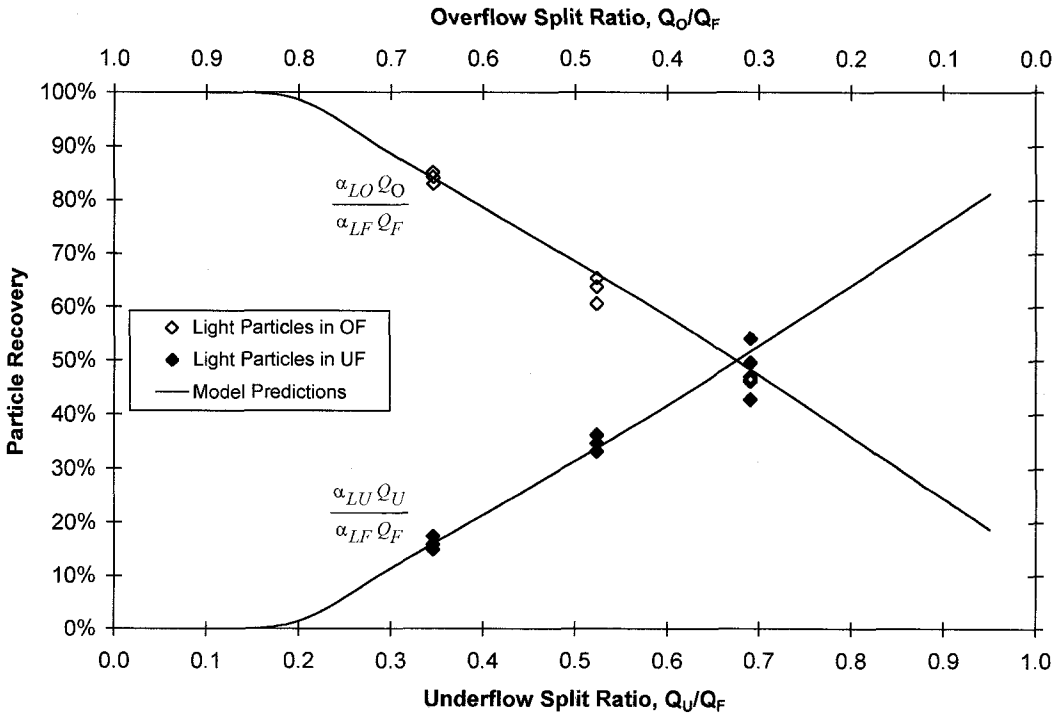

Figure A5-26. Recoveries of Light Particles in Overflow and Underflow for Column A, System II (α_{LF} = 0.134, α_{HF} = 0.163), Feed Rate 38.9 ml/s

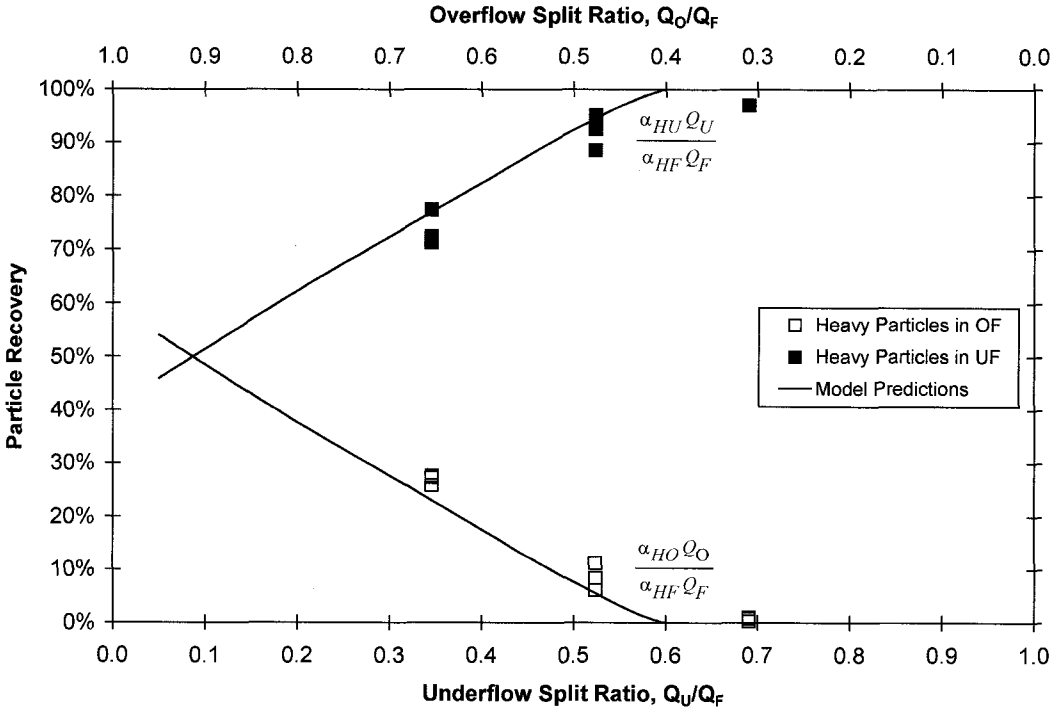

Figure A5-27. Recoveries of Heavy Particles in Overflow and Underflow for Column A, System II (α_{LF} = 0.134, α_{HF} = 0.163), Feed Rate 38.9 ml/s

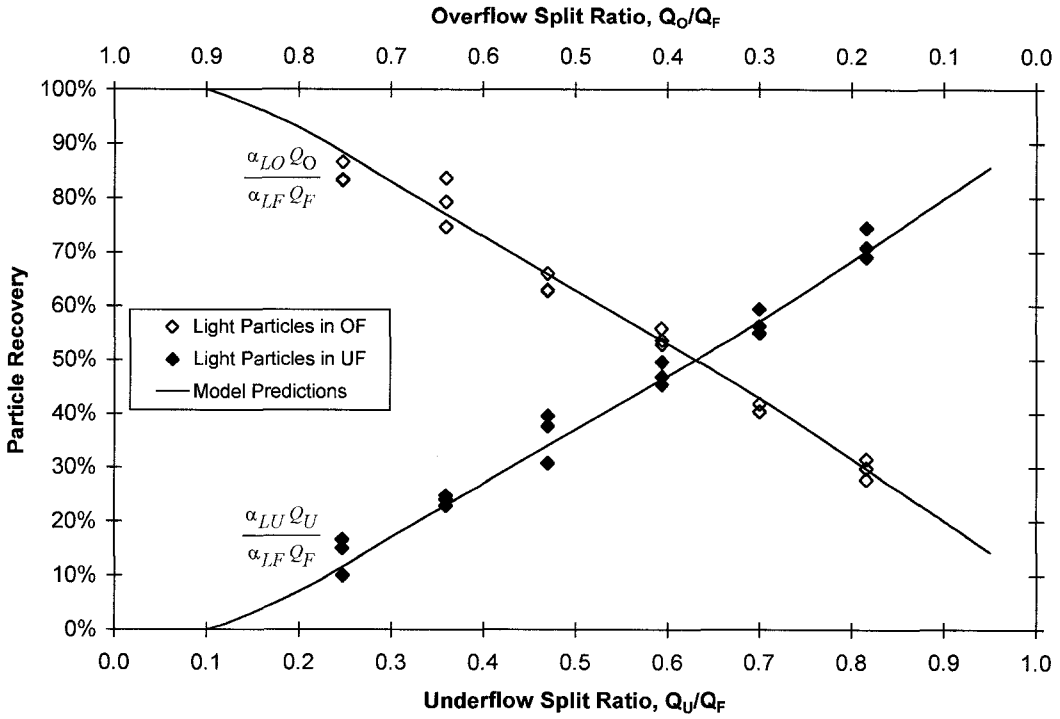

Figure A5-28. Recoveries of Light Particles in Overflow and Underflow for Column A, System II (α_{LF} = 0.134, α_{HF} = 0.163), Feed Rate 55.8 ml/s

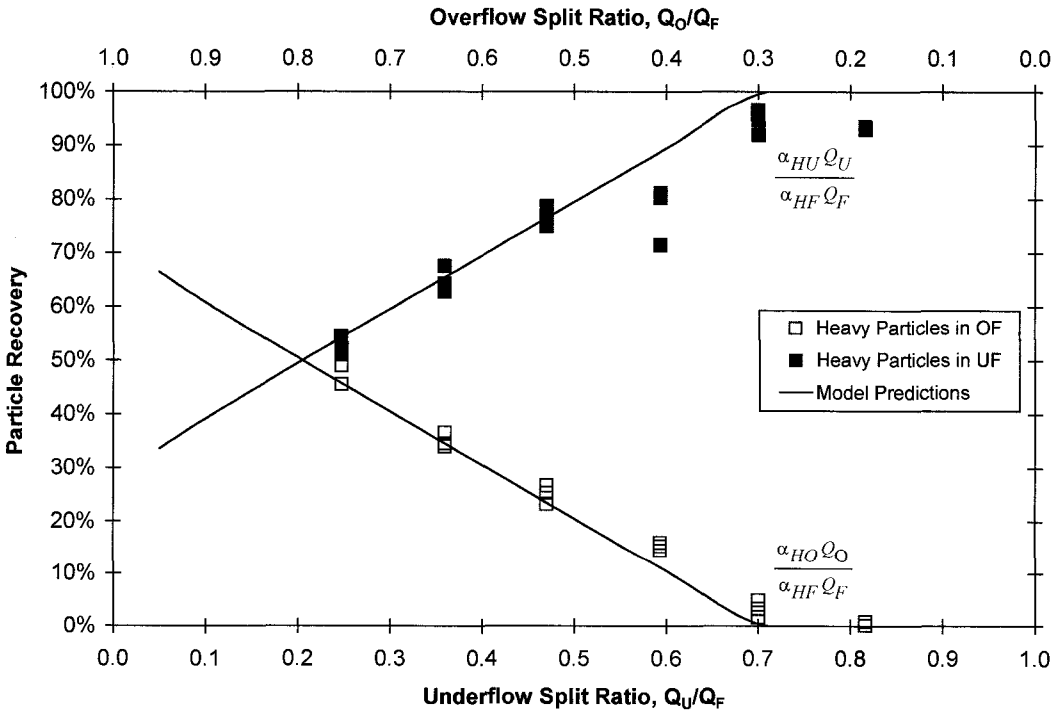

Figure A5-29. Recoveries of Heavy Particles in Overflow and Underflow for Column A, System II (α_{LF} = 0.134, α_{HF} = 0.163), Feed Rate 55.8 ml/s

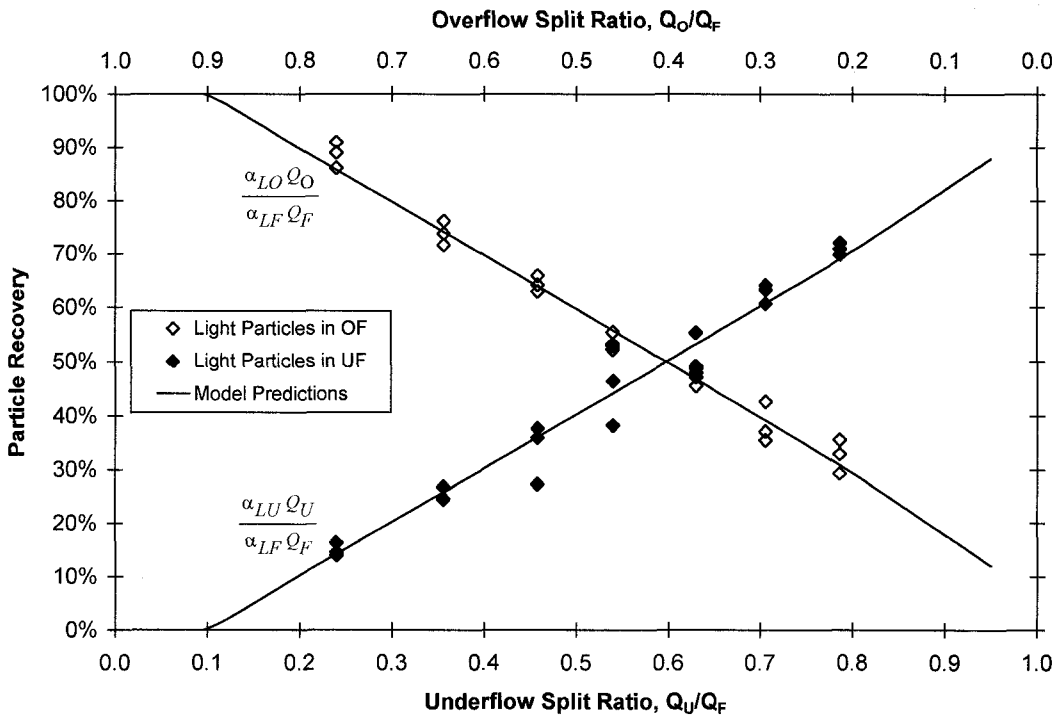

Figure A5-30. Recoveries of Light Particles in Overflow and Underflow for Column A, System II (α_{LF} = 0.134, α_{HF} = 0.163), Feed Rate 74.2 ml/s

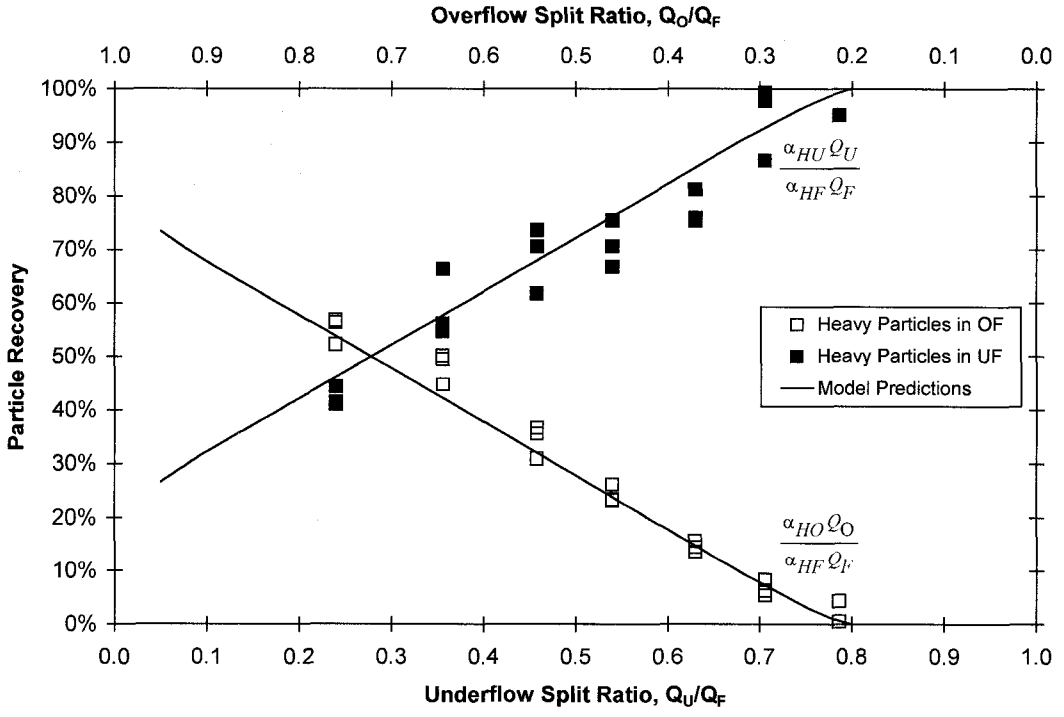

Figure A5-31. Recoveries of Heavy Particles in Overflow and Underflow for Column A, System II (α_{LF} = 0.134, α_{HF} = 0.163), Feed Rate 74.2 ml/s

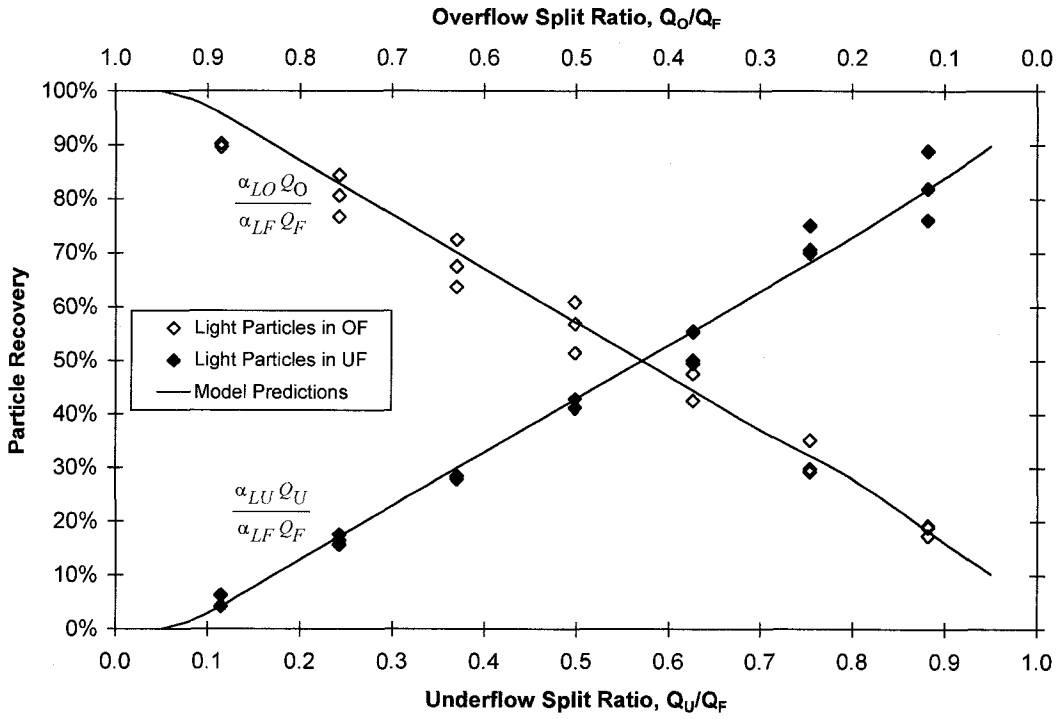

Figure A5-32. Recoveries of Light Particles in Overflow and Underflow for Column A, System II (α_{LF} = 0.134, α_{HF} = 0.163), Feed Rate 102 ml/s

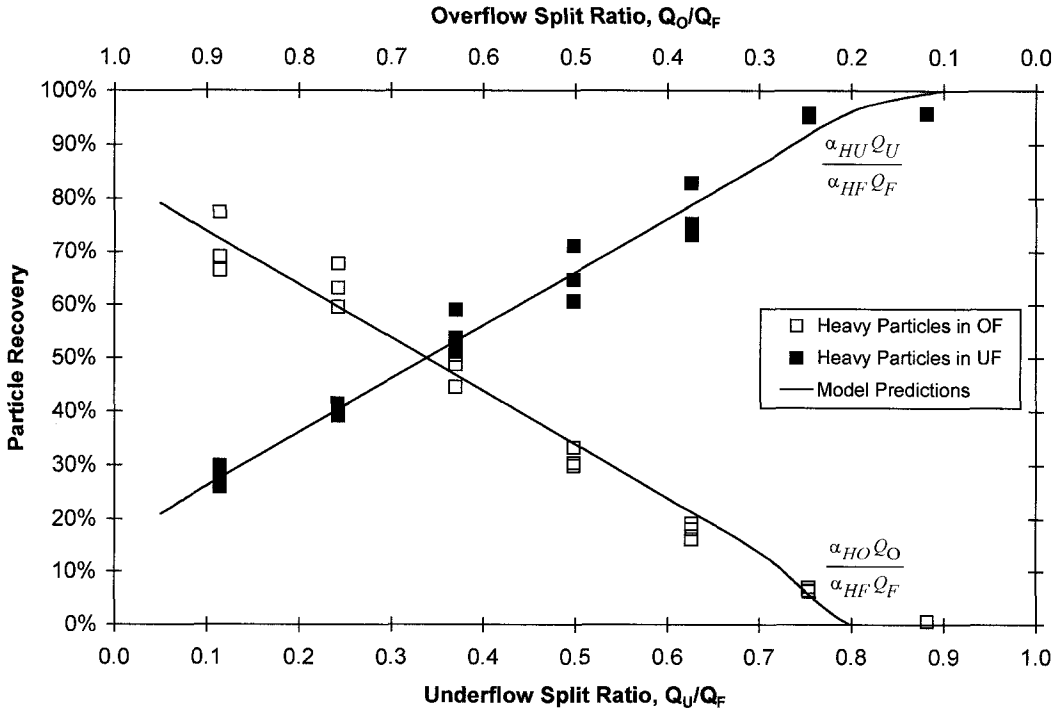

Figure A5-33. Recoveries of Heavy Particles in Overflow and Underflow for Column A, System II (α_{LF} = 0.134, α_{HF} = 0.163), Feed Rate 102 ml/s

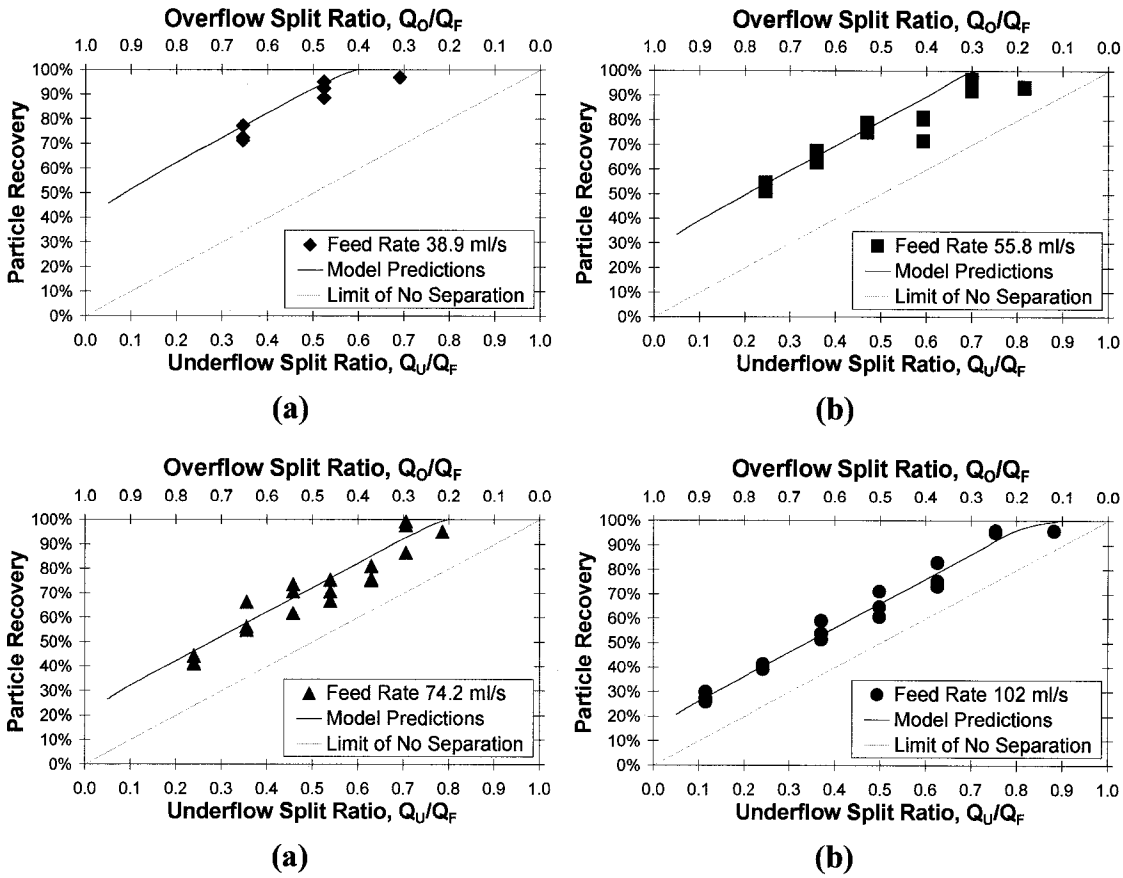

Figure A5-34a, b, c, d. Recoveries of Heavy Particles in Underflows of Column A, System II ($\alpha_{LF} = 0.134$, $\alpha_{HF} = 0.163$), all Feed Rates

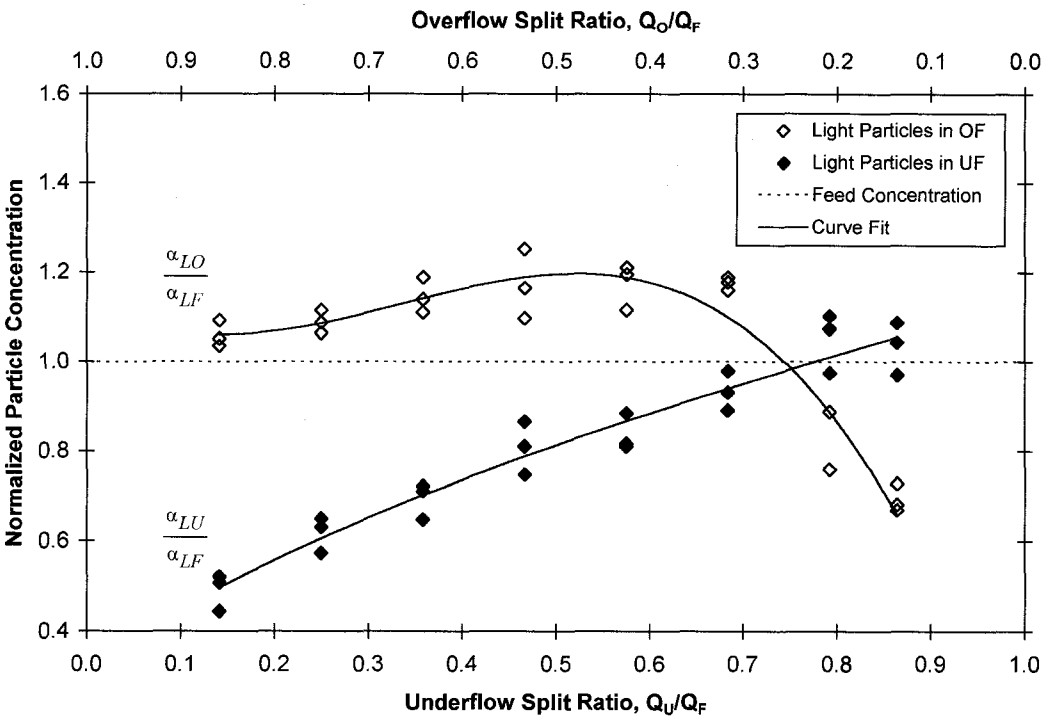

Figure A5-35. Concentrations of Light Particles in Overflow and Underflow for Column B, System I (α_{LF} = 0.058, α_{HF} = 0.122), Feed Rate 41.3 ml/s

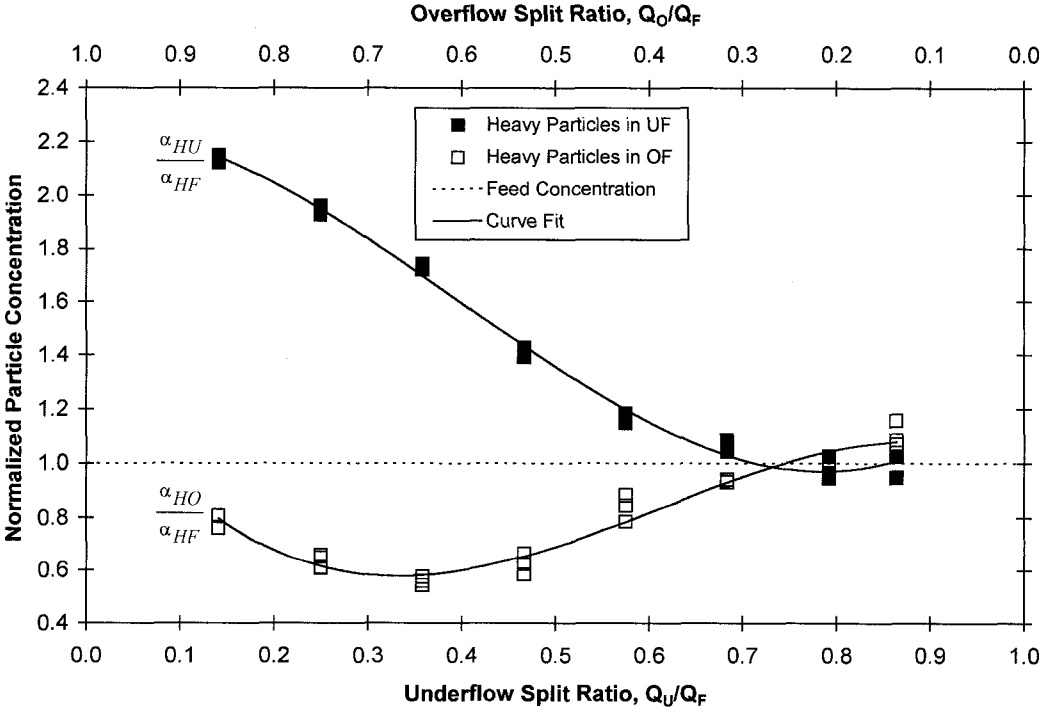

Figure A5-36. Concentrations of Heavy Particles in Overflow and Underflow for Column B, System I (α_{LF} = 0.058, α_{HF} = 0.122), Feed Rate 41.3 ml/s

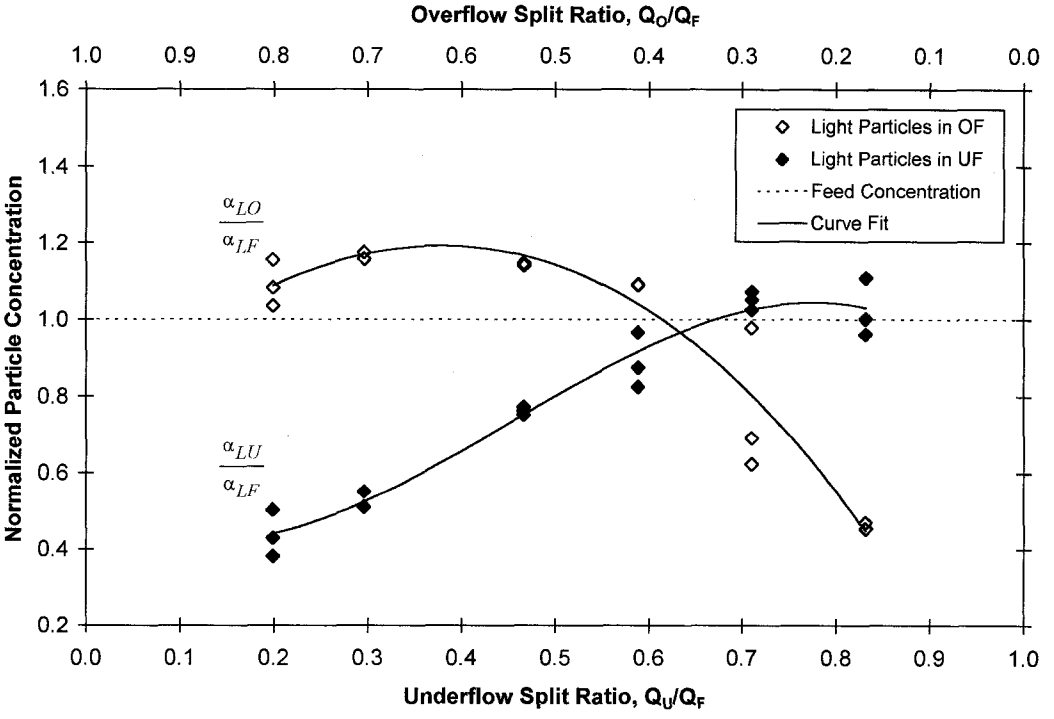

Figure A5-37. Concentrations of Light Particles in Overflow and Underflow for Column B, System I (α_{LF} = 0.058, α_{HF} = 0.122), Feed Rate 59.5 ml/s

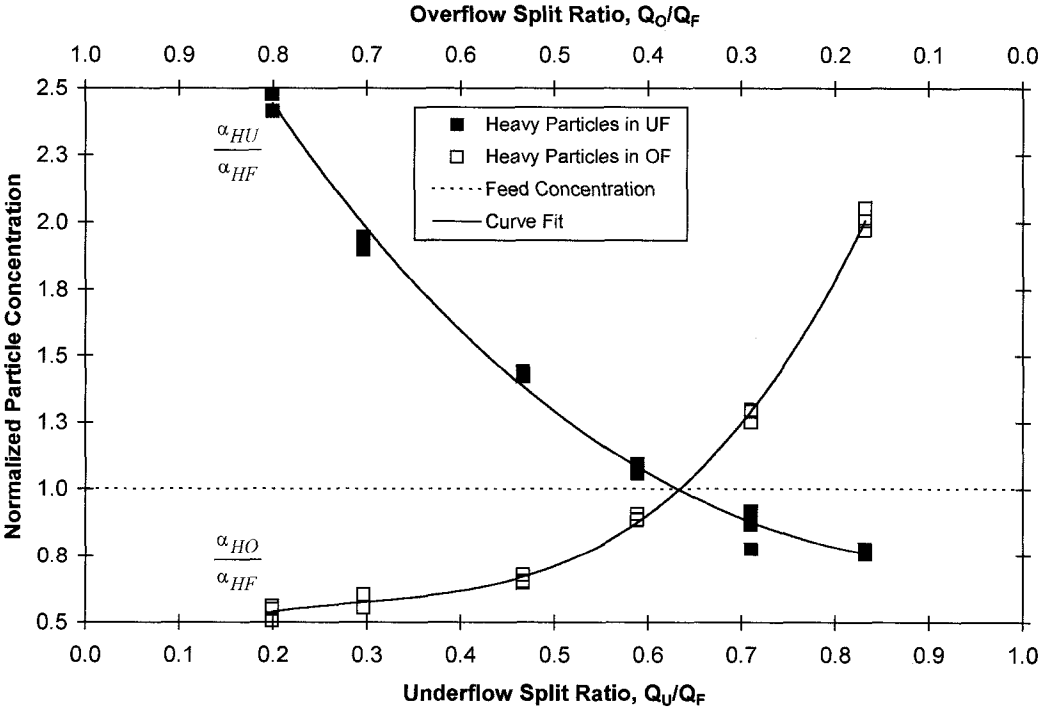

Figure A5-38. Concentrations of Heavy Particles in Overflow and Underflow for Column B, System I (α_{LF} = 0.058, α_{HF} = 0.122), Feed Rate 59.5 ml/s

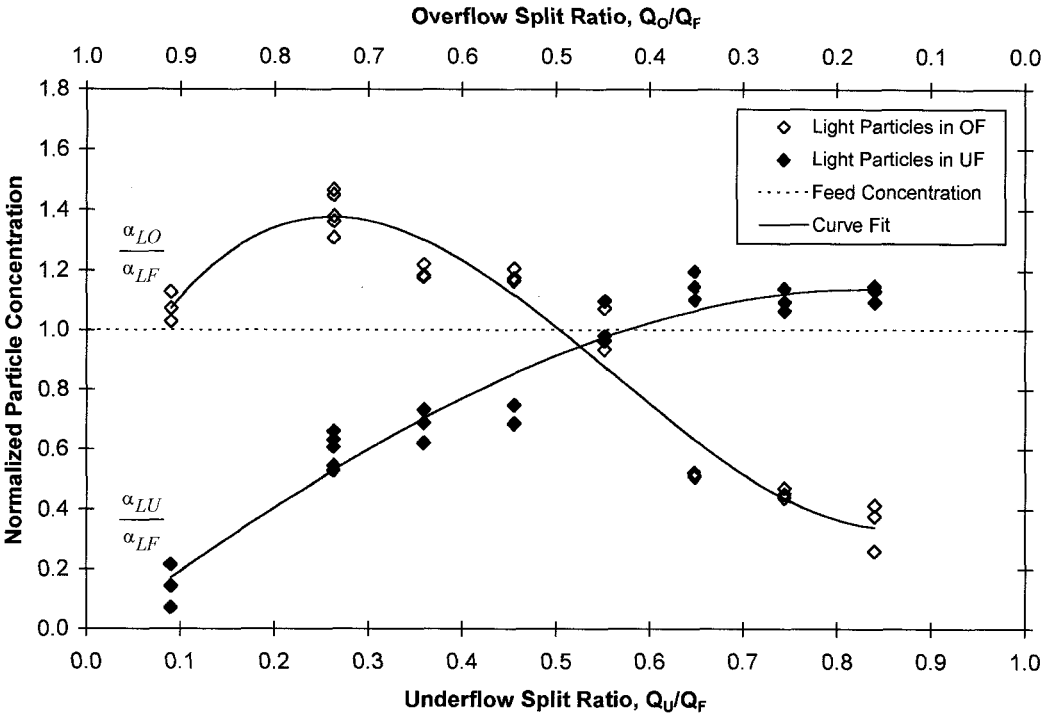

Figure A5-39. Concentrations of Light Particles in Overflow and Underflow for Column B, System I (α_{LF} = 0.058, α_{HF} = 0.122), Feed Rate 83.5 ml/s

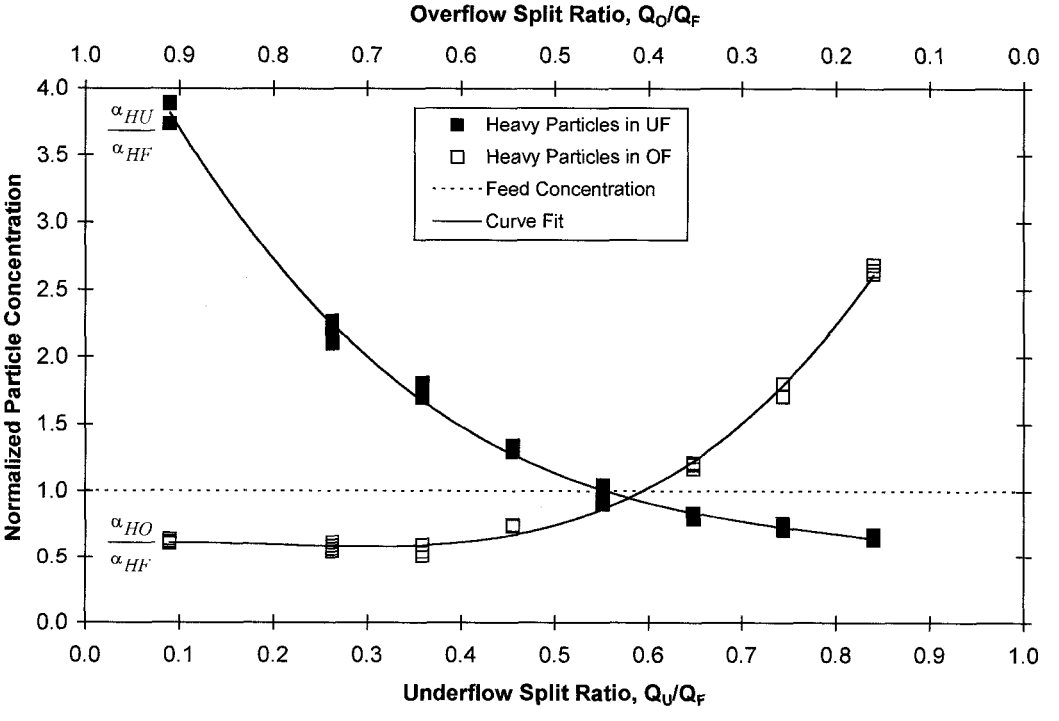

Figure A5-40. Concentrations of Heavy Particles in Overflow and Underflow for Column B, System I (α_{LF} = 0.058, α_{HF} = 0.122), Feed Rate 83.5 ml/s

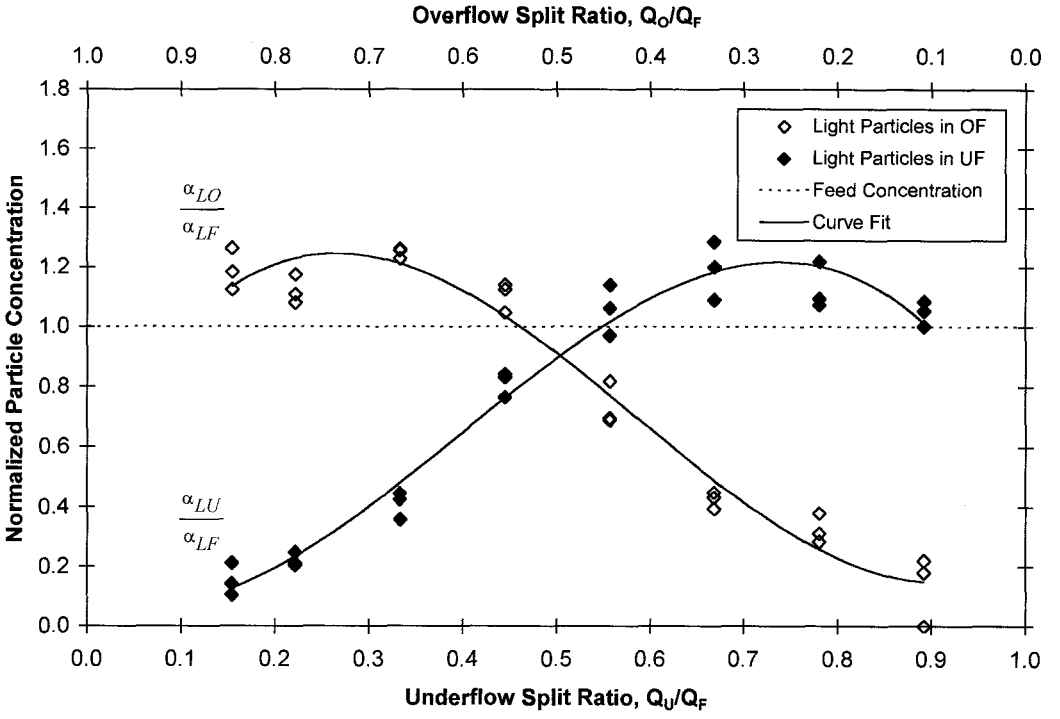

Figure A5-41. Concentrations of Light Particles in Overflow and Underflow for Column B, System I (α_{LF} = 0.058, α_{HF} = 0.122), Feed Rate 118 ml/s

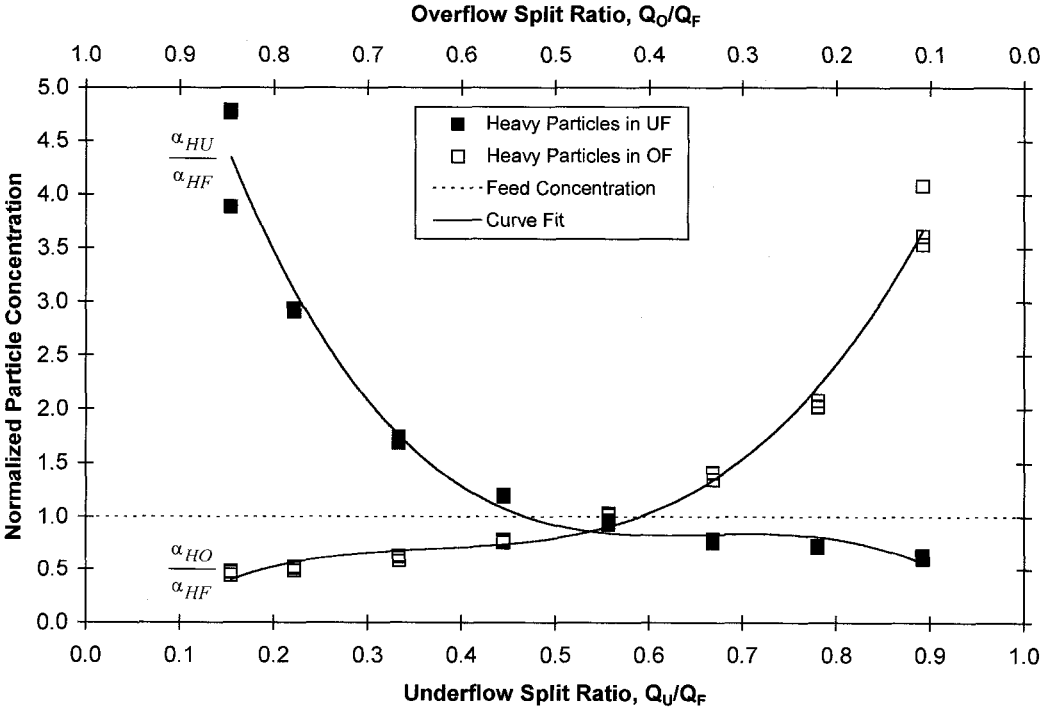

Figure A5-42. Concentrations of Heavy Particles in Overflow and Underflow for Column B, System I (α_{LF} = 0.058, α_{HF} = 0.122), Feed Rate 118 ml/s

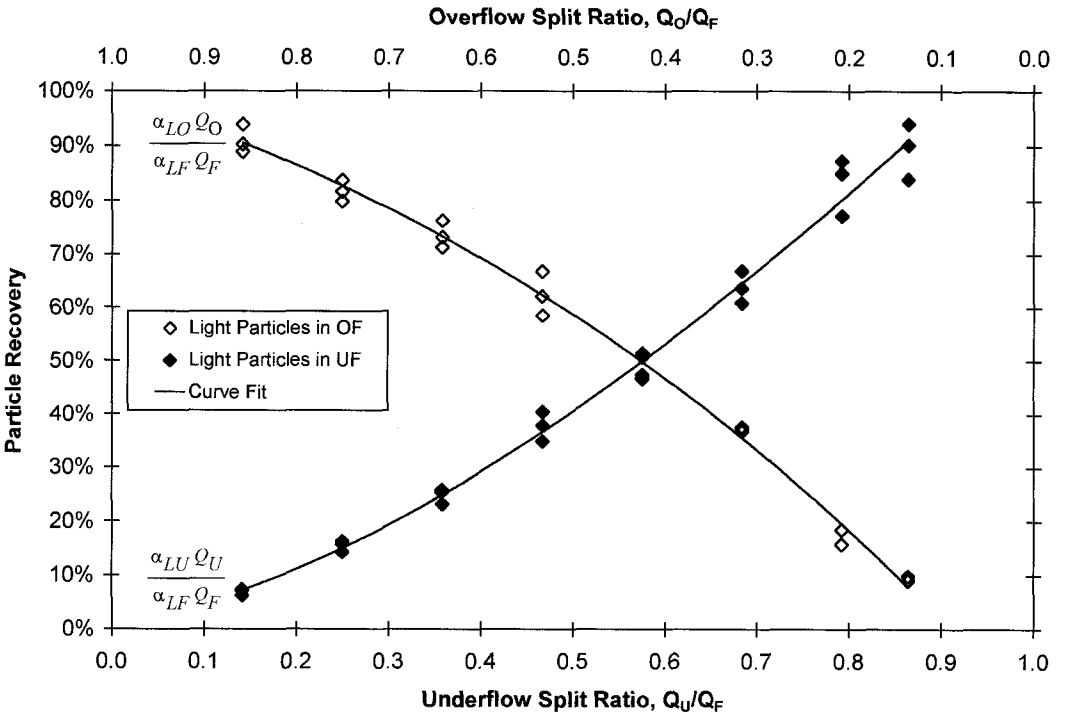

Figure A5-43 Recoveries of Light Particles in Overflow and Underflow for Column B, System I (α_{LF} = 0.058, α_{HF} = 0.122), Feed Rate 41.3 ml/s

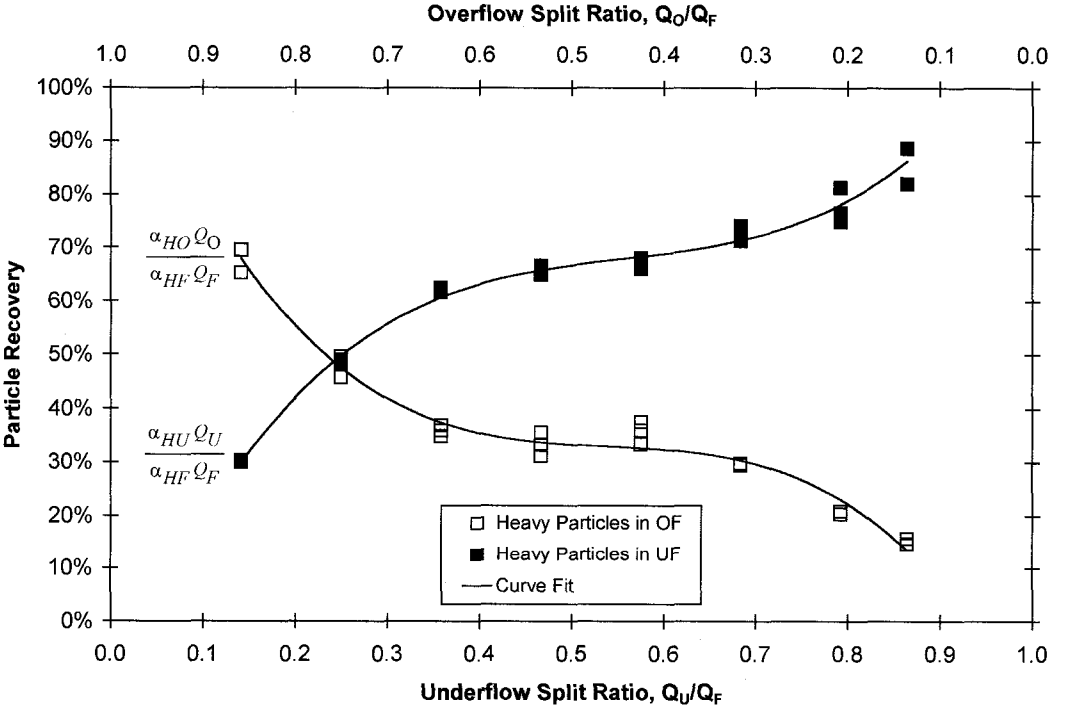

Figure A5-44. Recoveries of Heavy Particles in Overflow and Underflow for Column B, System I (α_{LF} = 0.058, α_{HF} = 0.122), Feed Rate 41.3 ml/s

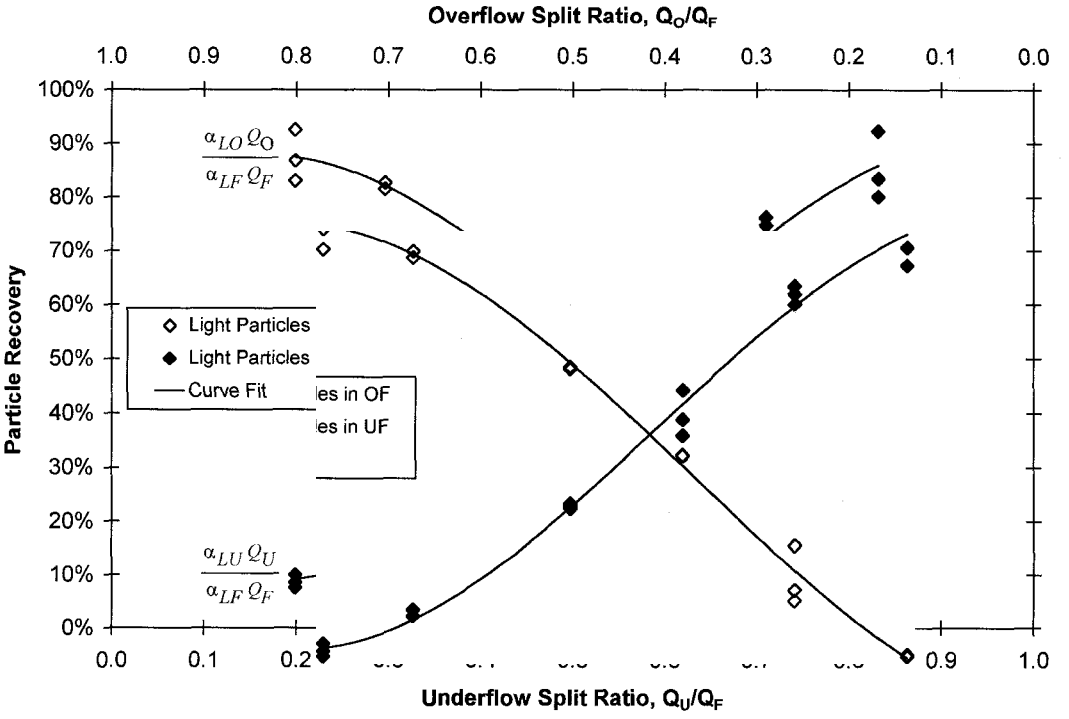

Figure A5-45. Recoveries of Light Particles in Overflow and Underflow for Column B, System I (α_{LF} = 0.058, α_{HF} = 0.122), Feed Rate 59.5 ml/s

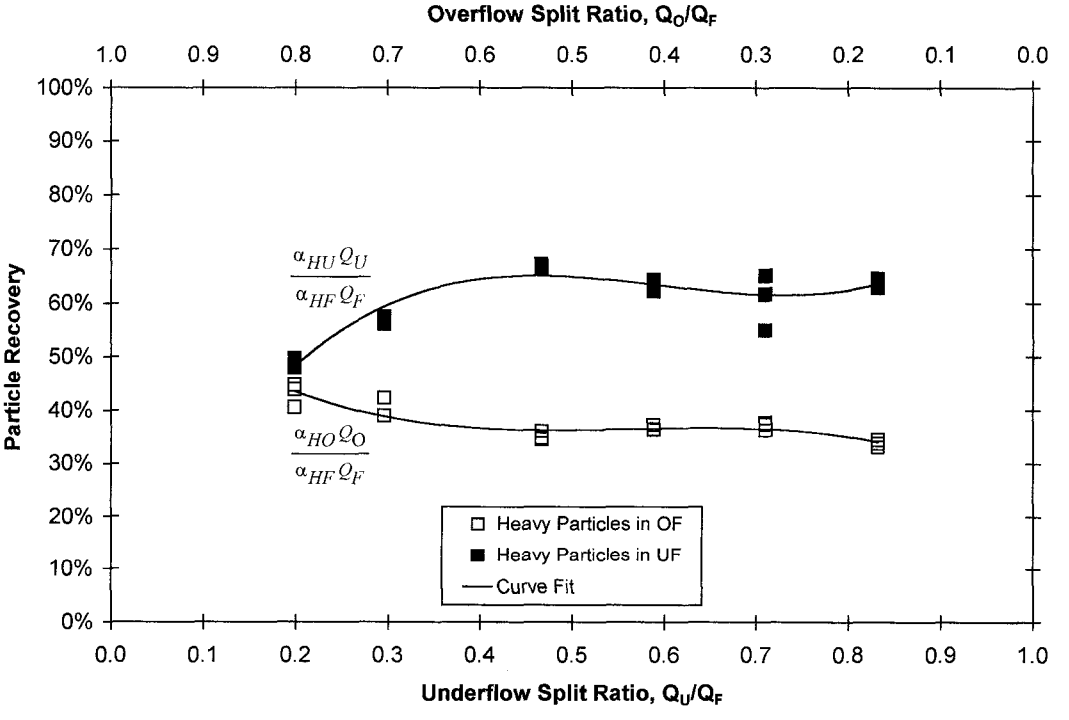

Figure A5-46. Recoveries of Heavy Particles in Overflow and Underflow for Column B, System I (α_{LF} = 0.058, α_{HF} = 0.122), Feed Rate 59.5 ml/s

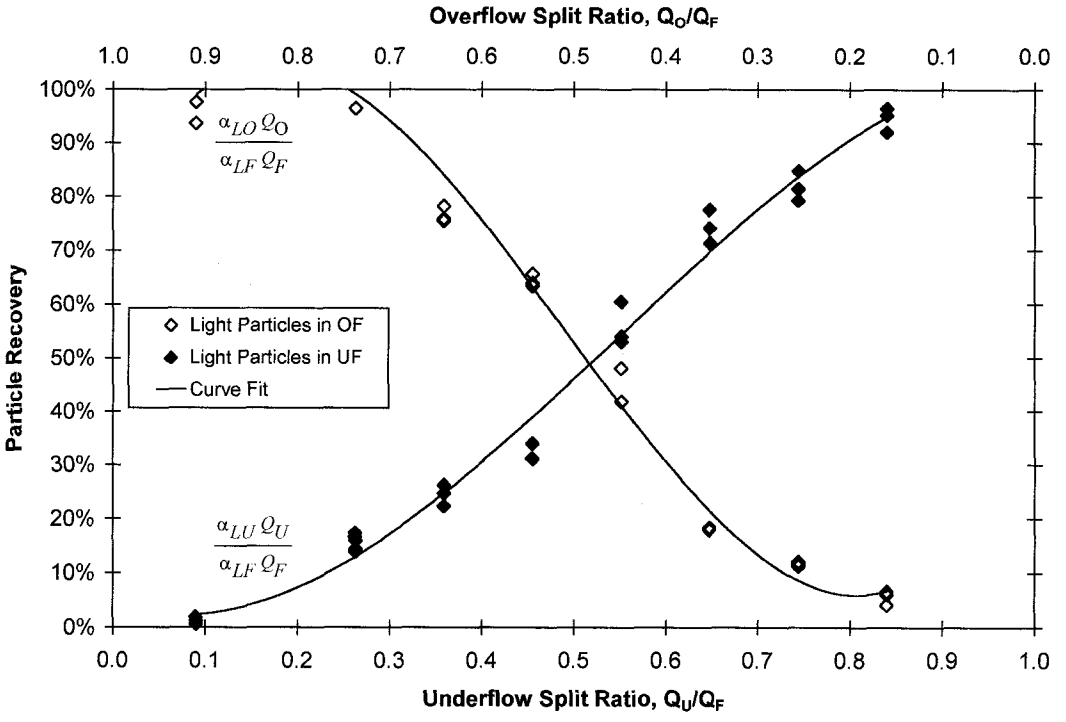

Figure A5-47. Recoveries of Light Particles in Overflow and Underflow for Column B, System I (α_{LF} = 0.058, α_{HF} = 0.122), Feed Rate 83.5 ml/s

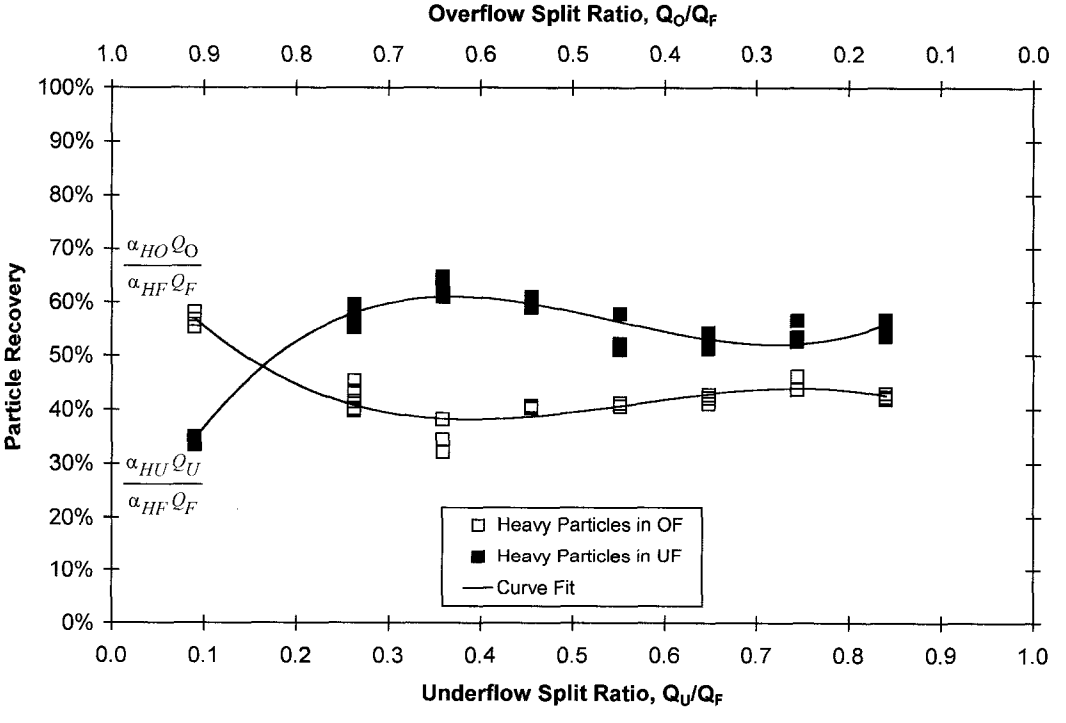

Figure A5-48. Recoveries of Heavy Particles in Overflow and Underflow for Column B, System I (α_{LF} = 0.058, α_{HF} = 0.122), Feed Rate 83.5 ml/s

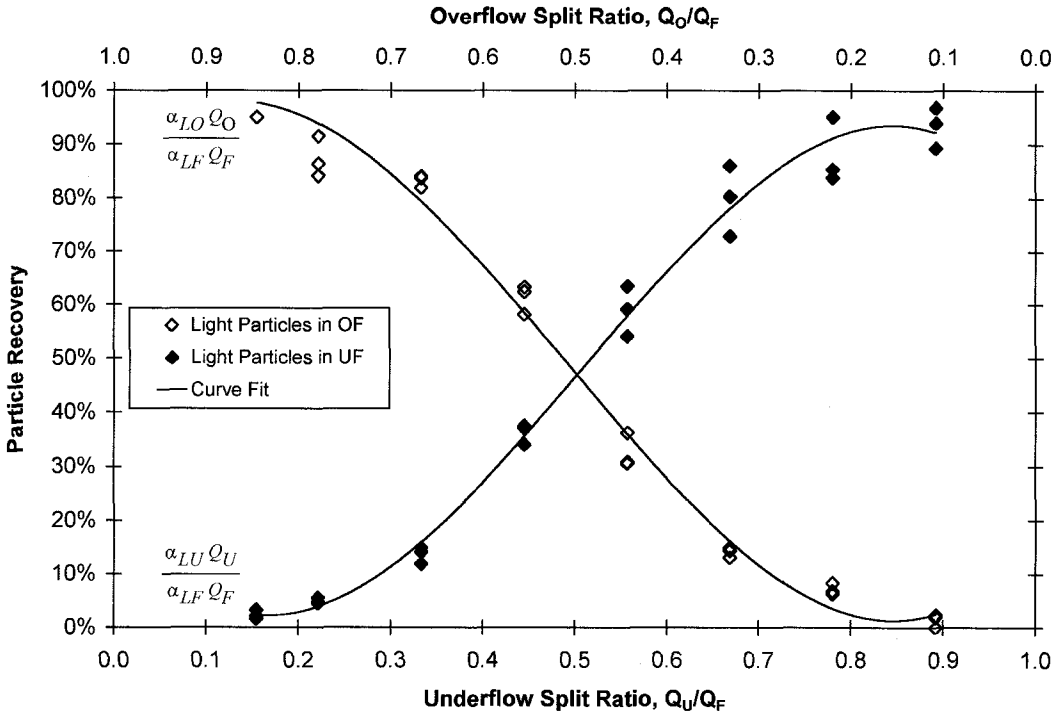

Figure A5-49. Recoveries of Light Particles in Overflow and Underflow for Column B, System I ($\alpha_{LF} = 0.058$, $\alpha_{HF} = 0.122$), Feed Rate 118 ml/s

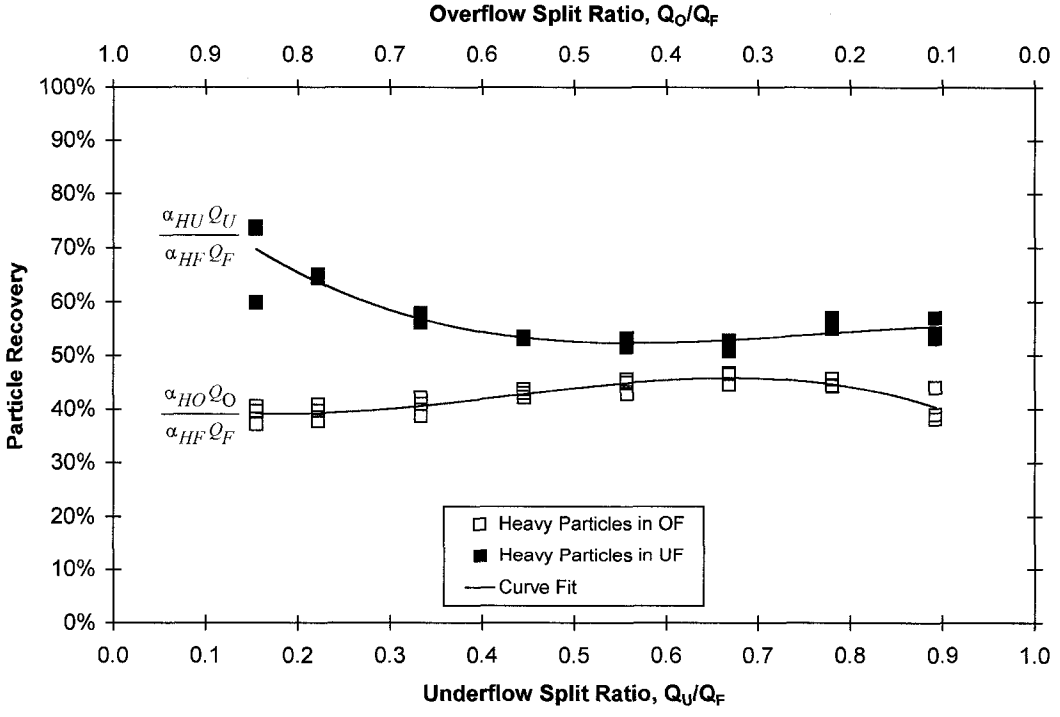

Figure A5-50. Recoveries of Heavy Particles in Overflow and Underflow for Column B, System I ($\alpha_{LF} = 0.058$, $\alpha_{HF} = 0.122$), Feed Rate 118 ml/s

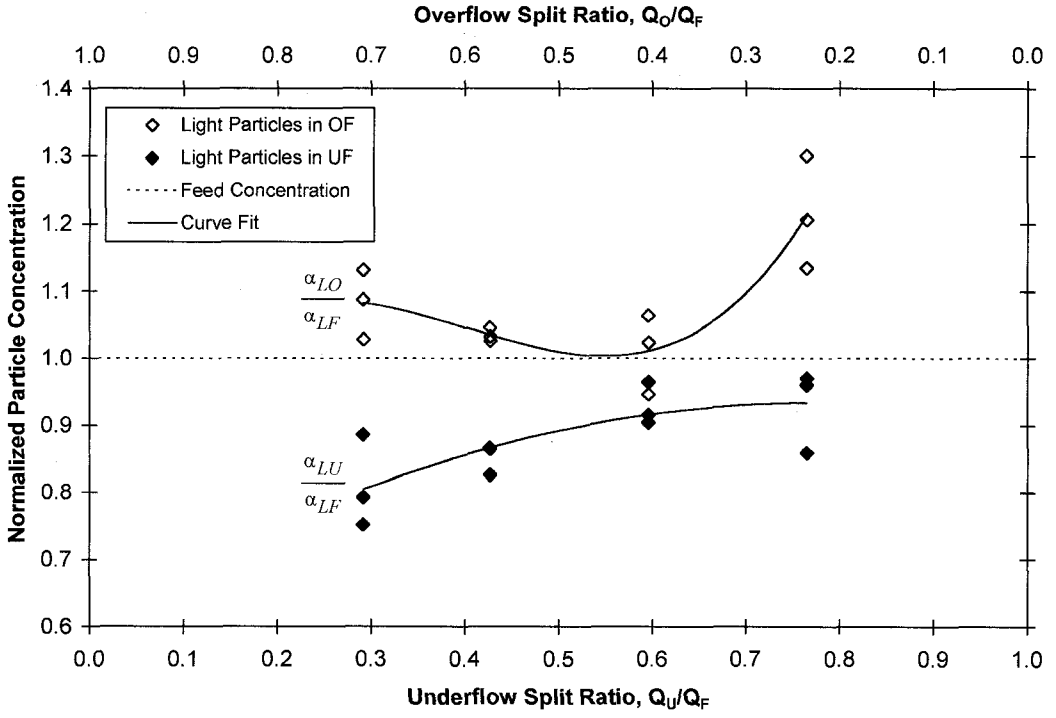

Figure A5-51. Concentrations of Light Particles in Overflow and Underflow for Column C, System I (α_{LF} = 0.058, α_{HF} = 0.122), Feed Rate 43.8 ml/s

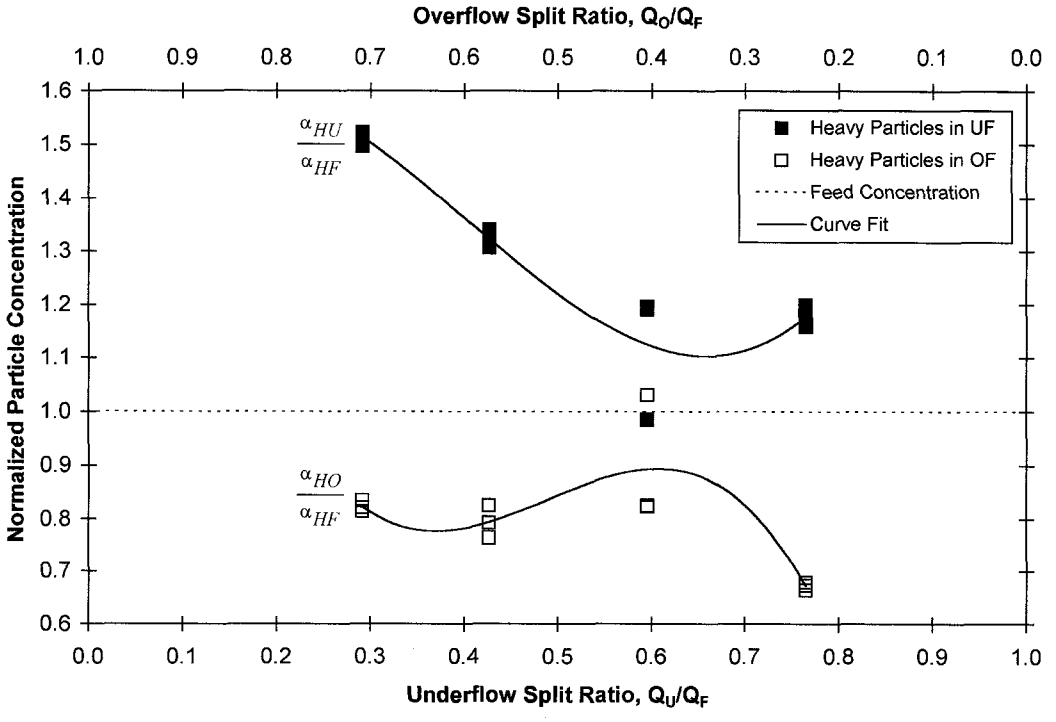

Figure A5-52. Concentrations of Heavy Particles in Overflow and Underflow for Column C, System I (α_{LF} = 0.058, α_{HF} = 0.122), Feed Rate 43.8 ml/s

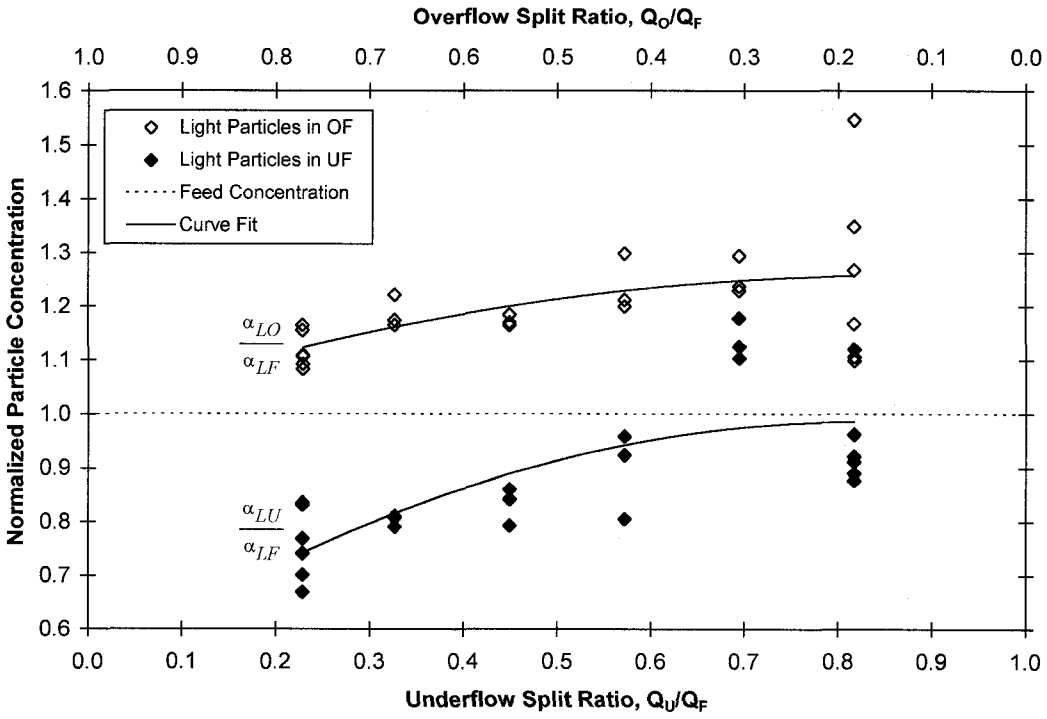

Figure A5-53. Concentrations of Light Particles in Overflow and Underflow for Column C, System I (α_{LF} = 0.058, α_{HF} = 0.122), Feed Rate 58.7 ml/s

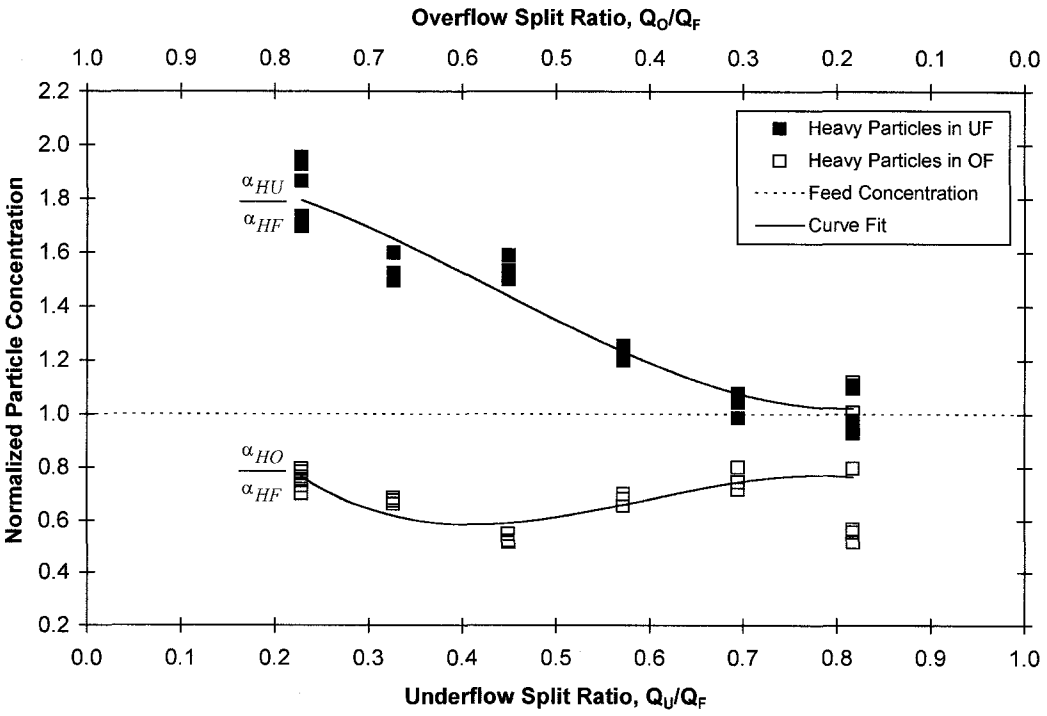

Figure A5-54. Concentrations of Heavy Particles in Overflow and Underflow for Column C, System I (α_{LF} = 0.058, α_{HF} = 0.122), Feed Rate 58.7 ml/s

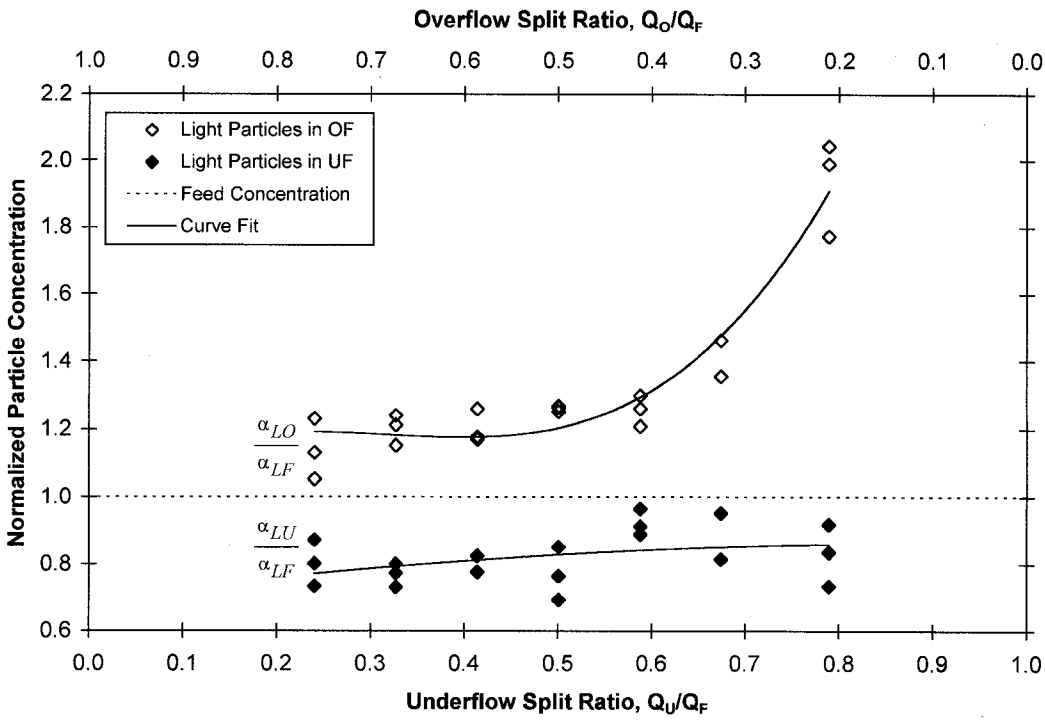

Figure A5-55. Concentrations of Light Particles in Overflow and Underflow for Column C, System I (α_{LF} = 0.058, α_{HF} = 0.122), Feed Rate 84.0 ml/s

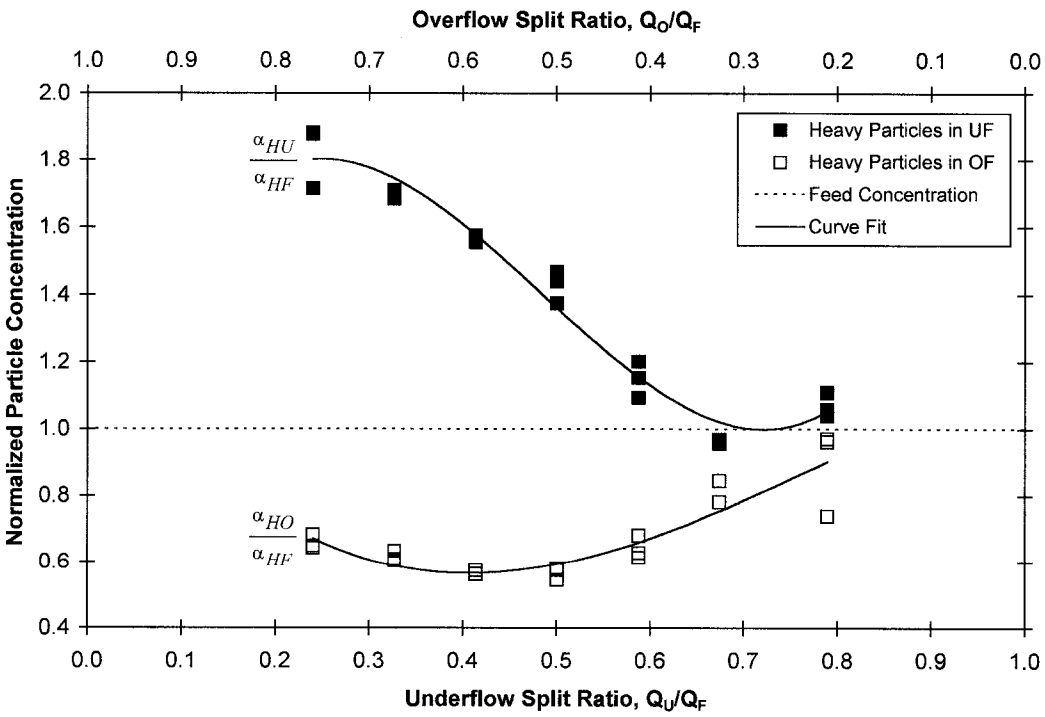

Figure A5-56. Concentrations of Heavy Particles in Overflow and Underflow for Column C, System I (α_{LF} = 0.058, α_{HF} = 0.122), Feed Rate 84.0 ml/s

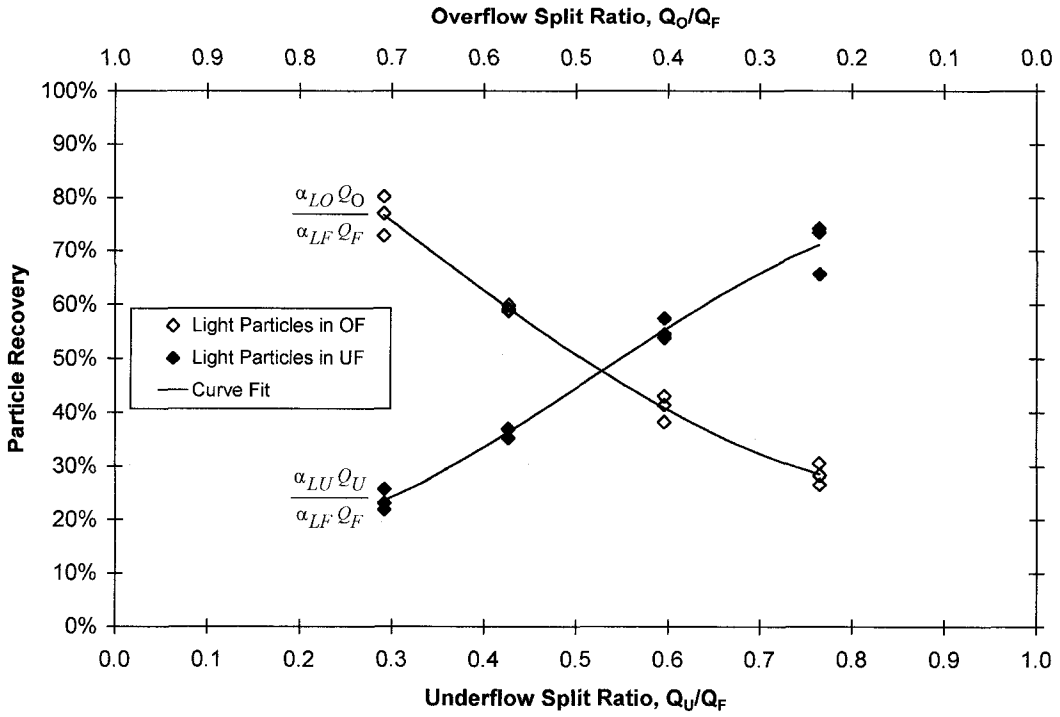

Figure A5-57. Recoveries of Light Particles in Overflow and Underflow for Column C, System I (α_{LF} = 0.058, α_{HF} = 0.122), Feed Rate 43.8 ml/s

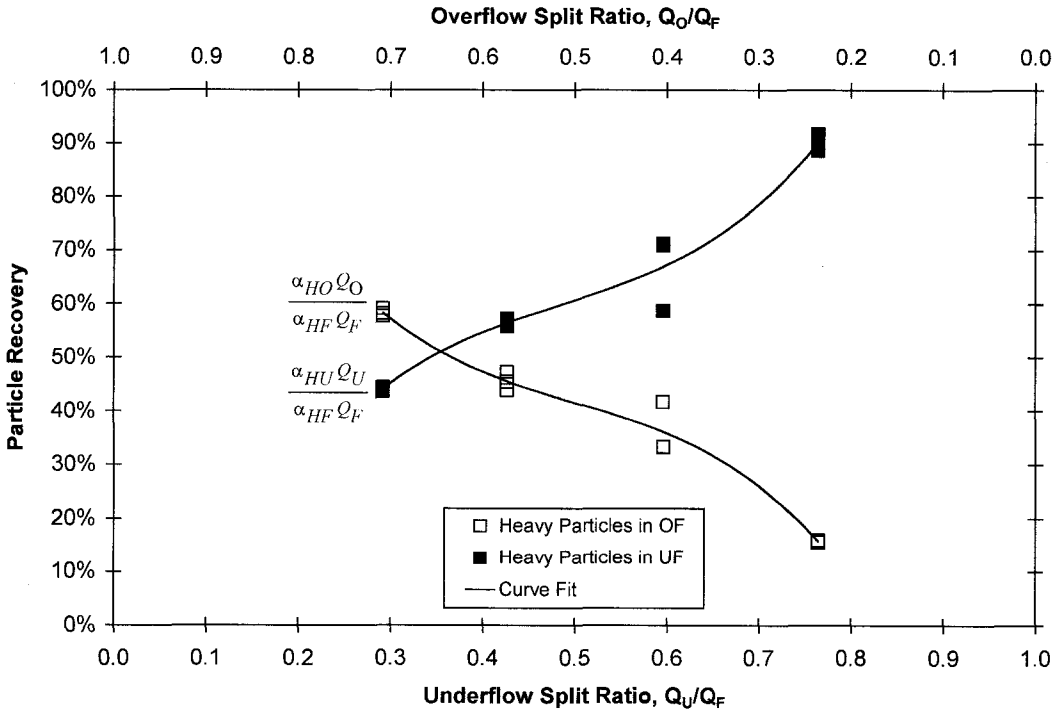

Figure A5-58. Recoveries of Heavy Particles in Overflow and Underflow for Column C, System I (α_{LF} = 0.058, α_{HF} = 0.122), Feed Rate 43.8 ml/s

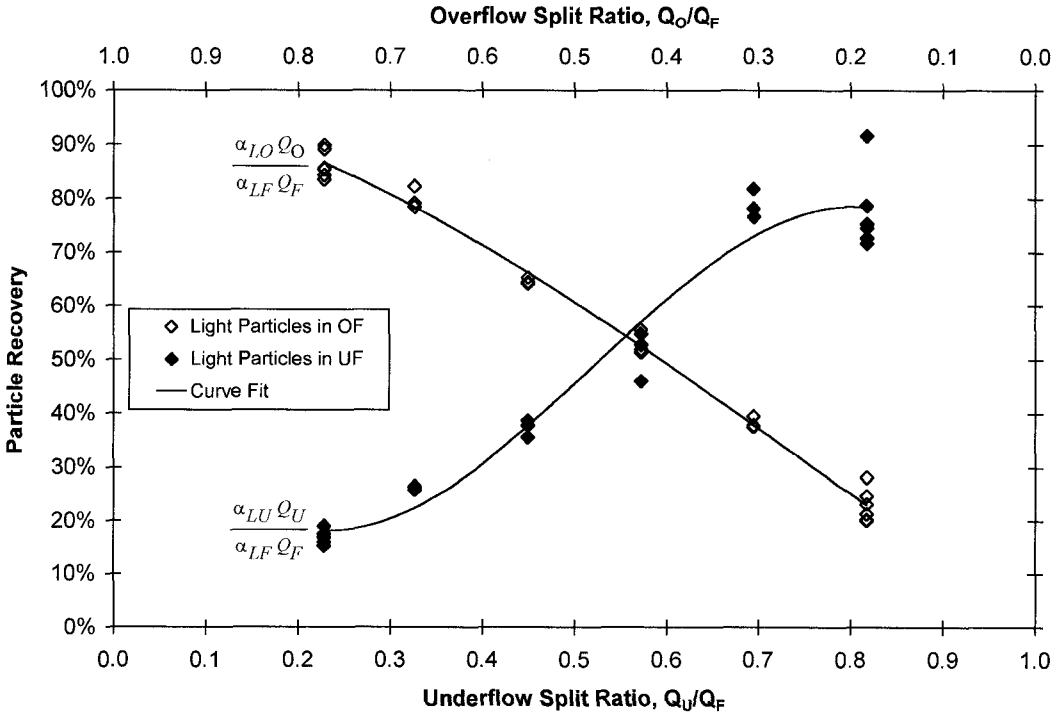

Figure A5-59. Recoveries of Light Particles in Overflow and Underflow for Column C, System I (α_{LF} = 0.058, α_{HF} = 0.122), Feed Rate 58.7 ml/s

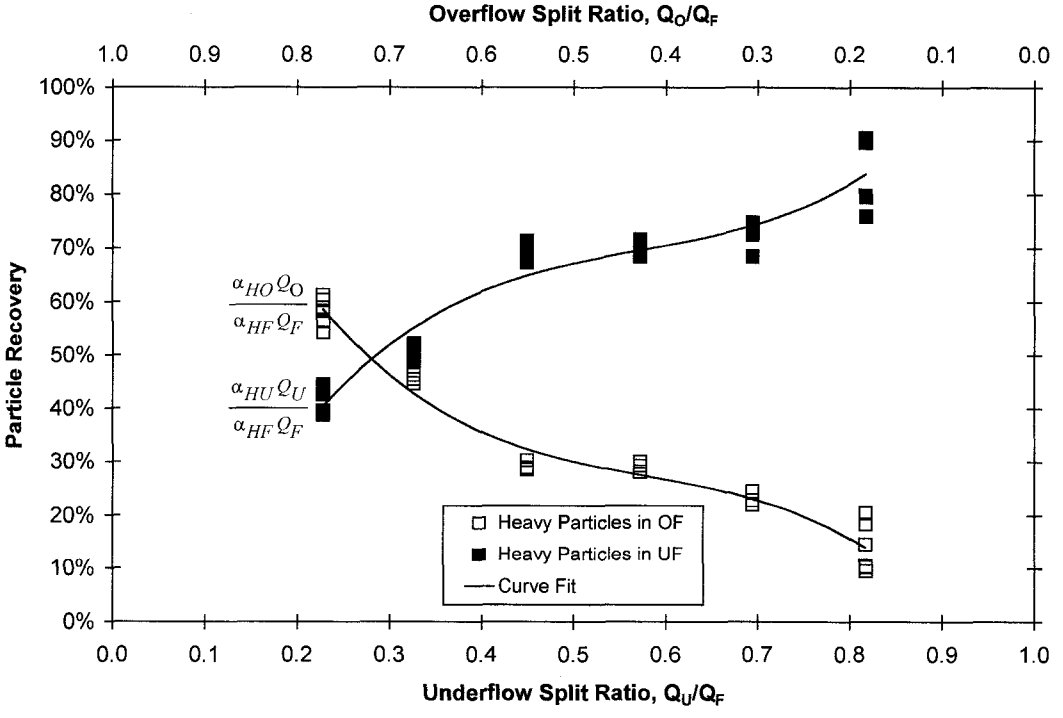

Figure A5-60. Recoveries of Heavy Particles in Overflow and Underflow for Column C, System I (α_{LF} = 0.058, α_{HF} = 0.122), Feed Rate 58.7 ml/s

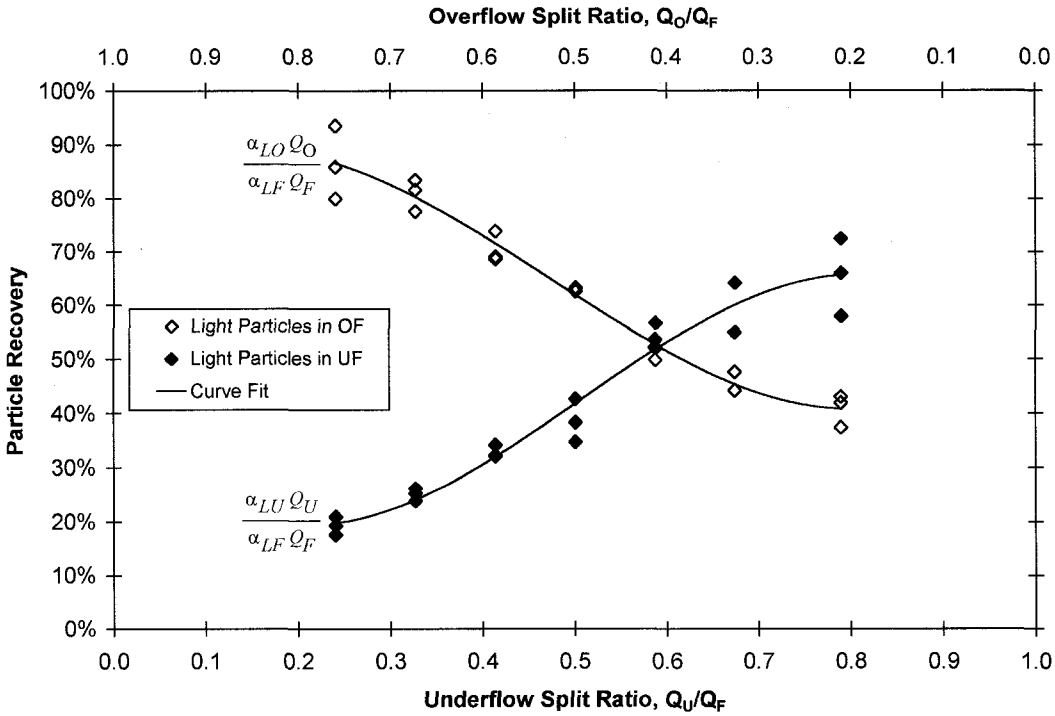

Figure A5-61. Recoveries of Light Particles in Overflow and Underflow for Column C, System I (α_{LF} = 0.058, α_{HF} = 0.122), Feed Rate 84.0 ml/s

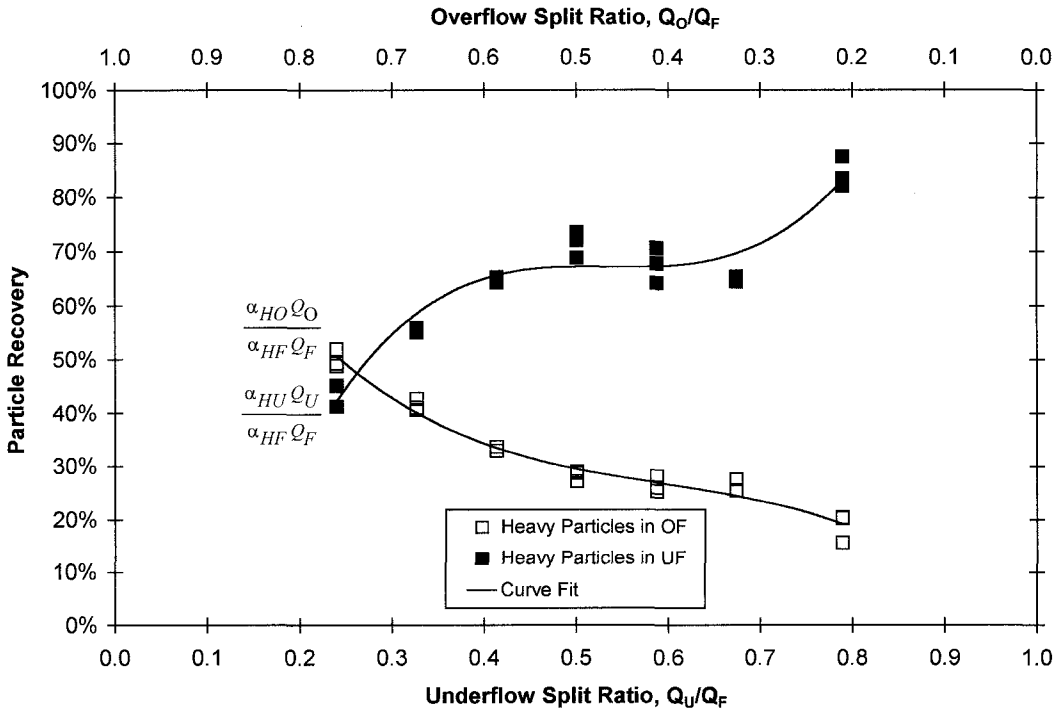

Figure A5-62. Recoveries of Heavy Particles in Overflow and Underflow for Column C, System I (α_{LF} = 0.058, α_{HF} = 0.122), Feed Rate 84.0 ml/s